Identification for Control Design with Application to a Compact Disk Mechanism

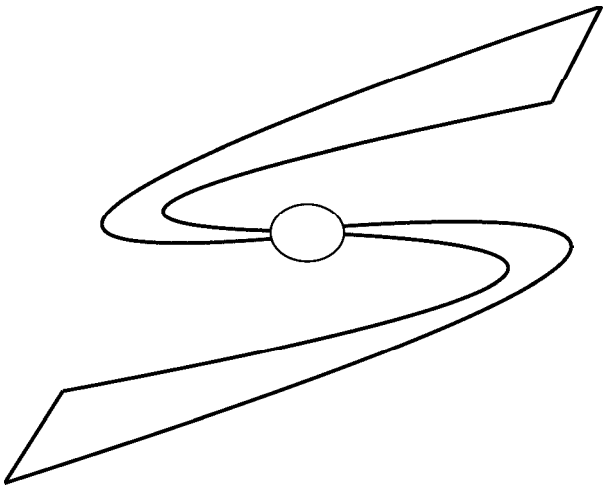

Hans Dötsch

Identification for Control Design with Application to a Compact Disk Mechanism

Identification for Control Design

with Application

to a Compact Disk Mechanism

PROEFSCHRIFT

ter verkrijging van de graad van doctor
aan de Technische Universiteit Delft,
op gezag van de Rector Magnificus Prof. ir. K.F. Wakker,
in het openbaar te verdedigen ten overstaan van een commissie,
door het College voor Promoties aangewezen,
op dinsdag 17 maart 1998 te 16.00 uur
door

Johannes Godfried Maria DÖTSCH

werktuigkundig ingenieur

geboren te Tegelen

Dit proefschrift is goedgekeurd door de promotor:
Prof. ir. O.H. Bosgra

toegevoegd promotor: Dr. ir. P.M.J. Van den Hof

Samenstelling Promotiecommissie:

Rector Magnificus, voorzitter
Prof. ir. O.H. Bosgra, Technische Universiteit Delft, promotor
Dr. ir. P.M.J. Van den Hof, Technische Universiteit Delft, toegevoegd promotor
Prof. dr. ir. J. Schoukens, Vrije Universiteit Brussel
Prof. dr. ir. J.J. Kok, Technische Universiteit Eindhoven
Prof. dr. ir. A. van den Bos, Technische Universiteit Delft
Prof. dr. ir. P.P.J. van den Bosch, Technische Universiteit Eindhoven
Dr. ir. M. Steinbuch, Nederlandse Philips Bedrijven B.V.

Published and distributed by:

Delft University Press
Mekelweg 4
2628 CD Delft
The Netherlands
Telephone: +31 15 2783254
Fax: +31 15 2781661
E-mail: DUP@DUP.TUDelft.NL

ISBN 90-407-1656-0 / CIP
NUGI: 841

Printed in the Netherlands

to Marja
Kennard, Kristan

Chapter 1

Voorwoord

Voorwoord

Het boek dat U thans leest rapporteert over mijn ruim vijf jaar durende onderzoek dat ik heb verricht als Assistent in Opleiding aan de Technische Universiteit Delft. De eerste gedachte bij het schrijven van dit voorwoord kan kort en krachtig worden weergegeven: eindelijk! Alle bevindingen en ervaringen van een intensieve periode hebben dan eindelijk hun beslag gekregen in dit proefschrift. Een gevoel van tevredenheid en niet in de laatste plaats voldoening kan hierbij moeilijk onderdrukt worden.

Ofschoon slechts de naam van één auteur op de omslag van dit proefschrift staat, is het verre van juist te veronderstellen dat het boekje in zijn huidige vorm slechts door één persoon tot stand is gekomen. Velen hebben een positieve invloed gehad op het verloop van het onderzoek, van wie ik de volgende met naam wil noemen. Een woord van dank gaat daarbij in de eerste plaats uit naar de personen die de mogelijkheid en de middelen hebben geboden om onderzoek te kunnen doen binnen een uitdagend project en van het begin tot en met het einde vertrouwen in een goede afloop hebben getoond: professor Okko Bosgra, wiens scherpe inzichten in en visie op de kern van de problematiek mij telkens weer verder op weg hebben geholpen en Budi Sastra van Philips' Natuurkundig Laboratorium, wiens kritische opmerkingen tijdens de kwartaalbesprekingen mij het noodzakelijke inzicht hebben verschaft in de technologische vragen die spelen in de industrie van de consumenten-electronica.

De discussies met Paul Van den Hof heb ik altijd zeer gewaardeerd en waren een grote steun voor een scherpe formulering van de onderzoeksproblematiek. De input van Maarten Steinbuch van Philips' NatLab heeft mij doen inzien dat het ontwerpen van een goede "loop shape" regeling een vak apart is; Gerrit Schootstra heeft mij in de beginfase geholpen een Compact Disk speler op een geheel andere wijze te leren bedienen dan ik gewend was. Discussies met collega's uit Delft en Eindhoven tijdens de reeds eerdere genoemde kwartaalbesprekingen heb ik zeer op prijs gesteld.

Ik heb het voorrecht gehad dat vier enthousiaste studenten de keuze voor hun afstudeeronderwerp hebben laten vallen op de Compact Disk speler: Henk

Smakman, Mohammad Daraei, Edwin van Donkelaar en Wouter Lap. Hun kritische vragen, opmerkingen en experimentele bijdragen zijn van grote waarde geweest, waarvoor dank.

Het werken met computers, netwerken en digitale signaal processoren heeft regelmatig tot momenten geleid die de wet van Murphy onderschrijven; de hulp van Henk Huisman, Peter Valk, Ben Wenneker, Jaap van Dieten, Rolf van Overbeek en Kees Slinkman is op die momenten zeer op prijs gesteld. Speciaal woord van dank gaat naar Guido Brown voor het uitlenen van zijn DSP.

Ondersteuning op het gebied van financiële en secretariële zaken, kopiëerfaciliteiten en maandelijkse kroketten door Els Arkesteijn, Maria Macherhi, Piet Ruinard en Cor Kremers is onmisbaar om de werkzaamheden als AIO aanzienlijk te veraangenamen.

Mijn kamergenoten Gregor van Baars en Thomas de Hoog waren altijd ongevraagd een luisterend oor voor de problematiek op het gebied van kinderopvang en de schrijnende situatie op de Nederlandse autowegen. Gesprekken over inhoudelijke dan wel niet-inhoudelijke zaken met collega AIO's Raymond, Dick, Hans, Sjirk, Marco, Edwin, David en Rob maakt promoveren tot een collectieve inspanning.

Er lijkt nu "eindelijk" weer tijd vrij te komen voor activiteiten die in de loop van de afgelopen periode steeds meer in het gedrang zijn gekomen zoals het verder verkennen van Afro-Cubaanse ritmepatronen en het voeren van levensbeschouwelijke discussies onder een goed maal met eetklup "de Eetklup". Het gevoel dat het nu "eindelijk" volbracht is zullen niet in de laatste plaats mijn ouders ten volle beamen; ik wil hen bedanken voor alle vrijheid en steun die ik van hen altijd heb mogen ontvangen, met name sinds zij opa en oma zijn geworden. Kennard en Kristan, papa hoeft niet meer naar "bofuh toe" en gaat weer wekelijks met jullie naar het dierenpark. Mijn laatste dankwoord gaat uit naar mijn lieve vrouw Marja. Zij heeft mij vrijwel niet anders gekend dan dat ik met een promotieonderzoek bezig was en heeft mij ten alle tijde daarin met liefde en daadkracht gesteund, wellicht meer dan zij zich ooit zal realiseren.

Hans Dötsch
Utrecht, 8 februari 1998

Chapter 1

Summary

Summary

Identification for Control Design with Application to a Compact Disk Mechanism

Hans Dötsch

Applications of optical disk drive systems in consumer electronic products require an enhancement of tracking behaviour in order to comply with stricter performance specifications that are imposed by an increasing information density on an optical disk and a faster accessability of this information. Moreover, in the application field of consumer electronic products an insensitivity to disturbances like shocks and vibrations, is required. Feedback control design is considered a viable tool to establish an enhanced tracking performance.

Specifications on track-following and disturbance attenuation of commercially available Compact Disk systems are achieved by controllers that are designed by means of "loop shape" design techniques, utilizing heuristic tuning rules. In view of enhanced performance specifications, heuristic design rules however lack sufficient refinement for utilization of available model knowledge for control design. To that end an enhanced tracking performance and disturbance attenuation is pursued by means of model-based control design, where controllers are designed on the basis of a mathematical, parametric model of the system. The design problem is phrased as an optimization problem. The quality of the resulting controller depends on the quality of the underlying model and, moreover, controllers generally are of a complexity similar to that of the underlying model. An important specification in view of implementation however is that a control design procedure should deliver controllers of restricted complexity.

In this research attention is directed towards the construction of parametric nominal models and model error bounds based on measurement data (system identification), that are suited for control design. The topic of identification

of parametric models that are suitable for control design has received a vast amount of attention in literature, resulting in the availability of tools for identification of approximate parametric models and model error bounds. What is not (yet) available is a systematic procedure for design of a restricted complexity, model-based controller that achieves an enhanced tracking performance for a system that is inaccurately known.

In this thesis a model-based control design procedure is proposed in view of design of restricted complexity controllers and is experimentally verified on a Compact Disk player. The basic ingredients of the proposed model-based control design procedure are identification of an approximate model, identification of model error bounds, design of a controller based on the approximate model and evaluation of the performance that is achieved for the (partially known) system utilizing a so-called system uncertainty description, incorporating model error bounds. Controller complexity is kept limited by utilizing low complexity models for design. Consequently, the limitations of the design need to be evaluated prior to controller implementation. A system uncertainty description based on a dual Youla model structure is shown to be suited for non-conservative evaluation of achieved disturbance attenuation, expressed in the sensitivity transfer function.

Experimental results obtained from two experimental Compact Disk systems indicate that utilization of model error bounds employing a dual Youla model structure is shown to enable a reliable and useful evaluation of performance that is achieved for the system prior to controller implementation. An important feature of the proposed procedure is that knowledge of the controller present in the feedback loop is required for identification and that inadequate controller knowledge becomes more critical in case of an increased bandwidth design.

Chapter 1

Introduction and problem motivation

1.1 Background motivation

The research reported in this thesis is motivated by the need for an enhanced technology for complying with harsher specifications on tracking behaviour in optical disk drive devices *and* the recent availability of promising tools in the field of feedback system design and modelling based on system measurements.

1.2 Optical disk drive systems

Demands on the dynamical behaviour of industrial processes have been growing more strict in terms of increasing technological demands at a decreasing environmental cost. This specifically holds for the application of optical disk drive systems (ODDS's) in information storage devices. The pace of developments in optical data storage technology during the last decennium has caused a broad application area of optical disk drive systems in industrial and in-home information storage devices. Especially the application of ODDS's in audio, video and computer-related electronic products has proven to be very profitable. As economic profit is dictated by a harsh competitive commercial activity in a rapidly changing consumer market, the demands on performance are constantly increasing.

For present applications in consumer products, optical disk systems are expected to perform well while being exposed to all kinds of disturbances (e.g. shocks, vibrations, scratches and grease stains on the disk surface). An optical disk system that is insensitive to disturbances but is too expensive will not sell; consequently, production costs must be kept low in order to be competitive in the consumer market. As optical disk systems are produced in large numbers at high production speed and low costs, every system will exhibit slightly different

behaviour. As the customer expects his or her purchased system to perform well, there are limits to which mass-produced systems are allowed to vary in performance.

In respect of future applications of ODDS's, important commercial breakthroughs are directed towards an increase of the amount of information contained on one disk. One way to realise this is to increase the information density on a disk. Optical data storage technology nowadays enables an increase of the information density by a factor 4. An alternative way is to construct multilayer optical disks, where several information layers are "glued" together in one disk. Disks containing 6 to 8 information layers have been proven to work well under optimally conditioned circumstances. In addition, the optical disk must rotate at higher velocities in order not to slow down information accessability due to an increased amount of information.

A critical part in the process of optical information read-out in view of the aforementioned performance specifications is the positioning of the optical read-out device with respect to the disk, which is enabled via an electro mechanical servo mechanism. The information on the disk can only be read in a correct way in case the optical device is placed with respect to the disk within prespecified distance margins, which we will further refer to as the problem of tracking of the information. Adequate tracking of information is achieved by means of altering the construction of the mechanical servo system or by application of a feedback controller. Although the problem of designing an enhanced tracking system is a combined problem of constructive design and control design, in this thesis we will view the construction of the tracking mechanism to be unalterable and restrict attention to design of a feedback controller.

One of the perhaps best known applications of an optical disk system in consumer electronic products is the Compact Disk player. Application of feedback controllers to a Compact Disk drive system has proven to establish an enhanced tracking performance and attenuation of disturbances. Controllers that satisfy present tracking specifications are obtained by employing heuristic tuning rules (loop shape design) and model-based control design techniques like Quantitative Feedback Theory (QFT) [14, 61] and robust design techniques that take model inaccuracy into account, like $\mathcal{H}_\infty$ and μ-synthesis design [36, 35]. A major issue in model-based control design is that in case specifications on tracking performance are set to a higher level, availability of models that accurately describe the system is a prerequisite.

In an industrial environment a cheap and fast way of obtaining models is to perform frequency response measurements by virtue of available dynamic signal analyzers. As signal analyzers employ a large number of measurement data,

frequency response estimates are presumed to be of high accuracy. Although frequency response estimates are of high accuracy, an indication of how good the estimates are is indispensable in case they underly the design of a controller in view of an enhanced performance for the system. Available signal analyzers do not (yet) provide a quantitative measure of the accuracy of frequency response estimates that is suitable for control design.

1.3 Problem formulation

In the previous section we have clarified that complying with increasing specifications on tracking performance of an electro mechanical servo mechanism via feedback compensator design requires the availability of accurate models. In recent years the topic of constructing mathematical models for design of high performance controllers has received a vast amount of attention in the research field of system identification. Research efforts have roughly branched into two directions.

One direction focusses on constructing nominal models that are to be used in a model-based control design in view of achieving a high performance for the system [69, 29, 53, 39]. Here a main issue is that a nominal model will at all times provide an approximate description of the system; attention has mainly been directed on *how* to approximate the system such that a resulting controller will do well for the system. The second direction focusses on development of identification techniques that provide a quantitative measure of the model quality in view of control design, delivering so-called model error bounds [90, 59, 37].

In view of the aforementioned need for accurate models for control design, the general problem statement addressed in this thesis reads as follows:

> In what way can available identification techniques contribute to achieving an enhanced tracking performance of an electro mechanical servo mechanism in a systematic way via model-based control design ?

From the above problem formulation, we discern the following questions that give further direction to our problem elaboration.

1. When is a controller a "good" one ?

Of course, a controller should achieve an enhanced performance since that is our main incentive to address control design. The question is directed towards requirements that are of a more pragmatic nature since we want to verify controllers experimentally on a physical system. Digital implementation of controllers puts restrictions on the maximum controller complexity, especially in case controllers are to be implemented at high sample rates. So a controller is designated a good one in case it realizes an enhanced tracking performance yet having a limited complexity.

2. Can we construct controllers that comply with our requirements via model-based control design in a straightforward manner, or do we have to take an alternative path ?

In case a system has complex dynamics, model-based control design in view of an enhanced tracking performance requires models to be of sufficient complexity to describe the system and its disturbances. As we do not know beforehand whether a model is sufficiently complex or not, a feasible approach is to model the system as accurately as possible and to account for (remaining) model errors by means of uncertainty models. Robust control design techniques [97] enable design of controllers that achieve some performance for the system. A disadvantage of optimization-based control design methods is that resulting controllers have a complexity similar to that of the model (i.e. nominal models and uncertainty models) underlying the design. This inevitably leads to controllers that are of a too high complexity.

One way to deal with high order controllers is to utilize controller order reduction techniques. A controller of lesser complexity is determined that achieves a similar performance as the complex controller. Work on reduction of the controller order, designed on the basis of a complex nominal model, is a.o. reported in [95]. Apart from the fact that it is not at all a straightforward exercise to find a controller of lower complexity that establishes a similar performance as a high order controller, a reduction approach heavily relies on the presumption that the high order controller achieves a desired performance for the system (which is the basic motivation to do control design!), yet can not be implemented. However, design of such a high order controller requires availability of a highly accurate nominal model, which is, as discussed in the previous section, not at all a self-evidency.

Summarizing, the answer to question 2 is that we adopt a strategy of employing models of limited complexity in order to come up with model-based

controllers of limited complexity yet achieving good performance for the system.

3. Does it suffice to utilize *nominal* models as a basis for control design such that controllers are obtained that answer to question 1 ?

Design of controllers based on low complexity models may yield low complexity controllers, yet hampers achieving an enhanced performance for the system due to the models inadequacy to capture the system dynamics. So sole utilization of nominal models does not guarantee performance for the system; hence the following question naturally pops up:

4. Does it suffice to utilize *uncertainty* models as a basis for control design such that controllers are obtained that answer to question 1 ?

Utilization of uncertainty models in a robust control design may lead to a robust controller, yet to achieve enhanced performance for the system the true model uncertainty should be limited. Consequently, uncertainty models that provide a high robust performance (again) imply a high order controller in case of a complex system, as the uncertainty model should be of sufficient high complexity to allow for *enhanced* robust performance.

5. Does there exist a model-based control design procedure that takes all the aforementioned aspects into account in a systematic way ?

The general problem stated above covers a broad range of various fields. We are on the one hand confronted with an industrial tracking system having complex dynamics that should comply with harsher tracking performance specs. In order to comply with these specifications, more insight in the system dynamics in terms of mathematical models is required and control design tools are needed that provide controllers that account for the systems complexity and its uncertain dynamical behaviour. On the other hand, the research fields of model-based control design and system identification have gained more insight into feedback control of complex dynamical systems that have uncertain dynamical behaviour. Tools have been developed for design of robust controllers and identification of nominal models and uncertainty models which have shown promising results being applied to a limited number of real-life applications.

In the light of the above answers to questions 1 to 4, the fields of model-based control design and identification of nominal models and uncertainty models play a role in the design of a controller of restricted complexity that achieves an enhanced tracking performance for a complex tracking mechanism as encountered in optical disk drive systems. What is yet unclear is the interplay between these tools such that they systematically contribute to an enhanced tracking performance. We will elaborate on this in more detail in the next section.

1.4 Modelling and feedback control design

In model-based control design, controllers are designed for a physical system with the presumption that the model underlying the design is an adequate system description. As models generally are idealized system descriptions, resulting controllers, designed on the basis of a model, may result in an unacceptably large difference between the designed performance and the performance actually achieved for the system (or even destabilize the system!). In order to account for differences between model and system (plant-model mismatch), robust control design techniques [26, 97] enable to incorporate so-called uncertainty models into the design, together with a nominal model. Resulting controllers are called robust if they achieve stability or performance for every system accounted for by the uncertainty model and hence, presumed the "true" system is accounted for by the uncertainty model, for the system. Whether a robust controller achieves a *prespecified* performance for the system however, depends on the shape and size of the modelled uncertainty, which boils down to selecting a suitable uncertainty structure. In case prior knowledge about the nature of uncertainty is at hand (e.g. varying gain, resonance modes), this can be fruitfully used to "decrease" the set of feasible systems, resulting in a less conservative design employing μ-synthesis techniques [97]. However, the more structure is incorporated into the uncertainty model, the more complex resulting controllers will be. The problem of high robust performance control design narrows down to the need for accurate yet simple models! In the field of system identification this need has been recognized and has led to research activity in two directions: identification of nominal models and uncertainty models. The common denominator in both directions is the identification of models that exhibit a small plant-model mismatch in view of high performance design. The pursued approaches however have different perceptions of a plant-model mismatch.

The starting point of nominal identification for control design is that a system

is too complex to model exactly and that the systems dynamics are (completely) unknown. As a result, a model is an approximate system description and the problem is then phrased as how to approximate a system such that controllers, designed on the basis of a model, exhibit high robust performance. The topic of approximate identification in view of high robust performance control design has received a great deal of attention in recent years [70, 29, 85, 53]. Resulting techniques employ available controller knowledge in the approximate identification and have proven to produce approximate models that are more appropriate for high performance design than in case no controller knowledge is employed.

However, the question "how much more" appropriate these approximate models are, remains unanswered. In order to answer this question satisfactorily, system knowledge is indispensable, which is presumed not (completely) available. In order to establish a sensible judgement in view of the *true* control suitability, uncertainty models are required.

The construction of model error bounds, based on measurement data, has received an increasing amount of research attention in recent years [59, 90, 37, 51, 47, 34]. Methods developed differ in presumptions on the sources and the nature of model uncertainty. Depending on the presumed nature of undermodelling errors and disturbances, resulting error bounds have a deterministic or stochastic character. Letting aside technical assumptions on error nature at this point, the main goal of identifying error bounds is to construct bounds that introduce little conservatism in a resulting robust design, implying that the bounds should be tight. For complex systems this inevitably results in complex error bounds and thus complex controllers. No specific attention has so far been given to identification of error bounds that are tight yet simple in view of restricted complexity, high robust performance design.

1.5 Problem elaboration and thesis outline

In the previous section we have given due prominence to the fact that the plant-model mismatch plays a significant role in view of high robust performance control design. Nominal (approximate) models and uncertainty models are both indispensable in a robust control design procedure. However, models underlying a robust design should be of limited complexity as resulting controllers are intended for implementation on a disk drive system. In this thesis a strategic choice is made to perform a high robust performance design of a restricted complexity controller in two stages:

1. a design step based on a low order nominal model and

2. a robust performance evaluation step based on utilization of tight (and thus complex) model error bounds.

The elaboration of this strategic choice results in the following thesis outline. The thesis structure is schematically depicted in figure 1.1.

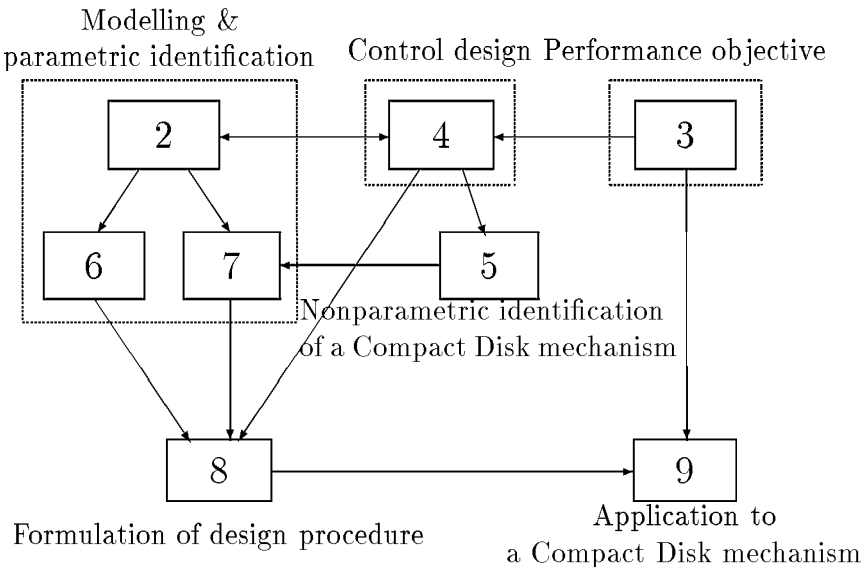

fig. 1.1: Schematic overview of the thesis outline.

Chapter 2: Modelling in view of control design

The mathematical framework used throughout this thesis is introduced and the role of approximate models and model error bounds in view of control design are clarified. At the end of chapter 2 we give a more detailed outline of the subsequent chapters.

Chapter 3: Compact Disk servo system

Physical properties of an electro mechanical actuator of a Compact Disc servo system are discussed; performance specifications in view of desired tracking behaviour are phrased and the significance of model-based control design for achieving these specifications is made plausible.

Chapter 4: Design of restricted complexity controllers

A control design procedure is proposed that employs a robustness optimization with respect to fractional model uncertainty in combination with a loop shape design technique. As the nominal design has no implicit robustness guarantee, robust performance evaluation constitutes an indispensable step in the control design.

Chapter 5: Nonparametric identification of a mechanical servo

The focus of this chapter is twofold. Firstly, frequency response estimation via periodogram averaging in conjunction with periodic excitation signals is put forward as a powerful means to estimate a system frequency response based on a large number of measurement data while the number of frequency domain data remains limited. Secondly, we will show that despite the presumed accuracy of frequency response measurements obtained via periodogram averaging they have limited accuracy as a basis for robust performance evaluation for a radial Compact Disk servo mechanism.

Chapter 6: Approximate identification of parametric models

Approximate identification of parametric models that are to be used for control design is the topic of this chapter. The use of coprime factor model structures for identification of feedback oriented models is motivated and the identification of (physically non-existent) coprime factors based on filtering of measured frequency domain data, clarified.

Chapter 7: Identification of model error bounds

The limited accuracy of frequency response measurements, as indicated in chapter 5, necessitates utilization of a so-called system uncertainty set, constituted of a nominal model and a model error bound. Identification of model error bounds employing a mixed worst case-probilistic error bounding technique [90] is elucidated. The utilization of error bounding is employed in a dual Youla parametrization of the model, enabling evaluation of robust performance for any stabilizing controller in a non-conservative manner.

Chapter 8: An iterative procedure of identification and control design

A methodology is formulated to gradually enhance robust performance, embodied by application of identification (chapter 6, 7) and model-based control design (chapter 4) in an iterative manner.

Chapter 9: Application to a Compact Disk servo mechanism

Experimental verification of the proposed method is carried for two experimental Compact Disk systems and results are presented and discussed. An approach is proposed for utilization of the error bounding technique for estimation of a system uncertainty set accounting for several systems having varying dynamics. The approach is experimentally verified.

Chapter 10: Conclusions and recommendations

The main results are summarized in chapter 10 and we will briefly discuss recommendations for further research.

Chapter 2

Modelling in view of control design

2.1 Introduction

In this thesis mathematical models are used for design of a feedback compensator with the aim to achieve a prespecified performance for an electro mechanical servo system, denoted further on as the plant. In the course of this research specific physical properties of the plant have given direction to the problem elaboration. In this chapter we elucidate a strategy for employing linear, time-invariant models and model error bounds in view of design of a feedback compensator, the incentive being the need for low complexity controllers.

The chapter is outlined as follows. Section 2.2 introduces a mathematical framework that enables us to phrase our problem in an unambiguous sense and in section 2.3 systems and system set representations are presented that are utilized throughout this thesis. In section 2.4 we discuss the role of nominal models and model error bounds in view of feedback compensator design and clarify how nominal models and model error bounds are employed for design of a restricted complexity controller. A further elaboration of approximate modelling for model based control design is addressed in section 2.5. Utilization of model error bounds in performance analysis is addressed in section 2.6. The chapter is concluded with an outline of the thesis in section 2.7.

2.2 Tools, notations, concepts

2.2.1 Modelling concepts

Selecting a suitable modelling framework, we are confronted with a number of questions. The first one is stated as follows:

- What is the intended model use ?

Our motivation to construct mathematical models is to use them for model-based control design. In addition, models are instrumental in analysis of the plant in the presence of a feedback controller. Generally, a physical plant is too complex to be described exactly and therefore models provide an approximate (and often simplified) description of the plant. Consequently, a model and a plant will exhibit discrepant behaviour when feedback controlled by the same controller. A desired feature of a model to be fit for control design is that it must provide some indication how large the discrepancy between model and plant will be in view of a feedback controller.

The second question is phrased as follows:

- What knowledge of the plant can be obtained for constructing mathematical models ?

There are roughly two ways to construct mathematical models of a physical plant. In case physical prior knowledge of the system is available, a model can be built based on first principles laws that govern the plant physics. First principles modelling of plants that have a highly structured nature provides a viable way to arrive at reliable models, however leading to high complexity models in case of complex plant dynamics. An alternative is to use measurement data, obtained directly from plant measurements, for constructing models, also known as system identification. As no prior knowledge of the plant physics is incorporated in building a model, the model complexity can be freely chosen. In addition, in case measurement data are attained relatively easy and fast system identification is an attractive alternative to physical modelling. As systems generally manifest themselves through signals that are available for measurement, an additional feature of employing measurement data for model construction is that the system is reflected in its bearest form, free from any prejudice induced by model assumptions.

As will be discussed in more depth in section 2.4, we give preference to models of restricted complexity in a model-based control design. Therefore, system identification is employed for constructing models in this thesis.

The last question concerns the validity of a model:

- When do we say a model is a "good" model ?

The primary goal is to come up with a feedback compensator that makes the physical plant behave in a desired fashion. So ultimately, a model is judged on whether the controller it is giving rise to, achieves a satisfactory behaviour for

the plant when feedback controlled by this controller. As discussed previously, models (inherently) are approximate system descriptions, leading to discrepant feedback dynamics of plant and model when feedback controlled by the same controller. Whether a model is good in view of control design can only be evaluated in case a model-based controller is available, implying an a posteriori evaluation of the model. This leads to a circular reasoning which makes the exercise of modelling in view of control design a non-trivial one.

Moreover, a controller that is not performing satisfactorily might very well be the result of a bad control design and not of a bad model.

Although the notions *plant*, *system* and *model* are seemingly used in an arbitrary manner, we point out that they all have a distinct meaning. The notion *plant* refers to the physical process that is object of study. In this thesis the plant constitutes an electro mechanical actuator as encountered in consumer electronic audio and video products. A *system* denotes a mathematical representation of a plant in terms of systematic relations between signals. A *model* is the mathematical object that describes the system.

In the remainder of this section, signals and systems are concretized in mathematical terms.

2.2.2 Notations and tools

Signals

A unified framework for dealing with deterministic and stochastic signals is provided by [55] by introducing the notion of quasi-stationary signals. We restrict ourselves to discrete time signal representations.

The autocovariance of a quasi-stationary signal is defined as

$$R_x(\tau) := \bar{E}\{x(t)x(t-\tau)\} = \lim_{N\to\infty} \frac{1}{N} \sum_{t=0}^{N-1} E\ x(t)x(t-\tau).$$

where E denotes the expectation operator. Quasi-stationary signals are most conveniently represented in terms of power spectral densities, attained by applying the DFT to the autocorrelation $R_x(\tau)$:

$$\Phi_x(\omega) := \lim_{N\to\infty} \sum_{\tau=-(N-1)}^{N-1} R_x(\tau)e^{-j\omega\tau}.$$

provided the sum exists. The cross-correlation of two quasi-stationary signals $\{x(t), y(t)\}$ is defined as

$$R_{yx}(\tau) := \lim_{N\to\infty} \frac{1}{N} \sum_{t=0}^{N-1} E\ y(t)x(t-\tau) \tag{2.1}$$

and the corresponding cross-spectral density as

$$\Phi_{yx}(e^{j\omega}) := \lim_{N\to\infty} \sum_{\tau=-(N-1)}^{N-1} R_{yx}(\tau)e^{-j\omega\tau},$$

Signals are often characterized in terms of boundedness with respect to some norm. Consider a discrete time signal $x(t)$, $\forall\ t$; signals often encountered in practical applications are suitably characterized in terms of bounded energy, denoted as

$$\|x(t)\|_2 := \sqrt{\sum_{t=0}^{\infty} |x(t)|^2} < \infty.$$

Periodic signals and realizations of stochastic processes however are not energy bounded but can be represented by power bounded signals. The notion of a power bounded signal is defined as follows:

Definition 2.2.1 *A signal $x(t)$ is power bounded if $\|x(t)\|_{\mathcal{P}} < \infty$ holds where $\|x(t)\|_{\mathcal{P}}$ is a semi-norm defined as* [48]*:*

$$\|x(t)\|_{\mathcal{P}} := \lim_{N\to\infty} \sqrt{\frac{1}{2N} \sum_{t=-N}^{N} |x(t)|^2}.$$

where $|\ .\ |$ denotes the Euclidean norm. □

Periodic signals may be conveniently represented in terms of a Discrete Fourier Transform (DFT) as follows:

$$X_N(e^{j\omega_k}) := \frac{1}{\sqrt{N}} \sum_{t=1}^{N} x(t)e^{-j\omega_k t},\quad \omega_k = \frac{2\pi k}{N},\quad k = 1,\ldots,N \tag{2.2}$$

In [48], (2.2) is referred to as the Discrete-to-Discrete Fourier transform. Parseval's identity states that the signal energy is preserved employing a DFT, meaning that $\|x(t)\|_2^2 = \|X_N(e^{j\omega_k})\|_2^2$ holds. For the sake of brevity of notation, the argument ω is discarded unless clarity of discussion may be lost.

Systems

A system is regarded a linear, time invariant (LTI) operator that maps one signal into another, denoted as

$$y = G\ u$$

where u and y are bounded signals and G denotes the system. A system that maps *any* bounded signal u onto a bounded signal y is called BIBO (bounded input bounded output) stable. A finite dimensional, linear, time-invariant discrete time system G is stable if it is analytic on and outside the unit circle in the complex plane, denoted as $G \in \mathbb{R}\mathcal{H}_\infty$. This implies that its poles all lie within the unit circle.

System design and analysis problems are often formulated in terms of a system norm, reflecting a characteristic system feature by a real positive number. Two system norms are utilized in this research; the infinity-norm (∞-norm) of a linear, time invariant stable system is defined as

$$\|G\|_\infty := \sup_\omega \bar{\sigma}(G(e^{j\omega}))$$

where $\bar{\sigma}(.)$ denotes the maximum singular value of a complex valued matrix, defined as

$$\bar{\sigma}(G) := \sqrt{\lambda_{\max}(G^*G)}$$

where $G^* := G^T(e^{-j\omega})$. Another system norm is the 2-norm, defined as

$$\|G\|_2 := \sqrt{\sum_{i=1}^{N} \mathrm{tr}\{G(e^{j\omega_i})^* G(e^{j\omega_i})\}}$$

which in fact is a semi-norm as $\|G\|_2$ can assume a zero value for $G(e^{j\omega}) \neq 0, \omega \neq \omega_i$. A stable system that maps bounded signals into bounded signals can be characterized in terms of so called signal induced norms which reflect, with slight abuse of terminology, the maximum signal amplification measured in an appropriate signal norm. A system norm that is induced by bounded power signals ($u \in l_\mathcal{P}$) equals the infinity-norm of G (see e.g. [97]) :

$$\|G\|_\infty = \sup_{\|u\|_\mathcal{P} \neq 0} \frac{\|Gu\|_\mathcal{P}}{\|u\|_\mathcal{P}}.$$

For brevity of notation, the argument ω will be left out in the sequel.

A norm that is not an induced system norm, is the Frobenius-norm. For a complex valued matrix $A \in \mathbb{C}^{p\times q}$ the Frobenius-norm is defined as follows ([97]):

$$\|A\|_F := \sqrt{\mathrm{tr}(A^*A)} = \sqrt{\sum_{i=1}^{p}\sum_{j=1}^{q}|a_{ij}|^2}. \tag{2.3}$$

Feedback systems

Feedback systems play a substantial role in this research. A general feedback system consists of a system P and a compensator C that are interconnected according to the configuration in the block diagram of figure 2.1. The transfer function of a feedback system that reflects the main properties of a closed loop system is the mapping

$$[r_2\ r_1]^T \rightarrow [y_p\ u_p]^T$$

defined as

$$T(P,C) := \begin{bmatrix} P \\ I \end{bmatrix} [I + CP]^{-1}[C \quad I] \tag{2.4}$$

where the feedback system $T(P,C)$ is expressed in its constituting parts, the system P and the compensator C. As the feedback configuration (2.4) is generally studied for formulation of control design problems and control relevant modelling problems, we refer to (2.4) as *the* feedback system in the remainder of this thesis.
The feedback system (2.4) is internally stable if $T(P,C) \in \mathbb{R}\mathcal{H}_\infty$ holds (e.g. [97]).

2.2.3 Performance

An important aspect of feedback system design is the specification of signals that are significant for feedback system behaviour. The feedback system depicted in figure 2.1 is a general feedback structure where plant input u_p, plant output y_p, control input u_c and control output y_c are signals that are feasible for describing performance. The transfer function that maps $[r_2\ r_1]^T$ into $[y_p\ u_p\ y_c\ u_c]^T$ can be expressed in terms of the feedback system (2.4) as follows:

$$\begin{bmatrix} y_p \\ u_p \\ y_c \\ u_c \end{bmatrix} = \left(\begin{bmatrix} I & 0 \\ 0 & I \\ 0 & -I \\ -I & 0 \end{bmatrix} T(P,C) + \begin{bmatrix} 0 & 0 \\ 0 & 0 \\ 0 & -I \\ I & 0 \end{bmatrix} \right) \begin{bmatrix} r_2 \\ r_1 \end{bmatrix}. \tag{2.5}$$

From (2.5) it is seen that requirements on the loop signals $[y_p\ u_p\ y_c\ u_c]^T$ can be transcribed into requirements on the transfer function (2.4), expressed by the equation:

$$W_{\text{out}} T(P,C) W_{\text{in}} + W_{\text{add}}$$

where $T(P,C)$ is expressed in (2.4) and $W_{\text{out}}, W_{\text{in}}, W_{\text{add}} \in \mathbb{R}\mathcal{H}_\infty$ are weightings of appropriate dimension reflecting e.g. properties of the loop signals. In the sequel we will pose $W_{\text{out}}, W_{\text{in}} \in \mathbb{C}^{2\times 2}$ and $W_{\text{add}} = 0$. Moreover, W_{out} and W_{in} are assumed to have a diagonal structure, leading to a closed loop transfer function

$$J(P,C) := W_{\text{out}} T(P,C) W_{\text{in}} \tag{2.6}$$

where $J(P,C) \in \mathbb{C}^{2\times 2}$.

The formulation of model-based controller synthesis and analysis problems is induced by the weighted transfer function (2.6). For controller synthesis, the $\mathcal{H}_\infty$-norm of (2.6),

$$\|J(P,C)\|_\infty,$$

constitutes the design criterion, as will be further elaborated in chapter 4. For analysis of the feedback system however, the magnitudes of the individual transfer functions of (2.6) are considered to be more informative compared to an $\mathcal{H}_\infty$-norm as they reflect frequency dependent feedback system properties like tracking behaviour and disturbance attenuation. To formalize analysis of performance, the following definition is made on notation:

Definition 2.2.2 *Consider a matrix Δ of which the elements are single variate, real rational functions. The notation $|\Delta|$ refers to a matrix of (frequency dependent) magnitudes of the elements of Δ, in contrast to $\|\Delta\|$ which attributes a real, non-negative number to Δ.*

Unless indicated otherwise, performance of a feedback system is evaluated in terms of

$$|J(P,C)|, \qquad \omega \in [0,\pi). \tag{2.7}$$

An advantageous feature of the transfer function (2.6) is that in the Single Input Single Output case, the magnitudes of the individual transfer functions of $J(P,C)$ enable evaluation of $\|J(P,C)\|_\infty$. This is shown in the next proposition.

Proposition 2.2.3 *Consider the weighted feedback transfer function $J(P,C)$ defined according to* (2.6) *for the SISO case; then the following equality holds*

$$\|J(P,C)\|_\infty = \sup_\omega \sqrt{\sum_{i=1}^{2}\sum_{j=1}^{2} |J_{ij}(P,C)|^2}$$

where $J_{ij}(P,C)$ indicates the (i,j)-element of $J(P,C)$.

Proof: *Consider the Frobenius norm $\|.\|_F$, as is defined in* (2.3). *We utilize the following result (*[97], *lemma 2.13):*

$$\|A\|_F^2 = \sum_{i=1}^{r} \sigma_i^2(A), \quad r = \min\{p,q\}$$

where $\sigma_i(A)$ is the ith singular value of A. By virtue of the fact that in the SISO case the matrix $J(P,C)$ has rank 1, hence having only one non-zero singular value, it follows from the above expressions that

$$\bar{\sigma}(J(P,C)) = \|J(P,C)\|_F$$

which leads to

$$\|J(P,C)\|_\infty = \sup_\omega \|J(P,C)\|_F.$$

□

From proposition 2.2.3 it follows that formulation of a design problem in terms of $\|J(P,C)\|_\infty$ and an analysis problem in terms of $|J(P,C)|$ are compatible.

2.3 System representations

2.3.1 Coprime factor representations

In this section fractional model representations are introduced that are used in this thesis. We consider a linear, time invariant (possibly unstable) system that is expressed in terms of a fraction of two stable transfer functions N and D as follows:

$$P = ND^{-1}.$$

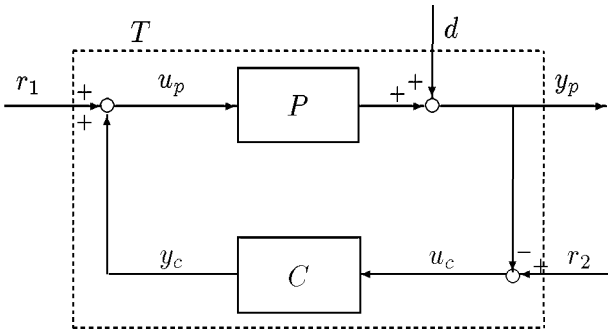

fig. 2.1: Block diagram of a feedback system with input signals $\{r_1, r_2, d\}$ and output signals $\{y_p, u_p, y_c, u_c\}$.

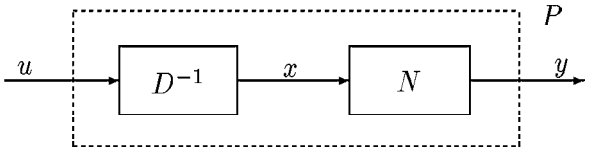

fig. 2.2: Block scheme of a coprime factor parametrization.

A block scheme of a coprime factor system representation is depicted in figure 2.2.
The fractional representation N, D is called right coprime if there exist transfer functions $X, Y \in \mathbb{R}\mathcal{H}_\infty$ such that

$$XN + YD = I$$

holds. In that case N and D share no common unstable zeros. An important class of fractional representations are right coprime factors that obey the relation

$$N^*N + D^*D = I, \quad \forall\omega,$$

in which case the factors are called *normalized.* Right coprime factors that are normalized are unique up to postmultiplication with a unimodular matrix.

In addition to representation of a model, the representation of a model set is instrumental in analysis and synthesis problems that deal with robustness properties of a nominal model. A plant model set based on a fractional model representation is defined as follows

$$\begin{aligned} &\mathcal{P}_{ND}(N, D, \delta_N, \delta_D) := \\ &\quad \{P = (N + \Delta_N)(D + \Delta_D)^{-1} \mid |\Delta_N| \leq \delta_N(\omega), |\Delta_D| \leq \delta_D(\omega)\}. \end{aligned} \tag{2.8}$$

where $N, \Delta_N, D, \Delta_D \in \mathbb{R}\mathcal{H}_\infty$. As will be discussed in sections 2.5 and 2.6, normalized coprime factors have favourable properties in view of feedback design and analysis problems.

2.3.2 Dual Youla representation

A system representation closely related to a feedback configuration and the fractional representation is the so called dual Youla parametrization [18]. Utilization of a dual Youla parametrization in feedback oriented modelling problems is found in [69, 53]. As knowledge of a controller is exploited to represent the set of all systems that are stabilized by this controller, it is a dual version of the well-known Youla parametrization that parametrizes the set of all controllers that stabilize a given system. A system P is parametrized in terms of a transfer function $R \in \mathbb{R}\mathcal{H}_\infty$ as follows:

$$P = (N_x + D_c R)(D_x - N_c R)^{-1} \tag{2.9}$$

where N_x, D_x are right coprime factors of an a priori chosen auxiliary model P_x; N_c, D_c are right coprime factors of a controller that stabilizes both the system P and the auxiliary model P_x. A block scheme of the dual Youla parametrization is depicted in figure 2.3.

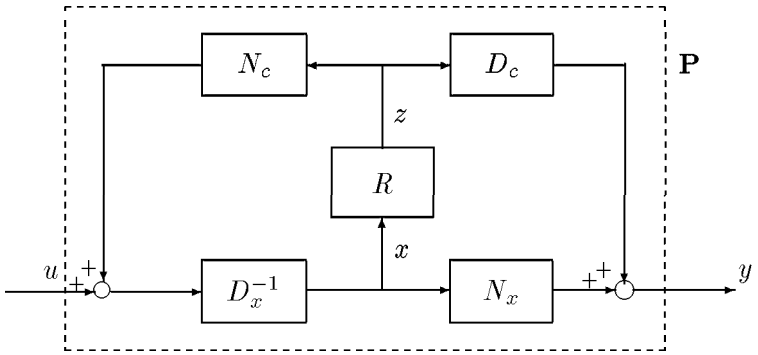

fig. 2.3: Block scheme of a dual Youla parametrization.

Given the coprime factors N_x, D_x, N_c, D_c, the transfer function R is uniquely related to the system P as

$$R = (D_c + PN_c)^{-1}(P - P_x)D_x \tag{2.10}$$

which follows from rewriting (2.9).
As (2.9) reflects a specificly parametrized coprime factor model representation, the freedom in choosing N_x, D_x, N_c, D_c can be exploited to induce factors $N_x + D_cR, D_x - N_cR$ that are normalized.

Proposition 2.3.1 *Denoting* $N_R := N_x + D_cR$ *and* $D_R := D_x - N_cR$ *then* N_R, D_R *are normalized right coprime factors, meaning*

$$N_R^* N_R + D_R^* D_R = I, \quad \forall\omega,$$

if

$$(D_x + CN_x)^*(D_x + CN_x) = (D_n + CN_n)^*(D_n + CN_n). \tag{2.11}$$

holds, where $\{N_n, D_n\}$ *are normalized right coprime factors of the plant* P.

Proof: *Substitution and straightforward manipulation of the expressions for* N_R, D_R *leads to the following expression:*

$$\begin{aligned}&\left(P(I+CP)^{-1}\right)^* P(I+CP)^{-1}+\\ &\quad (I+CP)^{-*}(I+CP)^{-1} = (D_x+CN_x)^{-*}(D_x+CN_x)^{-1}\end{aligned} \tag{2.12}$$

which can be rewritten as (2.11). □

This implies that normalization of $\{N_R, D_R\}$ is established if $\{N_x, D_x\}$ is determined such that $(D_x + CN_x)^{-1}$ is a spectral factor of the left hand side of (2.12).

A system uncertainty set employing a dual Youla system representation is defined in a similar fashion as in the coprime factor representation as follows

$$\begin{aligned}&\mathcal{P}_R(N_x, D_x, N_c, D_c, R, \delta_R) := \\ &\quad \{P = (N_x + D_c(R+\Delta_R))(D_x - N_c(R+\Delta_R))^{-1} \mid |\Delta_R| \leq \delta_R(\omega)\}.\end{aligned} \tag{2.13}$$

Without loss of generality one may impose $R = 0$, which leads to simpler expressions.

2.4 Modelling, feedback system design and robustness

In order to give direction to the elaboration in forthcoming chapters, in this section we put in perspective the role of nominal models and model error bounds in view of design of a restricted complexity controllers.

2.4.1 Feedback system design

Consider a feedback system $T(P, C_{\text{old}})$ as depicted in figure 2.1 constituted of a linear, time invariant system P that is presumed to be not exactly known and a feedback compensator C_{old} that is presumed to be known. The problem phrased in chapter 1 is to design a compensator C_{new} that realizes a prespecified (enhanced) performance of the feedback system $|J(P, C_{\text{new}})|$. A procedure for design of a controller that achieves an enhanced performance for the system via model based control design typically consists of the following two steps:

1. Construct a model $\hat{P}$ of the system P;
2. design a controller based on the model $\hat{P}$ such that a prespecified performance is achieved for the system P.

A controller is designed on the basis of a model $\hat{P}$ such that a certain prespecified performance is achieved for the model, according to following expression:

$$C_{\hat{P}} = \arg_{\tilde{C}} \min \|J(\hat{P}, \tilde{C})\|, \tag{2.14}$$

where $J(P, C)$ denotes a transfer function of a weighted feedback system that reflects performance expressed in (2.6). The performance that $C_{\hat{P}}$ achieves for the true system can be bounded by the following triangle inequality [69]

$$\|J(P, C_{\hat{P}})\| \leq \|J(\hat{P}, C_{\hat{P}})\| + \|J(P, C_{\hat{P}}) - J(\hat{P}, C_{\hat{P}})\|. \tag{2.15}$$

The inequality (2.15) shows that it makes no sense to design a controller that achieves a prespecified performance for the nominal model without accounting for the mismatch between system and model. A controller that looks suitable for the model $\hat{P}$ — implying a *low* value of $\|J(\hat{P}, C_{\hat{P}})\|$ — might prove disastrous for the system — implying a *high* value of $\|J(P, C_{\hat{P}}) - J(\hat{P}, C_{\hat{P}})\|$ — . So we require that a controller should provide a similar performance for model *and* system, in which case a controller is said to provide a robust performance for the model. In addition we demand that a prespecified (high) performance is achieved for the system. This brings us to defining the notion of high robust performance.

Definition 2.4.1 *Consider a model $\hat{P}$ and a controller $C_{\hat{P}}$ that is designed based on this model, then $C_{\hat{P}}$ achieves a high robust performance for the model $\hat{P}$ in case the following is satisfied*[1]

1. *$C_{\hat{P}}$ establishes a similar performance for the true system and for the model itself, formulated as follows:*

$$\|J(\hat{P}, C_{\hat{P}})\| \gg \|J(P, C_{\hat{P}}) - J(\hat{P}, C_{\hat{P}})\|;$$

   which implies that $\|J(P, C_{\hat{P}})\| \simeq \|J(\hat{P}, C_{\hat{P}})\|$;

2. *establishes a prespecified* **desired** *performance for the model (and, in view of the previous point, also for the true system), formulated as:*

$$\|J(\hat{P}, C_{\hat{P}})\| \simeq \gamma_{desired}.$$

[1] This definition has been phrased in similar terms by the formulation of the high performance control design problem in [69]. In fact, the definition stated here is dual as it is directed to the nominal model underlying the designed compensator, whereas in [69] enhanced robust performance control design is directed towards a compensator.

□

Note that both issues in definition 2.4.1 have to be satisfied to achieve a *high* robust performance as a controller can always be found such that the system and model have similar performances (robust performance) as long as the performance requirements are not too high.

The robustness requirement $\|J(\hat{P}, C_{\hat{P}})\| \gg \|J(P, C_{\hat{P}}) - J(\hat{P}, C_{\hat{P}})\|$ imposes that a model based control design procedure should provide a similar performance for the system and the model. This implies that the control design should anticipate or at least account for model imperfections.

2.4.2 Robust control design

In order to anticipate model imperfections in the control design, robust control design techniques explicitly account for the mismatch between model and system is by employing a nominal model and a model error bound as a basis for design. A control design problem in view of achieving some performance for a set of systems can be phrased as

$$C_{\mathcal{P}} = \arg_{\tilde{C}} \min_{P \in \mathcal{P}} \|J(P, \tilde{C})\|, \tag{2.16}$$

where $\mathcal{P}$ denotes a system set. The system set structure is immaterial for discussion at this point, but could be represented by system uncertainty set representations $\mathcal{P}_{ND}$ and $\mathcal{P}_R$, introduced in section 2.3, reflecting the plant-model mismatch in terms of coprime factor perturbations.

Control design using $\mathcal{H}_\infty$ and μ-synthesis design methods deliver compensators that are guaranteed to achieve stability and even some performance for every system contained in the uncertainty set. The issue remains whether a *prespecified* performance is attained for the whole set. Design of a controller that achieves a prespecified performance for every system in the set is not determined solely by the control design, but equally by the shape and the size of the uncertainty set.

This elucidates the fact that the problem of high performance model based control design is a combined problem of modelling and control design and that modelling and control design are mutually dependent. This observation has had a great influence on the developments in the field of modelling for control design as is discussed in the next subsection.

2.4.3 Modelling

The quest for models for design of enhanced performance controllers has branched into two directions: the construction of nominal models and model error bounds.

Construction of nominal models for enhanced feedback system design is based on the point of view that a prespecified robust performance limits the maximum allowable shape and size of the error between model and system. Having available an accurate system representation, nominal modelling amounts to problems of model reduction and/or system approximation, primarily based on tuning of the mismatch between a (high order) system and an approximate model in view of feedback system properties. Model reduction in view of feedback system design is elaborated in [95], where the system is described by a high order finite element model; approximate modelling in view of feedback system design based on measurement data is discussed in [69], where system knowledge is embodied by frequency responses.

The construction of model error bounds in view of feedback system design is founded on the belief that system knowledge underlying the modelling procedure is of limited accuracy; hence an uncertainty model that accounts for the mismatch between system and model is required to anticipate model imperfections in the design. Methods have recently been developed for constructing model error bounds, utilizing measurement data (see [90], [59] and [37]). A characteristic feature of model error bounding is that, although bounds can be moulded to their intended use, bounds can not be arbitrarily tuned, e.g. can not be made arbitrarily small without becoming unreliable, as available system knowledge can not be unambiguously be attributed to one LTI system.

We emphasize a subtle difference in the *perception* of the model error that underlies the nominal modelling and model error bounding. In nominal modelling it is presumed that exact system knowledge is available and the model error is due to the models inflexibility to describe this knowledge. In this perception of the model error, increasing the models flexibility delivers improved approximate system descriptions, implying a decrease of the model error.

Modelling of model error bounds however is founded on the presumption that system knowledge available is incapable of representing the system in an unambiguous way. In this respect the error between model and system is attributed to inadequate system knowledge. Increase of the models flexibility in this perspective does not necessarily lead to improved system approximations and, moreover, might lead to an unjust confidence in the model.

One might say that nominal modelling is a tool used by a designer that

is optimistic about the quality of the system representation and that error bounding is more in line with a pessimistic view on the system knowledge. In the following we argue that the "truth" lies somewhere in between.

2.4.4 Model errors: perception

Both nominal modelling and uncertainty modelling in view of feedback system design are directed towards minimizing the effect of uncertain plant dynamics on the achieved performance. The difference between nominal (or approximate) modelling and uncertainty modelling is the way model errors are perceived and accordingly manipulated.

In this thesis we will adopt both perceptions of model errors in a unified manner. In many cases the physical nature of the system under study allows us to acquire *very accurate* measurement data or to build highly accurate physically structured models. Although measurement data might be accurate and first principles models prove to be reliable, they provide no exact system representation. Disturbances will at all times be present in the data and we can never check the validity of measurement data as knowledge of the exact system dynamics is unavailable. Although system knowledge might be accurate and the construction of highly complex models is feasible, one must question whether high order modelling is the most sensible thing to do. As the nominal model is used for model-based control design, the controller complexity consequently will be high and unsuitable for implementation. Additionally, high order models are no prerequisite for a successful high robust performance design, as is indicated in literature. So the model quality is not solely hinged on a small model error but also (and not in the least) by a restricted model order.

Summarizing, modelling a physical system with complex dynamics in view of control design confronts us with a model error that can be viewed as being partly tunable as the model order is deliberately kept low, and partly non-tunable, since system knowledge does not *exactly* describe the system. Constructing nominal models for controller synthesis thus induces a "true" model error that is a mixture of a tunable part (corresponding to the optimistic view on model errors) and a non-tunable part (corresponding to the pessimistic view).

2.4.5 Model errors and control design

In this thesis both approximate models and model error bounds are employed to realize a prespecified robust performance via model based control design. Concluding our discussion on the role of models in view of design of a high

robust performance controller, we adopt the following strategy, in line with the observations made above.

Firstly, we choose to employ low order approximate models as a basis for control design. The motivation is that the controller complexity is kept limited which renders it useful for implementation and we wish to restrict modelling effort only to the system dynamics that are relevant in view of control design. The problem then boils down to *how* to determine a low order model that provides an approximate system description that allows for high robust performance design. Approximate modelling in view of enhanced robust performance design is not a clear-cut problem as will be further elaborated in section 2.5.

Secondly, as we do not account for model imperfections by employing model error bounds explicitly in the design, robustness of the designed controller has to be analysed prior to implementation. Performance analysis amounts confronting the controller with available system knowledge, while keeping in mind that system knowledge is not an exact system representation. To account for errors between system and system knowledge, model error bounds are employed in performance analysis. Utilization of model error bounds for analysis of robust performance is further addressed in section 2.6.

2.5 Approximate modelling

2.5.1 Feedback relevant approximation

In this section feedback relevant aspects of approximate identification for control design are highlighted from the perspective of approximate modelling, implying that system knowledge is presumed available in the form of a LTI high order system instead of measurement data. The actual identification problem is discussed in chapter 6.

A control relevant system approximation problem is based on determination of a model that minimizes the term $\|J(P,C) - J(\hat{P},C)\|$ in expression (2.15). With $J(P,C)$, expressed in (2.6), reflecting our feedback system, this leads to formulation of the following approximation problem:

$$\hat{P} = \arg_{\tilde{P}} \min \|J(P,C) - J(\tilde{P},C)\| \tag{2.17}$$

which is rewritten as $W_{\text{out}}(T(P,C) - T(\hat{P},C))W_{\text{in}}$. A model that satisfies (2.17) provides an approximate description of the system operating in a feedback configuration with a known controller. In this section the approximation is elaborated for coprime factor and dual Youla system representations. For notational convenience the weightings $W_{\text{out}}, W_{\text{in}}$ are discarded.

Coprime factor representation

Consider a (high order) system $P := ND^{-1}$ and a model of lower dynamical order $\hat{P} := \hat{N}\hat{D}^{-1}$ expressed in normalized right coprime factors and a controller $C := \tilde{D}_c^{-1}\tilde{N}_c$ expressed in normalized left coprime factors. The control relevant system approximation problem can be written as

$$\begin{bmatrix} N \\ D \end{bmatrix} (\tilde{D}_c D + \tilde{N}_c N)^{-1} [\tilde{N}_c \quad \tilde{D}_c] - \begin{bmatrix} \hat{N} \\ \hat{D} \end{bmatrix} (\tilde{D}_c \hat{D} + \tilde{N}_c \hat{N})^{-1} [\tilde{N}_c \quad \tilde{D}_c]$$

From the above expression it is clear that the control relevant approximation according to (2.17) is a non-affine expression of the coprime factors of system and model, due to the fractional structure of the feedback system. To make the approximation problem accessable for identification purposes, we aim for an approximation problem that is expressed in the approximation error $[(N - \hat{N})\ (D - \hat{D})]^T$ in an affine fashion.

The control relevant approximation problem formulated in (2.17) can be expressed into an affine expression of the approximation error $[(N - \tilde{N})\ (D - \tilde{D})]^T$ by imposing the restriction $\tilde{D}_c D + \tilde{N}_c N = \tilde{D}_c \hat{D} + \tilde{N}_c \hat{N}$; this leads to formulation of the following constrained approximation problem:

$$\hat{N}, \hat{D} = \arg_{\tilde{N},\tilde{D}} \min \left\| \begin{bmatrix} N - \tilde{N} \\ D - \tilde{D} \end{bmatrix} \Lambda^{-1} [\tilde{N}_c \quad \tilde{D}_c] \right\|_{\Lambda = \hat{\Lambda}} \tag{2.18}$$

where $\Lambda := \tilde{D}_c D + \tilde{N}_c N$ and $\hat{\Lambda} := \tilde{D}_c \hat{D} + \tilde{N}_c \hat{N}$.

Dual Youla parametrization

Consider a dual Youla parametrization of a high order system P and a model $\hat{P}$ as expressed in (2.9):

$$P := \frac{N_x + D_c R}{D_x - N_c R}, \quad \hat{P} := \frac{N_x + D_c \hat{R}}{D_x - N_c \hat{R}}$$

where $P_x := N_x D_x^{-1}$ is a model that is stabilized by $C := N_c D_c^{-1}$. One of the major features of a dual Youla parametrization in regard of the control relevant approximation problem (2.17), follows from straightforward substitution of a dual Youla parametrization of plant and model which gives the following expression:

$$T(P, C) - T(\hat{P}, C) = \begin{bmatrix} D_c \\ -N_c \end{bmatrix} (R - \hat{R}) [D_x + C N_x]^{-1} [C \quad I]. \tag{2.19}$$

Consequently, a dual Youla parametrization enables us to phrase the control relevant approximation problem in an affine expression of the approximation error $R - \hat{R}$. Utilization of a dual Youla parametrization in control relevant modelling problems has been elaborated by [40], [53] and [69]. A disadvantage of a dual Youla parametrization is that the associated model generally has a degree equal to $d(P_x) + d(C) + d(R)$[2] which consequently leads to models of high order. As high order models lead to high order controllers via optimization based control design, low order models are given preference in order to keep the controller order restricted.

The approximation problem formulated in expression (2.17) provides approximate models that exhibit a good system description in view of its feedback dynamics with an (known) available controller. As our primary purpose of system approximation is to design a new controller, the model resulting from (2.17) is not "optimal" for our purpose. An optimal approximate model can be determined via (2.17) only if the corresponding controller is known, which illustrates the inseparability of approximate modelling and model based control design.

As we will show in chapter 4, some knowledge of the dynamics of the new controller might be available, prior to the optimization based design. The issue arises whether we can exploit this prior knowledge of controller dynamics to "push" the approximation problem towards its intended purpose. This is further elaborated in the following two sections.

2.5.2 Fractional representations of feedback systems

In the following two sections we will show that a fractional representation of feedback systems enables to formulate an approximation problem that is closely related to (2.17) with incorporation of prior controller knowledge. Before we proceed, an important qualitative feature of fractional system representations in view of feedback system synthesis and analysis is discussed.

A well-known result by [88] is that, when studying approximation and robustness problems in view of feedback stability, systems should be metrized in the so called graph topology. A definition of the graph of a (possibly unstable) system is adopted from [88], phrased as

Definition 2.5.1 *The graph of a (possibly unstable) system P is defined as the set of all pairs of bounded input and bounded output signals $\{u, y\}$ that are related as $y = Pu$.* □

[2] $d(.)$ denotes the McMillan degree

Lemma 2.5.2 *Consider a (possibly unstable) system P with right coprime factors N, D. The graph of P can be parametrized using any right coprime factorization of P as* [88]*:*

$$\mathcal{G}_P := \begin{bmatrix} y \\ u \end{bmatrix} = \begin{bmatrix} N \\ D \end{bmatrix} x$$

where $\{y, u, x\}$ are bounded signals. □

The graph topology is known to be the weakest topology[3] that preserves stability of a feedback system. For more detailed elaborations we refer to [25], [88] and [89]. A metric that induces the graph topology is the so-called graph-metric, which is defined employing normalized right coprime factor representations [88], as follows:

$$\inf_{Q \in \mathbb{R}\mathcal{H}_\infty} \left\| \begin{bmatrix} N \\ D \end{bmatrix} - \begin{bmatrix} \tilde{N} \\ \tilde{D} \end{bmatrix} Q \right\|_\infty .$$

Note that this metric (and any other that induces the graph topology) is well defined for stable as well as unstable (yet stabilizable and detectable) systems. An important qualitative feature of the graph topology with respect to stability and performance of feedback systems, is that if two systems converge in the graph topology, meaning that $\hat{N} \to N, \hat{D} \to D$ holds, $T(P, C) \to T(\hat{P}, C)$ holds for the corresponding feedback systems. This is one of the major reasons to employ fractional system representations in view of feedback system design.

Instrumental in the formulation of an alternative feedback relevant approximation problem is the notion of a bicoprime factorization, introduced in the following

Definition 2.5.3 [88]. *Consider stable transfer functions N_r, N_l and D, then $N_r D^{-1} N_l$ is called a bicoprime factorization if N_r, D are right coprime and D, N_l are left coprime.* □

Taking a closer look at the feedback system transfer function

$$T(P, C) = \begin{bmatrix} N \\ D \end{bmatrix} (D + CN)^{-1} [C \quad I]$$

[3] A topology on a set of systems defines a set of neighbourhoods of systems, induced by a prespecified distance measure. A topology is called weaker with respect to another one if it allows for a larger number of neighbourhoods [58].

it can be verified that $\{[N \quad D]^T, (D+CN)^{-1}\}$ are right coprime and $\{(D+CN)^{-1}, [C \quad I]\}$ are left coprime in case C is stable and $\{N, D\}$ are right coprime, hence constituting a bicoprime factorization of the feedback system $T(P,C)$. Consequently, a feedback system $T(P,C)$ has a fractional structure that is affinely expressed in the coprime factors of P.

A fractional representation of the feedback system provides a quantitative notion to *how* the feedback systems $T(P,C)$ and $T(\hat{P},C)$ converge in case $\hat{N} \rightarrow N, \hat{D} \rightarrow D$ holds. If we express $T(P,C) := N_r D_T^{-1} N_l$ and $T(\hat{P},C) := \hat{N}_r \hat{D}_T^{-1} \hat{N}_l$ where

$$N_r := \begin{bmatrix} N \\ D \end{bmatrix}, \quad D_T := D + CN, \quad \hat{N}_l := [C \quad I],$$

$$\hat{N}_r := \begin{bmatrix} \hat{N} \\ \hat{D} \end{bmatrix}, \quad \hat{D}_T := \hat{D} + C\hat{N}, \quad N_l := [C \quad I],$$

we state the following:

$$\|T(P,C) - T(\hat{P},C)\| \rightarrow 0 \iff \left\| \begin{bmatrix} N_r - \hat{N}_r \\ N_l^T - \hat{N}_l^T \\ D_T - \hat{D}_T \end{bmatrix} \right\| \rightarrow 0$$

The expression on the right can be rewritten as

$$\left\| \begin{bmatrix} I & 0 \\ 0 & I \\ C & I \end{bmatrix} \begin{bmatrix} N - \hat{N} \\ D - \hat{D} \end{bmatrix} \right\| \rightarrow 0$$

as $N_l^T - \hat{N}_l^T = 0$.

Now we revert to the approximation problem as addressed in section 2.5 employing a fractional feedback system performance representation. An alternative formulation of a control relevant approximation problem is then defined as follows:

$$\hat{N}, \hat{D}, = \arg_{\tilde{N},\tilde{D}} \min \left\| W_{\text{out},f} \begin{bmatrix} I & 0 \\ 0 & I \\ \tilde{N}_c & \tilde{D}_c \end{bmatrix} \begin{bmatrix} N - \tilde{N} \\ D - \tilde{D} \end{bmatrix} W_{\text{in},f} \right\| \tag{2.20}$$

where $W_{\text{out},f}, W_{\text{in},f}$ denote user specified weightings. In case we choose $W_{\text{in},f} = (\tilde{D}_c D + \tilde{N}_c N)^{-1} \; [\tilde{N}_c \quad \tilde{D}_c]$ and $W_{\text{out},f} = I$ (putting $W_{\text{out}} = W_{\text{in}} = I$), it is

easily verified that the norm of (2.20) equals the norm of (2.18) in case $\Delta_\Lambda := \tilde{D}_c\Delta_D + \tilde{N}_c\Delta_N = 0$ holds. Hence the control relevant approximation problem according to (2.18) is equivalent to (2.20) in case $\tilde{D}_c D + \tilde{N}_c N = \tilde{D}_c\hat{D} + \tilde{N}_c\hat{N}$ holds.

We point out two features of the approximation problem formulated in (2.20). Firstly, the approximation criterion of (2.20) is well-defined for controllers that stabilize the system P but do not stabilize the approximate model $\hat{P}$, contrary to (2.6) which is well-defined only for controllers that stabilize both system and model. Now one may question the surplus value of an approximation that allows for unstable feedback systems in view of the present controller. As discussed in section 2.5, a desirable feature of a control relevant approximation is that a resulting model is robust in view of controller perturbations. The approximation criterion that minimizes the error should consequently have the same properties as a distance measure between systems that allows for the largest possible controller set such that both systems are yet stabilized. A distance measure that allows for destablizing controllers in that sense is more appropriate as it encompasses at least *all* stabilizing compensators. It is Concluded that an approximation according to (2.20) is more appropriate in view of robust approximation.

Secondly, an approximation according to (2.20) only differs from (2.6) with respect to the output weighting in case the input weight is chosen as $W_{\text{in},f} = \Lambda^{-1}[\tilde{N}_c\ \tilde{D}_c]$. The main difference however is that the optimization criterion is an affine expression in the approximation error $[(N - \tilde{N})\ (D - \tilde{D})]^T$ without imposing a parametric constraint as in (2.18). Instead of imposing $\Lambda = \hat{\Lambda}$ the error $[(N - \tilde{N})\ (D - \tilde{D})]^T$ is additionally penalized in the optimization of (2.20).

2.6 Uncertainty modelling

A controller that is designed based on an approximate model, according to expression (2.14), will exhibit a performance for the system different from the nominally designed performance, due to the error between system and model. To decide whether a controller is suited for implementation, a prediction of the performance achieved for the system is to be performed based on system knowledge available. As discussed in section 2.4, system knowledge is presumed not to be exact; to account for errors between system knowledge and the physical system in a performance analysis, we employ a system *set* representation, as defined in equation (2.9) and (2.14).

In this section we clarify the utilization of a system uncertainty set, constituted of a nominal model and a model error bound, for analysis of performance

$|J(P,C)|$ for *every* system in the set and for every (stabilizing) controller.

Evaluation of performance of a system set is phrased as verification of[4]

$$\Gamma_{\rm lo} \leq |J(P,C_{\rm new})| \leq \Gamma_{\rm up}, \quad \forall\ P \in \mathcal{P},\ \forall\ \omega. \tag{2.21}$$

where $\mathcal{P}$ is a system uncertainty set and $\Gamma_{\rm up}(\omega), \Gamma_{\rm lo}(\omega)$ are user specified frequency dependent upper and lower magnitude bounds. Analysis of performance is performed by evaluating whether the following inequalities hold:

$$\sup_{P\in\mathcal{P}} \ |J(P,C)| \ \leq \ \Gamma_{\rm up}(\omega) \tag{2.22}$$

$$\inf_{P\in\mathcal{P}} \ |J(P,C)| \ \geq \ \Gamma_{\rm lo}(\omega) \qquad \omega \in [0,\pi), \tag{2.23}$$

The sup- and inf-operation are performed element-wise.

Instrumental in performance analysis for $P \in \mathcal{P}$ is the availability of expressions of worst-case magnitude bounds of $|J(P,C)|$,

$$\sup_{P\in\mathcal{P}} \ |J(P,C)|\,, \quad \inf_{P\in\mathcal{P}} \ |J(P,C)| \qquad \omega \in [0,\pi),$$

The worst-case performance bounds should at least be *reliable*, meaning that the performance is captured for every $P \in \mathcal{P}$. In addition, the worst-case performance bounds should not be overly large, meaning that the performance bounds account not only for $P \in \mathcal{P}$. In this case the performance bounds are called conservative. We clarify the notion of conservative magnitude bounds employing system uncertainty sets by the following definition:

Definition 2.6.1 *Consider a system set $\mathcal{P}$ and frequency dependent upper and lower bounds of corresponding performance $|J(P,C)|$, denoted $|J(P,C)|_{up}$ and $|J(P,C)|_{lo}$. The performance bounds are said to be* **non-conservative** *if*

$$P \in \mathcal{P} \iff |J(P,C)|_{lo} < |J(P,C)| < |J(P,C)|_{up}, \quad \omega \in [0,\pi)$$

holds true and is said to be **conservative** *if*

$$P \in \mathcal{P} \ \Rightarrow \ |J(P,C)|_{lo} < |J(P,C)| < |J(P,C)|_{up}, \quad \omega \in [0,\pi)$$
$$P \in \mathcal{P} \ \not\Leftarrow \ |J(P,C)|_{lo} < |J(P,C)| < |J(P,C)|_{up}, \quad \omega \in [0,\pi)$$

holds true. □

[4]Recall from proposition 2.2.2 that | . | denotes the matrix of the magnitudes of the elements of a transfer function matrix.

We elaborate performance evaluation for the system uncertainty sets $\mathcal{P}_{ND}$ and $\mathcal{P}_R$, introduced in section 2.3.

Consider the plant model set $\mathcal{P}_{ND}$ defined in (2.9). Upper and lower magnitude bounds of the performance representation (2.7), that account for *any* system $P \in \mathcal{P}_{ND}$, are then defined as follows:

$$\sup_{P\in\mathcal{P}_{ND}} , \inf_{P\in\mathcal{P}_{ND}} |J(P,C)| := \tag{2.24}$$
$$\sup_{\substack{|\Delta_N|\le\delta_N \\ |\Delta_D|\le\delta_D}} , \inf_{\substack{|\Delta_N|\le\delta_N \\ |\Delta_D|\le\delta_D}} \left| \begin{bmatrix} N+\Delta_N \\ D+\Delta_D \end{bmatrix} (\tilde{D}_c(D+\Delta_D)+\tilde{N}_c(N+\Delta_N))^{-1} [\tilde{N}_c \quad \tilde{D}_c] \right|$$

Computation of upper and lower magnitude bounds according to (2.24) employing the system set bounds δ_N and δ_D, is not straightforward due to the fractional uncertainty structure. One approach is to make a worst case approximation of the magnitude bounds by employing the frequency dependent model uncertainty bounds δ_N, δ_D, i.e. we do not take phase information into account. The construction of worst case magnitude bounds for the feedback system (2.4) as is presented here, is described in [87].

Magnitude bounds are defined in a similar manner employing a system uncertainty set $\mathcal{P}_R(N_x, D_x, N_c, D_c, R, \Delta_R)$ as follows. Consider a feedback transfer function according to (2.4) of a model $P = (N_x + D_c(R+\Delta_R))(D_x - N_c(R+\Delta_R))^{-1}$ and a compensator $C_n = \tilde{D}_{cn}^{-1}\tilde{N}_{cn}$ that is evaluated for its robustness.

$$\sup_{P\in\mathcal{P}_R} , \inf_{P\in\mathcal{P}_R} |J(P,C)| := \tag{2.25}$$
$$\sup_{|\Delta_R|<\delta_R} , \inf_{|\Delta_R|<\delta_R} \left| \begin{bmatrix} N_x + D_c(R+\Delta_R) \\ D_x - N_c(R+\Delta_R) \end{bmatrix} \times \right.$$
$$\left. \left(\tilde{D}_{cn}D_x + \tilde{N}_{cn}N_x + \tilde{D}_{cn}(C_n - C)D_c(R+\Delta_R)\right)^{-1} [\tilde{N}_{cn} \quad \tilde{D}_{cn}] \right| .$$

The computation of non-conservative bounds employing a model uncertainty set $\mathcal{P}_R$, as defined in (2.14), is addressed in chapter 7. An important feature for computing non-conservative bounds is that the performance representation (2.7) based on the model uncertainty set $\mathcal{P}_R$, exhibits a structure that strongly relates to a Linear Fractional Transformation (LFT).

2.7 Elaboration outline

In this chapter the role of nominal models and model error bounds is discussed in view of the elaboration of our problem statement in chapter 1. Central theme in the utilization of models for model based control design is how to deal with the mismatch between the model and the system (for which the controller is primarily designed!), denoted as the model error. A conceptual distinction is made between model errors that can be tuned and model errors that are beyond tuning. The motivation for making this distinction is instigated by the insight that construction of approximate models of a complex plant allows for shaping of the model error within the restricted reliability of available plant knowledge, contained in measurement data. An experimental justification for this distinction is elaborated in chapter 5, where frequency response measurements of a radial Compact Disk servo mechanism are invalidated. We have phrased a performance relevant approximation problem based on shaping the tunable model error and a robust performance evaluation problem based on coping with non-tunable model errors.

In chapter 3 a Compact Disk servo system is discussed being the physical plant that motivates our problem formulation. The need for model based control design is clarified in case the present level of tracking performance is to be improved.

As low complexity controllers are to be obtained on the basis of low order models, the corresponding model error should be tuned such that a prespecified performance is achieved for the system. As we have discussed in section 2.4, the design of a prespecified robust performance controller imposes restrictions on the model error that are not likely to be met at first instant utilizing a low order model. The elaboration of the prespecified robust performance problem is hence split into two parts:

1. design of a restricted complexity controller that achieves a robust performance *enhancement* of the feedback system;

2. design of a restricted complexity controller that achieves a *prespecified* robust performance of the feedback system.

The first part is addressed in chapters 4, 6 and 7. A model based control design procedure is proposed in chapter 4 for design of restricted complexity controllers. Controller complexity is kept low via utilization of low order models, which directly reverts to the issue of how to tune the model error. Approximate identification of nominal models for control design is the topic

of chapter 6 and data based model error bounding and evaluation of robust performance is addressed in chapter 7.

The second part is set out in chapter 8, where an iterative approach towards prespecified performance enhancement is outlined, constituted of approximate modelling and robust performance evaluation and model based control design.

Experimental verification of the proposed procedure is presented in chapter 9.

Chapter 3

Compact Disk servo system

3.1 Introduction

In a broad spectrum of application areas of electro mechanical servo systems a tracking error must not exceed a prespecified value in the presence of disturbances, while requirements on tracking performance become more tight. Especially in the application area of optical data systems encountered in consumer electronic products, the still growing achievements in the field of electronics and optics dictate the pace of increasing performance demands. As this results in higher demands on tracking accuracy and speed in the presence of a wide range of disturbances, the achievable limits of performance of existing servo systems are by now more and more dictated by the mechanical part of the servo. In this chapter we clarify how model-based control design is employed in this research to achieve an enhanced tracking performance for optical disk drive systems with specific application to a Compact Disk player of the swing arm type.

This chapter addresses the following issues. Firstly, in section 3.2 the physical process of data reconstruction in optical data systems is elucidated; as a Compact Disk servo mechanism serves as a problem carrier, the physical lay out of a radial Compact Disk servo mechanism is discussed in more detail. Future requirements of optical data systems are discussed and the limitations to achieve these requirements are clarified in section 3.3. In section 3.4 we formulate the performance objective, directed towards reducing the contribution of periodic signal components in the tracking error due to periodic disturbances and the presence of flexibilities of the mechanical actuator. In section 3.5 we sketch a scenario how model based control is employed to realize the performance objective.

3.2 Compact disk drive

3.2.1 Optical data reading

The primary function of an optical disc system is to recover digital information, stored on an optical disk. For a thorough treatment of optical disc systems we refer to [7].

The digital information is physically contained in a relief of a spiral track, consisting of a sequence of pits of varying length. Data reading is the process of transformation the hight relief of the track into an electrical current, which is realized by projection of a laserbeam spot on the track and measurement of the intensity of the reflected beam. The light intensity of the reflected beam is the netto result of the part reflected by the pit and the part reflected by the pit surroundings. In case the pit reflected light path is longer by half the wave length of the light, it neutralizes the remaining light reflection. The netto intensity is almost zero in case the spot surface covers a pit and its surroundings in equal proportion and reaches its maximum value in case no pit is covered. A schematic depiction of a track on an audio disk is shown in figure 3.1.

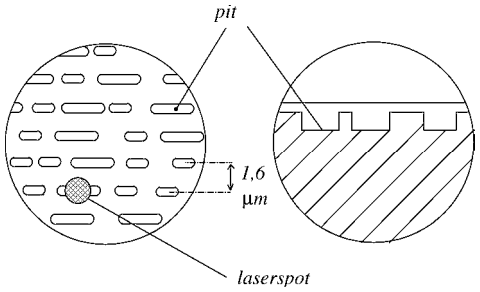

fig. 3.1: Schematic depiction (enlarged) of an audio disk surface.

Intensity of the reflected light is measured by a photo diode which converts light intensity into an electrical current. The audio signal is obtained through sampling at 44.1 kHz and adjusting the sampled signals for missing bits.

Correct detection of the relief on the disk is only established if the laserspot has a diameter with prespecified accuracy and a maximum allowed deviation of the spot position with respect to the track position. To keep the laserspot diameter within tolerated values, the optical part of the servo has to be focused accurately onto the information layer of the disk (positioning in focus direction). To establish accurate positioning of the laser spot position with respect to the

track, the optical part has to be positioned perpendicular to the track, in the plane of the disk (positioning in radial direction).

3.2.2 Physical lay out

The CD servo system consists of the following parts: the actuators, the information medium (disk) and a controller. We briefly describe the main features.

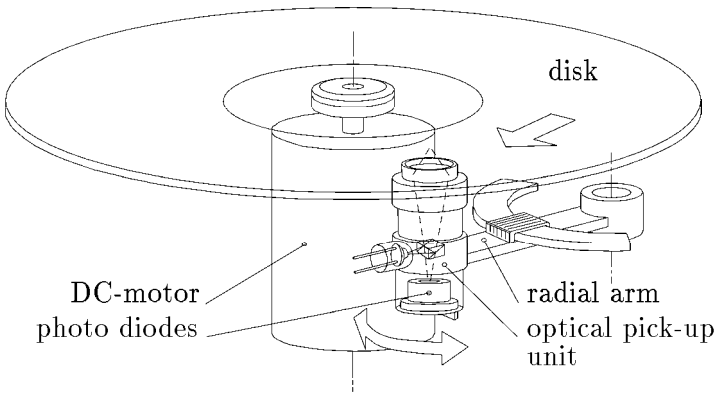

fig. 3.2: Schematic depiction of the physical lay out of the Compact Disk servo mechanism, consisting of a rotating arm and a leaf-spring actuator for spot focusing, mounted at its tip.

Actuators

The task of the mechanical servo in an optical data system is the positioning of the laserspot with respect to the track where the tracking error must not exceed prespecified margins. The compact disk servo that we address as our problem casus is of the swing-arm type (Philips CDM9) and is constituted of two electro mechanical actuators for positioning in perpendicular direction with respect to the disk surface (focus direction) and in radial direction, parallel to the disk surface.

The actuator enabling positioning in focus direction is constituted of two leaf springs that are actuated by an electro magnetic coil, onto which an optical lens is mounted. The optical construction of laser, lens and focus actuator is mounted on an actuator, consisting of an arm, that is driven by a current

driven rotating electro motor, enabling the positioning of the optical lens in radial direction. A schematic depiction of the CD servo mechanism is shown in figure 3.2.

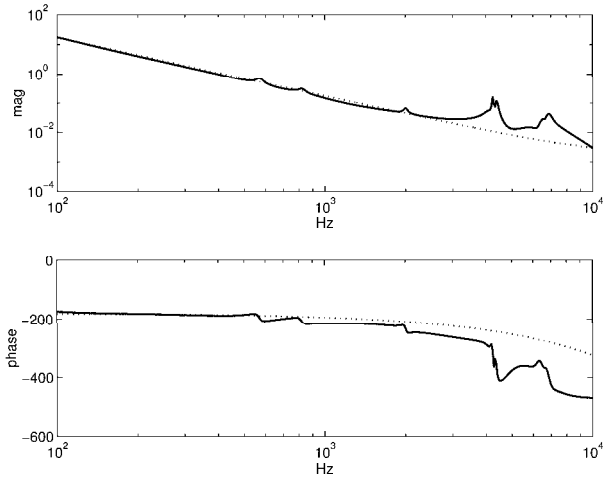

fig. 3.3: Bode diagram of a 32nd order model of a radial actuator of the swing-arm Compact Disk servo mechanism. Characteristic features are the presence of a double integrator and resonance modes due to actuator flexibilities at higher frequencies.

Both actuators are driven by a current that results in a position; as current is proportional to torque, the transfer function from current to position contains a double integrator. In specific the radial actuator behaves as a rigid body at low frequencies, but at higher frequencies the flexibilities of the arm dominate high frequent dynamical behaviour. As will be further discussed in section 3.4, the presence of flexible modes considerably complicates the design of controllers in case accurate tracking at higher frequencies is required. A Bode diagram of a model of a radial actuator of the CD mechanism is shown in figure 3.3 to illustrate the characteristic dynamics of a swing-arm type radial actuator. Although we specificly address a CD actuator, the actuator dynamics are characteristic for a broad range of electro mechanical motion control systems encountered in industrial and consumer electronic applications [82].

The fact that radial displacement of the optical device is enabled by rotation of an arm, has consequences for tracking performance. In figure 3.4 the relative gain of angular displacement of the arm to radial displacement with respect to the disk is depicted as a function of the radial position on the disk. The gain of angular rotation to radial displacement depends on the radial position in a

nonlinear manner.

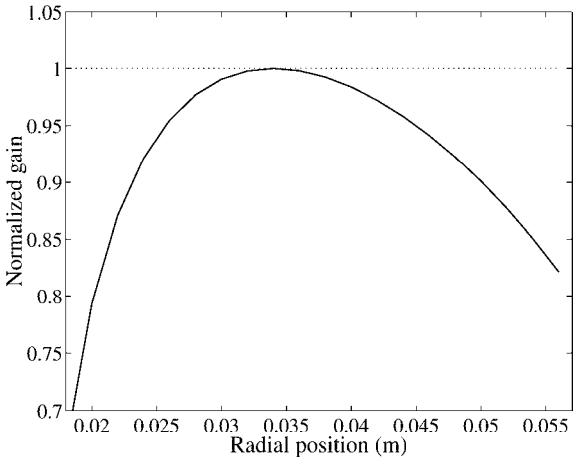

fig. 3.4: Nonlinear characteristic of relative gain of the radial actuator of a swing-arm type Compact Disk mechanism, expressed in radial displacement with respect to the disk centre.

The fact that the radial actuator gain varies with radial position implies that tracking performance also varies with radial position in case no precautions are taken. To be more specific, a decreasing actuator gain results in a decrease of the bandwidth[1] of the feedback system, which results in a decrease of disturbance attenuation at low frequencies. In order to keep the bandwidth constant for every radial position of the actuator, a commercially available CD player is equipped with an automatic gain control, that corrects for gain variations during play of a disk, using the so-called "wobbling"-method ([7]).

In chapter 9 we will revert to the nonlinear gain characteristic of the radial actuator, when addressing the exercise of acquiring measurement data in view of identification purposes.

Disk

Manufacturing of an audio disk is a process of injection of a liquid polycarbonate substrate into a mould, compression of the moulds and forced cooling. The moulds containing the information relief are manufactured by mastering [7]. The track shape of the master is almost a perfect spiral sequence of pits. The track geometry of the replicas however mostly deviates from the master

[1] A definition of the bandwidth is postponed until chapter 4

track due to the manufacturing process. Gass bubbles may be present in the disk due to injection and compression; track geometry is distorted by forced cooling leading to warp of the disk and a more or less potato shaped spiral track. After the disk is hardened, a hole is punched in the middle of the disk which hardly ever matches the geometrical centre of the track. As a result disk rotation implies eccentric spinning of the track.

Note that in mass-production of audio disks the cycle time of manufacturing is costly; so reducing the time of cooling and hole manufacturing results in a larger number of discs produced but inevitably poses higher demands on the tracking performance of the CD player.

A typical feature of audio applications of optical disks is that usage of the disks causes the presence of dirt, stains and scratches on the disk surface which severly hamper correct measurement of the intensity of the reflected light. Distortions in measured light intensity do not directly impair reconstruction of the audio information as it is attained by sampling of the light intensity, but have large effect on the analog error signals used for tracking. Consequently, the CD servo must also account for faulty tracking error signals. The error signals available for feedback compensation are discussed next.

Compensator

The position of the track on the disk is not available for measurement and neither is the position of the laser spot (or equivalently: position of the actuators). What can be measured is the difference between track and spot position which can be derived from fluctuations of light intensity in conjunction with an array of diodes. Error signals are thus available as analog currents for focus and radial actuator. The block diagram of figure 3.5 schematically depicts the closed loop configuration of a Compact Disk servo mechanism.
The presence of a feedback compensator is required for the following reasons. Firstly, the actuators are marginally stable due to the double integrator and can therefore not operate without a stabilizing controller.

Secondly, stability is not sufficient in view of accurate data reading as the tracking error magnitude must remain within prespecified values in the presence of disturbances. A major disturbance encountered in optical disk drive systems is the result of eccentric disk rotation in combination with track shape irregularities. The track position has the following properties due to its geometry and its rotating movement, observed from the radial actuator position:

- periodicity due to

1. eccentricity of the disk, which has dominating periodic components of which the period corresponds to the rotational frequency.
2. non-roundness of the track.

This results in presence of a fundamental frequency corresponding to the rotational frequency and its higher harmonics. These frequencies are clearly present in spectral estimates of the radial error signal. The presence of higher harmonics is due to modulation of the non-roundness by the eccentric rotation of the disk.

- time variance of the period: since the rotational frequency of the disk varies, the fundamental frequency and higher harmonics of the periodic disturbance vary in time.

- variability of the track shape: the contour of the track along two sequential disk revolutions (two periods) shows slight variations.

Another source of disturbances is due to acceleration forces that act on the servo system as a result of the mobility requirements of compact disk applications. Especially portable CD players and the car-CD are exposed to vibrations and shock-like disturbances. Due to the flexible construction and inertia of the servo mechanism and the disk the position of the actuators and the track will deviate from their nominal values. Of course it is crucial that these deviations are within the bounds that allow good track following. The nature of accelerations and the orientation with respect to the tracking actuator are hard to "predict".

Thirdly, the controller keeps the dynamics of the actuators within their linear operating range; translation of light intensity into position information implies a nonlinear relation that is approximately linear for relatively small displacements. For a detailed description we refer to Bouwhuis *et al.* ([7]).

3.3 Requirements and limitations

3.3.1 Requirements

The main performance specification for an optical disk drive servo mechanism is that the magnitude of the tracking error must not exceed a prespecified value, expressed as $|e(t)| < \delta$. If this specification is not satisfied, no correct reconstruction of information stored on a disk can take place. The following aspects are specific for commercial applications of optical data systems like the Compact Disk player.

Mobility requirements of CD systems impose that the servo should insensitive to external disturbances like mechanical shocks and vibrations, which manifest as accelerations of the servo mechanism. Due to flexibility and inertia of the construction and the disc, accelerations result in a relative displacement of the optical pick-up and the absolute track position. External accelerations are less structured than e.g. periodic disturbances due to eccentric disk rotation, which makes it hard to deal with them in a modelling framework.

An important feature is that consumer electronic products are produced in large numbers at lowest possible manufacturing costs. As a result, the dynamical behaviour of every single servo mechanism is not exactly known; moreover, mass-produced servo mechanisms will most unlikely exhibit exactly equivalent dynamic behaviour. The presence of a feedback controller therefore is required to reduce the effects of uncertain system dynamics on tracking performance, where the uncertainty is caused by inadequate knowledge of each servo system and the variability in dynamic behaviour of a large number of systems.

A performance requirement that is specific for portable applications is that power consumption should be low. From marketing point of view a product will not sell in case the customer is compelled to replace the batteries after short time spans of use. In audio applications of optical disk drives the servo produces audible noise in case controllers perform at high frequencies. This of course is an undesirable side effect from commercial point of view.

Towards future applications there are two fundamental requirements on the servo mechanism that should be complied with in view of an enhanced information capacity of Compact Disk systems and optical data systems in general:

- Information density on one disk should be substantially increased, implying that the track geometry and the radial distance increase of the track should be decreased. From optical point of view different types of laser light are available that enable read out of tracks having 4 times smaller dimensions.
- An increase of information density should not result in an increase of time needed to access the information. Consequently, data accessibility should be realized in shorter time spans which is feasible by an increase of the rotational velocity of the disk.

The above requirements impose that the value of δ is lowered and that disturbances due to eccentric disk rotation will deteriorate tracking performance. A general performance objective for the compact disk servo can thus be formulated as follows:

Definition 3.3.1 *High performance of a mechanical servo system is achieved if a prespecified upper bound of the tracking error is attained, phrased as* $|e(t)| < \delta, \forall t$, *at increased rotational speed of the disk and the power density of the controller output* $y_c(t)$ *is limited at high frequencies. These specifications should be attained for a set of servo mechanisms.*

In the following we will outline the limitations that we are confronted with in pursueing a high performance of an optical disk drive system via model-based control design.

3.3.2 Limitations

In this section we comment on the limitations of a model-based control design approach towards achieving a high performance according to definition 3.3.1 from the perspective of system physics.

Uncertain actuator dynamics

In a model-based control design approach mathematical models are utilized to describe the dynamical behaviour of the system. Requiring an enhanced tracking performance for a feedback system imposes a maximum allowable error between the model and the system. This means that in case knowledge of the system is limited, we can not expect a feedback controller, designed on the basis of available system knowledge, to achieve a satisfacory tracking performance for the system. So design of a feedback compensator that complies with prespecified tracking performance requires accurate knowledge of the system to be controlled.

Disturbances

One of the major reasons to design feedback controllers is to reduce the effect of disturbances on the performance of a system, as is adequately phrased in [57]. Attenuation of disturbances by means of feedback system design can be enhanced in case knowledge about the nature of the disturbances is at hand and, moreover, can be modelled effectively in view of control design. In view of reducing the tracking error magnitude in disk drive systems in the presence of periodic disturbances due to eccentric disk rotation, work has been reported on application of repetitive control schemes, where knowledge of the periodic nature of disturbances is employed in order to decrease its effect on the tracking error. For application results of repetitive control on disk drive systems, we

refer to [83] and [84]. Application of adaptive repetitive control to a swing-arm type Compact Disk mechanism to account for the varying rotation speed during play is reported by Smakman ([73]) and Dötsch *et al.* ([22]).

In the same line of argument of imposing a restriction to the extent of uncertain actuator dynamics, we argue that enhancement of tracking performance (decrease of the tracking error magnitude) requires more accurate knowledge of the disturbances. In this research we will not incorporate prior knowledge of the partly periodic nature of the disturbances explicitly in a design procedure, as we restrict our attention to modelling of the actuator.

Restricted complexity controllers

A practical issue in this research is that controllers are implemented utilizing a digital signal processor. The Compact Disk servo mechanism requires a high sample rate for digital controller implementation, which imposes constraints on the complexity of controllers that are liable for implementation with the current status of available hardware equipment.

3.4 Performance objective

To phrase a performance objective amenable for feedback system design, we consider the feedback system in figure 3.5. The actuator is denoted by $\mathcal{P}$, the feedback controller C, w is the track position on the disk, d denotes disturbances due to shocks, vibrations, grease stains, scratches, etc. The tracking error is denoted e and the controller output y_c; the filters $\mathcal{H}_{ext}, \mathcal{H}_w$ reflect how the disturbances d resp. w effect the feedback system.

The tracking error e is significant in view of accurate tracking in the presence of disturbances and the control output y_c is significant in view of audible noise production and power consumption. A performance formulation hence is based on the mapping of disturbance signals w and d on the tracking error e and the controller output y_c:

$$\begin{bmatrix} w \\ d \end{bmatrix} \rightarrow \begin{bmatrix} e \\ y_c \end{bmatrix}.$$

As we do not specificly account for different sources of disturbances in the further elaboration, disturbances are modelled by one signal entering the feedback loop. A general performance objective is phrased in terms of tracking and power consumption, embodied in the following transfer function:

$$\begin{bmatrix} e \\ y_c \end{bmatrix} = \begin{bmatrix} I \\ C \end{bmatrix} (I + PC)^{-1} H w_{\text{tot}}. \tag{3.1}$$

where H denotes a disturbance model accounting for all disturbances effecting the feedback system.

A performance objective amenable for model-based control design that complies with the formulation of high performance according to definition 3.3.1, can hence be phrased in terms assigning desired properties to the sensitivity transfer function $(I + PC)^{-1}$. In work by van Groos ([36]), van Groos *et al.* ([35]) and Steinbuch and Norg ([82]) on robust control design of a swing-arm type Compact Disk mechanism, the performance objective utilized for control design is formulated in terms of a maximum allowable magnitude characteristic of the sensitivity function. We adopt a similar line of argument for phrasing a performance objective. In order to achieve appropriate disturbance attenu-ation at higher disk rotation velocity and to simulaneously keep controller action (power consumption and production of audible noise) limited, the Bode magnitude diagram of the sensitivity should remain bounded by the magnitude characteristic depicted in figure 3.6.

Compensator characteristics that uphold in general for *any* compensator that potentially complies with the Bode magnitude characteristic in figure 3.6, irrespective of the way it is obtained, are based on following loop shape arguments [82]. In order to provide sufficient attenuation of periodic disturbances the sensitivity should have a $+3$ slope at low frequencies. As the radial actuator has a -2 slope this implies that the controller should have one integrator. To establish robustness of the feedback system in view of unknown or inaccurately known actuator dynamics, a phase lead is required in the cross-over frequency region. At higher frequencies a feedback controller should have sufficient roll-off in order to limit power of the controller output; generally a high frequent roll-off with a slope -2 is adequate. A Bode diagram of a feedback compensator that satisfies the above design specifications for a double integrator is depicted in figure 3.7.

An increase of rotation velocity of the disk consequently implies a shift of periodic disturbance components to higher frequencies. Consequently, the bandwidth of the feedback system should be enhanced to enable sufficient attenuation of periodic disturbances at higher frequencies.

In figure 3.8 the Bode diagram of the sensitivity function is depicted of the feedback system corresponding to the compensator of figure 3.7 and the model of the radial actuator of figure 3.3.

The Bode diagram of figure 3.8 illustrates that an enhanced bandwidth design

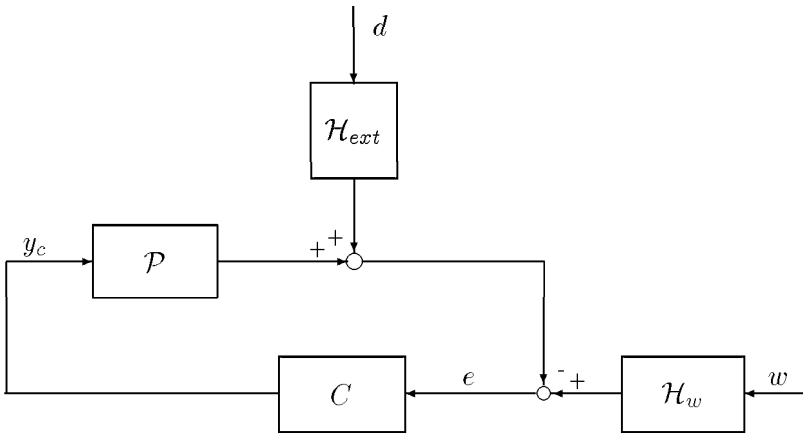

fig. 3.5: Block scheme of a servo mechanism consisting of an actuator $\mathcal{P}$, feedback controller C and disturbances $\mathcal{H}_{ext}d$ and $\mathcal{H}_w w$.

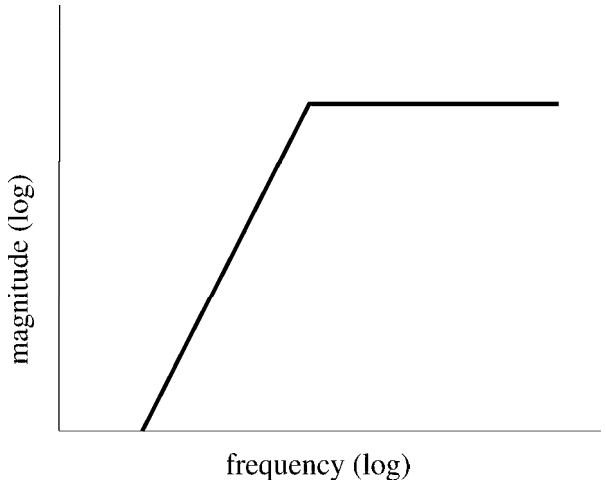

fig. 3.6: Bode magnitude diagram of the maximum sensitivity function magnitude that complies with sufficient disturbance attenuation and limited controller action.

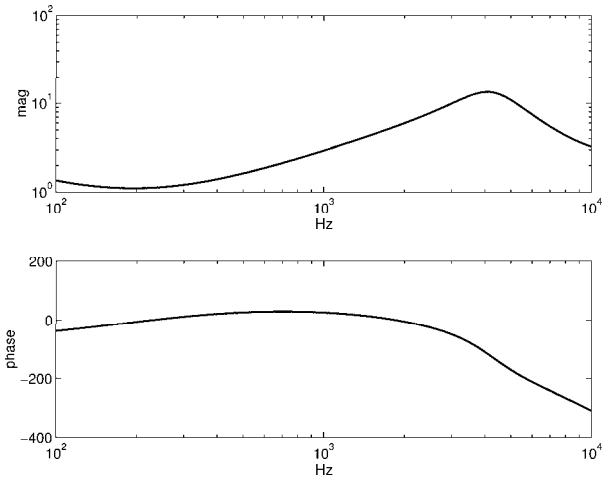

fig. 3.7: Bode diagram of a feedback compensator that achieves an enhanced bandwidth for a double integrator.

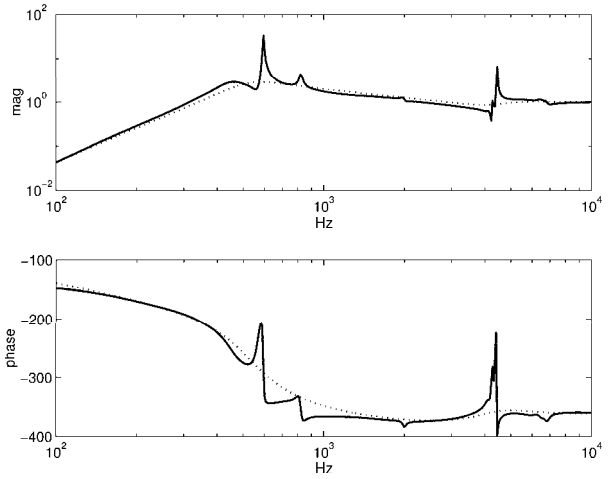

fig. 3.8: Bode diagram of the sensitivity function $(I+PC)^{-1}$ with the controller of figure 3.7 : a 32nd order model of the radial actuator of a swing-arm type Compact Disk mechanism (solid) and a double integrator (dot).

of an electro mechanical actuator based on a double integrator leads to a deterioration of tracking performance (or disturbance reduction) if we do not take account of resonance modes due to flexibilities. Concluding, an increase of the bandwidth of the radial feedback system is hindered by inaccurately known flexibilities of the mechanical construction of the servo system. Excitation of resonance modes results in periodic signals to occur in the tracking error that cause a drastic increase of the tracking error magnitude. We formalize the above line of argument in the following observation.

Observation 3.4.1 *An enhanced attenuation of disturbances via enlargement of the bandwidth, inevitably results in occurence of periodic components in the tracking error due to excitation of resonance modes of the mechanical servo in case flexibilities are not adequately accounted for in the control design.*

We will conclude this chapter by proposing a strategy that gives direction to the elaboration of our problem statement in chapter 1 in subsequent chapters.

3.5 Strategy towards enhanced performance

Based on the observation formulated above, the strategy of feedback control design that is adopted in this work in view of an enhanced attenuation of (periodic) disturbances at higher frequencies, is based on the following two arguments:

1. The bandwidth of the feedback system is enlarged based on loop shape arguments presuming the radial actuator is a rigid body;
2. To prevent resonance modes from being excited, model based control design is employed in order to "stiffen" the radial arm.

Instrumental is the availability of mathematical models that describe the flexibilities of an electro mechanical actuator sufficiently well.

Chapter 4

Design of restricted complexity controllers

4.1 Introduction

In this chapter a control design procedure is proposed for construction of a low complexity controller employing model-based control design that achieves an enhanced performance for the system. The need for controllers of restricted complexity is motivated in the previous chapter in view of keeping design cost low and to make digital controller implementation feasible in an experimental test environment.

Generally, model-based control design techniques constitute an optimization problem based on mathematical models of the system and weighting functions that incorporate performance specifications. Consequently, resulting controllers have a complexity similar to that of the model and weighting functions that underly the design. In case complex models and weightings are utilized in the design, this leads to controllers of an unacceptably high order.

The chapter is organized as follows. In section 4.2 the relation between model-based control design and models that underly the design is elucidated. Design of a controller on the basis of an approximate model that implicitly anticipates model imperfections, is the subject of section 4.3. The design of weighting functions that embody performance specifications for an electro mechanical actuator, as phrased in chapter 3, is discussed in section 4.4. Finally, a two stage control design procedure constituted of a design step and a robust performance evaluation step, is proposed in section 4.5.

4.2 Model-based control design

In order to clarify the control design procedure employed in this thesis, we revert to the discussion in section 2.4 and elucidate in more detail our view

point on model utilization for control design with application to a physical plant that is not exactly known.

A key presumption in model-based control design is that the model underlying the design is presumed equivalent to the system for which a compensator primarily is designed, which is known as the certainty equivalence principle. However, a model generally provides an approximate system description; consequently, controllers that are designed on the basis of a model will most likely exhibit a different performance for the nominal model and for the actual system. The extent of different performance not only depends on the difference between the model and system, but also on the performance specification that underlies the control design. A high performance model-based control design imposes a limitation on the allowable model error such that the difference between performance of model and system remains restricted.

Keeping in mind that a model at all times provides an approximate system description, we now discuss the consequences for design of a model-based controller of *restricted* complexity in view of a desired *high* performance for the physical plant. One way to arrive at controllers of low order reads as follows:

> Approach of **controller reduction**: construct a highly accurate (hence complex) model and design a controller based on this model; subsequently apply an order reduction technique on the high order controller.

In literature, e.g. Wortelboer ([95]), controller reduction is a well-defined problem. Techniques have become available to construct low order controllers given a complex controller, such that the difference of performance remains limited for a *high complexity model.* However, no performance guarantees are incorporated in the controller reduction for the plant. In order to perform a controller reduction in view of a limited performance degradation for the plant, knowledge of the mismatch between the plant and the high complexity model is a prerequisite. So, in case a controller reduction approach is taken to arrive at low order controllers (i.e. no information about the plant-model mismatch is employed), the designer inherently restricts him- or herself to a maximum achievable robust performance, induced by the quality of the underlying model.

Another way to design low complexity controllers reads as follows:

> Approach of **approximate modelling**: construct a low order model and subsequently design a full order compensator on the basis of that model.

The topic of approximate modelling for control design has received a vast amount of research attention, specificly in the field of approximate system

identification ([53, 69, 29, 85]). The problem motivation of approximate modelling has emerged from the insight that a plant is not exactly known, and hence a model necessarily is an approximate system description. Moreover, it is motivated and illustrated by several examples that a high order model is not a necessary prerequisite for design of a high robust performance controller.

An important feature of control design based on an approximate model is that robustness of the design can only be attained by a posteriori evaluation of the controller. We make a critical note at this point, since evaluation of performance in view of the plant requires information about the *true* plant-model mismatch, which is not available by presumption as the plant is presumed not to be exactly known. What is lacking in the above line of reasoning is the availability of a quality measure of the system knowledge, used for approximate modelling.

Both abovementioned approaches for design of a restricted complexity controller in view of a desired performance for the system in our point view require:

- a nominal model that constitutes the basis for *design* of a controller;
- a model error bound which accounts for the fact that a (restricted complexity) controller should work well for the physical plant.

Summarizing the above discussion, we state that the system knowledge that is available for modelling (e.g. frequency response measurements, first principle laws) constitutes an idealized description of the dynamical behaviour of the plant and therefore does not unambiguously represent the physical plant[1]. Therefore, any model-based control design procedure should account for inaccuracies of available system knowledge in order to ensure robustness of the design in view of the *plant*.

Controller reduction methods and approximate modelling procedures as available to date do not utilize model error bounds in a systematic manner for design of a high robust performance controller of restricted complexity. In this chapter a control design strategy is adopted where an approximate model is used for design and robustness of the designed controller is evaluated a posteriori, based on available system knowledge. This strategy requires an approach of repeated design and evaluation in order to systematicly explore the limitations of a high robust performance imposed by the mismatch between model and system.

[1] A similar statement is formulated by Skelton ([72])

4.3 Control design problem

4.3.1 An $\mathcal{H}_\infty$ loop shape design

In this section a control design technique is addressed that is known as an $\mathcal{H}_\infty$ loop shape design, developed by [49, 50]. The performance objective utilized in this control design is closely related to the closed loop transfer function (2.4) in chapter 2. We reconsider the block scheme of figure 4.1 of a system operating in closed loop. The signals r_1, r_2 are known and d denotes a disturbance, entering the closed loop system at the plant output.

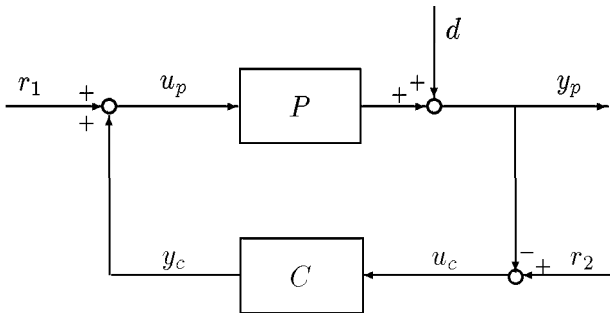

fig. 4.1: General block scheme of a system P operating in closed loop with a feedback controller C.

In chapter 2 we have clarified that the transfer function that maps $[r_2\ r_1]^T$ into $[y_p\ u_p]^T$, denoted as

$$\begin{bmatrix} P \\ I \end{bmatrix} [I + CP]^{-1} [C \quad I],$$

reflects a general performance measure of a feedback system. A feasible control design problem may be phrased as follows, employing an $\mathcal{H}_\infty$ performance objective:

$$C_{\hat{P}} = \arg_{\tilde{C}} \min \left\| W_{\text{out}} \begin{bmatrix} \hat{P}(I + \tilde{C}\hat{P})^{-1}\tilde{C} & \hat{P}(I + \tilde{C}\hat{P})^{-1} \\ (I + \tilde{C}\hat{P})^{-1}\tilde{C} & (I + \tilde{C}\hat{P})^{-1} \end{bmatrix} W_{\text{in}} \right\|_\infty \tag{4.1}$$

where $\hat{P}$ is an LTI model of the system and $W_{\text{in}}, W_{\text{out}}$ are user-specified weighting functions that reflect the desired performance.

In [50] a $\mathcal{H}_\infty$ control design procedure is phrased that shows great similarity with the control design formulated in (4.1). A similar design procedure is employed by [5]. First we introduce the control design strategy, formalized in the following definition.

Definition 4.3.1 *McFarlane and Glover ([50]).*
Loop shape control design procedure:

1. *Based on a nominal model $\hat{P}$, a weighting function W is designed such that the loop shape $W\hat{P}$ complies with desired performance of the feedback system.*

2. *Design a controller according to the following optimization problem:*

$$C_{\hat{P},W} = \arg_{\tilde{C}} \min \left\| \begin{bmatrix} W\hat{P} \\ I \end{bmatrix} [I + \tilde{C}W\hat{P}]^{-1} [\tilde{C} \quad I] \right\|_\infty .$$

3. *Construct the final controller as $C = WC_{\hat{P},W}$.*

□

Note that the controller resulting from the above design procedure is equivalent to the controller that results from the design problem stated in (4.1).

We make the critical observation that the controller order generally is determined twice by the order of the weighting W. This is undesirable in view of design of a restricted complexity controller. We will revert to this issue when discussing weighting functions in section 4.4.

4.3.2 Properties of the design

In this section we discuss the most relevant properties of the design procedure defined above.

Robustness

It is noted that the loop shape control design procedure, phrased as a nominal performance optimization problem, coincides with a specific robust stability optimization problem. To be more specific, the control design of (4.1) maximizes robust stability in view of perturbations on normalized right coprime factors

of the model $W\hat{P}$. This is shown by [5] and by [50] for normalized left coprime factors. An additional result is that evaluation of the maximum achievable robust stability margin is feasible prior to compensator calculation. The stability margin is expressed in terms of additive perturbations on the normalized right coprime factors of the loop shaped nominal model $W\hat{P}$:

$$\epsilon_{max} = \sqrt{1 - \left\| [\hat{N}_W \ \hat{D}_W] \right\|_H^2} \tag{4.2}$$

where $\{\hat{N}_W, \hat{D}_W\}$ are normalized right coprime factors of $W\hat{P}$. Whether robust stability actually is attained should be verified employing a system uncertainty set based on coprime factor representations, as introduced in chapter 2, that encompasses the true system. In case the loop shaped plant WP is captured by the set

$$\mathcal{P}_W := \left\{ P | P = (\hat{N}_W + \Delta_{\hat{N}_W})(\hat{D}_W + \Delta_{\hat{D}_W})^{-1}, \left\| [\Delta_{\hat{N}_W} \ \Delta_{\hat{D}_W}] \right\|_\infty < \epsilon_{max} \right\}$$

then a controller exists that robustly stabilizes $W\hat{P}$.

The maximum robust stability margin ϵ_{max} is employed by [50] as an indicator whether the weighting function has been chosen properly in terms of providing a sound trade-off between nominal performance and robust stability. In case a weighting leads to a stability margin that satisfies $\epsilon_{max} \ll 1$, the trade-off is too much in favour of nominal performance and robust stability properties are likely to be bad. In that case W should be modified in view of a lesser nominal performance.

Loop shape vs. robust design

A specific feature of the loop shape design procedure defined above is that the final controller is attained as the series connection of a weighting W and an optimal robust controller $C_{\hat{P},W}$. The weighting W has an interpretation of a loop shape compensator which is designed in view of a desired nominal performance with the presumption that a similar performance is achieved for the system. As the design procedure does not incorporate any knowledge of the system (high order model or system uncertainty set) we have to gain confidence in the controller by requiring that the robustness optimization does not alter the loop shape weighting too much. In case $C_{\hat{P},W}$ drastically degrades the nominal performance imposed by W, then it is stated that W is not suitably designed in view of robustness. In this respect we refer to the important result by [50] that is phrased as follows: " ... degradation in the loop shape caused

by the controller $C_{\hat{P},W}$ is limited at those frequencies where the desired loop shape is sufficiently large or sufficiently small."

In the next section we will use this result for design of a weighting that is suitable for an electro mechanical servo system.

4.4 Weighting functions

4.4.1 Considerations on weighting function design

Let us consider the feedback system depicted in the block diagram of figure 4.1. The signals that reflect performance are the controller input (tracking error) u_c and the controller output y_c. The operational situation dictates that $r_1 = r_2 = 0$. The performance objective is therefore embodied in the signal mapping $d \rightarrow [u_c \; y_c]^T$, expressed by the transfer function

$$\begin{bmatrix} u_c \\ y_c \end{bmatrix} = \begin{bmatrix} -(I+PC)^{-1} \\ -C(I+PC)^{-1} \end{bmatrix} d.$$

Here P represents the system; d is a disturbance entering the loop at the plant output and u_c is the tracking error that is to remain bounded. As discussed in chapter 3, we impose that $(I+PC)^{-1}$ has a $+3$ slope at low frequencies to provide sufficient disturbance attenuation and that $C(I+PC)^{-1}$ has a -2 slope at high frequencies to prevent from excessive power consumption and (audible) noise production. The characteristics of a controller that achieves these specifications for an electro mechanical CD actuator of the swing-arm type can be derived from loop shape arguments. The dynamical properties that are characteristic for a radial CD actuator are constituted of a double integrator and a number of resonance modes in the mid and high frequency region due to flexibilities, as we have discussed in chapter 3.

The above mentioned specifications on $(I+PC)^{-1}$ and $C(I+PC)^{-1}$ imply that the structure of a suitable compensator typically comprises an integrator to achieve a $+3$ slope of the sensitivity function at low frequencies, sufficient phase lead in the design cross-over region to ensure robustness and a roll-off of -2 at high frequencies. Hence a controller order of 4 is sufficient to comply with the above mentioned performance specifications.

Employing an (optimization-based) $\mathcal{H}_\infty$ control design method, it is imperative that the resulting controller complies with the above mentioned loop shape controller characterictics. For a given standard plant configuration defined in terms of $T(P,C)$, this imposes specific characteristics of the weighting functions.

In literature no guidelines are available for designing weighting functions for the $\mathcal{H}_\infty$ loop shape design of definition 4.3.1. Reported results only deal with a constant weighting where the system is presumed to have a high-frequent roll-off character. We refer to [50] and [69]. Increase of the gain in conjunction with high-frequent roll-off of the system causes the nominal loop gain to increase for all frequencies, thereby keeping the loop shape sufficiently high at low frequencies and sufficiently small at high frequencies in case of a steep roll-off.

In the subsequent subsection it is argued that a constant weight does not enable us to impose an integrator and a high frequent -2 slope on the control design for the $T(P,C)$ standard plant configuration and that we have to resort to dynamic weights. Note that a constant weighting is most favourable as compared to dynamic weightings from the view point of controller complexity.

4.4.2 Dynamic weighting design

In this section we will address the design of weighting functions $W_{\text{in}}, W_{\text{out}} \in \mathbb{C}^{2\times 2}$ such that a controller following from the optimization-based design

$$C = \arg_{\tilde{C}} \min \|W_{\text{out}} T(P,\tilde{C}) W_{\text{in}}\|_\infty$$

complies with the desired controller characteristics mentioned in the previous subsection.

An $\mathcal{H}_\infty$ control design objective that incorporates disturbance attenuation in conjunction with a restricted controller action is formalized as follows (leaving out $(j\omega)$ and the minus sign):

$$\left\| \begin{bmatrix} I & 0 \\ 0 & W_o \end{bmatrix} \begin{bmatrix} I \\ C \end{bmatrix} (I+PC)^{-1} W_i \right\|_\infty \tag{4.3}$$

The weighting W_i incorporates spectral information about the disturbance and W_o is a weighting reflecting spectral performance specifications for controller action.

To arrive at a suitable choice for the weighting function W_o, we employ loop shape arguments in conjunction with crude knowledge about the system dynamics, as has been put forward by [79]. In our case a crude model of the system is a double integrator with a gain, as has been discussed in chapter 3. As the system has a double integrator, a low frequent weight on the sensitivity having a -3 slope in magnitude is required to enforce an integrator; adding a weight with $+2$ slope at high frequencies is needed to enforce a -2 roll-off at

high frequencies. This results alltogether in a controller of order 7 (5 due to weights plus 2 due to the double integrator).

Compared to a loop-shape controller of order 4 that complies with performance requirements, the controller resulting from an optimization-based design is of a too high order. In [36] and [79] modification of the standard plant into

$$\begin{bmatrix} (I+PC)^{-1} & (I+PC)^{-1}P \\ C(I+PC)^{-1} & C(I+PC)^{-1}P \end{bmatrix} \tag{4.4}$$

is proposed that enables us to make fruitful use of the fact that the system has a -2 slope at low frequencies, requiring a -1 slope weight (instead of -3!) on $(I+PC)^{-1}P$ to enforce an integrator. Note that the modified standard plant (4.4) reflects the transfer function corresponding to the signal mapping $-[d\ r_1]^T \rightarrow [u_c\ y_c]^T$ in the block scheme of figure 4.1. If we set a -1 slope weight W_i at low frequencies on $(I+PC)^{-1}P$ and a $+2$ slope weight W_o at high frequencies on $C(I+PC)^{-1}$, a control design objective in view of nominal performance is formulated as:

$$\left\| \begin{bmatrix} (I+PC)^{-1} & (I+PC)^{-1}PW_i \\ W_oC(I+PC)^{-1} & C(I+PC)^{-1}P \end{bmatrix} \right\|_\infty \tag{4.5}$$

which can be rewritten in the Single Input Single Output case as

$$\left\| \begin{bmatrix} P(I+CP)^{-1}C & W_iP(I+CP)^{-1} \\ (I+CP)^{-1}CW_o & (I+CP)^{-1} \end{bmatrix} \right\|_\infty . \tag{4.6}$$

Presumed that $W_o = W_i^{-1}$ in order not to weight any other terms than $(I+CP)^{-1}C$ and $P(I+CP)^{-1}$, we define a performance objective criterion as follows:

$$\left\| \begin{bmatrix} W_i & 0 \\ 0 & I \end{bmatrix} \begin{bmatrix} P(I+CP)^{-1}C & P(I+CP)^{-1} \\ (I+CP)^{-1}C & (I+CP)^{-1} \end{bmatrix} \begin{bmatrix} W_o & 0 \\ 0 & I \end{bmatrix} \right\|_\infty . \tag{4.7}$$

The restriction $W_o = W_i^{-1}$ is not conflicting in terms of low frequent disturbance rejection (integrator in W_i) and high frequent roll-off of the controller ($+2$ slope of W_o in the high frequency region). Note that, starting from the performance objective (4.3), the performance objective in (4.6) imposes an indirect weighting of the sensitivity and complementary sensitivity in case $W_o = W_i^{-1}$.

A disadvantage of this restriction is that both weightings should at least be of order 3 instead of 2, implying an increase of the resulting controller order.

Moreover, the design phrased in definition 4.3.1 implies that the weighting order is counted twice (!) in the resulting optimization-based controller which is disadvantageous in view of our objective to design low complexity controllers. Therefore the controller order is reduced with the order of the weighting as is described by Bongers ([5]). As no prior guarantee can be given that performance deterioration due to controller reduction is limited, the reduced order controller is evaluated by visual inspection of the Bode diagrams of the full order and reduced order controller.

Before we specify weighting functions that comply with the above mentioned loop shape arguments, we specify the notion of bandwidth that is utilized throughout this thesis.

Definition 4.4.1 *Consider a Single Input, Single Output system P and a controller C that do not necessarily constitute a stable feedback system, then the bandwidth of the feedback system is defined as the lowest frequency for which $|PC| = 1$ holds, denoted ν_b.*

As disturbance attenuation is our main performance objective, it might have seemed more appropriate to designate the bandwidth as the lowest frequency for which $|(I+CP)| = 1$ holds to indicate the frequency region where feedback control establishes disturbance attenuation. In case of a stable system, increase of the gain of the (stable) controller provides an enhanced low frequent disturbance attenuation. In case the system is a double integrator however, increase of the controller gain is insufficient as the sensitivity is marginally stable, irrespective of the controller gain. In order to establish closed loop stability for a double integrator, additional phase lead is required in the frequency region near the point $(-1, 0)$ in the complex plane (continuous time case). The bandwidth being defined as the frequency for which $|PC| = 1$ in definition 4.4.1, complies with the frequency region that proves to be critical in view of enhanced disturbance attenuation for a double integrator.

Two weighting functions that achieve a prespecified bandwidth for a double integrator are formulated in the following definition.

Definition 4.4.2 *Consider a crude model of the system to be a double integrator with a gain, $\frac{K_p}{s^2}$. The following two weighting functions are defined for performance enhancement in an $\mathcal{H}_\infty$ loop shape control design procedure:*

- *A 4th order weighting that stabilizes $\frac{K_p}{s^2}$, parametrized as follows:*

$$W_4 := K \frac{\tau_0 s + 1}{\tau_0 s} \frac{\tau_1 s + 1}{\tau_2 s + 1} \frac{1}{\frac{s^2}{\omega_0^2} + 2\beta \frac{s}{\omega_0} + 1} \tag{4.8}$$

- *A 3rd order weighting that does not stabilize* $\frac{K_p}{s^2}$*, parametrized as follows:*

$$W_3 := K\frac{\tau_0 s + 1}{\tau_0 s}\frac{1}{\frac{s^2}{\omega_0^2} + 2\beta\frac{s}{\omega_0} + 1} \tag{4.9}$$

The choice of parameters $\tau_0 < \tau_1 < \tau_2 < \omega_0$ *is based on the desired location of poles and zeros to shape the lead-lag character of the weighting function.* □

The difference between W_4 and W_3 is a phase-lead that enables feedback stabilization of a double integrator by W_4 yet not by W_3. In order to simplify the weighting function design, the number of parameters is reduced to two by following definition.

Definition 4.4.3 *The parametrization of the weightings* W_4 *and* W_3*, defined in definition 4.4.2, is narrowed down to two parameters* ν_b *and* β*, defined as follows* [81]*:*

$$\tau_0 := \frac{\nu_b}{5}, \quad \tau_1 := \frac{\nu_b}{3}, \quad \tau_2 := 3\nu_b, \quad \omega_0 := 5\nu_b, \quad \beta = 0.4$$

where ν_b *denotes the design bandwidth for the closed loop system, defined as the frequency for which* $|W_3\frac{K_p}{s^2}| = 1$ *and* $|W_4\frac{K_p}{s^2}| = 1$ *holds. The weighting gain* K *is adjusted as such.* □

The structure of the weightings W_3 and W_4 reflects that we strive for enhancement of the bandwidth in view of a system consisting of a double integrator with a gain.

To clarify the fact that we have narrowed down our control design to specification of one parameter ν_b, reflecting the nominal design bandwidth (the relative damping β is kept fixed), the weightings are indicated as $W_3(\nu_b)$ and $W_4(\nu_b)$. What remains to be determined is the choice of the parameter ν_b, which is considered to be a most crucial one! Determination of ν_b is discussed in the subsequent section.

4.5 A procedure for restricted complexity controller design

4.5.1 Mechanisms underlying the design

We finally arrive at the main part of this chapter, being the formulation of a procedure for design of a restricted complexity controller.

Starting from a closed loop situation, the designer should be aware of the direction towards an enhanced performance. In many cases a crude model of

the plant is available that serves as a guideline for control design based on loop shape arguments. In the previous section 4th and 3rd order weighting functions are introduced that enable an enhancement of the design bandwidth ν_b for a double integrator.

The issue remains how ν_b should be assigned such that a controller C_{ν_b}, resulting from the optimization based design formulated in definition 4.3.1, achieves a similar bandwidth for the system [2].

An additional aspect is that low frequent controller modification may cause drastic performance deterioration in the cross-over and higher frequency region, due to the Bode-sensitivity "push-pop" effect. Specifically, adding an integrator for low frequent disturbance rejection results in a decrease of phase margin, which proves disastrous when resonance modes are present in the cross-over region. We take the view point that "pushing" towards a larger bandwidth is a valid strategy, as long as one is aware at what frequencies and to what extent the "popping" takes place.

The problem of determining an enhanced compensator that provides a similar performance for model and system is phrased as follows:

Problem 4.5.1 *Determine ν_b such that the controller $C_{\hat{P},\nu_b}$, resulting from the design in definition 4.3.1 based on a nominal model $\hat{P}$, achieves a performance for the model $|J(\hat{P}, C_{\hat{P},\nu_b})|$ and for the system $|J(P, C_{\hat{P},\nu_b} P)|$ that exhibit a similar enhancement.*

The key issue of problem 4.5.1 is to what extent the true model error allows for a simultaneous improvement of performance for model and system. As we can only evaluate a posteriori whether the model error is sufficiently small in view of the designed performance, a two stage control design procedure is proposed that is based on a design step and a robust performance evaluation step. By gradually increasing the nominal design bandwidth, the maximum achievable robust performance is obtained via trial-and-error. The two steps are subsequently elaborated.

4.5.2 Design of a weighting function trajectory

The controller $C_{\nu_b^0}$ is present in the loop and the goal is to design a controller that establishes the desired performance for the nominal model $\hat{P}$ and a similar performance for the plant P. Now the question is, having available a controller

[2] In [69] this problem is referred to as cautious controller enhancement of a high order system based on an approximate (low order) model.

$C_{\nu_b^0}$, how to choose $\nu_b^1 > \nu_b^0$ such that $C_{\nu_b^1}$ achieves an enhanced performance for $\hat{P}$ *and* the plant P.

As holds for loop shape design methods in general, the choice of ν_b is heuristic in nature and depends on how confident the designer is about the nominal model. As discussed in chapter 3, the loop shape weighting accounts for performance enhancement for a double integrator and the optimization step accounts for resonance modes in the cross-over frequency region, captured by the model. The more confident one is that the model describes resonances adequately, the larger the value of ν_b is assigned.

A feasible way is to designate a sequence of weightings corresponding with a gradually increasing value of ν_b and pick the corresponding (optimization-based) controller that provides a good trade-off between performance enhancement and robustness.

4.5.3 Performance evaluation

Although the controller resulting from the optimization problem in definition 4.3.1 is known to have optimal robustness properties, there is no guarantee that robust performance is achieved. A necessary additional step in the design procedure is to evaluate whether the designed controller achieves a similar performance for the system, prior to controller implementation. As we have introduced in chapter 2, a controller C_{ν_b} achieves a robust performance in case the following inequality is satisfied:

$$\Gamma_{\text{lo}} \leq |J(P, C_{\nu_b})| \leq \Gamma_{\text{up}}, \quad \forall\ P \in \mathcal{P},\ \forall\ \omega. \tag{4.10}$$

where $\Gamma_{\text{lo}}, \Gamma_{\text{up}}$ are prespecified performance magnitude bounds and $\mathcal{P}$ reflects available system knowledge, e.g. a high order LTI model or a frequency response of the physical system. In case one is confident about the accuracy of $\mathcal{P}$ reflecting the system, the above mentioned evaluation is straightforward. In case $\mathcal{P}$ constitutes a set of finitely or infinitely many feasible system representations, performance evaluation might wind up a laborious task.

As we want to try simple things first, frequency response measurements, obtained from an experimental Compact Disc mechanism, are validated in view of evaluation of robust performance in the next chapter. Based on the outcome of the validation, further direction towards robust performance evaluation will be given at the end of chapter 5.

4.6 Summary

A two stage model-based control design procedure is proposed that enables design of controllers having restricted complexity employing low order models, while achieving an enhanced performance for the system. Specific feature is that the design systematically explores the limitations imposed by the mismatch between model and system. The first step is to enforce an enhancement towards the desired performance via weighting function design based on loop shape arguments, followed by an optimization based design that is known to be optimally robust with respect to perturbations of normalized right coprime factors of the model, and hence anticipating model imperfections. The second step is evaluation of performance achieved for the system, based on available system knowledge.

The largest possible performance enhancement that can be achieved for the system depends not only on the design procedure but also on the models underlying the design. In line with the distinction between tunable and non-tunable model errors approximate identification of nominal models is addressed in chapter 6 and identification of model error bounds in chapter 7.

Chapter 5

Nonparametric identification of a mechanical servo

5.1 Introduction

In the control design procedure outlined in the previous chapter an approximate model is used for an optimization-based control design and an accurate system representation is subsequently used to evaluate the performance achieved for the system. Robustness properties of the proposed design procedure strongly depend on the accuracy of the system representation that is used for evaluation of performance.

In an industrial application area of electro mechanical servo systems, a fast (and hence cheap) way of obtaining accurate system representations is measurement of the system frequency response employing a dynamic signal analyzer ([44]). A signal analyzer provides the model builder with a large experimental freedom in terms of frequency range and resolution. In addition, commercial interests are not endangered (in contrast to plants that operate in process industry) and measurement time is relatively short (minutes) for high bandwidth servo systems. A signal analyzer produces frequency response measurements obtained via Fourier transformation of finite length time domain data sequences. As frequency responses are constructed by averaging on line, performed in a recursive manner, an arbitrarily large number of (Fourier transformed) time domain data is underlying the estimate. The number of time domain data points underlying a frequency response estimate virtually approaches the case that errors due to noise are no longer considered substantial.

In this chapter we address nonparametric identification of linear time invariant models and validation in view of their intended use as a basis for evaluation

of performance of the system in conjunction with a yet to be implemented controller. Validation of nonparametric models is performed experimentally for the radial actuator of a compact disc servo mechanism (described in chapter 3) utilizing a dynamic signal analyzer [44]. The contents are as follows.

In section 5.2 the estimation of frequency responses based on periodogram averaging is addressed. In section 5.3 the validation strategy is elucidated. The experiment design and implementation aspects of digital controllers are described in section 5.4. The results are shown and evaluated in section 5.5 and feasible explanations of the observed results are discussed in section 5.6. This chapter is concluded in section 5.7 where direction is given to further elaboration.

5.2 Frequency response estimation via periodogram averaging

5.2.1 Periodogram averaging

We consider a SISO discrete time, stable, linear time invariant system $P(q)$, a known input signal $u(t)$ and a disturbance $d(t)$ that produce an output $y(t)$, obeying the system equation

$$y(t) = P(q)u(t) + d(t), \quad -\infty < t < \infty, \tag{5.1}$$

where d represents an independent realization of an identically distributed random process having zero mean ($E\{d(t)\} = 0$) and variance σ_d^2. The block diagram of figure 5.1 depicts the system according to (5.1). The topic of this section is to produce an estimate of the systems frequency response $P(e^{j\omega})$ at a finite number of prespecified frequencies, based on measurements of (finite length) time domain data sequences $\{u(t), y(t)\}, t \in \{0, \ldots, N-1\}$. We recall from chapter 2 that signals are considered to be quasi-stationary, which enables us to treat deterministic and stochastic signals in a unified manner.

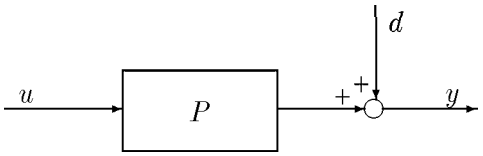

fig. 5.1: General identification setting.

Measurements of the input and output signals $\{u(t'), y(t')\}$ are taken during an

observation time $t' \in \{0, \ldots, N_o - 1\}$ and are collected as a batch of nonoverlapping sequences of data $\{u^i(t), y^i(t)\}$, $i = 1, \ldots, M$ of equal length N, written as

$$u^i(t) := w(t)u((i-1)N + n_i + t) \tag{5.2}$$
$$y^i(t) := w(t)y((i-1)N + n_i + t) \tag{5.3}$$

where $w(t) > 0$, $t \in \{0, \ldots, N-1\}$ denotes the window used during data measurement and i, $N \in \mathbb{Z}^+$ and $n_i \in \mathbb{Z}^+ \cup \{0\}$. The role of windowing the data will be discussed in the following section.

We allow for data sequences to be measured noncontiguously, indicated by the index n_i, which reflects the total number of data samples that are intermediate between data segments up to the i-th segment. In case M sequences are measured, then the total observation time must at least incorporate $N_o = MN + t_{d,M}$ samples. The Discrete Fourier Transforms of $u^i(t)$ and $y^i(t)$ are respectively defined as

$$U^i(e^{j\omega_k}) := \frac{1}{\sqrt{N}} \sum_{t=0}^{N-1} u^i(t)\, e^{-j\omega_k t}$$
$$Y^i(e^{j\omega_k}) := \frac{1}{\sqrt{N}} \sum_{t=0}^{N-1} y^i(t)\, e^{-j\omega_k t}$$

where $\omega_k = \frac{2\pi k}{N}, k = \{0, \ldots, N-1\}$ and $i \in \{1, \ldots, M\}$. $U^*(.), Y^*(.)$ denote the complex conjugate. A nonparametric estimate $\widehat{P}(e^{j\omega})$ of $P(e^{j\omega})$, based on observations of time domain sequences $\{u^i(t), y^i(t)\}$, is then obtained as

$$\widehat{P}(e^{j\omega_k}) = \frac{\sum_{i=1}^{M} (U^i(e^{j\omega_k}))^* Y^i(e^{j\omega_k})}{\sum_{i=1}^{M} (U^i(e^{j\omega_k}))^* U^i(e^{j\omega_k})}. \tag{5.4}$$

An estimate $\widehat{P}(e^{j\omega_k})$ according to (5.4) is expressed as the quotient of estimates of the cross spectral density of $u(t)$ and $y(t)$ and the auto spectral density of $u(t)$, also known as the periodogram (see [55], [60], [8]).

The motivation to consider periodogram averaging for frequency response estimation is that commercially available apparatus for measurement of spectral densities based on time domain data (signal analyzers), compute estimates via periodogram averaging. As computational effort is less elaborate — compared to for instance estimation of cross-correlation functions and subsequent Fourier

transformation — and as the number of data points virtually tends to infinity due to on-line averaging, signal analyzers provide very powerful means for accurate frequency response estimation.

5.2.2 Properties of the averaged periodogram

In this section we investigate properties of the averaged periodogram as a spectral density estimate in terms of bias, variance and the effect of unknown input signals.

We consider the cross spectral density $\Phi_{yu}(e^{j\omega})$, defined as

$$\Phi_{yu}(e^{j\omega}) := \lim_{N\to\infty} \sum_{\tau=-(N-1)}^{N-1} R_{yu}(\tau)e^{-j\omega\tau},$$

provided the sum exists, where $R_{yu}(\tau)$ is the the cross-covariance of two quasi-stationary signals $\{u(t), y(t)\}$, as is defined in chapter 2, expression (2.1)

$$R_{yu}(\tau) := \lim_{N\to\infty} \frac{1}{N} \sum_{t=0}^{N-1} E\{y(t)u(t-\tau)\}. \tag{5.5}$$

An estimate of Φ_{yu} is obtained via averaging the cross-periodogram of $u^i(t)$ and $y^i(t)$ for $i = 1, \ldots, M$ [8]. Consider $u^i(t)$ and $y^i(t), i = 1, \ldots, M$, to be measurements of $\{u(t), y(t)\}$ of finite length N, as defined above. An estimate of the cross-spectral density $\Phi_{yu}(e^{j\omega})$ is then obtained as

$$\widehat{\Phi}_{yu,M}(e^{j\omega}) = \frac{1}{M} \sum_{i=1}^{M} \widehat{\Phi}^i_{yu}(e^{j\omega}), \tag{5.6}$$

being the sample mean of $\widehat{\Phi}^i_{yu}$,

$$\widehat{\Phi}^i_{yu}(e^{j\omega}) = \left(U^i(e^{j\omega})\right)^* Y^i(e^{j\omega}).$$

Asymptotic analysis of (5.6) is concerned with properties as the number of data segments M tends to infinity. The main message of this section is that spectral density estimation via averaging of the periodogram requires periodic excitation signals in order to obtain an unbiased estimate and to reduce effects of transients in the measured output signal.

Let us first address biasedness in the next proposition.

Proposition 5.2.1 *Consider the averaged periodogram of expression* (5.6) *and measured data segments* $u^i(t), y^i(t),\ i = 1, \ldots, M$, *as defined by* (5.2) *and* (5.3). *The following holds as the number of data segments* M *tends to infinity:*

$$\lim_{M\to\infty} \widehat{\Phi}_{yu,M}(e^{j\omega}) = \frac{1}{2\pi}\int_{-\pi}^{\pi} P(e^{j\xi})\Phi_u(\xi)W(e^{j(\omega-\xi)})\, d\xi. \tag{5.7}$$

Proof: *Appendix B.* □

From (5.7) it is concluded that the averaged periodogram of $u(t)$ and $y(t)$ is a convolution of $P(e^{i\xi})$ and a weighted auto spectrum of $u(t)$, expressed as $\Phi_u(\xi)W(e^{j(\omega-\xi)})$.

In case a uniform window is used ($w(t) = 1, t \in \{0, \ldots, N-1\}$), $W(e^{j\omega})$ satisfies (found in [60] and [8])

$$W(e^{j\omega}) = \sum_{\tau=-N+1}^{N-1} \frac{N-|\tau|}{N} e^{-j\omega\tau} = \frac{1}{N}\left(\frac{\sin\frac{N\omega}{2}}{\sin\frac{\omega}{2}}\right)^2.$$

It is concluded that periodogram averaging obtained from finite length data segments provides an unbiased estimate of the system frequency response only in case an input signal is employed that satisfies $\Phi_u(\omega) \neq 0,\ \omega = \frac{2\pi k}{N}, k = 0, \ldots, N-1$ and $\Phi_u(\omega) = 0$ elsewhere. This implies that an excitation signal should be periodic with a period that fits an integer number into the window length N.

We point out a crucial difference between letting the number of data points tend to infinity ($N_o \to \infty$) and the number of data segments to infinity ($M \to \infty$). As the length of the data segments N in general will not be very large, transient responses of the system are present in every measured segment and will generally not average out in case the number of segments tends to infinity. Especially in case of badly damped systems transients are dominantly present and might deteriorate the estimate. This statement is formalized in the following

Proposition 5.2.2 *Consider measured data segments* $u^i(t), y^i(t),\ i = 1, \ldots, M$, *as defined by* (5.2) *and* (5.3). *Then in case the number* M *of data segments tends to infinity, the following holds:*

$$\lim_{M\to\infty} \frac{1}{M}\sum_{i=1}^{M} R_w(\tau)y(t_i+t)u(t_i+t-\tau) = R_w(\tau)(R_{yu_s}(\tau) + R_{ru}(\tau)).$$

Proof: *Appendix B.* □

The cross-correlation $R_{ru}(\tau)$ is due to the transient effect in measured output sequences due to previous unknown input signals. In case $u(t)$ is chosen as a realization of a white noise, it is easily verified that $R_{ru}(\tau) = 0$ which means that asymptoticly the effect of unknown inputs on the cross-periodogram, attained by averaging over data segments, is averaged out. Nevertheless, the estimate should be performed using a large number of data segments as unknown inputs introduce an additional noise term to the estimation problem. Concluding, averaging over a number of data segments employing a random excitation signal ($R_u(\tau) = 0, \tau \neq 0$) introduces an additional noise term that is to be averaged out and, more seriously, introduces a bias in case of a coloured excitation ($R_u(\tau) \neq 0, \tau \neq 0$).

The noise contribution due to unknown initial conditions when averaging over data segments, may be substantially reduced by employing periodic excitation. In case periodic excitation signals are applied to the system prior to measurement, the transient effects are tending to 0 as the system reaches a steady state. So when excitation is enforced, start of the measurement should be postponed until transient responses are presumed to have vanished.

It is noted that in case a periodic excitation signal u with period length N is utilized, which implies that $U^i(e^{j\omega}) = U^{i+1}(e^{j\omega}), i = 1, \ldots, M-1$ holds, the expressions of the averaged periodogram (5.4) can be simplified to

$$\widehat{P}(e^{j\omega}) = \frac{1}{M} \sum_{i=1}^{M} \frac{Y^i(e^{j\omega})}{U^i(e^{j\omega})}$$

which boils down to averaging the ETFE of each data segment.

In order to analyse the variance we follow the work of [90] and [8] for establishing an asymptotic distribution of the DFT of a random process having power spectrum σ_d^2. It is not our goal to derive an explicit expression for the variance of the second term of (5.6) but only to make plausible that the variance tends to 0 for $M \to \infty$.

Now the stochastic part is expressed as

$$\widehat{\Phi}_{yu,i}(e^{j\omega}) = \frac{1}{N} \sum_{\tau=-(N-1)}^{N-1} \sum_{t=(i-1)N}^{iN-1} w^i(t) w^i(t-\tau) d(t) u(t-\tau) e^{-j\omega\tau}$$

where $w^i(t)w^i(t-\tau)u(t-\tau)$ denotes a window of $d(t)$. In [8] it is shown that a windowed realization of a random proces $d(t)$ is asymptotically normally distributed ($N \to \infty$) where the variance is is expressed in σ_d^2 and $w^i(t)w^i(t-\tau)u(t)$.

It is assumed that the stochastic part of $\widehat{\Phi}_{yu,i}(e^{j\omega})$ is identically distributed and independent for $i = \{1, \ldots, M\}$. In that case the variance of $\widehat{\Phi}_{yu}(e^{j\omega})$ equals $\frac{1}{M}$ times the variance of $\widehat{\Phi}_{yu,i}(e^{j\omega})$.

5.2.3 Periodic excitation

Perhaps the most important observation in this section is that frequency response estimation attained by means of periodogram averaging, requires periodic excitation in order to get unbiased estimates. This rules out experiments using realizations of a random noise process for excitation, as is frequently employed in frequency response measurement.

A second observation is that averaging over data segments introduces an additional error term in the estimate as a result of the measured response to unknown input signals. The error contribution depends on the input signal used and, of course, the plant dynamics. In case the plant has badly damped poles (which is typical for a mechanical system having resonance modes) the contribution to the measured output may be substantial, at least for small values of t. Consequently, the cross-correlation $\hat{R}^i_{yu}(\tau)$ is noise corrupted for small values of τ (provided $R_u(\tau) = 0, \tau \neq 0$, otherwise $\hat{R}^i_{yu}(\tau)$ is biased) which implies this will affect the cross-periodogram for high frequencies. As accurate modelling of resonance modes is essential in line of consecutive control design, especially in the higher frequency region, it is imperative to reduce the effect of transients in the output. This, again, favours utilization of periodic excitation which enables to bring the system in a dynamic steady-state prior to measurement, thus reducing transient effects on the cross-periodogram estimate.

Utilization of periodic excitation signals has been advocated by Schoukens and Pintelon ([64, 68]) motivated by several advantageous features. We name the ones that are most important. Effects of measurement noise can be reduced by means of averaging of the signals, either directly of the time domain signals or on the DFT's; the noise contribution at frequencies that are not excited can straightforwardly be eliminated in this manner. Large numbers of time domain data can easily be reduced to a relatively small number of time or frequency domain data by means of averaging. In addition, data available from separate measurements are easily combined by employing the DFT which makes data acquisition much less dependent on memory restrictions of the measurement equipment. In chapter 9 we will address the combination of measurement data obtained from different radial actuators, making fruitful use of this feature. Also DFT signal representations allow for easy data manipulation in terms of filtering (multiplication opposed to convolution) where the effect of unknown

initial conditions can be reduced by employing periodic excitation.

5.3 Validation strategy

Our main objective in this chapter is to validate frequency response measurements of a radial actuator of a Compact Disk servo mechanism, in view of prediction of performance for a newly designed controller. Performance is expressed in chapter 2 in terms of $|J(P,C)|$; in this chapter we will confine performance evaluation to the magnitudes of $P(I+CP)^{-1}$ and $(I+CP)^{-1}$. As the responses are specified only in discrete frequency points the validation is restricted to these frequencies.

Validation of frequency response estimates is based on formulation of the following two questions:

1. Does a frequency response estimate provide an *exact* description of the system frequency response in the prespecified frequency points?

This question in itself does not seem to be a sensible one as exact plant knowledge is not available for validation. However, in case a frequency response is presumed to exactly describe the system a straightforward validation is to verify whether several frequency responses, obtained under different experimental conditions, are in accordance with each other. In case several responses obtained under different experimental conditions are different, one frequency response obviously is not sufficient to give an adequate description of the system.

In case several frequency responses are not in accordance with each other and therefore individually are inadequate system descriptions, this does not imply that they are inadequate in view of describing the system in the presence of a feedback controller. Hence, the second question is phrased as follows:

2. In case a frequency response estimate does *not* provide an exact system frequency response description, is it still suitable for evaluation of performance in view of a yet to be implemented controller ?

Invalidation in view of control design is an *a posteriori* evaluation and, moreover, becomes much more elaborate in case the control design is incorporated in the validation procedure. To circumvent a needless elaborate validation with respect to utility for high performance control design, a validation strategy is defined. Before we do so, we clarify the experimental configuration.

We recall from chapter 3 that the radial actuator of a swing-type Compact Disk mechanism is marginally stable and therefore has to operate in the presence of a stabilizing controller. Consequently, identification of the radial actuator has the feature that measurement data are to be acquired from the system in a closed loop configuration. A block diagram of a feedback configuration[1], consisting of a plant P and a (stabilizing) controller C is schematically depicted in figure 5.2.

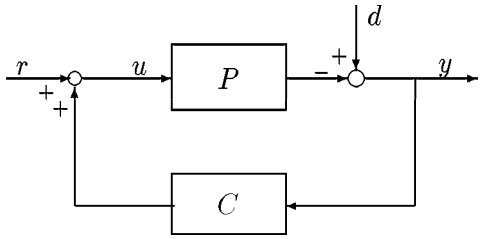

fig. 5.2: Block diagram of the experimental configuration of a Compact Disk mechanism of the swing-arm type, denoted P, and a controller C. The signal r is added for excitation purposes, d is a disturbance, u is the system input and y the system output.

The validation strategy is defined as follows.

Definition 5.3.1 Validation in view of performance evaluation: *consider two controllers C_0, C_1 that are known to stabilize the system and C_1 is known to achieve a larger bandwidth for the feedback system than C_0. Construct a frequency response of the system $\widehat{P}_0 := \widehat{PS}_0(\hat{S}_0)^{-1}$ where $\widehat{PS}_0$, $\hat{S}_0$ are estimated with C_0 in the loop via periodogram averaging in conjunction with periodic excitation.*

Conduct frequency response measurements $\hat{S}_1$ of $(1 + C_1P)^{-1}$ and $\widehat{PS}_1$ of $P(1 + C_1P)^{-1}$ with controller C_1 in the loop. Verify whether the achieved performance resembles the predicted performance, specified in terms of $(1 + C_1\widehat{P}_0)^{-1}$ and $\widehat{P}_0(1 + C_1\widehat{P}_0)^{-1}$, by evaluation of the following errors:

$$\left| (\widehat{PS})_1 - \widehat{P}_0 \left(1 + C_1\widehat{P}_0\right)^{-1} \right| < \delta(\omega) \tag{5.8}$$

[1]Note that the configuration in figure 5.2 only differs with the feedback configuration of the Compact Disk mechanism, described in chapter 3, with respect to the presence of an excitation signal at the system input.

and

$$\left|\hat{S}_1 - \left(1 + C_1\widehat{P}_0\right)^{-1}\right| < \delta(\omega) \tag{5.9}$$

at specified frequencies.

In case $C_0 = C_1$ the evaluation boils down to whether $PCS + S = 1$ holds.

The validation in view of control design requires information about the actual closed loop transfer function obtained from identification of frequency responses of $(1 + C_1P)^{-1}$ and $P(1 + C_1P)^{-1}$ according to the same procedure used for identification of $(1 + C_0P)^{-1}$ and $P(1 + C_0P)^{-1}$. So, actually the model $(\widehat{PS}_0, \hat{S}_0)$ is invalidated by another model $(\widehat{PS}_1, \hat{S}_1)$.

5.4 Carrying out the experiments

5.4.1 Measurement using a signal analyzer

A signal analyzer [44] provides facilities to generate an analog excitation signal and to measure two signals for estimation of frequency response models. Analog time signals are sampled at a sampling rate of 256 kHz having length $N = 2048$ and are anti aliasing filtered with a roll off at a frequency of 100 kHz; digital filters are used for anti aliasing in case data sequences are obtained via downsampling. The sample time of a (downsampled) data sequence may range from 3.9μsec to 38.16 sec, corresponding to a frequency resolution ranging from 12.8μHz to 125 Hz.

The discrete time signals are Fourier transformed to 1024 frequency domain samples. Only 801 frequency domain samples are used for calculation of a frequency response. The merits of the analyzer are that measurement and Fourier transformation can be repeated an arbitrarily large number of times for averaging. So the analyzer applies segmentation of measured data in segments of 2048 time domain samples and due to the averaging mechanism is capable of measuring a virtually infinite number M of 2048 samples.

Swept sine excitation

Periodic excitation signals are applied by means of sine sweep measurements, where the frequency of a sinusoid of prespecified magnitude is "swept" across the frequency range of interest. Frequency response measurements performed in this way may take a long duration of measurement. To have a basis for comparison with previously performed measurements frequency responses are measured in both cases starting from 100 Hz up to 10.1 kHz with a linear resolution of 12.5 Hz.

Two variables largely influence the estimation result: the integration time and the number of averages per frequency point. The integration time is the time span during which 2048 time samples are measured. It can be assigned a constant value during the sweep, but it is automatically adjusted to an integer number of times the length of one period. Hence the input spectrum is a spectral line at a specified frequency and the length of the time window is adjusted such that an unbiased estimate is obtained.

The periodogram of $\Phi_{yu}(e^{j\omega})$ is asymptotically efficient meaning that the variance asymptotically goes to 0. This can be established by choosing a large number of averages per frequency point (see also [60]) which inevitably increases the duration of the measurement.

The integration time is set to 500 msec and the number of averages is set to 3. The magnitude is set to 200 mV. A disadvantage of sine sweep excitation is the long duration of the measurement. One sweep measurement takes about 40 minutes.

5.4.2 Implementation of digital controllers

The experiments have been performed on the radial loop of a swing-arm type Compact Disk servo mechanism, as discussed in chapter 3. For implementation of digital controllers and excitation signals a TMS320C25 digital signal processor is used [16]. As the AD-board of the signal processor has no anti aliasing filters an analog 4th order filter having a roll off at a frequency of 10 kHz is used for the controller input signal.

The experiments are performed with three different controllers in the loop that establish an increasing bandwidth for the system: a 4th order controller C_{dr} is obtained from loop shaping and 8th order controllers C_{30} and C_{62} that are designed utilizing the $\mathcal{H}_\infty$ loop shape design procedure discussed in chapter 4; a constant weighting $W = 3,0$ resp. $W = 6,2$ and an 8th order nominal model have been used for the design, see [15]. In figure 5.3 the Bode figures of these controllers are shown. The state space representations of these controllers are given in appendix C.

As the controllers are implemented using a digital signal processor at a sampling frequency of 25 kHz, the performance of the implemented controller may deviate from the designed one as a result of saturation or quantisation of the control signals. In view of the closed loop invalidation, we must be confident that the implemented controller resembles the actual behaviour of the controller.

To reduce the effects of quantization the signals used in the calculation of the controller output have to be properly scaled. The dSPACE signal processor [16] provides l_1 scaling facilities of the states of an open loop controller. This

gives bad scaling results in case the controller contains an integrator. Since the controllers that are implemented contain an integrator closed loop scaling is preferred (see also [78]).

As adequate l_1 scaling depends on the controller present in the loop and the characteristics of the signals acting on the loop, separate scaling has to be performed for every controller and excitation signal. Calculation of the scaling factors is presented in appendix C.

5.5 Invalidation results

5.5.1 Open loop invalidation

In this section the frequency responses of the open loop system $\widehat{P}_C = \widehat{PS}_C \cdot \hat{S}_C^{-1}$ obtained under different experimental conditions are compared. The different experimental conditions are confined to experiments with different controllers in the loop using the same excitation. To ensure unbiased estimates according to the analysis of section 5.2.2, the excitation signal is chosen as a swept sine across the specified frequencies using a rectangular time window.

Figures 5.4, 5.5 and 5.6 each show two Bode plots of frequency responses of the radial actuator estimated with two different controllers C_i and C_j as presented in section 5.4.2 in the loop. Along with the frequency responses the values of $|\widehat{P}_{C_i} - \widehat{P}_{C_j}|$ and $\arg(\widehat{P}_{C_i}) - \arg(\widehat{P}_{C_j})$ are depicted.
From the results shown it is deduced that frequency responses of the radial actuator obtained with different controllers show an error in terms of $|\widehat{P}_{C_i} - \widehat{P}_{C_j}|$ and $\arg(\widehat{P}_{C_i}) - \arg(\widehat{P}_{C_j})$ that is larger in case the controllers present in the loop during measurement establish a larger bandwidth; the differences in figure 5.4 are less than in figure 5.5 and figure 5.6.

5.5.2 Closed loop invalidation

In this section the predicted and measured performance are compared according to expression (5.9). The closed loop performance is expressed in terms of the sensitivity function and the plant times sensitivity function.

Invalidation of frequency responses in conjunction with a known controller might lead to erroneous conclusions in case the implemented controller differs from the actual behaviour during experiments, as already mentioned in section 5.4.2. To evaluate the behaviour of the implemented controller a frequency response estimate of the controller is made.

The estimation of the controller is based on estimates of $(I + CP)^{-1} CP = C(I + PC)^{-1} P = CPS_i$ and $(I + PC)^{-1} P = PS_i$. The controller is deter-

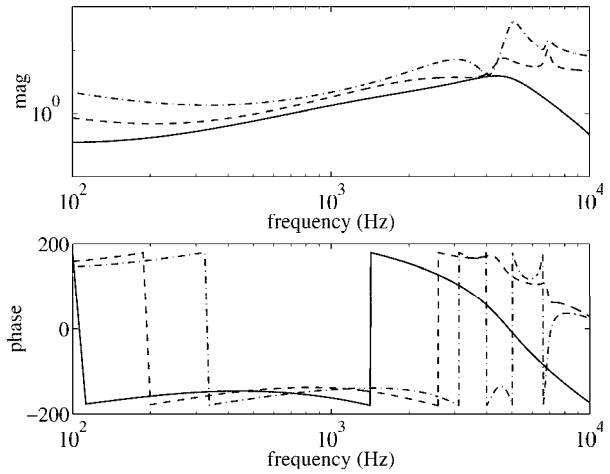

fig. 5.3: Controllers in the loop: C_{dr} (solid) of order 4, C_{30} (dot) and C_{62} (dash-dot), both of order 8

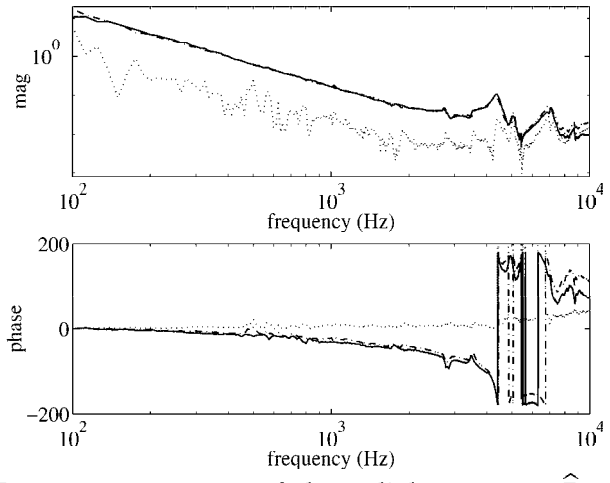

fig. 5.4: Frequency responses of the radial actuator: $\widehat{P}_{C_{30}}$ (solid), $\widehat{P}_{C_{dr}}$ (dash-dot) and $|\widehat{P}_{C_{30}} - \widehat{P}_{C_{dr}}|$ (dot,upper), $\arg(\widehat{P}_{C_{30}}) - \arg(\widehat{P}_{C_{dr}})$ (dot,lower).

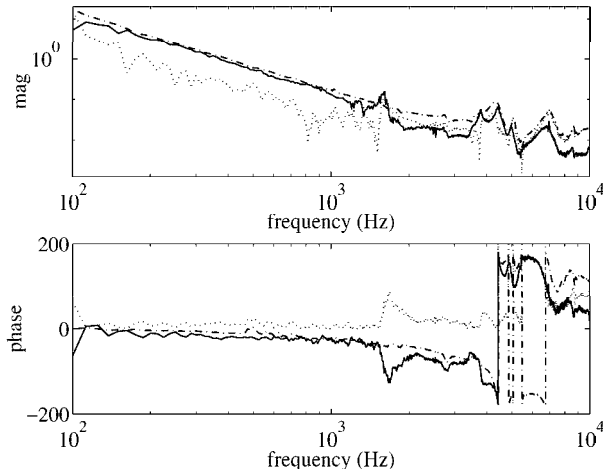

fig. 5.5: Frequency responses of the radial actuator: $\widehat{P}_{C_{62}}$ (solid), $\widehat{P}_{C_{dr}}$ (dash-dot) and $|\widehat{P}_{C_{62}} - \widehat{P}_{C_{dr}}|$ (dot, upper) and $\arg(\widehat{P}_{C_{62}}) - \arg(\widehat{P}_{C_{dr}})$ (dot, lower).

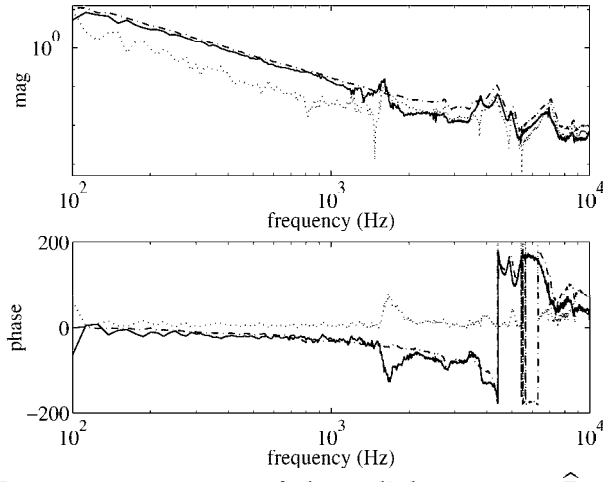

fig. 5.6: Frequency responses of the radial actuator: $\widehat{P}_{C_{62}}$ (solid), $\widehat{P}_{C_{30}}$ (dash-dot) and $|\widehat{P}_{C_{62}} - \widehat{P}_{C_{30}}|$ (dot, upper) and $\arg(\widehat{P}_{C_{62}}) - \arg(\widehat{P}_{C_{30}})$ (dot, lower).

mined as

$$\hat{C} = CPS_i(PS_i)^{-1}.$$

Figures 5.7 and 5.8 show the Bode diagrams of the designed and estimated frequency responses of resp. C_{30} and C_{62}. Up to approximately 1 kHz the implemented controller C_{30} coincides with the designed one, so model discrepancies up to 1 kHz are most likely not the result of bad controller implementation. The frequency response estimate of C_{62} however exhibits unacceptably large deviations from its design, which can be attributed to ill-conditioned implementation. It has to be noted that controller C_{62} is a bad one in view of limited controller action at high frequencies. The discrepancy in phase lag for high frequencies of both controllers is attributed to computational delay due to digital controller implementation.

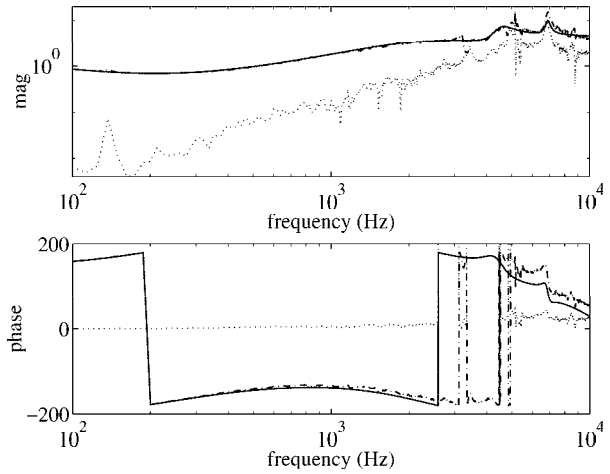

fig. 5.7: Controller C_{30}: designed (solid), a frequency response estimate $\hat{C}_{30}$ of the implemented controller (dash-dot) and the difference $|C_{30} - \hat{C}_{30}|$ (dot, upper), $\arg(C_{30}) - \arg(\hat{C}_{30})$ (dot,lower).

Figures 5.9 and 5.10 show the Bode diagrams of the sensitivity functions, measured and predicted with the same controllers C_{dr} resp. C_{30}. They indicate a larger difference between measured and predicted sensitivity in case of controller C_{30} than in case of C_{dr}. Bode diagrams of the plant times sensitivity PS, which are shown in appendix C, exhibit a similar difference between measured and constructed plant times sensitivity.
Figure 5.11 shows the sensitivity measured with controller C_{dr} in the loop and predicted based on frequency responses obtained with C_{30} in the loop.
The discrepancies between predicted and measured performance are evident.

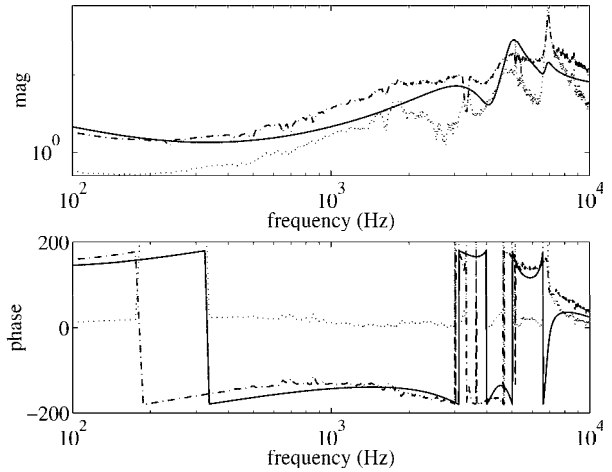

fig. 5.8: Controller C_{62}: designed (solid), a frequency response estimate $\hat{C}_{62}$ of the implemented controller (dash-dot) and the difference $|C_{62} - \hat{C}_{62}|$ (dot, upper), $\arg(C_{62}) - \arg(\hat{C}_{62})$ (dot,lower).

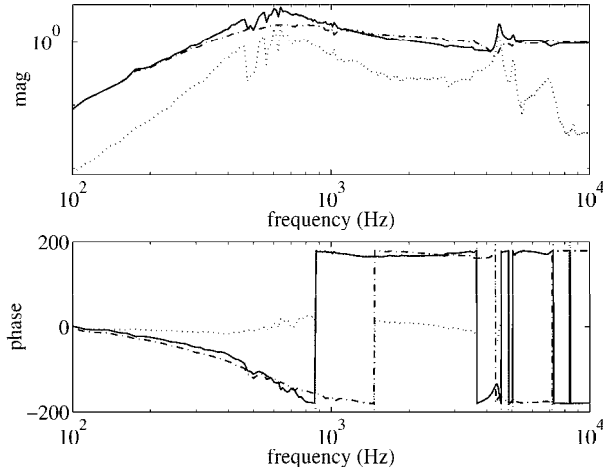

fig. 5.9: Sensitivity: $\hat{S}_{C_{dr}}$ (dash-dot) and $\hat{S}_{C_{dr}}(\hat{S}_{C_{dr}} + C_{dr}\widehat{PS}_{C_{dr}})^{-1}$ (solid)

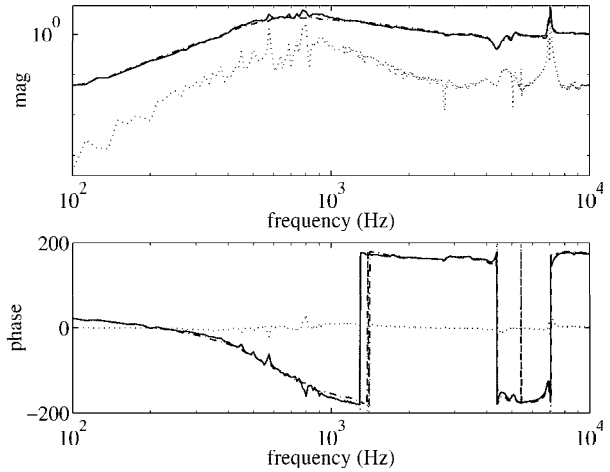

fig. 5.10: Sensitivity: $\hat{S}_{C_{30}}$ (dash-dot) and $\hat{S}_{C_{30}}(\hat{S}_{C_{30}} + C_{30}\widehat{PS}_{C_{30}})^{-1}$ (solid)

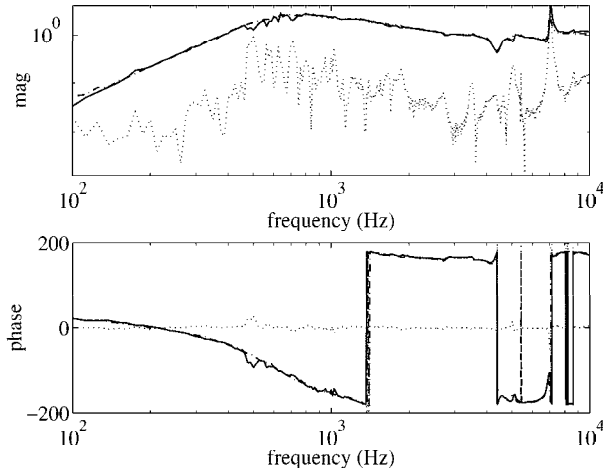

fig. 5.11: Sensitivity: $\hat{S}_{C_{dr}}$ (dash-dot), $\hat{S}_{C_{30}}(\hat{S}_{C_{30}} + C_{dr}\widehat{PS}_{C_{30}})^{-1}$ (solid), $|\hat{S}_{C_{dr}} - \hat{S}_{C_{30}}(\hat{S}_{C_{30}} + C_{dr}\widehat{PS}_{C_{30}})^{-1}|$ (dot, upper) and $\arg(\hat{S}_{C_{dr}}) - \arg(\hat{S}_{C_{30}}(\hat{S}_{C_{30}} + C_{dr}\widehat{PS}_{C_{30}})^{-1})$ (dot, lower).

Two observations are made. Firstly, the discrepancies are larger in case the controller used during experimentation enables a higher bandwidth for the closed loop system. Secondly, the predicted sensitivity functions are typically "nonsmooth" compared to the measured ones and discrepancies are predominantly present in the cross-over and high frequency region.

For controller C_{30}, depicted in the Bode diagram of figure 5.7, we may deduce that frequency responses of the sensitivity transfer function are not invalidated due to bad controller implementation alone, at least up to approximately 1.5 kHz. A similar observation holds for the validation of the plant times sensitivity according to expression (5.8); the corresponding Bode diagrams are shown in appendix C for brevity of presentation.

Let us consider the error $|\hat{S}_{C_j} - \hat{S}_{C_j}(\hat{S}_{C_j} + C_j\widehat{PS}_{C_j})^{-1}|$ for C_{dr} and C_{30}. We do not regard the sensitivity measured and constructed with controller C_{62}, depicted in the Bode diagram of figure 5.8, for the reason that differences that may occur can not be attributed unambiguously to invalidity of system frequency responses. The measured and constructed sensitivity in figures 5.9 and 5.10 exhibit relatively large discrepancies in amplitude in the cross-over frequency region and for the higher frequencies. In case the controller achieves a higher bandwidth the discrepancies obviously seem more evident (compare figures 5.9 and 5.10).

We emphasize that frequency response measurements of a controller obtained via an estimation procedure that is similar to the one as performed for the system, indicate that one must be cautious with the presumption that exact knowledge of the controller is available. As we will see in chapter 9, similar observations can be made in a parametric identification of the Compact Disk mechanism.

In figure 5.11an error $|\hat{S}_{C_{dr}} - \hat{S}_{C_{30}}(\hat{S}_{C_{30}} + C_{dr}\widehat{PS}_{C_{30}})^{-1}|$ is clearly present at all frequencies. The error seems larger for frequency responses estimated with a controller in the loop that achieves a higher bandwidth.

The validation procedure carried out in this section serves one single purpose, being the verification of frequency response measurements of plant times sensitivity and sensitivity of a radial Compact Disk mechanism in view of their utility for evaluation of performance (see chapter 4) for a controller that has not been implemented yet. Given the invalidated measurements, we stress that it is not explicitly our aim to find the feasible causes of the observations made, but to motivate from physical experience that we need some indication of the error contained in measurement data in order to enable a *reliable* evaluation of system performance. In the next section however we will discuss some issues that might provide an explanation for the observed differences in order to

inventorise the kind of errors that we might have to account for.

5.6 Potential causes of invalidity

In this section we discuss some issues that might and might not constitute feasible explanations for the observed errors.

MIMO configuration

As has been clarified in chapter 3, a Compact Disk servo mechanism consists of two actuators for track following in radial and focus direction of a disc where interaction between both actuators is present.

For invalidation we consider the radial part of the servo mechanism. As both actuators are marginally stable, experiments have to be performed in presence of stabilizing controllers. For validation of frequency responses of the radial servo mechanism the focus part will have influence on the results due to the closed loop configuration and the dynamic interaction. We consider the consequences of estimating SISO frequency response models in a multivariable closed loop configuration in view of the validation results. The plant P and the controller C are resp. denoted as

$$P = \begin{bmatrix} P_{11} & P_{12} \\ P_{21} & P_{22} \end{bmatrix}, \qquad C = \begin{bmatrix} C_{11} & 0 \\ 0 & C_{22} \end{bmatrix}.$$

Frequency response models of

$$S_{\text{in}} = [I + CP]^{-1}, \quad S_{\text{out}}P = [I + PC]^{-1} P$$

are estimated elementwise, where S_{in} denotes the input sensitivity and S_{out} the output sensitivity. In case of a square invertible system P, it holds that $S_{\text{out}}P = PS_{\text{in}}$. An estimate of P is obtained by element-wise calculation of $PS_{\text{in}}S_{\text{in}}^{-1}$. Here the multivariable character of the plant is ignored. After manipulation the $(1,1)$-element of PS_{in} can be expressed as

$$P_{11}\,(1 + C_{11}P_{11}^{*})^{-1} + P_{12}\,(C_{11}P_{12}^{*})^{-1}$$

where

$$P_{11}^{*} = P_{11} - C_{22}P_{12}P_{21}(1 + C_{22}P_{22})^{-1}, \quad P_{12}^{*} = P_{12} - P_{21}^{-1}(C_{11}^{-1} + P_{11})(C_{22}^{-1} + P_{22})$$

An estimate $\hat{P}_{11}$ is obtained as

$$\begin{aligned}(PS_{\text{in}})_{11}\, S_{\text{in},11}^{-1} &= P_{11} - C_{22}P_{12}P_{21}\,(1 + C_{22}P_{22})^{-1} \\ &=: P_{11}^{*} \end{aligned} \tag{5.10}$$

From (5.10) it is evident that, when discarding the multivariable closed loop configuration, a biased frequency response of the radial actuator is obtained due to interaction. The bias term however does not depend on the controller C_{11}, which means that estimation with any controller C_{11} but with the same controller C_{22} gives the same bias. Validation of consistency and in view of performance evaluation of a frequency response are therefore equally well evaluated from a biased estimate of the actuator. So validation results are not basically affected due to element-wise calculation of frequency responses. Note however that the observed invalidition results can not be attributed *directly* to the dynamics of the radial actuator.

Nonlinear plant dynamics

The physics of the radial Compact Disk actuator is known to exhibit nonlinear behaviour in case of large tracking errors, due to the nonlinear relation between light intensity and electrical current, discussed in chapter 3. We evaluate to what extent nonlinearities may explain the results. In case the plant is nonlinear two situations are distinguished as a result of the fact that identification is performed in presence of a controller.

PS and S are linear

The closed loop dynamics of the plant are linearized by the controller [2] implying that the plant times sensitivity and the sensitivity are linear. Frequency responses obtained with different (sinusoidal) excitation signals are expected to be equal. As the specific controller in the loop linearizes the system, open loop frequency responses obtained with different controllers are expected to differ. This is observed in the Bode diagrams of the frequency responses of the radial actuator in figures 5.4, 5.5 and 5.6.

The frequency responses of PS_{C_i} and S_{C_i} and the ones reconstructed with the controller C_i are also expected to be similar. From figures 5.9 and 5.10 it is evident that this is not the case for either controllers C_{dr} and C_{30}; so one may conclude that nonlinear behaviour of the actuator indeed may explain the observed differences.

[2] In fact this can be seen as a desirable property of a controller.

Using another controller C_j however may be expected to lead to different frequency response measurements for the system; this is clearly the case in figure 5.11.

PS and S are nonlinear

Suppose the closed loop plant dynamics are nonlinear. In that case frequency response estimates are linearized estimates determined by the experimental conditions, being the controller and the signals acting on the system during the experiment. As measurements have been performed using the same excitation signal we can only indicate possible nonlinearity of S based on figures 5.9 and 5.10 where the measured sensitivity S is compared to the reconstructed one in conjunction with the same controller. In appendix C Bode diagrams of the plant times sensitivity are shown for the similar case. They evidently differ in the cross over and for higher frequencies which might be explained by nonlinearity of PS and S.

We stress that nonlinear behaviour of the radial Compact Disk actuator *might* explain the validation results. However, a more thorough analysis of possible nonlinear behaviour is imperative to scrutinize the above results.

5.7 Discussion

The issue addressed in this chapter is validation of frequency response estimates of the radial part of a Compact Disk servo mechanism in view of their utility for evaluation of robust performance for any stabilizing controller. As the (marginally stable) radial actuator operates in a feedback loop, frequency responses of the plant times sensitivity and the sensitivity are obtained by means of a signal analyzer (type HP 3562A), which enables frequency response estimation based on periodogram averaging utilizing swept sine excitation. Validation of frequency response estimates is performed for the open loop dynamics (reconstructed by dividing plant times sensitivity and sensitivity) and the dynamics in conjunction with three different stabilizing controllers, as defined in definition 5.3.1. Based on experimental results, we can summarize the following outcome: frequency responses of the actuator, obtained with three different controllers in the loop and sine sweep excitation, exhibit errors that are unacceptably large in view of evaluation of robust performance for a any stabilizing controller. Frequency response estimates of the plant times sensitivity and the sensitivity are invalidated in conjunction with a known controller. Measured and predicted sensitivity functions are compared and show large discrepancies

in case frequency responses are measured with a high bandwidth controller in the loop.

The main observation is that in view of a *reliable* evaluation of performance of a radial Compact Disk mechanism, as phrased in section 4.5.3, a frequency response estimation should provide an accurate frequency response together with a quantitative measure of its validity.

In the field of system identification, techniques have recently been developed that provide a nominal model together with an upper bound of the model error, based on measurement data (a.o. [90], [59], [37]). As in any system identification method, presumptions on the system dynamics, the nature of disturbances and experimental conditions under which data are acquired, underly the development of the tools. The quoted references have employed a framework where finite length time domain data sequences are available for identification. As a result of the presumptions on available data, model error bounds are attributed to undermodelling, measurement noise and unknown initial conditions.

So basically there are two paths to construct a high order system representation based on measurement data. The first one is frequency response measurement utilizing a signal analyzer. Although the number of (time domain) data underlying the frequency response estimate virtually tends to infinity, the frequency responses exhibit limited reliability in view of performance analysis, as shown in this chapter. An alternative path is to construct a complex model (or frequency response) in conjunction with a bound on the error, which enables a robustification of the performance analysis with respect to inaccurate system knowledge. Both paths are schematically depicted in figure 5.12 where the left branch depicts the identification of frequency responses based on a virtually "infinite" data length and the right branch reflects the identification framework that underlies available error bounding techniques.
We make two comments regarding the utilization of available model error bounding techniques in view of robust performance analysis.

1. Although a frequency response estimate is of limited accuracy, they are very accurate as a direct consequence of the large number of averages used for estimation. Available model error bounding procedures have not (yet) been applied based on a number of data points similar to that underlying an analyzer estimation. To enable a fair justification for employing model error bounds, at least a similar amount of data points should be underlying the bounding procedure.

2. In chapter 2 parametric system uncertainty sets $\mathcal{P}_R$ have been introduced that provide an adequate way of representing a system set by means of a

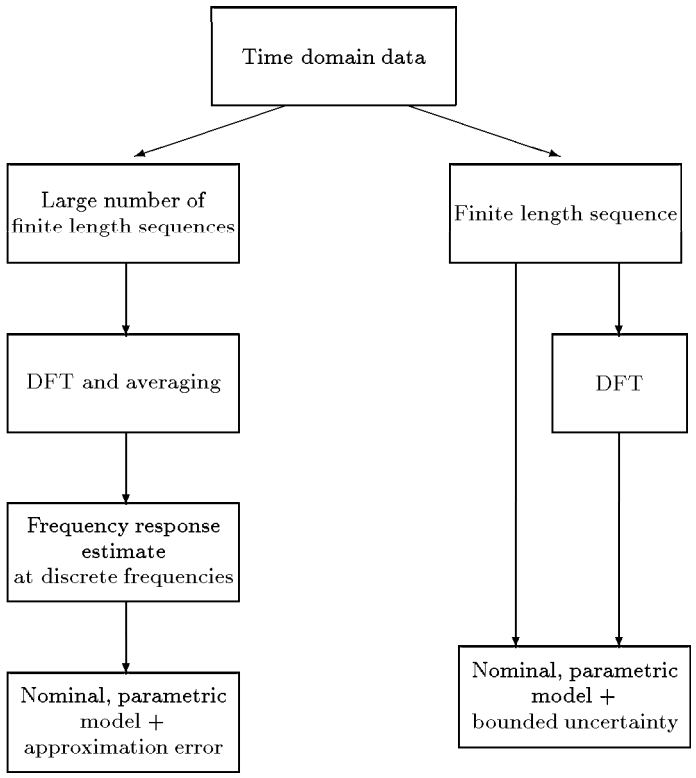

fig. 5.12: Identification of nonparametric models by means of averaging, utilizing a signal analyzer (left branch), and identification of model error bounds (right branch).

model error bound. It is however unclear in what way a structured system uncertainty set can be employed in view of robust performance analysis as phrased in section 4.5.3.

Data based construction of nonparametric and parametric model error bounds is the topic of chapter 7. Identification of parametric models based on frequency response measurements is addressed in chapter 6.

Chapter 6

Approximate identification of parametric models

6.1 Introduction

In this chapter we address the construction of linear time invariant, parametric models of low order from measurement data, also referred to as approximate system identification. As suggested by the chapter title, aspects of approximate modelling and system identification come together in this chapter. Our motivation for constructing *approximate* models is to enable design of restricted complexity controllers via model-based control design employing low order models, as we have discussed in chapter 4, section 4.2. The problem has been conceived in chapter 2 from an approximate modelling point of view, using fractional system representations.

The merger of approximation and identification in feedback relevant modelling problems has been incented by the recognition that approximate identification for control design and model-based control design are closely intertwined. Illuminating treatisis on the subject are given by [85] and [29].

The chapter outline is as follows. The identification framework, based on frequency domain representations of measurement data, is addressed in section 6.2. Identification of parametric fractional model representations is addressed in section 6.3. The formulation of a feedback relevant approximate identification problem in section is elaborated in section 6.4; an alternative approximate identification is proposed in order to account for prior knowledge of a yet to be designed controller in the approximation. Finally, some issues on excitation signal design are discussed in section 6.5.

6.2 Identification framework

System identification has a broad range of application areas for constructing mathematical models, not in the least due to the appealing feature that models are solely inferred from physical observation, not from presumption. Well-known accounts on the subject of system identification are given by [55] and [76]. In this section we address the identification framework of this research.

6.2.1 Experimental configuration

In chapter 5 we have clarified that measurement experiments on a Compact Disk swing-arm type mechanism have to be performed in the presence of a (stabilizing) feedback controller. Let us reconsider the block diagram of figure 5.2. The signal r is added to the experimental set up for excitation purposes and is available for measurement. The output signal y is fed back to the compensator C and induces a correlation between the input signal u and the disturbance d. From the block diagram in figure 5.2 the following signal relations are derived

$$\begin{aligned} u &= (I+CP)^{-1}r - (I+CP)^{-1}Cd \\ y &= P(I+CP)^{-1}r + (I+CP)^{-1}d. \end{aligned}$$

A well-known fact in identification literature is that in case an estimate of P is solely based on measurements of the loop signals $\{u, y\}$, also known as the direct method, that the asymptotic estimation of the system P is biased. A number of techniques has been developed to enable unbiased identification based on closed loop measurement data [55, 69]. One way to deal with estimation based on closed loop measurements is to estimate models of $P(I+CP)^{-1}$ and $(I+CP)^{-1}$, which is feasible as $\{r, u, y\}$ are available for measurement and r is presumed uncorrelated with d. The resulting estimates are subsequently used to construct a model of P. We recall from chapter 5 that the validation of frequency responses attained via a signal analyzer, is performed in a similar manner: frequency response estimates of $P(I+CP)^{-1}$ and $(I+CP)^{-1}$ are obtained via open loop identification based on averaging of Y_N^i/R_N^i resp. U_N^i/R_N^i; an unbiased estimate is subsequently attained by pointwise division of the frequency response estimates of $P(I+CP)^{-1}$ and $(I+CP)^{-1}$. In this chapter, averaged frequency response estimates Y_N^i/R_N^i resp. U_N^i/R_N^i serve as a basis for parametric identification, employing coprime factor model parametrizations.

6.2.2 Frequency domain data representation

Consider the block diagram in figure 6.1.

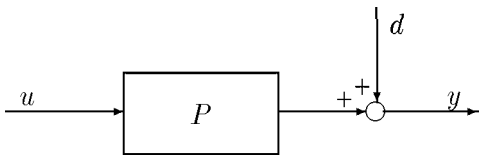

fig. 6.1: General identification setting.

The plant, represented by an LTI system P, is driven by an input signal u and produces an output signal y, consisting of the plants response to u and some disturbance d that is not available for measurement. The system P is represented as a linear, time invariant operator of discrete time signals, expressed as

$$y(t) \;=\; P(q)\; u(t) \;+\; d(t). \tag{6.1}$$

The disturbance d is a realization of a stochastic noise process with zero mean value and variance σ_d^2. The signals available for measurement are presumed quasi-stationary, as discussed in chapter 2. Measurements of u and y are presumed to be taken during an observation time $t' = 0, \ldots, N_0 - 1$ and are available in the form of a finite number of data segments, denoted as

$$\begin{array}{rcl} u^i(t) & := & w(t)u((i-1)N + n_i + t) \\ y^i(t) & := & w(t)y((i-1)N + n_i + t). \end{array}, \qquad t = 0, \ldots, N-1 \tag{6.2}$$

where N is the segment length and i the segment index. The index n_i denotes the total number of samples that are intermediate the segments up to the i-th segment and is introduced to indicate that data segments are not necessarily measured contiguously. As we do not consider the case where measured segments are overlapping, we impose $n_{i+1} - n_i \geq 0, i = 1, \ldots, M-1$. In case M segments are measured, then the minimum length of the observation sequence equals $NM + n_M$.

Applying the Discrete Fourier Transform (discussed in chapter 5) to the ith data segment gives the following frequency domain expression of the system equation (6.1):

$$Y_N^i(e^{j\omega_k}) = P(e^{j\omega_k})\, U_N^i(e^{j\omega_k}) + D_N^i(e^{j\omega_k}) + S_N^i(e^{j\omega_k}),$$
$$\omega_k = \frac{2\pi k}{N}, k = 0, \ldots, N-1,$$

where $S_N^i(e^{j\omega_k})$ reflects the effect on $Y_N^i(e^{j\omega_k})$ as a result of the unknown past input $u(t)$, $t \leq 0$. An estimate of the systems frequency response at a finite number of prespecified frequencies ω_k is then straightforwardly written as (see also [55])

$$\begin{aligned}\hat{P}_i(e^{j\omega_k}) &= \frac{Y_N^i(e^{j\omega_k})}{U_N^i(e^{j\omega_k})} \\ &= P(e^{j\omega_k}) + \frac{D_N^i(e^{j\omega_k})}{U_N^i(e^{j\omega_k})} + \frac{S_N^i(e^{j\omega_k})}{U_N^i(e^{j\omega_k})}. \end{aligned} \tag{6.3}$$

The complex numbers $\hat{P}_i(e^{j\omega_k})$ constitute an ETFE of the system and are corrupted with disturbance terms $D_N^i(e^{j\omega_k})/U_N^i(e^{j\omega_k})$ due to random (measurement) noise and $S_N^i(e^{j\omega_k})/U_N^i(e^{j\omega_k})$ due to unknown past input signals. An estimate $\hat{P}(e^{j\omega_k})$ of the systems frequency response is attained via averaging of ETFE's over a number of data segments:

$$\hat{P}^M(e^{j\omega_k}) = \frac{1}{M}\sum_{i=1}^{M} \hat{P}_i(e^{j\omega_k}). \tag{6.4}$$

In case an excitation signal is utilized that is periodic with period length N and the input signals of the data segments satisfy $U_N^{i+1}(e^{j\omega_k}) = U_N^i(e^{j\omega_k})$, $i = 1, \ldots, M-1$, frequency response estimation via averaging of the ETFE's is strongly related to periodogram averaging, which has been discussed in chapter 5. Consequently, based on the analysis in section 5.2.1, frequency response estimates attained via ETFE averaging are presumed unbiased and the effects of disturbances and transients in the measured output segments are substantially reduced by means of averaging.

6.2.3 Identification of normalized coprime factors

In this section we address identification employing coprime factor model representations. Utilization of a fractional modelling framework in feedback related identification problems is reported by [53] in an adaptive robust control design scheme and by [39, 40] for experiment design issues. In [69] coprime factor

models and a dual Youla parametrization are exploited in view of approximate modelling for control design. In [13] fractional model representations are employed in an iterative method of identification and control design.

Recalling from chapter 5, from the experimental configuration in figure 5.2 we have available frequency response estimates of $P(I+CP)^{-1}$ and $(I+CP)^{-1}$. In case the controller C is stable, it follows from the definition of right coprimeness in chapter 2, that $P(I+CP)^{-1}$ and $(I+CP)^{-1}$ are right coprime factors of the system P as

$$X\ P(I+CP)^{-1} + Y\ (I+CP)^{-1} = I$$

holds for $X = C$ and $Y = I$ (see [11]). A coprime factor representation of a system is far from unique, hence it is desirable to exploit the freedom in representing coprime factor representations to a much broader range than those accessable via measurement data. Additional freedom in designating specific coprime factors for identification is feasible via filtering of the excitation signal r. The corresponding factors that are accessible from closed loop measurements are then parametrized as

$$\begin{aligned} N_F &:= P(I+CP)^{-1}F^{-1} \\ D_F &:= (I+CP)^{-1}F^{-1}. \end{aligned} \tag{6.5}$$

where F denotes a stable and stably invertible filter, determining the specific plant factors induced by the data $\{Fr, u, y\}$. The use of a filter F in order to provide access to coprime factors other than $\{P(I+CP)^{-1}, (I+CP)^{-1}\}$ has been addressed by [11]. There the filter F is parametrized as $F := (D_x + CN_x)^{-1}$ where $\{N_x, D_x\}$ constitute r.c.f.'s of a model P_x stabilized by the same controller C; corresponding factors $\{N_F, D_F\}$ are right coprime. Consequently, the right coprime factors $\{N_x, D_x\}$ parametrize the freedom in specifying the coprime factors of P in terms of (6.5) that can be identified from (filtered) measurement data.

As coprime factors are physically non-existent and, moreover, not unique, the filter F designates the specific coprime factors (representing the plant) that are to be identified. From an identification point of view, the system that generates the data, being expressed in terms of coprime factors, is determined by the choice of the filter F. Consider a coprime factor representation of the plant $P = ND^{-1}$, operating in a feedback configuration with a compensator C, as depicted in figure 6.2.
The signals $\{r_1, u_p, y_p\}$ are directly available for measurement. The (artificial) signal x is written as

$$x = (D + CN)^{-1}(r_1 + Cr_2) - (D + CN)^{-1}Cd$$

and can not be constructed as such as d is unknown. Substitution of x in the signal equations

$$\begin{bmatrix} y_p \\ u_p \end{bmatrix} = \begin{bmatrix} N \\ D \end{bmatrix} x + \begin{bmatrix} I \\ 0 \end{bmatrix} d$$

gives

$$\begin{bmatrix} y_p \\ u_p \end{bmatrix} = \begin{bmatrix} N \\ D \end{bmatrix} (D + CN)^{-1}(r_1 + Cr_2) + \begin{bmatrix} (I + CP)^{-1} \\ -(I + CP)^{-1}C \end{bmatrix} d.$$

If we denote $x_r := F(r_1 + Cr_2)$ where F is a stable and stably invertible filter, we can recast a closed loop identification problem into two open loop identification problems as $\{r_1, r_2\}$ are uncorrelated with d.

As discussed in chapter 2, *normalized* coprime factor representations correspond to systems of lowest McMillan degree. Consequently, it is imperative that identification within a fractional framework is feasible based on data that correspond to *normalized* coprime factors of the system. If we consider coprime factors $\{P(I + CP)^{-1}F^{-1}, (I + CP)^{-1}F^{-1}\}$, accessible via closed loop measurements, then normalized factors are attained if

$$\left(P(I + CP)^{-1}F^{-1}\right)^* P(I+CP)^{-1}F^{-1} + \left((I + CP)^{-1}F^{-1}\right)^* (I+CP)^{-1}F^{-1} = I$$

holds, which can be rewritten as

$$\left(P(I + CP)^{-1}\right)^* P(I + CP)^{-1} + \left((I + CP)^{-1}\right)^* (I + CP)^{-1} = F^*F \quad (6.6)$$

and implies that F should be assigned as a spectral factor of the left hand expression in (6.6), which is available from measurement. It follows that a filter F that provides access to *normalized* coprime factors via measurement of $P(I + CP)^{-1}$ and $(I + CP)^{-1}$ can be determined by means of a spectral factorization problem.

An alternative approach to obtaining access to normalized coprime plant factors is presented by [86]. Their rationale is based on the following proposition.

Proposition 6.2.1 *Consider the coprime factors accessible through measurement* (6.5) *and the dual Youla parametrization* (2.9)*; then the following holds:*

$$\begin{aligned} N_x + D_c R &= P(I+CP)^{-1}(I+CP_x)D_x \\ D_x - N_c R &= (I+CP)^{-1}(I+CP_x)D_x. \end{aligned} \tag{6.7}$$

Proof: *See* [11]. □

The above proposition implies that the coprime factor representation according to (6.5) and the dual Youla parametrization according to (2.9) are algebraically equivalent. Consequently, considerations concerning the choice of the filter $F := (D_x + CN_x)^{-1}$, that induce normalized coprime factor data, also uphold in view of the choice of N_x, D_x that are associated with a dual Youla parameter. In other words, identification of a dual Youla parameter of *normalized* associated plant factors is feasible if and only if $(D_x + CN_x)^{-1}$ is a spectral factor of the left hand side of (6.6). In the following we elaborate on the choice of $\{N_x, D_x\}$ in view of normalized coprime factors and a dual Youla parameter, associated with normalized coprime factors.

In case coprime factors $\{N_x, D_x\}$ are available as normalized coprime factors of a (high order) model that gives a good overall description of the plant, then the associated dual Youla parameter will satisfy $R \simeq 0$ according to (2.10). Consequently,

$$\begin{aligned} N_x &\simeq P(I+CP)^{-1}(I+CP_x)D_x \\ D_x &\simeq (I+CP)^{-1}(I+CP_x)D_x \end{aligned}$$

holds and $\{N_x, D_x\}$ are (almost) equivalent to normalized plant factors. The issue remains that a model P_x must be identified that approximates P in a sense such that $R := D_c^{-1}(I+PC)^{-1}(P-P_x)D_x \simeq 0$ holds. This is tackled by performing an iterative procedure of filtering the data based on an available, not necessarily good, model $\hat{P}_{x,i}$ and subsequent identification of the corresponding coprime factors, leading to a model $\hat{P}_{x,i+1}$ that in its turn is used for construction of a new filter, until sufficient normalization of filtered data is attained. Concluding, access to normalized coprime factors via measurement data is obtained by means of following filter operation:

$$\begin{aligned} \hat{N}(e^{j\omega_k}) &:= \tfrac{Y}{R}(e^{j\omega_k})(D_x + CN_x) \\ \hat{D}(e^{j\omega_k}) &:= \tfrac{U}{R}(e^{j\omega_k})(D_x + CN_x) \end{aligned} \tag{6.8}$$

where $\{N_x, D_x\}$ are nrcf's of a model that accurately decribes the system and C is the controller in the loop during data acquisition. We will address normalization of measurement data in more detail in chapter 9.

6.3 Parametric identification

In parametric identification, a model is selected from a set of candidate models, described by a prefixed model structure, by estimation of parameters that may vary over some prespecified range of values. An important aspect of parameter identification is the selection of a model structure that parametrizes the set of candidate models. Although the identification addressed in this research has a single input, two output configuration, we confine the discussion at this point to Single Input, Single Output model structures.

Model structures

In this research two model structures are utilized for identification of parametric models. The first one we address provides a linear expression of a transfer function in the unknown parameters and is based on a generalization of the concept of finite impulse response models, generally referred to as orthogonal finite impulse response (ORTFIR) model structures. The development of system based functions and their application in problems of approximate identification is elaborated upon in [41] and have already proven their existential rights in applications in Prediction Error Identification and uncertainty bounding identification procedures ([90] and [37]). A thorough treatment on the subject of ORTFIR system representations is given in [41]; here we confine ourselves to a brief description of ORTFIR models and motivate their usage for modelling in view of control design.

An ORTFIR model structure of order n_p is a linearly parametrized model structure, expressed as

$$\begin{aligned} P(e^{j\omega},\theta) &= D + \sum_{k=0}^{\bar{n}_p-1} L_k \mathcal{V}_k(e^{j\omega}) \\ &= \vartheta(e^{j\omega})\,\theta \end{aligned} \tag{6.9}$$

where

$$\begin{aligned} \theta &= [D \;\; L_0 \;\; \ldots \;\; L_{\bar{n}_p-1}]^T \in \mathbb{R}^{n_b\bar{n}_p+1} \\ \vartheta(e^{j\omega}) &= [1 \;\; \mathcal{V}_0^T(e^{j\omega}) \;\; \ldots \;\; \mathcal{V}_{n_p-1}^T(e^{j\omega})]. \end{aligned}$$

It is noted that $\{1, \mathcal{V}_0(e^{j\omega}), \ldots, \mathcal{V}_\infty(e^{j\omega})\}$ constitutes an orthonormal basis of $\mathcal{H}_2$ and can be constructed utilizing a basis generating dynamical system of

order n_b; we refer to [41, 42] for detailed elaborations on the construction of orthonormal bases.

We list the most important basic features of employing system based model representations in system identification:

- As is shown below, linearly parametrized models enable the formulation of an analytic solution in case of a least squares optimization problem and, moreover, this solution is a global minimum.
- A major impetus to the development of system based functions has been the philosophy that, if one is capable of putting more system knowledge in a basis with respect to which the system is described, one needs lesser parameters to produce an adequate system description. From system identification point of view this is a desirable feature as parsimonity in model parameters keeps the variance of the parameter estimates low. As almost any stable system can be employed for construction of an orthonormal basis, the model builder has a large freedom in choosing a basis that is most suitable to his or her purposes.

Another model structure that is typically employed for identification of low order models is expressed as the ratio of two polynomials in $e^{-j\omega}$, written as

$$P(e^{j\omega}, \theta) = \frac{\sum_{k=0}^{n_b} b_k e^{-j\omega k}}{1 + \sum_{k=1}^{n_a} a_k e^{-j\omega k}} \tag{6.10}$$

where $\theta \in \mathbb{R}^{n_a+n_b+1}$, defined as $\theta^T := [a_1 \; a_2 \; \ldots \; a_{n_a} \; b_0 \; b_1 \; \ldots \; b_{n_b}]$.

Parameter identification

In Prediction Error methods as described by [55], the formulation of an identification criterion is built on the squared difference between measured output and the output predicted by the model, leading to familiar least squares optimization problems. Employing frequency domain data for parameter identification, a least squares optimization can be phrased in terms of the elementwise squared difference between two complex valued operators, which can suitably be expressed in terms of a Frobenius-norm[1] of a complex matrix, see also [64] and [92]. As $tr\{A^*A.\} = \|A\|_F^2$ holds, the $\mathcal{H}_2$ operator norm is well suited from an identification point of view by summing the Frobenius-norm over prespecified frequencies — note that frequency response data are available only at a

[1] Recall from chapter 2 that the Frobenius-norm of a matrix $A \in \mathbb{C}^{p\times q}$ is defined as $\|A\|_F := \sqrt{tr(A^*A)} = \sqrt{\sum_{i=1}^{p}\sum_{j=1}^{q} |a_{ij}|^2}$

finite number of frequencies $\omega_k, k = 1, \ldots, N$, hence parameter identification actually is performed as an optimization of a semi-norm — which leads to the following optimization problem:

$$\hat{\theta} = \arg_\theta \min \left\| W(e^{j\omega_k}) \left(\hat{P}^M(e^{j\omega_k}) - P(e^{j\omega_k}, \theta) \right) \right\|_2^2 \tag{6.11}$$

where $\hat{P}^M(e^{j\omega_k})$ is an averaged ETFE, expressed in (6.4) and $W(e^{j\omega_k})$ reflects a weighting function and $\| \cdot \|_2$ denotes the l_2-norm defined in chapter 2.

In case of a model parametrization according to (6.9), an analytic expression of the parameter estimate can be obtained. Consider the following expressions:

$$\begin{aligned} \hat{\mathcal{P}} &= [\hat{P}(e^{j\omega_1}) \;\; \hat{P}(e^{j\omega_2}) \;\; \ldots \;\; \hat{P}(e^{j\omega_N})]^T, \\ \Psi &= [\vartheta^T(e^{j\omega_1}) \;\; \vartheta^T(e^{j\omega_2}) \;\; \ldots \;\; \vartheta^T(e^{j\omega_N})]^T, \\ \mathcal{W} &= \mathrm{diag}(W(e^{j\omega_1}),\, W(e^{j\omega_2}),\, \ldots,\, W(e^{j\omega_N})) \end{aligned}$$

then (6.11) is rewritten as - note that the trace-operator is discarded in the SISO case -

$$\hat{\theta} = \arg_\theta \min \left(\mathcal{W}(\hat{\mathcal{P}} - \Psi\theta) \right)^* \left(\mathcal{W}(\hat{\mathcal{P}} - \Psi\theta) \right)$$

which is expressed as

$$\hat{\theta} = \left(\Psi^* \mathcal{W}^* \mathcal{W} \Psi + (\Psi^* \mathcal{W}^* \mathcal{W} \Psi)^T \right)^{-1} \left(\Psi^* \mathcal{W}^* \mathcal{W} \hat{\mathcal{P}} + (\hat{\mathcal{P}}^* \mathcal{W}^* \mathcal{W} \Psi)^T \right) \tag{6.12}$$

which shows the advantageous feature of linear model parametrizations as they allow for an analytic computation of a parameter estimate.

Frequency domain identification of parametric coprime factor models, employing a rational model structure as in (6.10), is formulated as

$$\hat{\theta} = \arg_\theta \min \left\| V_{\mathrm{out}} \begin{bmatrix} \frac{Y}{X}(e^{j\omega_k}) - \frac{B(e^{j\omega_k})}{F(e^{j\omega_k})} \\ \frac{U}{X}(e^{j\omega_k}) - \frac{A(e^{j\omega_k})}{F(e^{j\omega_k})} \end{bmatrix} V_{\mathrm{in}} \right\|_2^2 \tag{6.13}$$

where

$$\begin{aligned} \theta &:= [b_0 \ldots b_{n_b} \; a_0 \ldots a_{n_a} \; f_1 \ldots f_{n_f}]^T \\ B(e^{j\omega}) &:= b_0 + b_1 e^{-j\omega} + b_2 e^{-2j\omega} + \ldots + b_{n_b} e^{-n_b j\omega} \\ A(e^{j\omega}) &:= a_0 + a_1 e^{-j\omega} + a_2 e^{-2j\omega} + \ldots + a_{n_a} e^{-n_a j\omega} \\ F(e^{j\omega}) &:= 1 + f_1 e^{-j\omega} + f_2 e^{-j\omega} + \ldots + f_{n_f} e^{-n_f j\omega}. \end{aligned}$$

and $X(e^{j\omega_k}) = (D_x + CN_x)^{-1}R(e^{j\omega_k})$. A rational model structure (6.10) leads to a nonlinear optimization problem. To tackle the optimization as phrased by (6.13) we will employ a Sanathanan-Koerner iteration [66], which enables us to utilize analytic solutions as expressed by (6.12) in an iterative manner to approximate the actual solution.

The identification problem (6.13) gives parametric transfer function estimates

$$N(\hat{\theta}) := \frac{\hat{B}(e^{j\omega_k})}{\hat{F}(e^{j\omega_k})}, \quad D(\hat{\theta}) := \frac{\hat{A}(e^{j\omega_k})}{\hat{F}(e^{j\omega_k})}.$$

The corresponding model $P(\hat{\theta}) := N(\hat{\theta})D^{-1}(\hat{\theta})$ is constructed utilizing state space model descriptions of $N(\hat{\theta})$ and $D(\hat{\theta})$, as is elaborated in [11].

The optimization problem (6.13) constitutes the problem of identification of approximate models that are to be used for model-based control design. The one issue remaining is the choice of the weightings $V_{\text{out}}, V_{\text{in}}$ such that feedback relevant properties are incorporated in the approximation; this is the topic of the subsequent section.

6.4 Approximate identification

6.4.1 Approximation in view of present controller

The problem of approximate identification of (low order) models is closely related to the problem of system approximation. In this section we continue our discussion in section 2.5 on approximate modelling for high robust performance compensator design. Recalling the weighted feedback system $J(P, C)$ in equation (2.6), we have posed a feedback relevant approximation problem in expression (2.17) as follows

$$\hat{P} = \arg_{\tilde{P}} \min \|J(P, C) - J(\tilde{P}, C)\|.$$

where C is a known and stabilizing controller. The model $\hat{P}$ is subsequently used to design a high robust performance controller by means of the control design procedure presented in chapter 4, phrased as

$$C_{\hat{P}} = \arg_{\tilde{C}} \min \|J(\hat{P}, \tilde{C})\|.$$

A resulting controller achieves an enhanced robust performance if the following two inequalities are satisfied

$$\begin{aligned} \|J(\hat{P},C)\| &> \|J(\hat{P},C_{\hat{P}})\| \\ \|J(\hat{P},C_{\hat{P}})\| &\gg \|J(P,C_{\hat{P}}) - J(\hat{P},C_{\hat{P}})\|. \end{aligned}$$

The first inequality implies that the nominal performance is enhanced, which is most likely the case as $C_{\hat{P}}$ is designed based on $\hat{P}$. The second inequality states that the nominally designed performance is (approximately) achieved for the system P, which makes the designed controller a *robust* controller. Consequently, an approximate model is adequate for an enhanced robust design in case it also provides a feedback relevant approximation in view of the newly designed controller $C_{\hat{P}}$. As this controller obviously is not known, the extent of robust performance enhancement is restricted by the model underlying the design.

Consider the block diagram of figure 6.3 of the general feedback system, consisting of a plant P and a compensator C. If we denote $r := r_1 + Cr_2$, we have access to the plant times sensitivity $P(I+CP)^{-1}$ and sensitivity $(I+CP)^{-1}$ via closed loop measurement data $\{r, u_p, y_p\}$[2].
Reverting to the feedback relevant approximation formulated in (8.3), rephrased here as

$$\hat{\theta} = \arg_\theta \min \left\| \begin{bmatrix} \frac{Y}{X}(e^{j\omega_k}) \\ \frac{Y}{X}(e^{j\omega_k}) \end{bmatrix} (D_x + CN_x)^{-1}[C \quad I] - \begin{bmatrix} N(\theta) \\ D(\theta) \end{bmatrix} (D(\theta) + CN(\theta))^{-1}[C \quad I] \right\|_2^2, \tag{6.14}$$

we can recast the feedback relevant approximation objective into an affine expression in the approximation error

$$[\frac{Y}{X}(e^{j\omega_k}) - N(\theta) \quad \frac{U}{X}(e^{j\omega_k}) - D(\theta)]^T$$

in case $D(\theta)+CN(\theta) = D_x+CN_x$ is satisfied. This leads to an approximation problem with an additional parametric constraint, formulated as

$$\hat{\theta} = \arg_\theta \min \left\| \begin{bmatrix} \frac{Y}{X}(e^{j\omega_k}) - N(\theta) \\ \frac{U}{X}(e^{j\omega_k}) - D(\theta) \end{bmatrix} (D_x + CN_x)^{-1}[C \quad I] \right\|_2^2 \Bigg|_{F=(D(\theta)+CN(\theta))^{-1}}. \tag{6.15}$$

[2] $P(I+CP)^{-1}$ and $(I+CP)^{-1}$ are right coprime factors of the plant in case $C \in \mathbb{R}\mathcal{H}_\infty$.

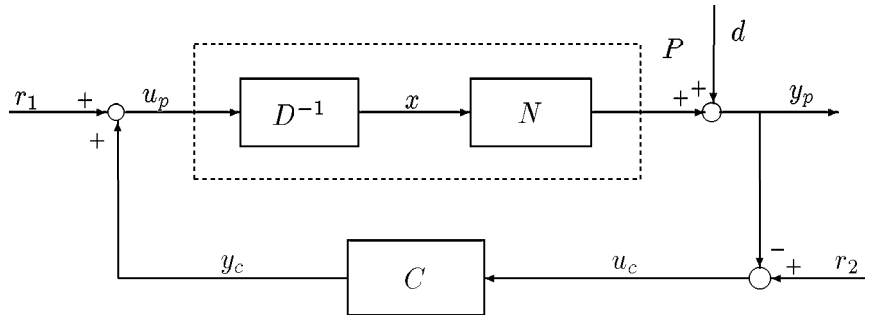

fig. 6.2: Coprime factor representation in a feedback loop.

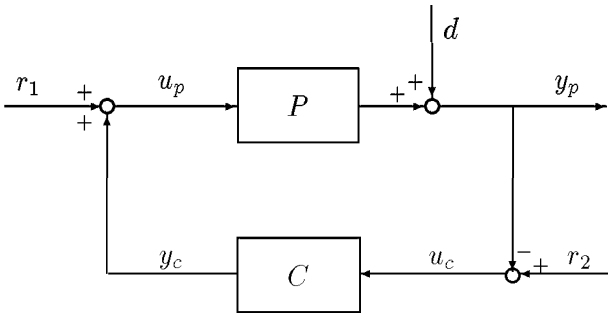

fig. 6.3: Block scheme of a closed loop system consisting of a linear, time invariant system P and a controller C.

A feasible procedure to tackle this constrained optimization is proposed in [86]. A high order model P_x is identified by performing an unconstrained identification according to (6.15); a filter $F = (D_x + CN_x)^{-1}$ is constructed, based on its normalized factors, and corresponding filtered data are evaluated for normalizedness. This exercise is repeated until filtered data are (almost) normalized. In order to identify a parametric model that satisfies the parametric constraint, coprime factors are identified according to (6.15) without imposing the constraint and normalized factors of the resulting model $P(\theta) = N(\theta)D(\theta)^{-1}$ are used for constructing a filter $(D_n(\theta) + CN_n(\theta))^{-1}$. The signal r is filtered and normalizedness of corresponding data is checked. Performing the unconstrained identification and subsequent filtering a number of times, the parametric constraint is satisfied in case the sequence of repeatedly identified models converges.

The point stressed in the above discussion is that getting access to normalized (and thus controller independent) plant factor data and the actual parametric identification based on normalized data, seem to constitute inseparable problems. This is results from the fact that the auxiliary model P_x (of which normalized coprime factors $\{N_x, D_x\}$ induce normalized factor data) and the identified model $P(\theta)$ are the one and the same model.

We take a slightly different approach towards complying with the parametric constraint. The auxiliary model P_x obtained from the normalization is employed to construct the filter $(D_x + CN_x)^{-1}$ which emphasizes the control relevant dynamics of the system. The corresponding normalized frequency response measurements

$$\frac{Y}{X} := \frac{Y}{R}(D_x + CN_x), \quad \frac{U}{X} := \frac{U}{R}(D_x + CN_x),$$

are the data that underly the estimation, where $X := (D_x + CN_x)^{-1}R$. The model parameters are identified via an unconstrained optimization according to

$$\hat{\theta} = \arg_\theta \min \left\| \begin{bmatrix} W_{\text{out}} & 0 \\ 0 & I \end{bmatrix} \begin{bmatrix} \frac{Y}{X}(e^{j\omega_k}) - N(e^{j\omega_k}, \theta) \\ \frac{U}{X}(e^{j\omega_k}) - D(e^{j\omega_k}, \theta) \end{bmatrix} (D_x + CN_x)^{-1} [C \quad I] \begin{bmatrix} W_{\text{in}} & 0 \\ 0 & I \end{bmatrix} \right\|_2^2 . \tag{6.16}$$

The parametric constraint is evaluated a posteriori.

The motivation for taking this approach is that we already have available a control relevant model, being the model P_x, that provides access to normalized

data. However, the order of P_x is too high to serve as a basis for model-based control design. Instead of repeated filtering and identification (and hence repeatedly modifying the normalization) we keep the normalized data fixed to $\{\frac{Y}{X}, \frac{U}{X}\}$ and estimate a model of low order. As control relevancy of a model and accessibility to *normalized* coprime factor data via a filter based on a model in fact determine the same model, a model resulting from the optimization above will approximately satisfy the parametric constraint.

6.4.2 Approximation in view of future controller

An approximate identification problem as phrased in the previous section provides a model that gives an approximate system description reflecting the system properties in view of a known controller. The primary aim of approximate identification however is to construct models that provide a basis for design of a *new* controller, hence a model should reflect system properties that are significant in view of this new controller. The above formulated approximate identification does thus not embody the approximation problem that is actually to be solved; this has also been stressed in [70].

We reason that a system approximation incorporating prior knowledge of the "future" controller produces models that enable a larger enhancement of robust performance than in case this knowledge is not exploited. Two questions are hence phrased:

1. Do we have some prior controller knowledge ?

The answer to question 1. is affirmative. An attractive feature of the robust control design procedure formulated in definition 4.3.1, chapter 4, is that some knowledge of the optimization-based controller is available prior to the optimization in terms of the weighting function $W(\nu_b)$. The weighting is designed by means of loop shaping (see definition 4.4.2 for expressions of loop shape weightings used in this thesis).

2. How do we utilize prior controller knowledge in an approximate identification?

Question 2. has not found a satisfying answer yet in literature. Here we propose the formulation of an approximate identification problem that enables incorporation of prior controller knowledge and that is closely related to the approximate identification of expression (6.15).

In section 2.5.2 a feedback system representation in terms of the graph (see also appendix A) of a (possibly unstable) system is introduced which enables

to phrase a feedback relevant mismatch in an affine expression of the difference between the corresponding normalized coprime factors. A feedback relevant approximation objective then is expressed in the approximation error $[N - N(\theta), D - D(\theta)]^T$ in terms of the following expression

$$\left\| \begin{bmatrix} I & 0 \\ 0 & I \\ C & I \end{bmatrix} \begin{bmatrix} N - N(\theta) \\ D - D(\theta) \end{bmatrix} \right\|.$$

A feedback relevant approximate identification that incorporates a weighting $W(\nu_b)$ that follows from the design of a controller according to the procedure in chapter 4, can thus be phrased as

$$\hat{\theta} = \arg_\theta \min \left\| \begin{bmatrix} I & 0 \\ 0 & I \\ W(\nu_b) & I \end{bmatrix} \begin{bmatrix} \frac{Y}{X} - N(\theta) \\ \frac{Y}{X} - D(\theta) \end{bmatrix} \right\|_2^2. \tag{6.17}$$

where $\{\frac{Y}{X}, \frac{U}{X}\}$ are frequency response estimates of normalized coprime factors of the system.

Note that the optimization problem of expression (6.17) is nearly equivalent with the optimization phrased in (6.15) in case a weighting $(D_x + CN_x)^{-1}[C \;\; I]$ is added on the right side of (6.17) and in case $W(\nu_b) \simeq C$, where C is the controller in the loop during data measurement.

We will not employ the approximate identification of (6.17) as at this stage many questions emerge that first need some clarification before utilization in a model-based control design procedure is feasible. One of the questions that we raise is: how does the optimization of (6.17) relate to the optimization based control design problem in chapter 4? Clearly, the compatibility of identification and model-based control design is more or less violated.

6.5 Excitation signal design

In this section we briefly address a number of considerations is underlying the construction of an excitation signal.

As discussed in chapter 5, periodic excitation signals are advantageous in view of frequency response estimation via ETFE averaging. Periodic signals can be straightforwardly constructed as a realization of a random process or as a sum of sinusoids. Two aspects in favour of employing multi-sinusoids are the following:

- One can assign the exact frequencies for excitation in case of a multi-sinusoid;
- The power spectral density of a multi-sinusoid can be directly assigned.

A multi-sine is expressed as follows

$$u(t) = \sum_{l \in \{0,\ldots,N-1\}} a_l \, cos(\omega_l t + \phi_l)$$

where frequencies ω_l can be chosen from $\omega_k = \frac{2\pi k}{N}, k = 0, \ldots, N-1$ and a_l^2 denotes the spectrum at ω_l. The magnitude a_l and the phase ϕ_l are to be determined such that $u(t)$ complies with the considerations discussed above. Detailed accounts on designing multi-sinusoidal signals are given in [32]. In general, the design consists of two consecutive steps, the first one being determination of the desired spectrum followed by minimization of the maximum time domain magnitude (also known as minimization of the Crest-factor [32]) in order to comply with physical input limitations imposed by the plant under consideration. Before we comment on both steps, some general considerations regarding excitation signal design are mentioned.

When performing experiments it is imperative to ensure beforehand whether the data are sufficiently informative. This is often referred to as the input signal being persistently exciting, implying that any two different models within a prespecified set can be discriminated based on the data [55]. In the case of frequency response estimation this boils down to specifying the number of frequency points and the location on the frequency axis that should be available for parametric identification. The minimum number of frequency points is determined by the order of the model that is to be identified (see section 6.3). The exact location along the frequency axis is guided by what frequency region is important for modelling; in case of control design the low-frequent region is less important than the cross-over and higher frequencies. Moreover, any prior knowledge of e.g. resonance modes is an important hint to choose more frequency points in the suspected region than elsewhere.

A second consideration is the desire to decrease the effect of measurement noise on the estimation by choosing the input spectrum such that a favourable signal-to-noise ratio is attained in important frequency regions. We make the observation that when measuring under closed loop conditions the noise contribution is not only affected by increase of input spectral power in the frequency region of concern, but also by the controller in the loop. Especially in case a controller is to be designed that enhances the bandwidth one may expect

that the disturbances will play a more dominating role in the cross-over region, as the sensitivity will inevitably peak up in this region. One might choose to increase the input power in the cross-over region in order to preserve a low variance, but there are limitations due to the fact that tracking is endangered, which is undesirable from the point mentioned previously. So it is expected that the limitations of accuracy of frequency response estimates will occur in the cross-over frequency region.

A conceptual guideline is that an excitation signal should be reflecting the situation in which the model is going to used [55]. In the identification framework presented above, a physical plant is represented as a linear, time invariant system that behaves equally under all experimental conditions, meaning that it is independent of the input signal. It should however be borne in mind that this is an idealized reflection of reality and that a perhaps more realistic representation would be to model a physical system as an LTI system that depends on (circumstantial) operational conditions, as "the" system to be modelled may not exist. In the context of modelling for control design, this observation has been made by Skelton ([72]), where a three-model theory is proposed in order to be alert to self-deception: an LTI system representation should only be employed for analytical predictions to evaluate properties of a low order model. A third model, reflecting the true systems performance, should be used for testing.

Input spectrum

Specification of the input power spectral density predominantly is based on considerations concerning a maximum signal-to-noise ratio in frequency bands of interest in the case of nonparametric identification.

To that end prior knowledge of disturbance spectral densities and of the sensitivity transfer function (the closed loop situation is addressed!) is required, which usually is not at hand. Therefore the input spectrum at first instant is chosen to be flat, implying the coefficients a_l are equal.

Employing a flat input spectrum, a frequency response estimate of the sensitivity is attained in conjunction with upper bounds of the estimation error — as will be addressed in chapter 7 — based on which the uniform spectrum can be adjusted. In case uncertainty bounds are large due to variance in specific frequencies (most likely in the cross-over frequency region), it is obvious that the disturbance power spectrum is large in that area and consequently the magnitude of corresponding sinusoids should be increased as to maintain an acceptable signal-to-noise ratio. In this manner, nonparametric uncertainty bounds may give good guidance towards an improved input spectrum. We will

revert to spectral input design in more detail in chapter 9.

Time domain properties

Different multi-sinusoids have the same spectrum, so there is freedom left to specify what specific signal is suited to our purpose. The design freedom is embodied in the phases ϕ_l that enable signals to look totally different in the time domain, while keeping the spectral properties unaltered. Restrictions on the time domain signal often are translated in terms of minimization of the magnitude such that the signal-to-noise ratio may be maximized, which results in an optimization of the Crest-factor or peak-to-peak value of the input signal, as discussed in [32]. Roughly two ways are reported in literature to determine the phase parameters in view of minimizing the Crest-factor. One way is based on analytical rules, either based on heuristic arguments [71] or on some optimization criterion. The second way is less sophisticated in that phases are randomly picked from the interval $[0, 2\pi)$.

What seems to be the best option for our case, is motivated by the conceptual guidance rule, discussed above, that excitation signals should not deviate too much from intended model use. As measurements are performed in closed loop, we translate this as follows: the loop signals (being plant input and tracking error) must not differ too much when observed with and without excitation. From experiments it is deduced that randomly phased sinusoids show the least deviation from the non-excited case and as such prove best suitable.

Chapter 7

Identification of model error bounds

7.1 Introduction

In this chapter we address the identification of model error bounds and their utilization in analysis of robust performance. We briefly recapitulate the main observations discussed in previous chapters that motivate the utilization of model error bounds in this thesis.

In the control design procedure, proposed in chapter 4, evaluation of robust performance is a crucial step in the design prior to controller implementation. We have verified experimentally in chapter 5 that frequency response estimates of a compact disc servo mechanism are of limited accuracy in view of providing reliable predictions of the achieved performance. In order to make the performance evaluation step robust in view of inaccurate system knowledge, utilization of model error bounds is a necessity.

An additional motivation for employing model error bounds is confined in a problem that is relevant for consumer electronic products that are produced in large numbers, as has been clarified in chapter 3. Due to the mass-production process no single product will exhibit exactly equivalent dynamical properties; a specific feature of electro mechanical systems is that resonance frequencies (which may drastically deteriorate performance!) slightly vary. To that end a control design procedure is desired that achieves a high performance for a batch of systems, taking account of the fact that slight deviations in dynamical behaviour occur. As varying system dynamics can be well captured in terms of system uncertainty sets, a feasible option is employment of the proposed control design scheme in conjunction with model error bounds that account for varying system dynamics, implying that measurement data are taken from different physical systems. The uncertainty bounding method presented in this chapter will be applied to two experimental systems in chapter 9.

The chapter is organized as follows. In section 7.2 we sum up requirements on utilizing model error bounds, that are to be met in view of evaluation of robust performance. In section 7.3 it is shown that the utilization of a system uncertainty set based on a dual Youla model representation enables non-conservative evaluation of robust performance for any stabilizing controller. A mixed worst-case probabilistic error bounding technique, developed by [90], is presented in section 7.4. The topic of validation of model error bounds is addressed in section 7.6. The chapter is concluded with some remarks in section 7.7.

7.2 Requirements

Let us revert to the performance evaluation step in the control design procedure in section 4.5. In section 2.6 analysis of robust performance for a system uncertainty set $\mathcal{P}$ is phrased in terms of the following inequality

$$\Gamma_{\rm lo}(\omega) \leq |J(P, C_{\rm new})| \leq \Gamma_{\rm up}(\omega), \quad \forall P \in \mathcal{P}, \quad \omega \in [0, \pi). \tag{7.1}$$

where $\mathcal{P}$ denotes system set, $C_{\rm new}$ is a newly designed controller and $\Gamma_{\rm up}, \Gamma_{\rm lo}$ are prespecified lower and upper magnitude bounds. We have shown in chapter 5 that frequency response measurements obtained via periodogram averaging, are insufficiently reliable for performance evaluation. Moreover, frequency response measurements are only defined at a finite number of frequencies which makes evaluation of (7.1) feasible only at these frequencies. In order to robustify the performance evaluation with respect to inaccurate system knowledge and to enable performance evaluation for the continuous frequency axis, a system uncertainty set is required such that for every model in that set the performance evaluation according to (7.1) can be performed.

As is discussed in section 2.6, robust performance analysis requires the availability of non-conservative expressions for

$$\sup_{P \in \mathcal{P}} |J(P, C)|, \qquad \inf_{P \in \mathcal{P}} |J(P, C)|, \qquad \omega \in [0, \pi)$$

employing a structured system uncertainty set $\mathcal{P}$. This brings us to the first requirement regarding the utilization of model error bounds in view of robust performance analysis.

> **Requirement 1:** A system uncertainty set should enable *non-conservative* expressions of worst-case magnitude error bounds of the closed loop transfer function $J(P, C)$ for $\omega \in [0, \pi)$, according to the expression (7.1).

Evaluation of (7.1) should be performed only for those systems that are contained in the system uncertainty set, meaning that the construction of magnitude bounds of the feedback system from the system uncertainty set should be done in a non-conservative manner. The notion of non-conservative feedback system magnitude error bounds is defined in chapter 2, definition 2.6.1. In chapter 2, section 2.3, two system uncertainty sets $\mathcal{P}_{ND}$ and $\mathcal{P}_R$ are defined that describe a set of systems in terms of a nominal model and a frequency dependent bound on the magnitude of the error. The suitability of a system uncertainty set structure in view of performance evaluation according to (7.1) is determined whether it allows for construction of non-conservative error bounds according to definition 2.6.1.

> **Requirement 2:** Error bounds due to disturbances should have a decaying character for a larger number of data points used.

In chapter 5 we have observed that although frequency response estimates deliver no exact system representations, a very accurate estimate can be attained by averaging of an arbitrarily large number of sample estimates. This indicates that the effect of disturbances can adequately be reduced by means of averaging. An implicit presumption underlying a frequency response estimation based on averaging is that system dynamics do not average out while disturbance effects do.

A third requirement concerns the number of data samples underlying the error bounding procedure:

> **Requirement 3:** An error bound estimation procedure must handle a large number of data points, in similar amount as is underlying a frequency response estimation attained with a signal analyzer. In addition, computational effort must remain acceptable.

When constructing a model from frequency response data one naturally prefers a frequency response one trusts most, whether an explicit error bound is available or not. If error bounds are not at hand, some uncertainty will always be accounted for in a high robust performance control design. Data based error bounds are considered to be of surplus value only in case these bounds are in compliance with experimental experience gained from signal analyzer estimates. Consequently a gap is to be bridged between a frequency response, presumed very accurate but having no explicit error bound, and a frequency response being less accurate — due to the much smaller number of data points used — but with an error bound.

First we will address requirement 1. Expressions of nonconservative magnitude error bounds of open and closed loop transfer functions are not available in

literature. In the next section we will derive nonconservative expressions of additive transfer function error bounds of open as well as closed loop systems, employing a model uncertainty structure based on a dual Youla parametrization.

7.3 Performance evaluation employing model error bounds

Requirement 1, formulated in the previous section, states that a structured system uncertainty set $\mathcal{P}$ is suitable for robust performance evaluation, in case expressions of performance bounds $\Upsilon_{\rm up}(\mathcal{P},C), \Upsilon_{\rm lo}(\mathcal{P},C)$ can be determined, based on $\mathcal{P}$, such that

$$P \in \mathcal{P} \iff \Upsilon_{\rm lo}(\mathcal{P},C) \leq |J(P,C)| \leq \Upsilon_{\rm up}(\mathcal{P},C), \quad P \in \mathcal{P}, \quad \omega \in [0,\pi),$$

is satisfied for any robustly stabilizing controller. Evaluation of robust performance hence requires construction of magnitude bounds of $J(P,C)$ based on a structured system uncertainty set $\mathcal{P}$ such that the magnitude bounds are non-conservative (recall definition 2.6.1, chapter 2, for definition of conservative magnitude bounds), which is phrased as follows:

$$\begin{aligned} \sup_{P\in\mathcal{P}} \ |J(P,C)| \ &\leq \ \Gamma_{\rm up}(\omega) \\ \inf_{P\in\mathcal{P}} \ |J(P,C)| \ &\geq \ \Gamma_{\rm lo}(\omega) \end{aligned}$$

for $\omega \in [0,\pi)$. In chapter 2, section 2.3, two model uncertainty structures $\mathcal{P}_{ND}(N,D,\delta_N,\delta_D)$ (equation (2.9)) and $\mathcal{P}_R(N_x,D_x,N_c,D_c,R,\delta_R)$ (equation (2.14)) have been introduced that are based on fractional model representations. Bounds on the additive error of coprime factors and dual Youla parameter are both attainable via measurement data employing the model error bounding technique of section 7.4. Hence, system uncertainty sets $\mathcal{P}_{ND}(N,D,\delta_N,\delta_D)$ and $\mathcal{P}_R(N_x,D_x,N_c,D_c,R,\delta_R)$ can be constructed from model error bounds and nominal models via system identification.

Employing the system uncertainty set $\mathcal{P}_R(N_x,D_x,N_c,D_c,R,\delta_R)$, defined in (2.14), upper and lower performance bounds of $|J(P,C)|$ are expressed in expression (2.25),

$$\begin{aligned} \sup_{|\Delta_R|<\delta_R}, \inf_{|\Delta_R|<\delta_R} \Bigg| \begin{bmatrix} N_x + D_c(R+\Delta_R) \\ D_x - N_c(R+\Delta_R) \end{bmatrix} \ \times \\ (D_x + C_{\rm new}N_x + (C_{\rm new}-C)D_c(R+\Delta_R))^{-1} \begin{bmatrix} C_{\rm new} & I \end{bmatrix} \Bigg| . \end{aligned}$$

where $\tilde{D}_{cn}^{-1}\tilde{N}_{cn} = C_{\text{new}}$. If we consider the case that $C = C_{\text{new}}$, the following expressions for non-conservative performance bounds are derived based on $\mathcal{P}_R$:

$$\begin{aligned} \inf_{P\in\mathcal{P}_R} |J(P,C)| &:= |J_{\text{nom}}(\mathcal{P}_R,C)| - \delta_J(\mathcal{P}_R,C) \\ \sup_{P\in\mathcal{P}_R} |J(P,C)| &:= |J_{\text{nom}}(\mathcal{P}_R,C)| + \delta_J(\mathcal{P}_R,C) \end{aligned}$$

where

$$|J_{\text{nom}}(\mathcal{P}_R,C)| = \left| \begin{bmatrix} N_x + D_c R \\ D_x - N_c R \end{bmatrix} (D_x + CN_x)^{-1} \begin{bmatrix} C & I \end{bmatrix} \right| \tag{7.2}$$

$$\delta_J(\mathcal{P}_R,C) = \left| \begin{bmatrix} D_c \\ -N_c \end{bmatrix} \right| \delta_R \left| (D_x + CN_x)^{-1} \begin{bmatrix} C & I \end{bmatrix} \right|. \tag{7.3}$$

As performance bounds simplify into an affine expression in δ_R for $C_{\text{new}} = C$, the bounds are non-conservative. However, in case $C_{\text{new}} \neq C$, δ_J is no longer affinely expressed in δ_R.

The main result shown in this section is that a system uncertainty set $\mathcal{P}_R$ enables the construction of upper and lower magnitude bounds of $J(P, C_{\text{new}})$ for any newly designed controller C_{new} without introducing conservatism. We merely mention at this point that additive magnitude error bounds of the closed loop transfer function $J(P,C)$ can be constructed element-wise for any controller in a non-conservative manner by virtue of the fact that a closed loop uncertainty structure employing a system uncertainty set $\mathcal{P}_R(N_x, D_x, N_c, D_c, R, \delta_R)$, is a Linear Fractional Transformation (LFT). Fruitful use is made of a result known from complex functional analysis [65], that in the SISO case an LFT maps circles in the complex plane into circles, which is straightforwardly extended to transformation of discs in the complex plane. The result is formalized in the next proposition.

Proposition 7.3.1 *Consider a system uncertainty set $\mathcal{P}_R(N_x, D_x, N_c, D_c, R, \delta_R)$ as defined in* (2.14) *and performance of a feedback system defined by* (2.7)*, then non-conservative lower and upper bounds of performance for a stabilizing controller C_{new} are resp. expressed as:*

$$\begin{aligned} \inf_{P\in\mathcal{P}_R} |J(P,C_{\text{new}})| &= |J_{\text{nom}}(\mathcal{P}_R,C_{\text{new}})| - \delta_J(\mathcal{P}_R,C_{\text{new}}) \\ \sup_{P\in\mathcal{P}_R} |J(P,C_{\text{new}})| &= |J_{\text{nom}}(\mathcal{P}_R,C_{\text{new}})| + \delta_J(\mathcal{P}_R,C_{\text{new}}) \end{aligned}$$

where

$$J_{\text{nom}}(\mathcal{P}_R, C_{\text{new}}) = \begin{bmatrix} N_x + D_c R & -D_c \\ D_x - N_c R & N_c \end{bmatrix} \times \tag{7.4}$$
$$\begin{bmatrix} (D_x + C_{\text{new}} N_x + (C_{\text{new}} D_c - N_c) R)^* \\ (C_{\text{new}} D_c - N_c)^* \delta_R^2 \end{bmatrix} D(\mathcal{P}_R, C_{\text{new}})^{-1} \; [C_{\text{new}} \quad I]$$

and

$$\delta_J(\mathcal{P}_R, C_{\text{new}}) = \tag{7.5}$$
$$\begin{bmatrix} I \\ |C_{\text{new}}| \end{bmatrix} |(D_x + C N_x) D_c| \; \delta_R \; D(\mathcal{P}_R, C_{\text{new}})^{-1} \; [|C_{\text{new}}| \quad I]$$

where

$$D(\mathcal{P}_R, C_{\text{new}}) := |D_x + C_{\text{new}} N_x + (C_{\text{new}} D_c - N_c) R|^2 - |C_{\text{new}} D_c - N_c|^2 \; \delta_R^2 \tag{7.6}$$

provided $D(\mathcal{P}_R, C_{\text{new}}) > 0$.

Proof: *Appendix D.* □

Note that in case $C_{\text{new}} = C$, expressions (7.4) resp. (7.5) simplify into (7.2) and (7.3).

As the system uncertainty set $\mathcal{P}_R(N_x, D_x, N_c, D_c, R, \delta_R)$ itself has an uncertainty structure equivalent to an LFT,

$$P = \frac{N_x + D_c(R + \Delta_R)}{D_x - N_c(R + \Delta_R)},$$

a similar result can be derived for an open loop system:

Proposition 7.3.2 *Consider a system P for which $P \in \mathcal{P}_R(N_x, D_x, N_c, D_c, R, \delta_R)$; the following equivalence then holds:*

$$P \in \mathcal{P}_R(N_x, D_x, N_c, D_c, R, \delta_R) \quad \equiv \quad |P_{\text{nom}}| - \delta_P \leq |P| \leq |P_{\text{nom}}| + \delta_P, \quad \forall \omega$$

where

$$P_{\text{nom}} := \frac{(N_x + D_c R)(D_x - N_c R)^* + D_c N_c^* \delta_R^2}{(D_x - N_c R)(D_x - N_c R)^* - N_c N_c^* \delta_R^2} \tag{7.7}$$

$$\delta_P := \frac{|N_x N_c + D_c D_x| \, \delta_R}{(D_x - N_c R)(D_x - N_c R)^* - N_c N_c^* \delta_R^2} \tag{7.8}$$

provided $(D_x - N_c R)(D_x - N_c R)^* > N_c N_c^* \delta_R^2$.

Proof: *Appendix D.* □

In the following two sections identification of a system uncertainty set $\mathcal{P}_R$ is addressed. A mixed worst-case probabilistic error bounding technique is discussed in section 7.4 for a stable system; in section 7.5 the identification of a dual Youla parameter is addressed.

7.4 Mixed worst-case probabilistic bounding

In recent years research effort in the field of system identification has delivered theories and tools for data based construction of system uncertainty sets, constituted of a nominal model and a model error bound. Methods are reported in [59, 37, 90] that provide data based model error bounds that are to be used for robust control design. An identification procedure is discussed developed by [90] that provides a nominal LTI model in conjunction with a bound on the model error from measurement data. The results presented in this section are mainly taken from the thesis of [90], chapter 5, to which we refer for a (much) more detailed elaboration on the subject.

7.4.1 Identification framework

The measurement data are presumed to obey the system equation

$$y(t) = G(q)u(t) + d(t)$$

where $G(q)$ denotes a stable system which can be written as

$$\begin{aligned} G(e^{j\omega}) &= \sum_{k=0}^{\infty} g(k) e^{-j\omega k} \\ &= D + \sum_{k=1}^{\infty} L_k \mathcal{V}_k(e^{j\omega}) \end{aligned}$$

where $u(t)$ is a known input signal and $d(t)$ is a realization of a stochastic noise process, added to the (measurable) output $y(t)$; $\mathcal{V}_k(e^{j\omega})$ denote system based orthonormal basis functions, discussed in chapter 6, section 6.3. The input $u(t)$ and the disturbance $d(t)$ are presumed to be uncorrelated.

Measurement data $\{u, y\}$ are presumed available in terms of a number of data segments of equal length N, similar to the data format introduced in

section 6.2.2. The input signal is periodic with period length N and the data segment length is an integer multiple of N; moreover, measurement of data segments $\{u, y\}$ is not required to be performed contiguously. Measurement data are consequently denoted as

$$\begin{array}{rcl} u^i(t) & := & u((i-1)N + n_i + t) \\ y^i(t) & := & y((i-1)N + n_i + t). \end{array}, \quad t = 0, \ldots, N-1 \tag{7.9}$$

where N is the segment length and i the segment index. The index n_i denotes the total number of samples that are in between segments up to the i-th segment. The number of data samples in between two subsequent segments is presumed to be an integer multiple of N, indicated by $n_{i+1} - n_i \geq pN; p \in \mathbb{Z}; i = 1, \ldots, M-1$.

The following assumptions are instrumental in derivation of uncertainty bounds:

1. the input $u(t)$ is bounded in magnitude prior to measurement, i.e. $|u(t)| \leq \bar{u}^p$, $t < 0$ where $\bar{u}^p$ is known.

2. the system pulse response is presumed bounded as $|g(k)| \leq K\rho^{-k}$ for $k \in \mathbb{Z}$, where $K \in \mathbb{R}^+, \rho \in \mathbb{R}^+$ and $\rho > 1$;

3. the generalized pulse response is presumed bounded as $|L_k| \leq \mathcal{K}\eta^k$ for $k \in \mathbb{Z}$ where $\mathcal{K} \in (\mathbb{R}^+)^{1 \times n_b}$ and $\eta \in \mathbb{R}$ with $\eta < 1$.

7.4.2 Discrete transfer function bounds

In this subsection a procedure is discussed to construct a nonparametric estimate $\hat{G}(e^{j\omega_k})$ of $G(e^{j\omega_k})$ together with a bound $\delta_G(\omega_k)$ such that $|G(e^{j\omega_k}) - \hat{G}(e^{j\omega_k})| < \delta_G(\omega_k)$ holds with prespecified probability at a finite number of frequencies. The motivation to address discrete error bounding is twofold. Firstly, continuous error bounding is based on the same methodology but is more involved, so discrete error bounding provides a quick preliminary indication. Secondly, as discrete error bounds are mainly attributed to measurement noise (this will be clarified shortly in this section), they provide us with valuable information as to how to improve the excitation signal design to reduce variance.

It is not our intention to present the method in full detail, as this would only obscure the main features. We restrict the elaboration to elucidation of the mechanisms of the uncertainty bounding technique as to how to make the right choices regarding prior assumptions, excitation signal design, etcetera in view of obtaining useful and reliable bounds.

An estimate of the systems frequency response at a finite number of prespecified frequencies ω_k based on averaging of the ETFE, is expressed as (see also section 6.2.2)

$$\begin{aligned} \hat{G}_i(e^{j\omega_k}) &= \frac{Y^i(e^{j\omega_k})}{U^i(e^{j\omega_k})}, \\ \hat{G}^M(e^{j\omega}) &= \frac{1}{M}\sum_{i=1}^{M}\hat{G}_i(e^{j\omega_k}) \end{aligned} \tag{7.10}$$

where $Y^i(e^{j\omega_k})$ and $U^i(e^{j\omega_k})$ are DFT's of resp $y^i(t)$ and $u^i(t)$. Applying the system equation gives

$$\hat{G}_i(e^{j\omega_k}) = G(e^{j\omega_k}) + \frac{D^i(e^{j\omega_k})}{U^i(e^{j\omega_k})} + \frac{S^i(e^{j\omega_k})}{U^i(e^{j\omega_k})}.$$

For the construction of a bound on the error $|\hat{G}(e^{j\omega_k}) - G(e^{j\omega})|$ a distinction is made between the error contribution due to random (measurement) noise $(D^i(e^{j\omega_k})/U^i(e^{j\omega_k}))$ and the error contribution due to unknown past input signals $(S^i(e^{j\omega_k})/U^i(e^{j\omega_k}))$. For analysis the error is split up into two terms, introducing an auxiliary transfer function $\tilde{G}_i(e^{j\omega})$ defined as

$$\tilde{G}_i(e^{j\omega_k}) := \hat{G}_i(e^{j\omega_k}) - \frac{S^i(e^{j\omega_k})}{U^i(e^{j\omega_k})} = G(e^{j\omega_k}) + \frac{D^i(e^{j\omega_k})}{U^i(e^{j\omega_k})}$$

that solely accounts for errors due to measurement noise. The following inequality can then be derived:

$$|G(e^{j\omega_k}) - \hat{G}(e^{j\omega_k})| \leq |G(e^{j\omega_k}) - \tilde{G}(e^{j\omega_k})| + |Q(e^{j\omega_k})|$$

where $Q(e^{j\omega_k})$, expressed as

$$Q(e^{j\omega_k}) := \hat{G}(e^{j\omega_k}) - \tilde{G}(e^{j\omega_k}) = \frac{1}{M}\sum_{i=1}^{M} Q_i(e^{j\omega_k})$$

denotes the error due to unknown input signals and $|G(e^{j\omega_k}) - \tilde{G}(e^{j\omega_k})|$ accounts for the variance error. An expression for the error bound due to unknown inputs $|Q(e^{j\omega_k})|$ is shown in appendix E.

To calculate the error due to variance an estimate of the variance

$$\hat{\sigma}^2(\tilde{G}(e^{j\omega_k})) = \frac{1}{M(M-1)}\sum_{i=1}^{M}\left|\tilde{G}(e^{j\omega_k}) - \tilde{G}^i(e^{j\omega_k})\right|^2 \tag{7.11}$$

is needed, which can not be attained as $\tilde{G}(e^{j\omega_k})$ is not available. Based on measurement data $\hat{G}_i(e^{j\omega_k})$ we can however find an approximate estimate of the variance (7.11) as

$$\hat{\sigma}^2(\hat{G}(e^{j\omega_k})) = \frac{1}{M(M-1)} \sum_{i=1}^{M} \left| \hat{G}(e^{j\omega_k}) - \hat{G}^i(e^{j\omega_k}) \right|^2 \tag{7.12}$$

and a bound on the approximation error of the variance estimate

$$|\hat{\sigma}^2(\tilde{G}(e^{j\omega_k})) - \hat{\sigma}^2(\hat{G}(e^{j\omega_k}))| \leq \mathcal{S}(\omega_k)$$

where $\mathcal{S}(\omega_k)$ is a calculable term shown in appendix E. The bound on the approximation error accounts for the fact that the variance estimate is corrupted due to effects of unknown initial conditions, present in the measurement data.

We formalize the construction of a nonparametric error bound in the following proposition.

Proposition 7.4.1 *Consider the prior assumptions on the magnitude bound on past input signals and the bound on the system impulse response. The input signal $u(t)$ is periodic with period length N and M data segments are acquired, each segment corresponding to one period of $u(t)$. An upper bound on the error between the averaged ETFE and the system frequency response is constructed as follows*

$$|G(e^{j\omega_k}) - \hat{G}(e^{j\omega_k})| \leq \delta_1(\omega_k) + \delta_2(\omega_k, \alpha) \quad w.p. \quad \geq \begin{cases} F_\alpha(2, 2(M-1)) & \omega_k \neq 0, \pi \\ F_\alpha(1, M-1) & \omega_k = 0, \pi \end{cases}$$

where $F(n,m)$ denotes the F-distribution with n degrees in the numerator and m degrees in the denominator and $\delta_1(\omega_k)$ and $\delta_2(\omega_k, \alpha)$ satisfy

$$|\delta_1(\omega_k)| \leq \frac{1}{M\sqrt{N_o}} \frac{\bar{u}^p + \bar{u}}{|U^i_{N_o}(e^{j\omega_k})|} \frac{L\rho(1-\rho^{-MN_o})}{(\rho-1)^2} \rho^{-N_s}$$

and

$$\delta_2(\omega_k, \alpha) = \sqrt{\alpha} \left(\hat{\sigma}_r^2(\hat{G}(e^{j\omega_k})) + \mathcal{S}(\omega_k) \right)^{\frac{1}{2}}$$

Proof: *see* [90], *appendix B.4.* □

An estimate of the error bound of $|G(e^{j\omega_k}) - \hat{G}(e^{j\omega_k})|$ is constructed as the sum of a deterministic error bound $\delta_1(\omega_k)$ and stochastic error bound $\delta_2(\omega_k, \alpha)$ as noise is modelled in terms of realizations of a random process. The total

error bound thus constitutes a frequency dependent confidence interval for the system frequency response, hence explaining the mixed worst-case stochastic character of the bounds.

Essential in the derivation of bounds for the separate error terms is that the subdivision between unknown input signals and variance is an error classification based on system theoretic considerations but can not be extracted from measurement data as such. As a result the formulation of an error bound in terms of a sum of (physically) independent error contributions might give the wrong impression that the separate bounds can be identified independently. In the expressions for the error bound due to variance it is evident that the bound is determined not only by presumptions on measurement noise but also by the prior assumptions on input magnitude $\bar{u}^p$ and bound on the system impulse response, reflected by K, ρ. The magnitude bound $\bar{u}^P$ follows from e.g. actuator constraints. Values of K, ρ however are based on presumed system dynamics and it should always be verified a posteriori whether they are consistent with the identified bounds. If not, they should be adjusted and the bounding procedure repeated. In practice this amounts to performing the bounding exercise a number of times, tuning the priors until they are compatible with the resulting bounds.

7.4.3 Continuous transfer function bounds

In this subsection we address the identification of an LTI parametric model $\hat{G}(e^{j\omega}, \theta)$ of $P(e^{j\omega})$ in conjunction with an error bound $\delta_G(\omega)$ that satisfies $|G(e^{j\omega}) - \hat{G}(e^{j\omega}, \theta)| < \delta_G(\omega)$ with prespecified probability for $\omega \in [0, \pi)$.

The procedure is quite similar to the nonparametric case, although it is more involved since a parameter estimation has to be performed as an intermediate step in order to enable construction of a continuous transfer function error bound.

Parameter estimation

Parameter estimation is carried out employing an ORTFIR model structure, as is discussed in chapter 6, section 6.3. Consider an ORTFIR model structure where n_b denotes the McMillan degree of the basis generating model, the number of basis functions used is $\bar{n}_p$ and the number of parameters equals $1 + n_b \bar{n}_p$,

$$\begin{aligned} G(e^{j\omega},\theta) &= D + \sum_{k=0}^{\bar{n}_p-1} L_k \mathcal{V}_k(e^{j\omega}) \\ &= \vartheta(e^{j\omega})\,\theta \end{aligned}$$

where[1]

$$\begin{aligned} \theta &= [D \;\; L_0 \;\; \ldots \;\; L_{\bar{n}_p-1}]^T \in \mathbb{R}^{n_b\bar{n}_p+1} \\ \vartheta(e^{j\omega}) &= [1 \;\; \mathcal{V}_0^T(e^{j\omega}) \;\; \ldots \;\; \mathcal{V}_{\bar{n}_p-1}^T(e^{j\omega})]. \end{aligned}$$

A parameter estimate $\hat{\theta}^i$ is attained via the expression in (6.12) employing ETFE's corresponding to the several data segments. Denoting

$$G(e^{j\omega}) = \vartheta(e^{j\omega})\theta_0 + \sum_{k=\bar{n}_p}^{\infty} L_k \mathcal{V}_k(e^{j\omega})$$

the following expression is obtained from the system equation:

$$\hat{G}^i(e^{j\omega_k}) = \vartheta(e^{j\omega_k})\theta + \sum_{k=\bar{n}_p}^{\infty} L_k \mathcal{V}_k(e^{j\omega}) + \frac{D^i(e^{j\omega_k})}{U^i(e^{j\omega_k})} + \frac{S^i(e^{j\omega_k})}{U^i(e^{j\omega_k})}.$$

From this expression it can be derived that the parameter error $\theta_0 - \hat{\theta}^i$ is constituted of three terms,

$$\theta_0 - \hat{\theta}^i = \mathcal{Z} + \mathcal{S}^i + \mathcal{F}^i \tag{7.13}$$

where $\mathcal{Z}$ is the contribution due to undermodelling, $\mathcal{S}^i$ due to unknown input signals and $\mathcal{F}^i$ due to measurement noise. The expressions for $\mathcal{Z}, \mathcal{S}^i$ and $\mathcal{F}^i$ can be derived by virtue of the linear parametrization of an ORTFIR model structure and are quite technical; for a detailed elaboration we refer to de Vries [90]), section 5.4.2.

Transfer function estimation

Based on a parameter estimate, an estimate of the transfer function is obtained as[2]

$$\hat{G}_f^i(e^{j\omega}) = \vartheta_{\bar{n}_f}(e^{j\omega}) \;\; [\mathcal{W} \;\; 0] \;\; \hat{\theta}^i$$

[1] In order to prevent any misunderstandings, notation is adopted from de Vries ([90]).

[2] Note that the number of basis functions of the transfer function estimate $\bar{n}_f$ need not be the same as the number of basis functions $\bar{n}_p$ employed in the parameter identification.

where $\mathcal{W} \in \mathbb{C}^{\bar{n}_f \times \bar{n}_f}$ denotes a weighting that enables regularization of estimated parameters that correspond to the tail of the ORTFIR sequence. Typically these parameters are expected to show lesser contribution to the input-output dynamics of the model and for the same reason are expected to be hard to estimate accurately. As a result bad tail parameter estimates might deteriorate the overall transfer function estimate due to large variance. To deal with bad tail parameter estimates, prior assumptions on the decaying character of the generalized pulse response parameters can be enforced by choosing the weighting $\mathcal{W}$ diagonal with a decaying sequence of positive real numbers on the main diagonal, thus reducing the effect of variance at the cost of only little bias.

The final estimate is obtained by averaging the estimates in a similar manner as in the nonparametric case:

$$\hat{G}_f(e^{j\omega}) = \frac{1}{M} \sum_{i=1}^{M} \hat{G}_f^i(e^{j\omega}).$$

From equation (7.13) the following expression is found

$$G - \hat{G}_f^i = \Gamma + \Xi - \vartheta_{\bar{n}_f}[\mathcal{W} \;\; 0]\mathcal{S}^i - \vartheta_{\bar{n}_f}[\mathcal{W} \;\; 0]\mathcal{F}^i$$

where

$$\Gamma(e^{j\omega}) = \vartheta_{\bar{n}_f}(I - \mathcal{W})\theta_0$$

is an error due to the weighting $\mathcal{W}$ in the construction of the transfer function;

$$\Xi(e^{j\omega}) = \sum_{k=\bar{n}_f}^{\infty} L_k \mathcal{V}_k - \vartheta_{\bar{n}_f}[\mathcal{W} \;\; 0]\mathcal{Z}$$

reflects an undermodelling error term being the netto effect of the undermodelling error in $\hat{\theta}^i$ (second term on the right hand side) and the undermodelling error due to utilization of only the first $\bar{n}_f$ basis functions in the construction of the model (first term on the right hand side). The term

$$\vartheta_{\bar{n}_f}[\mathcal{W} \;\; 0]\mathcal{S}^i$$

is due to the effect of unknown input signals on the measured output signals and

$$\vartheta_{\bar{n}_f}[\mathcal{W} \;\; 0]\mathcal{F}^i$$

is due to measurement noise.

An expression for the error bound of $|G(e^{j\omega}) - \hat{G}_f(e^{j\omega})|$ is constituted of the sum of separate error bounds due to unknown inputs and measurement

disturbances, as is similar to the nonparametric case, and an additional error due to undermodelling. As transfer function errors are induced by parameter errors, the real and imaginary part of the transfer function are dependent; construction of error bounds hence is performed for real and imaginary part separately and are subsequently combined into an uncertainty region in the complex plane using results of simultaneous probability density theory.

We state the main result in the following proposition:

Proposition 7.4.2 *de Vries ([90]). Consider the transfer function estimate $\hat{P}_f(e^{j\omega})$; let the input signal be periodic with period N and let M segments of measurement data $\{u^i(t), y^i(t)\}$ be available such that $U^i(e^{j\omega}) = U^{i+1}(e^{j\omega})$, $i = 1, \ldots, M-1$ holds. In that case the following holds, asymptotic in N,*

$$G(e^{j\omega}) - \hat{G}_p(e^{j\omega}) \in \mathcal{A}(e^{j\omega}) \quad w.p. \geq F_\alpha(2, M-2)$$

where $\mathcal{A}(e^{j\omega})$ constitutes the set of stable transfer functions, denoted $\Delta_1(e^{j\omega}) + \Delta_2(e^{j\omega})$, that satisfy

$$\begin{bmatrix} Re\{\Delta_1(e^{j\omega})\} \\ Im\{\Delta_1(e^{j\omega})\} \end{bmatrix}^T \left(\hat{\Sigma}^2_M(\hat{P}_f(e^{j\omega})) + 2\mathcal{S}_p(\omega)I\right)^{-1} \times \begin{bmatrix} Re\{\Delta_1(e^{j\omega})\} \\ Im\{\Delta_1(e^{j\omega})\} \end{bmatrix} \leq \frac{2(M-1)}{M-2}\alpha$$

$$|Re\{\Delta_2(e^{j\omega})\}| \leq |S_p(e^{j\omega})| + |Re\{\Xi(e^{j\omega})\}| + |Re\{\Gamma(e^{j\omega})\}|$$

$$|Im\{\Delta_2(e^{j\omega})\}| \leq |S_p(e^{j\omega})| + |Im\{\Xi(e^{j\omega})\}| + |Im\{\Gamma(e^{j\omega})\}|$$

where $\mathcal{S}_p(\omega)$ is an upper bound of the variance estimate and $S_p(e^{j\omega})$ is an upper bound of the error due to unknown initial conditions.

Proof: *see* [90], *appendix B.7.* □

As the construction of parametric transfer function bounds goes along the same line as the nonparametric bounds, the distinction between unknown initial conditions and variance is more of theoretic nature. As both effects are present in measurement data, any attempt to distinct between the two is dependent on presumptions on system dynamics and noise characteristics, as is discussed in the previous subsection.

The error due to undermodelling however is not present in the data but results from modelling choices and hence the bounding procedure is equipped

with more tuning handles that enable to tune the model error to one's purpose. Utilization of a generalized FIR model structure enables to discern between undermodelling errors and other errors, due to the fact that undermodelling is attributed to the "tail" expansion that is discarded in the identification. Moreover, parameter estimation and parameter error bounding is feasible via clear-cut expressions.

A last feature of parametric uncertainty bounding that we would like to mention is the feasibility to make a trade-off between undermodelling and variance contributions in the total model error bound and therefore creating more insight in how the overall model error can be reduced. This provides informative bounds as how to decrease the model error, either by the experiment design to obtain smaller model error bounds due to variance or by adjusting the model order. This in fact enables tuning of the model error with respect to the overall error instead of solely the undermodelling part.

As we have discussed in chapter 6, the identification problem that we are confronted with is that a model is to be identified from measurement data acquired under closed loop conditions. In the face of the uncertainty bounding procedure previously discussed, the remarks are made.

Firstly, the presumption that $u(t)$ and $d(t)$ are uncorrelated is no longer valid for closed loop measurements. As is clarified in chapter 6, this problem can be alleviated by utilization of coprime factor model representations and a dual Youla representation as they enable to rephrase a closed loop identification problem into an open loop identification of a stable transfer function. Recasting the closed loop problem into an open loop one is feasible via appropriate filtering of the data.

Secondly, filtering of finite length data attained from closed loop experiments, as is elaborated in chapter 6, results in input signals corresponding to the open loop problem that may no longer be exactly periodic, due to transients of the filter. However, employing periodic excitation signals — the excitation signal design is elaborated in section 6.5 — allows to reduce the transient effects due to filtering; filtering of periodic signals is most easily performed in the frequency domain, employing DFT's of the signals and frequency responses of the filters.

7.5 Error bounding of a dual Youla parameter

Recalling from chapter 2, section 2.3, a system P can be parametrized in terms of a transfer function $R \in \mathbb{R}\mathcal{H}_\infty$ as follows (see also equation (2.9)):

$$P = (N_x + D_c R)(D_x - N_c R)^{-1}$$

where N_x, D_x are right coprime factors of an a priori chosen auxiliary model P_x. The transfer function R is uniquely related to the plant P as (see also expression (2.10))

$$R = (D_c + PN_c)^{-1}(P - P_x)D_x$$

which follows from rewriting (2.9). In figure 7.1 a block scheme of a dual Youla parametrization of a model P operating in closed loop is depicted, where a disturbance d enters the loop as an additive signal on the system output y_p.

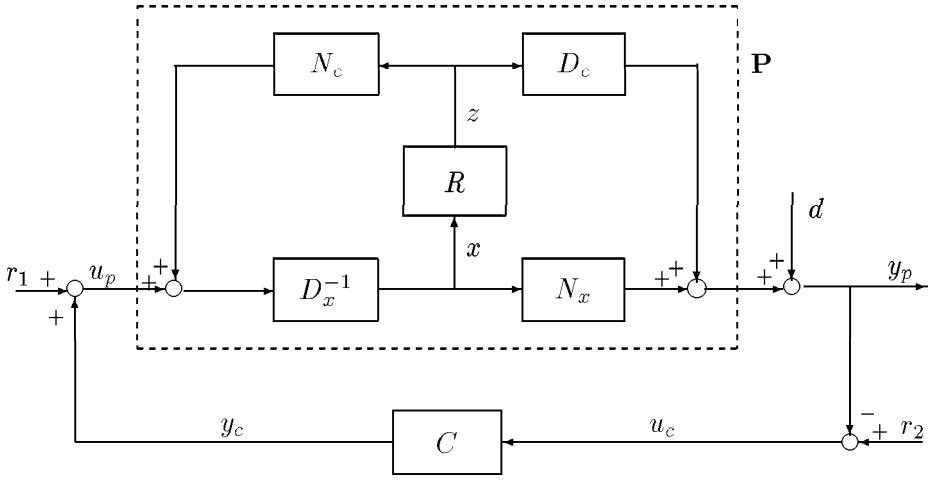

fig. 7.1: Block scheme of a dual Youla parametrization of an LTI model operating in closed loop with an additive disturbance d entering the loop at the plant output y_p.

The input x and output z of the transfer function R are related to the external signals $\{r_1, r_2, d\}$ as follows:

$$\begin{aligned} x &= (D_x + CN_x)^{-1}(r_1 + Cr_2 - Cd) \\ z &= D_c^{-1}[P(1+CP)^{-1} - P_x(1+CP_x)^{-1}]\,(r_1 + Cr_2) + \\ &\qquad [(D_c + PN_c)^{-1} - (D_c + P_x N_c)^{-1}]\,d \end{aligned} \tag{7.14}$$

Although x is correlated with d, we can construct the part of x that is uncorrelated with d, by performing the filter operation

$$x_r := (D_x + CN_x)^{-1}\ (r_1 + Cr_2) \tag{7.15}$$

which is feasible as r_1, r_2 are uncorrelated with d and are available for measurement[3]. The signal x can consequently be written as $x_r + x_d$, where $x_d := (D_x + CN_x)^{-1}\ d$ holds. The signal z however can not be constructed from available signals $\{r_1, r_2\}$ as z is correlated with $r_1 + Cr_2$ via the plant P, which of course is unknown. From the block diagram in figure 7.1 the following relation is derived:

$$R\ x + (D_c + P_x N_c)^{-1} d = (D_c + P_x N_c)^{-1}(y_p - P_x u_p)$$

providing a noise corrupted output signal $z_d := R\ x_r + (D_c + P_x N_c)^{-1} d$ that can be constructed via the filter operation

$$z_d = (D_c + P_x N_c)^{-1}(y_p - P_x u_p). \tag{7.16}$$

Access to the associated dual Youla parameter consequently is attained via signals x_r and z_d as

$$z_d = R\ x_r + H\ d$$

where x_r is uncorrelated with the disturbance d; R is the dual Youla parameter associated with $\{N_x, D_x, N_c, D_c\}$ as defined by (2.10) and the noise model H is expressed as

$$H := (D_c + P_x N_c)^{-1}. \tag{7.17}$$

Consequently, the closed loop identification problem is transcribed into an open loop identification that can be tackled by available open loop techniques.

We point out that in literature modelling of disturbances in a dual Youla framework usually is formulated in a so-called (R, S)-parametrization. We refer to work reported by [39], [40] and [69]. Consider the block scheme of figure 7.2. The signals r_1, r_2 are known and a disturbance w enters the loop as an additive signal on z. The following relations can be derived for the (R, S)-parametrization:

$$\begin{aligned} x &= (D_x + CN_x)^{-1}(r_1 + Cr_2) \\ z &= D_c^{-1}(I + P_x C)^{-1}(y_p - P_x u_p) \end{aligned} \tag{7.18}$$

[3]Note that in case r_1 and r_2 are not available for measurement, we can construct an uncorrelated input signal from $\{u_p, y_p\}$ and knowledge of C, as $r_1 + Cr_2 = u_p + Cy_p$ holds.

As $r_1 + Cr_2 = u_p + Cy_p$ holds, the above relations imply that input and output signals $\{x, z\}$ can be reconstructed from $\{u_p, y_p, N_c, D_c, N_x, D_x\}$. Note that the signal x is uncorrelated with the disturbance w, contrary to the situation where a disturbance enters the loop at the plant output. This results from the fact that the transfer from z to x is 0; so any signal that is uncorrelated with $\{r_1, r_2\}$ and enters the loop at the output of R, is uncorrelated with x. Identification of a system operating in closed loop can consequently be phrased as an open loop identification of an associated, stable transfer function as follows:

$$z = R\ x + S\ w$$

where R is the dual Youla parameter defined by (2.10) and S equals the noise filter H.

7.5.1 Access to normalized coprime factor data

From the algebraical equivalence between filtered coprime factors and a dual Youla parametrization, expressed by (6.7), it follows that access to normalized coprime factor data may also be attained by filtering in a dual Youla parametrization of the system. The frequency responses of the associated coprime plant factors are attained via the filter operation

$$\begin{aligned} &N_x + D_c \frac{Z}{X}(e^{j\omega}) \\ &D_x - N_c \frac{Z}{X}(e^{j\omega}). \end{aligned} \tag{7.19}$$

where the signals $X(e^{j\omega})$ and $Z(e^{j\omega})$ are available through filter operations (7.15) and (7.16).

Although (6.8) and (7.19) are algebraically equivalent, we point out that there is a difference in sensitivity with respect to inadequate knowledge of the controller C. In case N_x, D_x are normalized factors that accurately describe the system, accessability of normalized coprime plant factors still is dependent on accurate controller knowledge in case of (6.8). Filtering via a dual Youla parametrization however is less sensitive to controller inaccuracies as the associated signal z is small and consequently reduces the influence of N_c, D_c in the filter operation. Especially in case of controllers that impose a high bandwidth and, consequently, result in "peaking" of the sensitivity function, slight deviations between the designed and actually implemented controller might exhibit huge differences in the cross-over region. This phenomenon is experimentally verified in chapter 9.

7.6 Validation of uncertainty bounds

In general, validation of identified models is concerned with the evaluation whether a model sufficiently answers to predetermined demands. To phrase the validation problem of identified model error bounds, we pose two questions, adopted from [55], that phrase the main aspects of our validation problem:

1. Does the model (in our case: model error bound) agree sufficiently well with the observed data ?
2. Is the model error bound good enough for its intended use ?

It is stressed that validation of model error bounds applies to the uncertainty set induced by the bounds. Bounds by themselves are not informative without specificiation of a model with respect to which the bounds describe model uncertainty.

The first question addresses whether identified bounds provide a credible description of model uncertainty. Bounds are "credible" if they comply with prior knowledge or for that matter any knowledge available of the system. To that end a first judgment requires that error bounds should not be too small (or too optimistic) as they should at least capture the "true system", or too large (too pessimistic) as they should not account for uncertainty that can not be validated. If either bounds are too small or too large, they lose credibility and one prefers to redo the identification. In case error bounds *seem* credible — in engineering terms bounds "look good" — credibility can be enlarged by checking whether the bounds are consistent with prior assumptions on system and disturbance behaviour. We refer to error bounds as being *reliable* in case they capture the true system and simultaneously are not overly large.

The second question in fact judges models in view of their intended use, regardless the way they are attained. As control design is the purpose of modelling, a general guideline is that the error bound should be small in view of feedback relevant properties of the system. To enhance performance of the system employing a nominal design, a zero error would be the ideal case. But in view of credibility, a zero error bound would instantaneously be rejected. We refer to error bounds as being *useful* in case they allow for an enhanced performance.

7.7 Discussion

Now that we have clarified the utilization of model error bounds, we can deepen the role of model uncertainty in the control design scheme adopted in this

research. The goal of the control design is to achieve a prespecified performance for the system with a restricted complexity controller. Employing a model based control design procedure, there are two issues that dictate to what extent a prespecified performance for the system can be achieved:

1. How accurate is the system knowledge that is available for constructing models ?

2. What is the allowed controller complexity ?

In case a model is attainable having zero model error and the controller complexity is unrestricted, virtually *any* performance can be achieved for the *plant*. Unfortunately, this situation never will occur.

Let us first consider question 2. As is clarified in chapter 4, an important feature of our control design problem is that the controller order should remain limited; we have taken the road of employing *low order* models for control design to achieve this. Although approximate models are underlying the control design, far more accurate (and thus more complex) models are attainable via measurement data. Consequently, the specific choice of not incorporating *all* system knowledge into the design of a compensator, implies that the model error is constituted of a part imposed by the design method, and a part resulting from inaccurate or inadequate system knowledge.

It is the distinction between these two conceptually different types of model uncertainty that is characterictic for the approach taken in this work. In line of the control design strategy in chapter 4, we thus make an artificial partition of the actual model error in terms of a part that is tunable in view of performance enhancement *and* a part that is non-tunable, due to inadequate system knowledge. Consequently, there is a limit to the extent to which we can view the model error as being a design variable.

The accuracy of available system knowledge dictates the non-tunable model error, which is the issue addressed in question 1. As system knowledge is available or obtainable via measurement data, non-tunable model errors are due to the fact that measurement data only capture system dynamics during a finite time (therefore possibly lacking information) and are contaminated with measurement noise. An additional aspect is that the physical plant might not match the LTI modelling framework.

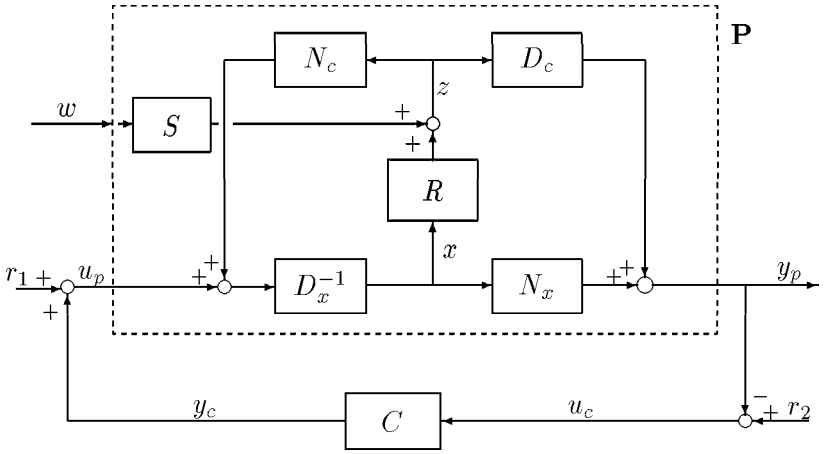

fig. 7.2: (R, S)-parametrization of an open loop model operating in a feedback loop.

Chapter 8

An iterative procedure of identification and control design

8.1 Introduction

In this chapter we will formulate a procedure in view of a systematic enhanced robust performance design for an electro mechanical servo mechanism. The basic tools that constitute the ingredients for a model-based control design procedure are an $\mathcal{H}_\infty$ loop shape control design (chapter 4), approximate identification of low order models suitable for control design (chapter 6) and identification of a system uncertainty set (chapter 7).

The performance that is pursued for an electro mechanical servo system in terms of tracking performance and disturbance attenuation is formulated in this research in terms of a desired sensitivity transfer function, as we have clarified in chapter 3. Design of controllers that comply with specifications on the sensitivity requires accurate knowledge of the dynamics of mechanical part of the servo. In case the system is inaccurately known, a controller might even deteriorate rather than improve tracking. Hence design of controllers based on adequate models is the approach followed in this thesis in order to enhance tracking performance.

The chapter outline is as follows. In section 8.2 we briefly clarify the mechanisms that underly a model-based control design procedure in view of design of *restricted* complexity controllers, touching upon the discussion in section 2.4. The basic aspects of a model-based control design procedure are discussed in section 8.3, constituting an iterative approach of approximate identification and model-based compensator design. A specific feature of the proposed scheme is that a data-based system uncertainty set is employed for evaluation of robust performance. Finally, a detailed iterative procedure is formulated in section

8.4.

8.2 Robust performance enhancement

Let us revert to the discussion on restricted complexity control design in view of an enhanced feedback system performance in section 2.4 in order to put the control design of chapter 4 and the identification of chapters 6 and 7 in an appropriate perspective.

Consider a system P operating in conjunction with a feedback controller C according to the feedback configuration depicted in figure 8.1. Performance is denoted as $\|J(P,C)\| := \|W_{\text{out}}T(P,C)W_{\text{in}}\|$; W_{out} and W_{in} are user defined weighting functions that will be discussed in more detail in section 8.4.

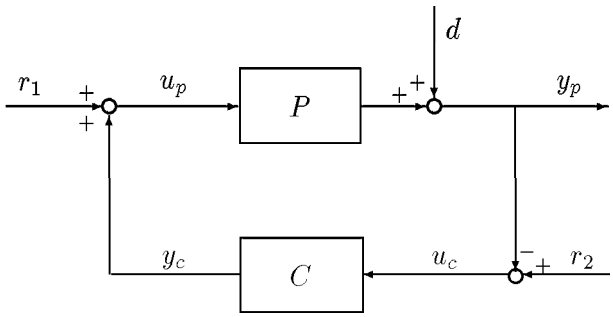

fig. 8.1: Block diagram of the feedback system $T(P,C)$, constituted of a system P in feedback configuration with a controller C.

Instrumental in design of an enhanced robust controller is the availability of a nominal model $\hat{P}$ that underlies the control design. Design of an enhanced robust controller $C_{\hat{P}}$ is performed by the optimization according to

$$C_{\hat{P}} = \arg\min_{\tilde{C}} \|J(\hat{P},\tilde{C})\|_\infty$$

which has been addressed in chapter 4. The designed controller $C_{\hat{P}}$ achieves an enhanced robust performance in view of the previous controller C in case

$$\|J(P,C_{\hat{P}})\|_\infty < \|J(P,C)\|_\infty$$

is satisfied[1] where P denotes the plant.

[1] Recall from section 2.2.3, proposition 2.2.3, that evaluation of performance in terms of

In order to obtain controllers of restricted complexity (recall the discussion in chapter 4), the nominal model $\hat{P}$ is chosen to be of limited complexity, which implies that the model provides an *approximate* description of P. Consequently, the designed controller $C_{\hat{P}}$ will exhibit a different performance for the model $\hat{P}$ and the system P, which is expressed by the triangle inequality (see also expression (2.15), section 2.4),

$$\|J(P, C_{\hat{P}})\| \leq \|J(\hat{P}, C_{\hat{P}})\| + \|J(P, C_{\hat{P}}) - J(\hat{P}, C_{\hat{P}})\|. \tag{8.1}$$

A controller $C_{\hat{P}}$ provides a *robust* enhanced performance in case the following two relations are satisfied:

$$\begin{aligned} \|J(\hat{P}, C_{\hat{P}})\| &< \|J(\hat{P}, C)\| \\ \|J(\hat{P}, C_{\hat{P}})\| &\gg \|J(P, C_{\hat{P}}) - J(\hat{P}, C_{\hat{P}})\|, \end{aligned}$$

which in words indicate that nominal performance is improved and simultaneously robust performance is preserved. The extent to which robust performance can be enhanced utilizing $\hat{P}$ is determined by the actual error between P and $\hat{P}$. Especially in case low order models are used for control design, an approximate model only allows for a limited enhancement of robust performance, indicated by the above inequalities.

The main point stressed is that the model error imposes limitations on the maximum achievable robust performance enhancement. Hence the problem boils down to determining a model $\hat{P}$ of limited complexity that allows for the largest possible enhancement of robust performance. Approximate modelling for enhanced robust control design is therefore directed towards "shaping" of the approximation error. We have clarified in section 2.5 that an approximate model is regarded suitable for design of an enhanced robust performance controller in case it complies with the following two inequalities:

$$\begin{aligned} \|J(\hat{P}, C)\| &\gg \|J(P, C) - J(\hat{P}, C)\| \\ \|J(\hat{P}, C_{\hat{P}})\| &\gg \|J(P, C_{\hat{P}}) - J(\hat{P}, C_{\hat{P}})\|. \end{aligned}$$

Consequently, a performance relevant approximation is not only determined by the known controller (which is the controller present in the feedback loop), but also by a future controller. As a future controller yet has to be designed on the basis of the nominal model, the utility of an approximate model in view of enhanced robust control design can only be evaluated a posteriori. This

$\|J(P,C)\|_\infty$ can be derived from $|J(P,C)|$; so we do not fundamentally change the performance evaluation problem stated in section 2.6 in this way.

necessitates an iterative approach towards approximate modelling and model-based control design in view of an enhanced robust performance.

Design of a controller based on an approximate model requires an evaluation of the achieved performance to inspect the (inevitable) discrepancy between designed and achieved performance prior to controller implementation. To that end, performance evaluation is performed based on system knowledge available, which in our case is embodied in measurement data.

In chapter 5 we have addressed frequency response measurements of a radial Compact Disk servo system in view of their utility for performance evaluation. It is shown that a sole frequency response, although seemingly accurate at first sight, constitutes an insufficiently accurate basis for evaluation of *robust* performance; this observation has led us in chapter 2 to make a discern between a model error that is tunable and a model error that is non-tunable. In order to enable a performance evaluation that is robust in view of inaccurate system knowledge (frequency response measurements), we have motivated in the final discussion in chapter 5 the incorporation of data based model error bounds in a procedure for evaluation of the achieved performance.

In chapter 7 the identification of model error bounds has been addressed. Evaluation of robust performance employing model error bounds is expressed as

$$\sup_{P \in \mathcal{P}} \|J(P, C_{\hat{P}})\|_\infty \leq \gamma_{\text{spec}} \tag{8.2}$$

where the value γ_{spec} denotes a prespecified performance level. It has been shown in section 7.3 that employing a dual Youla model uncertainty structure enables evaluation of robust performance in terms of error bounds of $|J(P, C)|$, which provides in terms of disturbance attenuation (sensitivity).

In most cases it will be very likely that a robust performance *enhancement* may be feasible, but achieving a *prespecified* robust performance may yet be beyond reach as a result of the limitations of a model-based control design based on *approximate* models. The issue rises what to do next?

In order to arrive at a prespecified robust performance employing approximate models for control design we adopt a scenario where we start from one feedback situation going to another in small steps where in every step a critical evaluation of performance enhancement is pursued. This leads to formulate a control design strategy in terms of a repeated exercise of gradually enhancing robust performance until a prespecified robust performance is established. At this point we make a critical note that there is no guarantee that a prespecified

performance actually will be achieved.

In literature iterative schemes of approximate system identification and model-based control design are proposed (we refer to [69], [85] and [29]). In the next section the principal steps taken in an iterative approach *towards* a prespecified robust performance are discussed.

8.3 Principal scheme

In this section we discuss a general iterative procedure and will comment on the separate steps of approximate identification and model-based control design.

The index i refers to the model $\hat{P}_i$ that is identified and the controller C_i that is designed on the basis of $\hat{P}_i$ in the i-th iteration; $J_i(P,C)$ refers to $W_{\text{out},i}T(P,C)W_{\text{in},i}$. An iterative scheme basically boils down to a repeated execution of the following consecutive steps[2].

Data acquisition

Consider the feedback system in figure 8.1 and denote C_{i-1} as being the compensator resulting from a preceding design or, in case $i = 1$, an initial compensator present in the feedback loop. Measurements of $\{r_1, u_p, y_p\}$ are obtained under closed loop conditions. In the approximate identification discussed in chapter 6 and the identification of model error bounds, discussed in chapter 7, time domain measurement data are represented in terms of their Discrete Fourier Transforms $\{R_N(e^{j\omega}), U_N(e^{j\omega}), Y_N(e^{j\omega})\}$.

Approximate identification

A feedback relevant approximate model is identified according to the following optimization problem

$$\hat{P}_i = \arg_{\tilde{P}} \min \|J_{i-1}(P, C_{i-1}) - J_{i-1}(\tilde{P}, C_{i-1})\|, \tag{8.3}$$

where measurement data are confined in the expression for $J_{i-1}(P, C_{i-1})$. In order to preserve robust performance, the nominal performance must not be deteriorated, phrased in the requirement

$$\|J_{i-1}(\hat{P}_{i-1}, C_{i-1})\| \simeq \|J_{i-1}(\hat{P}_i, C_{i-1})\|.$$

The rationale is that a decrease of the upper bound on achieved performance, expressed by the triangle inequality (8.1), is established in each separate step

[2]It is noted that this scenario strongly hinges on the primary iterative scheme as developed by Schrama ([69]).

of approximation and control design. The approximation problem can thus be interpreted as determining a model that achieves an enhanced performance robustness while maintaining nominal performance for the *present* controller C_{i-1}.

As discussed in the previous section, an approximate model suitable for our purpose must exhibit satisfactory robust performance properties in view of the present controller *and* the future controller. So, we do not specificly aim at approximating a model in view of the controller C_{i-1}, as is expressed by the above approximation problem, but in fact in view of both controllers C_{i-1} and C_i. Of course, controller C_i is not (yet) available.

Control design

A controller is designed based on a model $\hat{P}_i$, according to the $\mathcal{H}_\infty$ loop shape design method discussed in chapter 4, definition 4.3.1, leading to

$$C_i = \arg_{\tilde{C}} \min \|J_i(\hat{P}_i, \tilde{C})\|_\infty \tag{8.4}$$

A decrease of the upper bound on $\|J(P,C)\|$ expressed by the triangle inequality by means of control design, imposes an additional requirement on the controller, expressed as

$$\|J_i(P, C_{i-1}) - J_i(\hat{P}_i, C_{i-1})\| \simeq \|J_i(P, C_i) - J_i(\hat{P}_i, C_i)\|$$

which indicates that an enhanced robust performance is achieved via enhancing nominal performance in case the difference of achieved and nominal performance only slightly deteriorates.

We have clarified in chapter 4 that the control design according to (8.4), phrased as a nominal design, implicitly anticipates model imperfections in terms of fractional perturbations in view of stability. Whether the performance deterioration increases of course depends on the true error between model and system. In case the system is only a slight perturbation of the model, expressed in terms of normalized coprime factor representations, the requirement is likely to be met for a designed controller. This poses an additional motivation for phrasing an approximate identification problem in view of robust performance enhancement in terms of identification of normalized coprime factors, as has also been put forward by [69].

Performance evaluation

To evaluate whether a controller is suitable for implementation, analysis of the actually achieved performance is imperative. To that end we want to

evaluate the value of

$$\sup_{P \in \mathcal{P}} \|J(P, C_{\hat{P}})\|_\infty < \gamma_{\text{desired}}$$

where $\mathcal{P}$ denotes a set of systems to which the plant is presumed to belong. Performance evaluation is instrumental in making the right trade-off between nominal performance enhancement and robustness; based on the outcome of the evaluation a controller is found suitable (or not) for implementation. Performance relevant model error (PREME) evaluation constitutes the second stage of the control design procedure as proposed in chapter 4.

Performance evaluation is performed utilizing a system uncertainty set, identified from measurement data as addressed in chapter 7. Typically, a data based system uncertainty set represents the most accurate system representation that we can extract from measurement data and accounts for model errors that are beyond tuning. As performance is evaluated based on a system uncertainty set, it is referred to as system uncertainty-based performance relevant model error (SUPREME) evaluation.

The above mentioned steps are schematically depicted in figure 8.2.

8.4 Detailed scheme

Finally we come to the proposition of a procedure for model based robust performance enhancement that is to be applied to a mechanical servo system. In line with the scheme discussed in previous section, an iterative scheme of system identification and control design is constituted of the following steps:

Data acquisition

A periodic excitation signal, denoted r_1 in figure 8.1, is applied to the feedback system and, when transient effects have vanished, measurements of the signals $\{r_1, u_p, y_p\}$ are obtained from the system operating in conjunction with a known controller, depicted in the block diagram in figure 8.1. Averaging of the segments of r_1, u_p and y_p is performed on the time domain signals, prior to DFT, as this saves computation time; averaged DFT's are denoted as $R(e^{j\omega_k}), U(e^{j\omega_k})$ and $Y(e^{j\omega_k})$. Each DFT signal is stacked in a data matrix of dimension $N_f \times M$, N_f denoting the number of sinusoids contained in $R(e^{j\omega_k})$ and M the number of periods measured. Data matrices are denoted $\mathcal{R} \in \mathbb{C}^{N_f \times M}$, $\mathcal{U} \in \mathbb{C}^{N_f \times M}$ and $\mathcal{Y} \in \mathbb{C}^{N_f \times M}$.

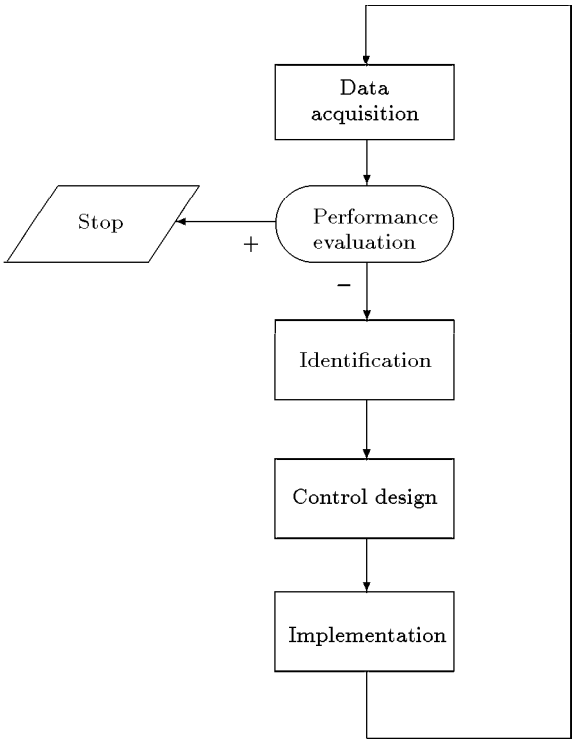

fig. 8.2: Schematic diagram of an iterative procedure of identification and control design in view of robust performance enhancement.

Identification of an auxiliary model

Identification of approximate models (chapter 6) and system uncertainty sets (chapter 7) is performed in this thesis using fractional model representations. The main motivation to use fractional model representations is that they exhibit favourable properties in view of feedback relevant modelling. We briefly recapitulate the main features encountered in this work:

- The $\mathcal{H}_\infty$ loop shape control design is known to provide controllers that have optimal robust stability properties with respect to additive perturbations of normalized coprime factors of the model. In order to comply with the anticipated nature of model imperfections by the controller, approximate modelling should preferrably be done in the same way.
- A system uncertainty set that is based on a dual Youla model representation (see expression (2.14)) enables the derivation of non-conservative error bounds of the closed loop system with any (stabilizing) controller in the loop. This is a powerful tool to evaluate the achieved performance prior to controller implementation.

Instrumental for coprime factor identification of approximate models and model error bounding employing a dual Youla uncertainty set, is the availability of a model P_x that provides an accurate description of the system operating in the presence of a known stabilizing compensator. We list three reasons.

Firstly, as coprime factors do not represent unique model representations, identification within a coprime factor model structure requires measurement data to correspond to normalized coprime factors of the systems to ensure well-posedness of the identification problem. Normalized factor data are accessable via filtering on the basis of accurate system knowledge, embodied in an accurate model P_x.

Secondly, a model P_x that provides an accurate system description constitutes an adequate auxiliary model for a dual Youla system uncertainty set identification. This is seen from the expression (also referred to in chapter 6, expression (2.10))

$$R = (D_c + PN_c)^{-1}(P - P_x)D_x \tag{8.5}$$

which indicates that in case $P_x \simeq P$, the corresponding dual Youla parameter satisfies $R \simeq 0$. A small value of R is favourable in view of a tight uncertainty set.

Thirdly, $\{N_x, D_x\}$ are used in the construction of control relevant weightings for identification of an approximate model.

Identification of an auxiliary model is carried out in the course of constructing a filter that induces normalized coprime factor data. Access to normalized coprime factor frequency domain data is established via the filter operation

$$X(e^{j\omega_k}) = (D_x + CN_x)^{-1} R(e^{j\omega_k})$$

such that Y/X and U/X satisfy

$$\left(\frac{Y}{X}\right)^* \frac{Y}{X} + \left(\frac{U}{X}\right)^* \frac{U}{X} \simeq I.$$

Instrumental for the construction of a "normalizing" filter $(D_x + CN_x)^{-1}$ is the identification of a parametric model P_x that accurately describes the system dynamics in view of the controller present in the loop. To that end we employ an ORTFIR model structure for identification of normalized coprime factors of P_x. Normalization of coprime factor data is based on a procedure proposed by [86] and consists of the following steps:

1. Consider DFT's $\{R(e^{j\omega_k}), U(e^{j\omega_k}), Y(e^{j\omega_k})\}$ of the time domain measurement data $\{r_1, u_p, y_p\}$, obtained in the closed loop configuration of figure 8.1. First a low order basis generating model is attained via coprime factor identification with common denominator, discussed in chapter 6, by means of the following optimization problem:

$$\hat{B}, \hat{A}, \hat{F} = \arg_{B,A,F} \min \left\| V_o \begin{bmatrix} \frac{Y}{R}(e^{j\omega_k}) - \frac{B(e^{j\omega_k})}{F(e^{j\omega_k})} \\ \frac{U}{R}(e^{j\omega_k}) - \frac{A(e^{j\omega_k})}{F(e^{j\omega_k})} \end{bmatrix} V_i \right\|_2^2$$

   where

$$\begin{aligned} B(e^{j\omega}) &:= b_0 + b_1 e^{-j\omega} + b_2 e^{-2j\omega} + \ldots + b_{n_b} e^{-n_b j\omega} \\ A(e^{j\omega}) &:= a_0 + a_1 e^{-j\omega} + a_2 e^{-2j\omega} + \ldots + a_{n_a} e^{-n_a j\omega} \\ F(e^{j\omega}) &:= 1 + f_1 e^{-j\omega} + f_2 e^{-2j\omega} + \ldots + f_{n_f} e^{-n_f j\omega}. \end{aligned}$$

2. A high order auxiliary model P_x is identified employing an ORTFIR model structure (chapter 6), utilizing the previously identified model as a basis generating system.

3. Based on normalized right coprime factors of the model P_x, denoted $\{N_x, D_x\}$, access to normalized coprime factor frequency domain data is obtained as:

$$\begin{aligned}\frac{Y}{X}(e^{j\omega_k}) &:= \frac{Y}{R}(e^{j\omega_k})(D_x(e^{j\omega_k}) + CN_x(e^{j\omega_k})) \\ \frac{U}{X}(e^{j\omega_k}) &:= \frac{U}{R}(e^{j\omega_k})(D_x(e^{j\omega_k}) + CN_x(e^{j\omega_k})).\end{aligned}$$

or alternatively as, employing the dual Youla parametrization:

$$\begin{aligned}\frac{Y}{X}(e^{j\omega_k}) &:= N_x(e^{j\omega_k}) + D_c(e^{j\omega_k})\frac{Z}{X}(e^{j\omega_k}) \\ \frac{U}{X}(e^{j\omega_k}) &:= D_x(e^{j\omega_k}) - N_c(e^{j\omega_k})\frac{Z}{X}(e^{j\omega_k}).\end{aligned}$$

where

$$\begin{aligned}X(e^{j\omega_k}) &= (D_x + CN_x)^{-1}R(e^{j\omega_k}) \\ Z(e^{j\omega_k}) &= D_c^{-1}(I + P_xC)^{-1}(Y(e^{j\omega_k}) - P_xU(e^{j\omega_k}))\end{aligned}$$

4. Verify whether $(Y/X)^*Y/X + (U/X)^*U/X \simeq I$ is satisfied; if not, revert to step 1 employing $\frac{Y}{X}(e^{j\omega_k})$ and $\frac{U}{X}(e^{j\omega_k})$ as frequency domain data.

Repeating the above steps a number of times gradually improve the normalizedness of the frequency domain coprime factor data.

Identification of a model error bound

A tight and accurate system uncertainty set is identified employing the system uncertainty set representation $\mathcal{P}_R(N_x, D_x, N_c, D_c, R, \delta_R)$, employing the frequency domain data $\{X(e^{j\omega_k}), Z(e^{j\omega_k})\}$ obtained by the filter operation shown above. A nominal model $R(e^{j\omega}, \theta)$ of the dual Youla parameter is identified together with a continuous transfer function error bound $\delta_R(\omega)$, using the procedure in chapter 7.

The dual Youla parameter associated with an auxiliary model P_x that accurately describes the system will hardly contain relevant information. Moreover, as $\{N_x, D_x\}$ are determined as normalized coprime factors, the corresponding system factors $N_x + D_cR$ and $D_x - N_cR$ indicate that the dual Youla parameter constitutes a perturbation of normalizedness of the filtered coprime factor data. As we have obtained data that are (presumed) sufficiently normalized from the procedure phrased above, an important consequence is that the identified uncertainty set of R contains 0 for all frequencies. If this is not the case, the identified uncertainty set is not consistent with the fact that coprime factor frequency domain data are sufficiently normalized.

Identification of an approximate model

Based on the (almost) normalized frequency domain data $\{Y/X, U/X\}$, a low order parametric model is identified employing a least-squares curve-fit of coprime factors as follows (chapter 6):

$$\hat{\theta} = \arg_\theta \min \left\| V_{\text{out}} \begin{bmatrix} \frac{Y}{X}(e^{j\omega_k}) - N(e^{j\omega_k}, \theta) \\ \frac{U}{X}(e^{j\omega_k}) - D(e^{j\omega_k}, \theta) \end{bmatrix} V_{\text{in}} \right\|_2^2 \Bigg|_{D(\hat{\theta})+CN(\hat{\theta})=D_x+CN_x} .$$

where the weightings $V_{\text{out}}, V_{\text{in}}$ are chosen as

$$V_{\text{out}} = \begin{bmatrix} W(\nu_b) & 0 \\ 0 & I \end{bmatrix}$$

$$V_{\text{in}} = (D_x + CN_x)^{-1} [C \quad I] \begin{bmatrix} W^{-1}(\nu_b) & 0 \\ 0 & I \end{bmatrix}$$

where $W(\nu_b)$ is a weighting resulting from the control design, discussed in chapter 4, expressions (4.9) and (4.8). In order to comply with the parametric constraint, we adopt the approach discussed in chapter 6, section 6.4.1, to perform the approximate identification in an unconstrained manner and to check a posteriori whether the parametric constraint is sufficiently satisfied. For arguments in favour of this approach, we refer to the discussion in section 6.4.1.

Control design

Control design is based on a $\mathcal{H}_\infty$ loop shape design, treated in chapter 4 and formulated in detail in definition 4.3.1. The design basically comprises the following two steps

1. Design of a trajectory of weighting functions using a $4th$ resp. $3rd$ order lead-lag filter $W_4(\nu_b^i)$ or $W_3(\nu_b^i)$, $\nu_b^{i+1} > \nu_b^i$, for $i = 1, \ldots, p$.

   Some observations regarding the difference of the weighting functions are at place. The $4th$ order lead-lag filter contains a phase lead near the cross-over frequency region and hence enables to stabilize the nominal model, while the $3rd$ order weighting does not stabilize the nominal model. Note that stabilization of the nominal model is not required as the consecutive optimization based design optimizes stability robustness. As we have indicated in chapter 4, the robustness optimization step must not alter the

nominal design too much since then the trade-off between nominal performance and robust stability is not in proper balance. In this perspective, a $4th$ order weighting has preference. On the other hand, a $3rd$ weighting, resulting in a controller order lower by 2, establishes less cautious steps towards performance enhancement, but may lead to a larger enhancement for the system in each control design step.

Robust controllers $C_{\hat{P},\nu_b^i}$ are computed according to the procedure phrased in definition 4.3.1 for every weighting.

2. Although the controllers $C_{\hat{P},\nu_b^i}$ have optimal robustness properties, they are not guaranteed to be robust for the system. Therefore the sequence of robust controllers $C_{\hat{P},\nu_b^i}, i = 1, \ldots, p$ is evaluated in view of the performance achieved for the system, referred to as robust performance evaluation. To that end the identified system uncertainty set $\mathcal{P}_R$ is employed by virtue of transformation of the identified model error bounds δ_R into additive error bounds of the feedback system, as expressed in proposition 7.3.1, section 7.3. The controller that provides the largest possible performance enhancement within the prespecified margins of robust performance is picked from the sequence of designed controllers for implementation.

Controller implementation

In case robust stability and performance analysis turn out right, the controller is implemented and new data acquired in presence of the new controller according to the data acquisition step above. Details on implementation issues are postponed until the next chapter.

Validation system uncertainty set

Once the newly designed controller is successfully implemented and new data measurements are obtained, the estimated uncertainty set can be validated in view of its capability of reliably predicting the sensitivity and plant times sensitivity for the newly designed controller. Two situations are liable to occur.

The achieved performance is reliably predicted by the system uncertainty set, hence the identified model error bounds are validated in view of their intended purpose. We draw the conclusion that presumptions underlying the modelling and the control design in conjunction with performance evaluation are (still) valid for further enhancement of the feedback systems performance.

The achieved performance is *not* well predicted; this implies that the identified uncertainty set is invalidated in view of the enhanced feedback situation.

As models are instrumental in the design and analysis of enhanced controllers, we at least demand that the controllers should establish a performance for the system within the validity range of the models underlying its design and analysis. In case a controller proves to be operating beyond the models validity range, we do not claim that the models are wrongly estimated, but that the controller is wrongly designed in view of the available models. To that end, we modify the design by specifying a lesser performance in a subsequent control design, which is established by using weightings reflecting lesser nominal performance enhancement — taking smaller steps in the weighting function design — or identification of higher order models in order.

Performance evaluation

In case the system uncertainty set is validated, we evaluate whether the actually achieved performance complies with the desired performance. If so, the iteration is stopped, otherwise continued.

An important aspect is that iterative schemes have not yet been demonstrated to converge to an optimal controller. We therefore require that after one iteration a minimum level of performance enhancement of the system must be established in order to make a renewed iteration worthwhile. A scenario that may be expected is that, starting with low performance, robust enhancement steps will gradually decrease and that it will become more and more difficult to achieve a substantial performance enhancement. Ultimately, the designer will have to make the decision whether the effort still weights up against the profit. Moreover, the performance objective primarily set out might prove to be beyond reach which means he has to settle for less performance.

In figure 8.3 the above steps and their mutual relations are schematically depicted in a flow diagram.

We conclude this section with a last remark.

Employing a low order model as a basis for model based control design is instrumental in keeping the controller complexity low. In order to realize an enhancement of robust performance we are consequently compelled to make small steps, which implies that establishing a prespecified robust performance may require more iterations then in case a higher order model is underlying the control design. So with respect to choosing a suitable model order, we are confronted with a trade-off between a high model order in view of a large robust performance enhancement and a low model order in view of implementation restrictions of high order controllers.

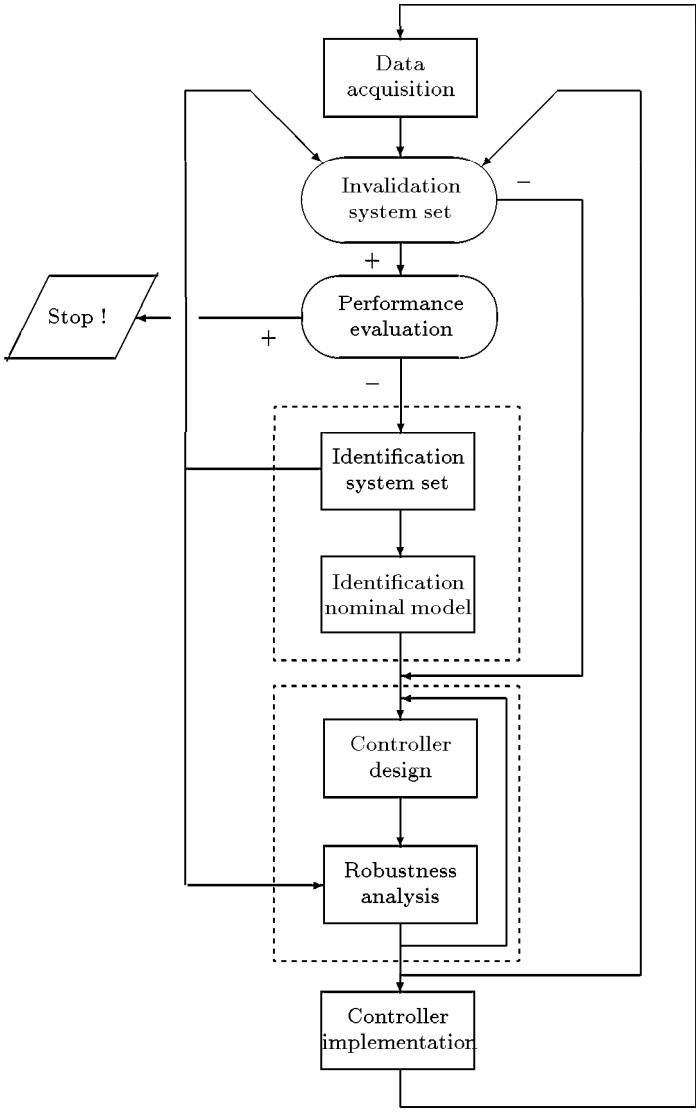

fig. 8.3: Schematic diagram of the detailed iterative scheme of identification and control design in view of performance enhancement.

8.5 Summary

In this chapter we have proposed an iterative approach of approximate identification and model based control design with the aim to design controllers of restricted complexity that establish a prespecified, performance for the system. Let us briefly review the main issues presented.

The need to resort to an iterative approach towards modelling and control design has been put forward by the fact that we deliberately want to keep the model order low in view of a (resulting) low order controller. Design of a controller on the basis of this model, in such a way that a similar performance is achieved for the system as is designed on the model, renders the robust performance enhancement that can be achieved by design of a single controller, to be restricted. Repeating the design of controllers that subsequently establish small steps of enhanced performance should finally lead to the prespecified performance.

A feature of the design procedure is that the controller anticipates model imperfections, although robustness is not guaranteed a priori. Therefore we must evaluate the achieved robust performance prior to implementation. To that end a system uncertainty set description, constructed from measurement data, is employed to provide a *reliable* prediction of how a newly designed controller performs for the system.

The iterative approach presented in this chapter is formulated in a more concise manner by Dötsch *et al.* ([23]). In the next chapter the proposed procedure is applied to an experimental Compact Disk servo system.

Chapter 9

Application to a Compact Disk servo mechanism

9.1 Introduction

In this chapter the iterative procedure of identification and control design, proposed in the previous chapter, is applied to two experimental set ups of a Compact Disk servo mechanism of a swing-arm type.

The experimental environment for controller implementation and data acquisition is described and the experimental lay out of the Compact Disk servo mechanism, discussed in chapter 3, is discussed in more detail in section 9.2. In section 9.3 we clarify considerations regarding the initialization of the proposed procedure. The subsequent steps taken in one iteration are carried out in section 9.4 for one Compact Disk set up. Evaluation of the results in view of the theoretical developments in previous chapters is the topic in section 9.5.

In section 9.6 the system uncertainty set identification discussed in chapter 7 is applied to measurement data obtained from two different experimental Compact Disk mechanisms, in order to construct an uncertainty set that accounts for distinct dynamical behaviour. We conclude this chapter in section 9.7 with a discussion of observed results.

9.2 Experimental environment

9.2.1 Hardware equipment

For experiment purposes two Compact Disk servo mechanisms, as described in chapter 3, are available. For implementation of digital controllers, data measurement and implementation of periodic excitation signals, two digital

signal processors are used [17]. The hardware equipment utilized for performing experiments is treated in this section.

Compact Disk player

The experimental system is equipped with an interface that enables measurement of tracking error signals and application of control and excitation signals. As the system has a double integrator, a stabilizing internal controller is present. Implementation of an external controller is performed by switching from the internal controller to the external one, which is feasible by a hardware switch on the interface. A schematic overview of the physical lay out and a photograph picture of the experimental environment are depicted in figure 9.1 resp. 9.2.
A block diagram of the experimental Compact Disk feedback system is depicted in figure 9.3.

We address some features specific for a radial actuator that affect the elaboration of the measurement experiments. In chapter 3 it is clarified that a radial actuator causes the servo system to have a non-linear gain, depending on the radial position on the disk where data are read. The available internal controller automatically corrects for gain variations by injecting a sinusoide with a frequency just above the closed loop bandwidth. This is the so-called "wobble" [7]. However, an external controller does not correct for gain drifts; hence measurements acquired in the presence of an external controller inherently are subjected to gain drifts. In order to minimize the effect of static non-linearities on measurement data, in figure 9.4 the relative gain drifts are shown as a function of radial measurement position for measurement time intervals $\{60, 120, 240, 480\}$ secs. The drift in relative gain is depicted for a given measurement time for radial positions ranging from $0.02m$ to $0.057m$, which covers the total radial range of an audio compact disc. According to figure 3.4, chapter 3, the radial position on a disk where gain drifts are minimal for a large radial displacement — which is equivalent to a large measurement time — corresponds to a normalized gain of 1; thus measurements with little gain drift during a longer measurement time are obtained at approximately $0.03m$ distance from the disk centre.
As is indicated in chapter 3, radial tracking is severely hindered by the dominant presence of periodic disturbances due to eccentric disk rotation. From an identification point of view, the influence of (periodic) disturbances on measurement data should be minimized. The effect of periodic disturbances on the tracking error (and hence on the signal-to-noise ratio) is influenced by two

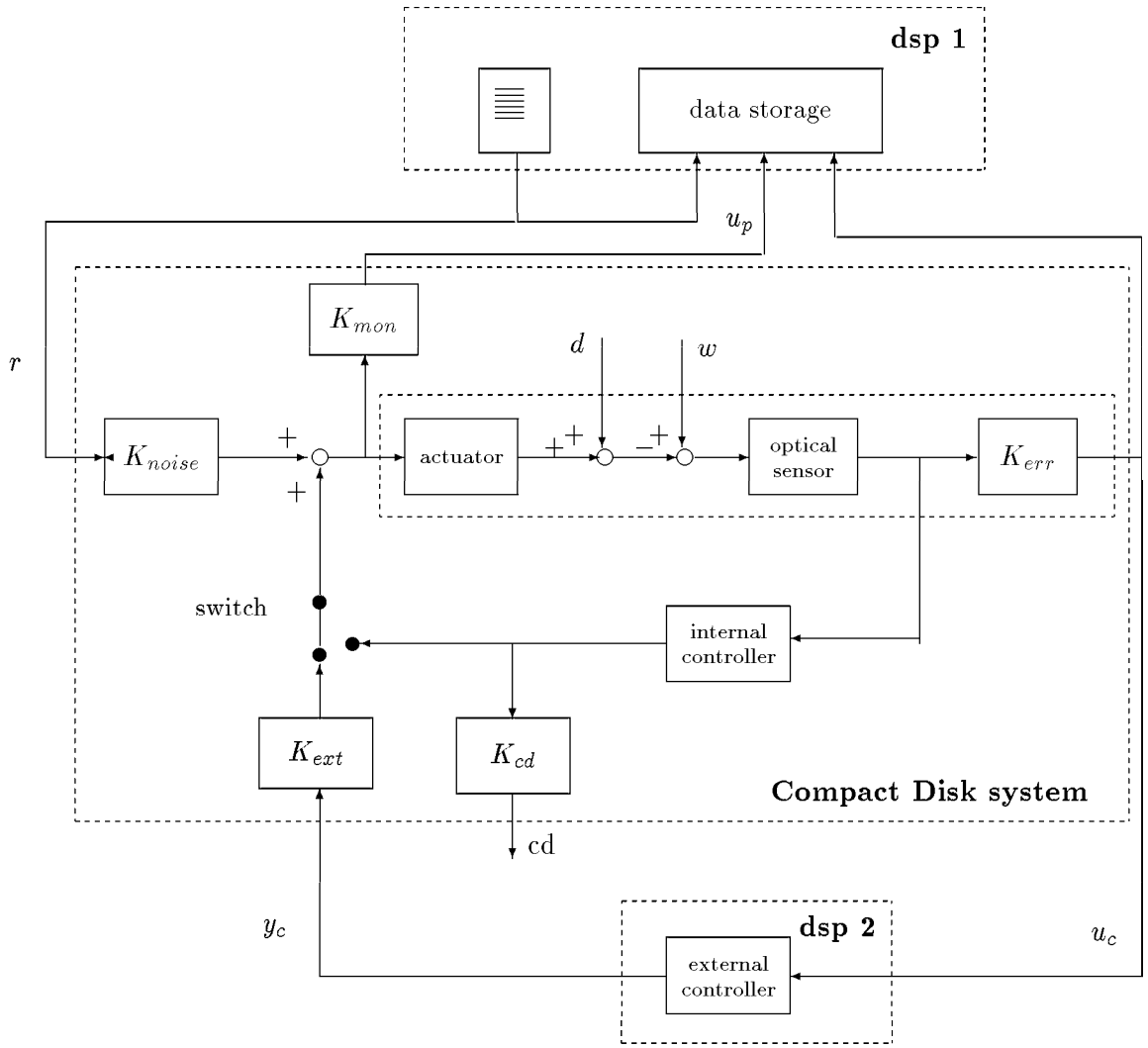

fig. 9.1: Schematic diagram of the physical lay out of the experimental environment: Compact Disk system, a digital signal processor for data measurement and implementation of periodic excitation signals (DSP 1) and a digital signal processor for controller implementation (DSP 2).

fig. 9.2: Photographic impression of the experimental environment.

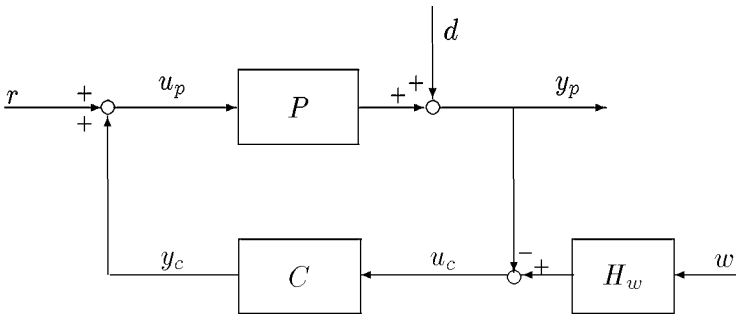

fig. 9.3: Block diagram of the experimental Compact Disk servo system of figure 9.1, constituted of the optical pick-up unit, denoted P, and an external controller C. The signals u_p, u_c are available for measurement, r is the excitation signal; w is the position of the track and y_p is the position of the actuator, which are both not available for measurement.

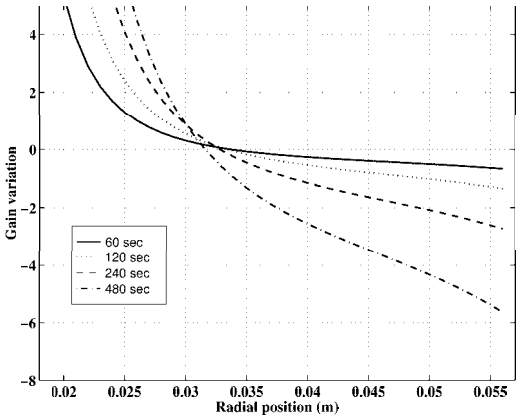

fig. 9.4: Relative gain drifts expressed as a function of radial measurement position for measurement time $\{60, 120, 240, 480\}$ secs.

mechanisms:

- Disk rotation velocity varies approximately from 8 Hz at the centre of the disk (start of the track) to 3 Hz at the edge of the disc. Periodic disturbance components due to eccentric disk rotation hence shift to lower frequencies in case of a low disk rotation velocity, which is the frequency region where the sensitivity function of the feedback system is more capable of attenuation.

- The non-linear gain characteristic of the radial actuator (shown in figure 3.4, chapter 3) also applies to the gain with which radial displacement disturbances induce an angular arm displacement for accurate tracking. From figure 3.4 it is concluded that measurement at a radial position $0.05m$ enables a relative decrease of the disturbance gain of approximately 11%, compared to a radial position of approximately $0.033m$. Consequently, measurement experiments with a high signal-to-noise ratio are preferrably performed while the radial actuator is tracking at the edge of the disc.

An optimal choice of the radial position for doing measurement experiments is based on a compromise between the two above mentioned aspects: reducing the effects of gain drift on the one hand and a low disturbance gain on the other hand. An important factor in this respect is the time needed to acquire the measurement data as gain drift increases with increasing measurement time. Data acquisition is discussed in the section on implementation issues; at this

point we mention that time required for data measurement amounts to approximately 120 secs. From figure 9.4 it is deduced that in case measurements are performed at a radial position of $0.05m$, a measurement time of 120 secs corresponds to a gain drift less than 1%, which is acceptable.

Signal processor

For implementation of digital controllers, measurement of data sequences and implementation of periodic excitation signals, two DS1003 processor boards are used that are built around a TMS320C40 floating point digital signal processor (DSP) [17].

As the frequency region of interest ranges up to 10.000 Hz, the sample frequency for data acquisition and digital controller implementation is set out at 25 kHz, which corresponds to a sample time of 40 μ sec. Utilization of two processor boards is required in order to implement controllers at a sample rate of 25 kHz (DSP 2 in figure 9.1) and enable periodic excitation and data acquisition at the same sample rate (DSP 1 in figure 9.1). Controller and signal design and subsequent downloading onto the processor board is performed within a MatLab software environment.

9.2.2 Implementation issues

Controller implementation

Controller implementation at a sample rate of 40 μ sec puts a hard constraint on the maximum controller order viable for implementation. Minimization of the number of calculations during one sample time required for a given controller, enables maximization of the implementable controller order. Using a real Jordan canonical state space form, the maximum controller order that can be implemented at a sample time of 40 μ sec is 15.

If we recall the control design of chapter 4, this implies that using weighting functions of order 3 resp. 4, the maximum order of a model underlying the design is 9 resp. 7 (note that the loop shape weightings effect the controller order twice). This means that approximately half of the controller order is determined by weightings instead of the model, which is undesirable for the following reason.

The practical motivation for doing *approximate* identification for model-based control design is due to hardware restrictions for controller implementation. By keeping the model order low, we are able to design low order controllers viable for implementation. A low complexity model however restricts an increase of robust performance; we refer to the discussion on model errors

in section 2.4. Within the constraint of a prefixed controller order, a model of largest possible order hence enables the largest possible enhancement of robust performance. Consequently, to balance the model order and weighting order in accordance with our design philosophy, a controller order reduction step is performed such that the weighting effects the controller order only once. This implies that models can be identified of a maximum order 11 in case of a 4-th order weighting and order 12 in case of a 3-rd order weighting.

Data acquisition

Due to limited memory capacity of the DS1003 processor board, data sequences are measured as separate segments, which expands limitations of the number of measured data to the internal memory capacity of the computer. The maximum segment length equivalent to a power of 2 is 8192 samples in case 3 signals are to be measured; this implies that the maximum period length that can be measured is also 8192 samples.

As is discussed in chapter 5, segmented data measurement in conjunction with periodic excitation signals does not effect contributions of noise and unknown initial conditions to the estimation results any differently from the case that data would have been acquired contiguously.

The number of segments that can be measured is restricted by the internal memory capacity of the host computer. In order to limit computation time, we choose to employ 40 periods with a length of 4096 samples for identification, which amounts to measurement of 20 data segments. Measurement of every segment is triggered on the first data sample of the excitation signal period. The total number of measured time domain data $\{r, u, y\}$ then equals $4096 \times 40 \times 3 = 491.520$ data samples. After Fourier transformation (recall that one period contains 99 sinusoids) $99 \times 40 \times 3 = 11.880$ complex data samples are obtained.

The data are stacked matrix-wise as $\mathcal{R} \in \mathbb{C}^{99\times 40}$,$\mathcal{U} \in \mathbb{C}^{99\times 40}$ and $\mathcal{Y} \in \mathbb{C}^{99\times 40}$ in view of uncertainty bounding; in view of identification of nominal parametric models the averaged DFT's of $\{r, u, y\}$ are used, obtained by averaged the 40 time domain signals:

$$U_N^{\mathrm{av}}(e^{j\omega_k}) = \frac{1}{\sqrt{N}} \sum_{t=0}^{N-1} \left(\frac{1}{40} \sum_{i=1}^{40} u^i(t) \right) e^{-j\omega_k t} \tag{9.1}$$

$$Y_N^{\mathrm{av}}(e^{j\omega_k}) = \frac{1}{\sqrt{N}} \sum_{t=0}^{N-1} \left(\frac{1}{40} \sum_{i=1}^{40} y^i(t) \right) e^{-j\omega_k t}. \tag{9.2}$$

9.3 Initialization

9.3.1 Periodic excitation signal design

The most important feature of employing periodic excitation signals for identification is that they allow for an unbiased frequency domain representation of measurement data, as is shown in chapter 5. Utilization of periodic excitation signals has several additional properties as is clarified in chapter 6, as substantial data reduction and filtering and noise reduction via simple computational operations.

Design of a periodic excitation signal has been addressed in section 6.5 and boils down to specifying the frequencies ω_k of interest for identification and the magnitudes of the individual sinusoids, expressed as

$$r(t) = \sum_{k \in \{0,\ldots,N-1\}} a_k \cos(\omega_k t + \phi_k).$$

The period length is prefixed to a maximum of $N = 8192$ samples, restricted by the memory capacity of the processor board. The magnitudes are chosen equivalent for all frequencies.

Once frequencies and magnitudes are fixed, the phases of a multisinusoid allow for "shaping" the time domain features of one period. Two considerations are underlying the determination of the phase values:

- The excitation signal should not deviate too much from signals that are present in operational conditions (see discussion in section 6.5);
- The signal-to-noise ratio should be as large as possible.

Phase values are therefore determined by performing 30 iterations with random phase selection and picking the signal having a minimal Crest-factor. The resulting signal period is subsequently scaled to a maximum magnitude of 80 mV.

The specific excitation that is utilized in the subsequent experiments has a period length of 4096 samples with a logarithmic frequency scaling along the frequency range. This results in an excitation signal containing 99 sinusoids for a frequency range of $[100, 10.000]$ Hz. A period of the excitation signal and its DFT are shown in figure 9.5.

9.3.2 Design of an initial compensator

Performing one iteration towards an enhanced performance, the system has to be feedback controlled by a known stabilizing compensator. In case a compensator is available that stabilizes the system, it can be used as an initial controller

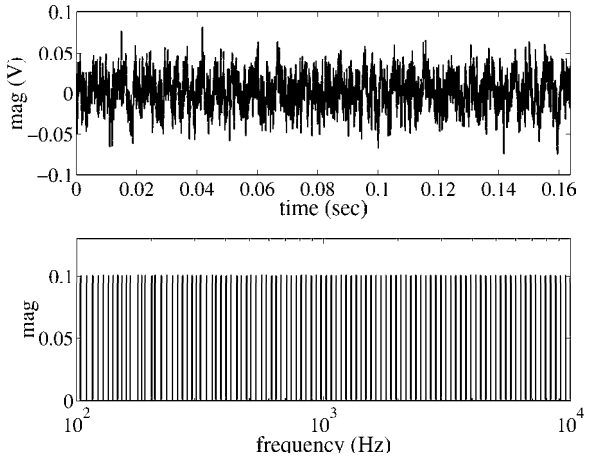

fig. 9.5: Excitation signal: 1 period of the time domain signal with period length of 4096 samples and sample time: 40 μ sec.(upper) and the DFT (lower) for a frequency range [100, 10.000] Hz.

that is to be enhanced. As in many iterative calculation schemes, the initial controller has a substantial effect on the evolution of designed compensators and convergence towards an optimal controller (if it converges at all!). One of the reasons for exploiting an iterative approach is to systematically tune the model in view of an enhanced controller design, thereby dealing with resonance modes via optimization based design step by step. To that end we prefer an initial controller that is not obtained via optimization based design or that already achieves some level of performance as we want the scheme do the job. Therefore, design of an initial compensator is carried on the basis of loop shape arguments using a frequency response of the system.

Frequency response measurement and loop shape compensator design constitute the initialization of the first iteration.

Frequency response measurements of $P(I+CP)^{-1}$ and $(I+CP)^{-1}$, with a stabilizing controller C in the loop, are obtained from cross-periodogram estimates of $\Phi_{yr}(e^{j\omega})$ and $\Phi_{ur}(e^{j\omega})$ via averaging the ETFE's $\frac{Y^i}{R^i}$ and $\frac{U^i}{R^i}$ over 40 periods. A frequency response of the system is obtained as $Y_N^{\mathbf{av}}(e^{j\omega_k})/U_N^{\mathbf{av}}(e^{j\omega_k})$, using expressions (9.2) and (9.1), and is shown in figure 9.6.

Based on the system frequency response, the 4th order lead-lag compensator $W_4(\nu_b)$ of expression (4.8) is designed with a nominal design bandwidth $\nu_b =$

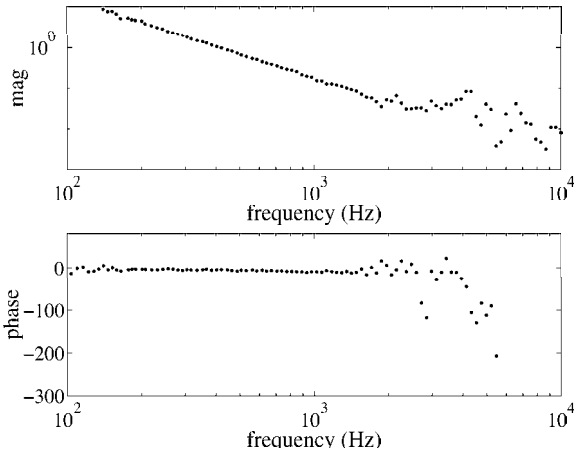

fig. 9.6: Frequency response measurement of the radial actuator by means of periodogram averaging of 40 periods, employing a multi-sinusoidal signal containing 99 frequencies.

500 Hz:

$$W_4(\nu_b) = K\frac{\tau_0 s+1}{\tau_0 s}\frac{\tau_1 s+1}{\tau_2 s+1}\frac{\omega_0^2}{s^2+2\beta\omega_0 s+\omega_0^2}$$
$$\tau_0 = \frac{\nu_b}{5},\quad \tau_1 = \frac{\nu_b}{3},\quad \tau_2 = 3\nu_b,\quad \omega_0 = 5\nu_b,\quad \beta = 0.4$$

A Bode diagram of $W_4(500)$ is shown in figure 9.7, providing low-frequent disturbance attenuation by adding a pole almost in $(1,0)$ and phase lead in the cross-over region.

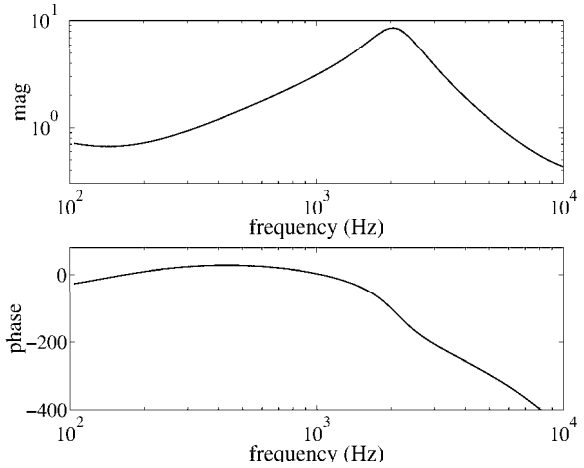

fig. 9.7: Initial 4th order compensator $K\frac{\tau_0 s+1}{\tau_0 s}\frac{\tau_1 s+1}{\tau_2 s+1}\frac{\omega_0^2}{s^2+2\beta\omega_0 s+\omega_0^2}$, nominal design bandwidth $\nu_b = 500$ Hz.

9.4 Iteration towards enhanced performance

9.4.1 Identification of an auxiliary model

In the course of identification of an approximate model and a system uncertainty set, employing fractional model representations, a model P_x is required that provides an accurate system description. In chapter 8, section 8.4, we have clarified the significance of such a model on three counts. Firstly, identification of coprime factor models based on frequency response measurement data $\{\frac{U(e^{j\omega_k})}{R(e^{j\omega_k})}, \frac{Y(e^{j\omega_k})}{R(e^{j\omega_k})}\}$ requires that they correspond to *normalized* coprime factors of the system as has been addressed in chapter 6. To that end a filter operation of the data must be performed, which is feasible via an accurate plant model. Secondly, data-based construction of a system uncertainty set $\mathcal{P}_R(N_x, D_x, N_c, D_c, R, \delta_R)$ is based on identification of an error bound on the dual Youla parameter that is associated with a model P_x. As is discussed in chapter 7, a tight system uncertainty set can be identified provided the model P_x is an accurate system description. Thirdly, in control relevant identification of an approximate model, addressed in chapter 6, section 6.4.1, the optimization is subjected to a parametric constraint (see expression (6.15)) utilizing an accurate system model.

In chapter 8 it is discussed that a model P_x that provides access to normalized coprime factors via filtering of measurement data, in fact is an accurate system model in view of control relevant approximate identification and pro-

vides an adequate auxiliary model for construction of a system uncertainty set $\mathcal{P}_R(N_x, D_x, N_c, D_c, R, \delta_R)$. Concluding, normalization of measurement data, uncertainty bounding employing a dual Youla parametrization and control relevant approximation are intertwined by means of an accurate, high order model P_x of the system. The term "auxiliary" model is adopted from [69], where it is employed in the context of the dual Youla parametrization of models. In our context, the notion "auxiliary" also applies to P_x being an intermediate model of a system uncertainty set, as follows from the above.

The first step in an iteration therefore is the normalization of measurement data by means of identification of an auxiliary model P_x. Identification of P_x is performed via the procedure presented in section 8.4; parametric coprime factor estimates $\{N_x, D_x\}$, employing an ORTFIR model structure of order 48 (utilizing 6 basis functions of order 8), and the normalized frequency response data $\{\frac{Y(e^{j\omega_k})}{X(e^{j\omega_k})}, \frac{U(e^{j\omega_k})}{X(e^{j\omega_k})}\}$ are shown in the Bode diagram of figure 9.8.

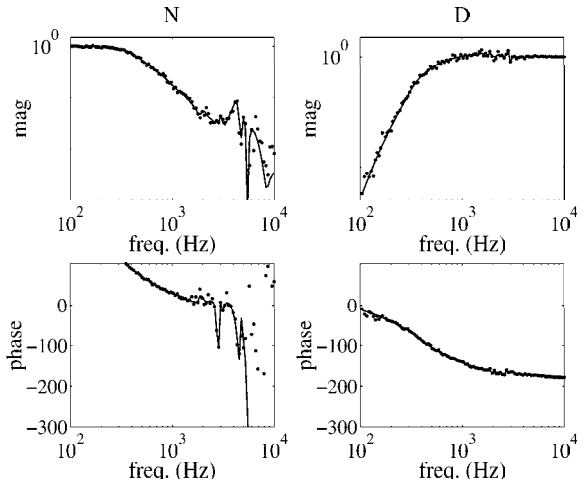

fig. 9.8: Identification of coprime factors of an auxiliary model P_x (ORTFIR model of order 48, using 6 basis generating model of order 8).

The procedure of identification of P_x and subsequent filtering to obtain normalized frequency response data, is repeated until normalizedness of the filtered data is sufficient. Figure 9.9 shows the normalization of the filtered data $\{\frac{Y}{X}(e^{j\omega_k}), \frac{U}{X}(e^{j\omega_k})\}$ and frequency response measurements $\{\frac{Y}{R}(e^{j\omega_k}), \frac{U}{R}(e^{j\omega_k})\}$, where $X(e^{j\omega_k}) := (D_x + CN_x)^{-1}R(e^{j\omega_k})$.

The Bode diagrams of the open loop model P_x, constructed from N_x, D_x and the frequency response $Y_N^{\mathrm{av}}(e^{j\omega_k})/U_N^{\mathrm{av}}(e^{j\omega_k})$ are shown in figure 9.10.

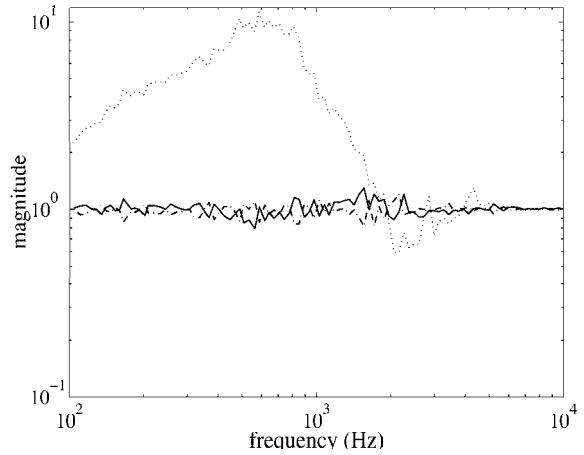

fig. 9.9: Normalization of frequency response data: measured frequency responses (dot), filtered via coprime factor representation and constructed via a dual Youla representation (dash-dot).

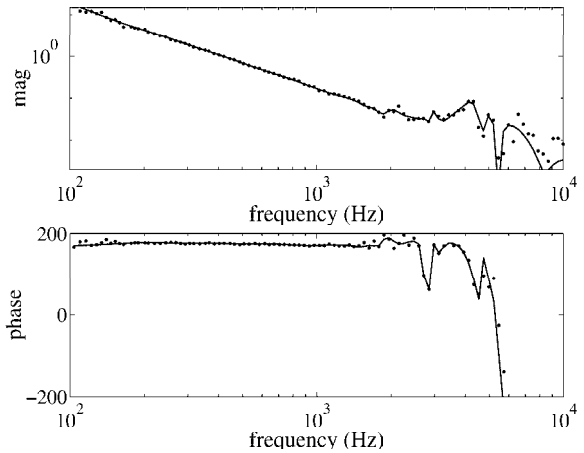

fig. 9.10: Auxiliary model P_x constructed on the basis of coprime factor estimates. $\{N_x, D_x\}$ and frequency response $\frac{Y_N(e^{j\omega_k})}{U_N(e^{j\omega_k})}$

9.4.2 Identification of an error bound

Identification of a system uncertainty set $\mathcal{P}(N_x, D_x, N_c, D_c, R, \delta_R)$ amounts to identification of a dual Youla parameter R together with a model error bound δ_R, as discussed in chapter 7. The auxiliary model P_x is obtained from data normalization in the previous section and $\{N_c, D_c\}$ are nrcf's of the controller C present in the loop during measurement.

Frequency response data $\mathcal{X}(e^{j\omega_k}) \in \mathbb{C}^{N_f \times M}$, $\mathcal{Z}(e^{j\omega_k}) \in \mathbb{C}^{N_f \times M}$, that are associated to the dual Youla parameter are obtained via the filter operation

$$X(e^{j\omega_k}) = (D_x + CN_x)^{-1} R(e^{j\omega_k}) \tag{9.3}$$

$$Z^i(e^{j\omega_k}) = D_c^{-1}(I + P_x C)^{-1}(Y^i(e^{j\omega_k}) - P_x\ U^i(e^{j\omega_k})). \tag{9.4}$$

where $i = 1, \ldots, M$; in this case $N_f = 99$ and $M = 40$ holds. As $\{N_x, D_x\}$ are the same factors as utilized for filtering of normalized coprime factor data, the following equivalence holds

$$\begin{aligned} \frac{Y^i}{R}(e^{j\omega_k})(D_x + CN_x) &= N_x + D_c \frac{Z^i}{X}(e^{j\omega_k}) \\ \frac{U^i}{R}(e^{j\omega_k})(D_x + CN_x) &= D_x - N_c \frac{Z^i}{X}(e^{j\omega_k}), \end{aligned}$$

which is easily verified by substitution of (9.3) and (9.4) in the expressions above. This implies that, as discussed in chapter 7, access to normalized coprime factor data can equally be obtained based on the frequency domain data $\{Z^i(e^{j\omega_k}), X(e^{j\omega_k})\}$ via construction as indicated by the right hand side of the expressions above. Normalizedness of data obtained employing a dual Youla parametrization is also shown in figure 9.9; although both frequency domain data representations are algebraically equivalent according to the above expressions, there are minor differences in the normalizedness of the corresponding filtered data. An explanation is postponed until section 9.5.

The error bounding technique of chapter 7 is applied to the filtered data $\{\mathcal{X}(e^{j\omega_k}), \mathcal{Z}(e^{j\omega_k})\}$, providing discrete and continuous magnitude error bounds of the dual Youla parameter, associated with nrcf's $\{N_x, D_x\}$ of the auxiliary model P_x and nrcf's $\{N_c, D_c\}$ of the controller C present in the loop during measurement. The averaged ETFE and the (nonparametric) discrete error bound of the dual Youla parameter are shown in the Bode magnitude in figure 9.11.a. A continuous error bound of the dual Youla parameter, identified based on ORTFIR parameter estimates is shown in figure 9.11.b; the separate contributions of noise and undermodelling to the bounds are shown in figure 9.11.c where the error bound due to noise is estimated with a 99.9% probability.

As we have discussed in section 7.6, validation of model error bounds is performed on two counts.

The first validation issue is: are the bounds credible ? Validation of the credibility of the discrete or continuous error bounds could be carried out by verifying whether of a 1000 averaged ETFE's or parametric models of the dual Youla parameter, based on a 1000 independent measurements, just one is not be captured by the corresponding bounds. Of course, this is a too elaborate undertaking; we are confident with respect to the reliability of the discrete bounds by the fact that the averaged ETFE is completely captured.

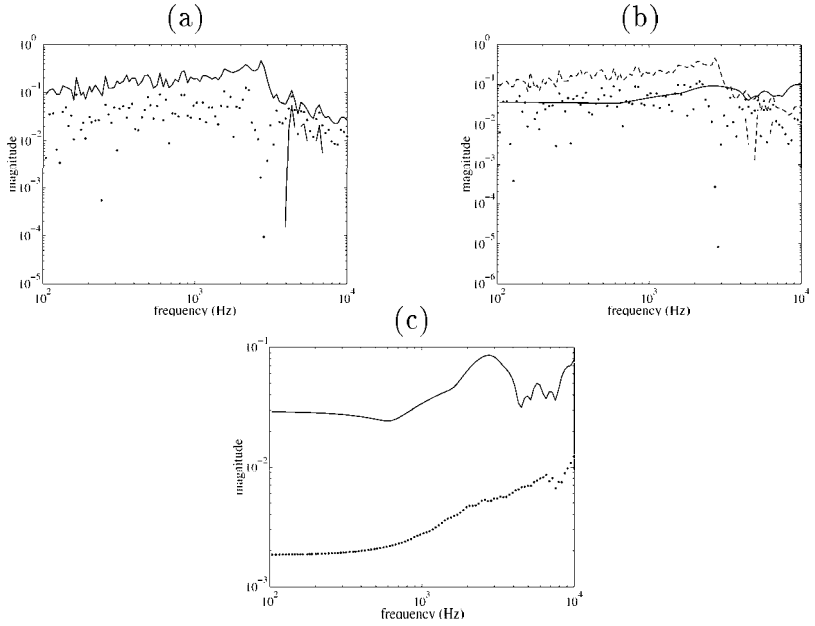

fig. 9.11: Error bounds of a dual Youla parameter: discrete (a) and continuous (b) transfer function error bound and ETFE; figure (c) depicts the separate error bounds due to noise (probabilistic, solid) and undermodelling (deterministic, dot), error due to unknown inputs is neglegible.

We observe that 0 is contained in the uncertainty set for almost all frequencies for the discrete as well as the continuous error bound. The fact that 0 is comprised by the identified uncertainty bounds for almost all frequencies indicates that the auxiliary model P_x is a sufficiently accurate system description and hence a solid uncertainty reference model. In this case we choose $R = 0$ as the uncertainty reference model and adjust the model error bound to $|\hat{R}(\theta, e^{j\omega})| + \delta_R(\omega), \omega \in [0, \pi)$.

In order to evaluate credibility of dual Youla model error bounds in view of the corresponding open loop dynamics, we utilize the expressions in proposition 7.3.2 to construct additive error bounds of the magnitude of the associated open loop system in a non-conservative way. Continuous upper and lower magnitude bounds of the open loop system and the averaged ETFE $Y_N^{\mathrm{av}}(e^{j\omega_k})/U_N^{\mathrm{av}}(e^{j\omega_k})$ of the system are shown in the Bode magnitude diagram of figure 9.12.

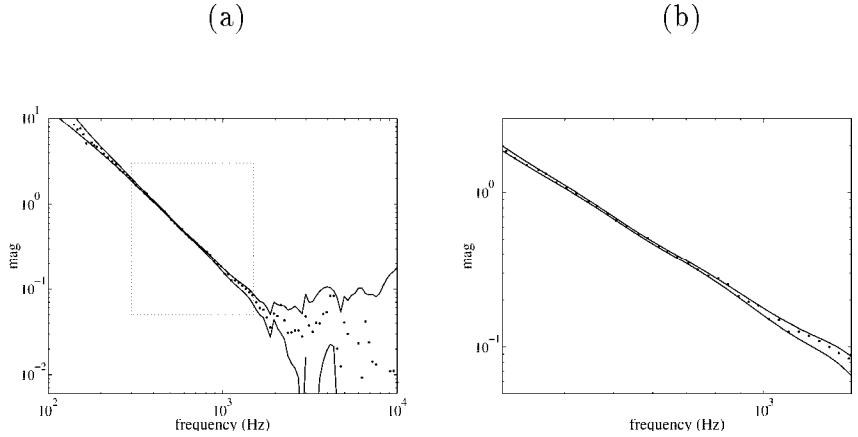

fig. 9.12: Upper and lower continuous magnitude bounds and averaged ETFE (dot) of the radial actuator: frequency range [100, 10.000] Hz (a) and [300, 1.500] Hz (b).

The open loop bounds capture the system frequency response quite tightly, especially in the cross-over frequency region, which is depicted in the "zoomed-in" Bode magnitude diagram of figure 9.12.b. We observe that the open loop bounds seem to be tightest in the frequency region [400, 700] Hz, which is the frequency region of interest for the controller C in the loop during measurement, depicted in the Bode diagram in figure 9.7, having a design bandwidth of 500 Hz.

The second validation issue is: are the bounds useful ? The main purpose for error bounding is to evaluate robust performance of a yet to be implemented controller, as is clarified in chapter 7. A preliminary validation of the identified model error bounds regarding their utility for evaluating feedback system performance, is to evaluate whether the transformed bounds are consistent with the measured closed loop frequency response data. Performance evaluation for a controller that was present in the loop during data acquisition is referred to as performance monitoring (see also [87]). In chapter 7 it has been shown that

a model uncertainty structure based on a dual Youla model parametrization, denoted as $P \in \mathcal{P}_R(N_x, D_x, N_c, D_c, R, \delta_R)$, enables performance monitoring of $T(P,C)$ in a non-conservative way, which directly follows from the expressions (7.2) and (7.3) for $C = N_c D_c^{-1}$.

Continuous upper and lower magnitude bounds of the closed loop transfer function matrix $T(P,C)$, constructed from the identified system uncertainty set $\mathcal{P}_R$, and the corresponding averaged ETFE's $Y_N^{\text{av}}(e^{j\omega_k})/R_N^{\text{av}}(e^{j\omega_k})$ and $U_N^{\text{av}}(e^{j\omega_k})/R_N^{\text{av}}(e^{j\omega_k})$ are shown in the Bode magnitude diagrams of figure 9.13.

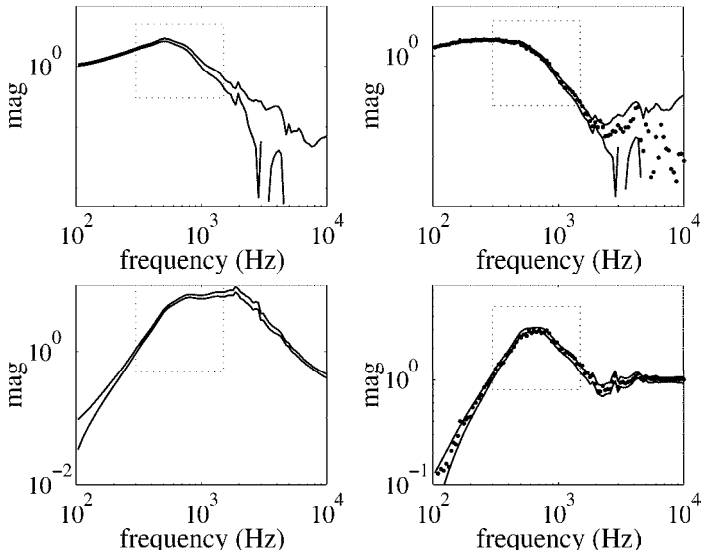

fig. 9.13: Upper and lower continuous magnitude bounds and averaged ETFE (dot) of $T(P,C)$: frequency range [100, 10.000] Hz.

The magnitude error bounds of $T(P,C)$ are quite tight and the bounds for $P(I+CP)^{-1}$ and $(I+CP)^{-1}$ capture the frequency response estimates in an accurate manner.

Considering the "zoomed-in" frequency region in figure 9.14, the closed loop error bounds seem less tight than the bounds of the open loop system in the corresponding frequency region. An open loop error bound that is much tighter in the cross-over frequency region than for other frequencies corresponds to a closed loop error bound that "looks" tight for all frequencies. This observation stresses the suitability of error bounding within a dual Youla parametrization in view of feedback properties of a system, as the above Bode magnitude diagrams are complying with statements in literature that a feedback relevant model should be close to the system specificly in the cross-over frequency area ([69,

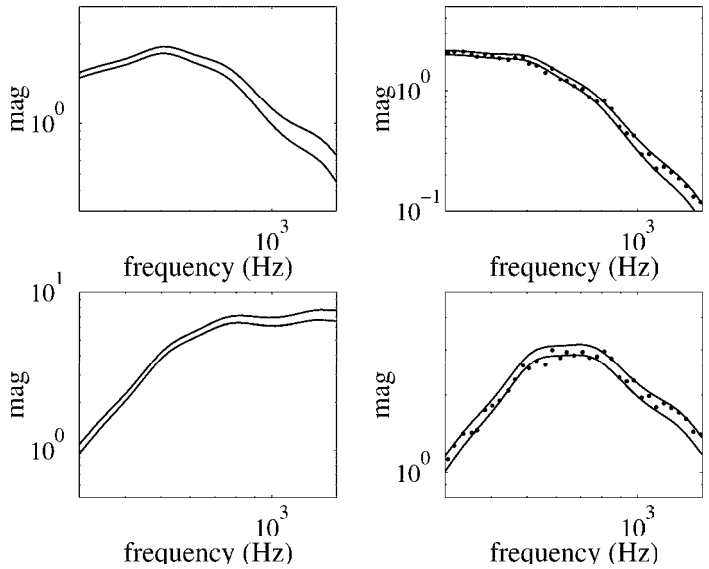

fig. 9.14: Upper and lower continuous magnitude bounds and averaged ETFE (dot) of $T(P,C)$: frequency range [300, 1.500] Hz.

29]).

9.4.3 Identification of an approximate model

An approximate model is identified utilizing a coprime factor model structure, based on (almost) normalized frequency response data obtained from the normalization in section 9.4.1. We address the identification of an approximate model that provides a control relevant approximation of the system as we have discussed in section 2.5, expression (2.17),

$$\hat{P} = \arg_{\tilde{P}} \min \|J(P,C) - J(\tilde{P},C)\|_2^2.$$

Identification of an approximate model that complies with the control relevant approximation above is formulated in terms of the following parameter estimation problem (see also chapter 6)

$$\hat{\theta} = \arg_\theta \min \left\| V_{\text{out}} \begin{bmatrix} \frac{Y}{X}(e^{j\omega_k}) - N(e^{j\omega_k},\theta) \\ \frac{U}{X}(e^{j\omega_k}) - D(e^{j\omega_k},\theta) \end{bmatrix} V_{\text{in}} \right\|_2^2,$$

where $X(e^{j\omega_k}) = (D_x + CN_x)^{-1}R(e^{j\omega_k})$. The coprime factor models are

parametrized as follows:

$$N(e^{j\omega_k},\theta)=\frac{B(e^{j\omega_k})}{F(e^{j\omega_k})},\quad D(e^{j\omega_k},\theta)=\frac{A(e^{j\omega_k})}{F(e^{j\omega_k})}$$

where

$$\begin{aligned}
B(e^{j\omega}) &:= b_0+b_1e^{-j\omega}+b_2e^{-2j\omega}+\ldots+b_{n_b}e^{-n_bj\omega}\\
A(e^{j\omega}) &:= a_0+a_1e^{-j\omega}+a_2e^{-2j\omega}+\ldots+a_{n_a}e^{-n_aj\omega}\\
F(e^{j\omega}) &:= 1+f_1e^{-j\omega}+f_2e^{-j\omega}+\ldots+f_{n_f}e^{-n_fj\omega}\\
\theta &:= [b_0\ \ldots b_{n_b}\ a_0\ \ldots\ a_{n_a}\ f_1\ \ldots\ f_{n_f}]
\end{aligned}$$

which constitutes a nonlinear optimization problem. As is discussed in chapter 8, the parameter estimation problem is made compatible with the control relevant approximation problem by following two issues:

1. Selecting the weightings V_{out} and V_{in} as

$$\begin{aligned}
V_{\text{out}} &= \begin{bmatrix} W(\nu_b) & 0\\ 0 & I\end{bmatrix}\\
V_{\text{in}} &= (D_x+CN_x)^{-1}[CW^{-1}(\nu_b)\ \ I].
\end{aligned}$$

$W(\nu_b)$ is the weighting function resulting from a previous control design. Weighting function design is confined in the control design and is discussed in section 9.4.4; in the first iteration, the loop shape compensator obtained from the initialization in the previous section is used as weighting function.

2. Imposing the constraint $D(\hat{\theta})+CN(\hat{\theta})=D_x+CN_x$ on the parameter estimation.

The nonlinear optimization is tackled via a Sanathanan-Koerner iteration, as discussed in chapter 6, without imposing the parametric constraint. In case no significant changes occur in the estimated transfer functions, the iteration is presumed to have converged and stopped.

The weightings that emphasize the feedback relevance of the approximation, $W(\nu_b), I, (D_x+CN_x)^{-1}CW^{-1}(\nu_b)$ and $(D_x+CN_x)^{-1}$, are shown in the Bode magnitude diagrams in figure 9.15.
The results of a coprime factor identification of order 8 is shown in the Bode diagram of figure 9.16.
The resulting 8th order open loop model is shown in the Bode diagram of figure figure 9.17.
The resulting estimate is evaluated a posteriori in view of the parametric constraint in the Bode magnitude diagram of figure 9.18; in case the constraint is not satisfied, the model order is increased.

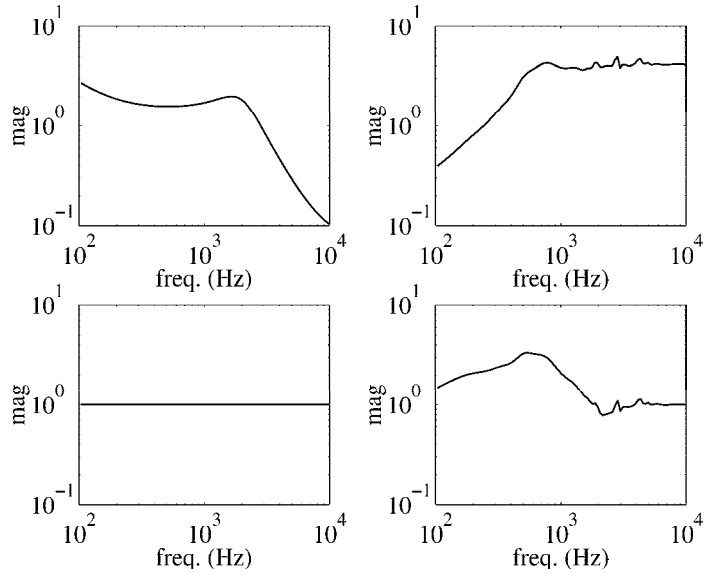

fig. 9.15: Weightings that emphasize feedback relevant aspects of the approximate coprime factor identification: $W(\nu_b)$ (left-upper), I (left lower), $(D_x + CN_x)^{-1}CW^{-1}(\nu_b)$ (right-upper) and $(D_x + CN_x)^{-1}$ (right-lower).

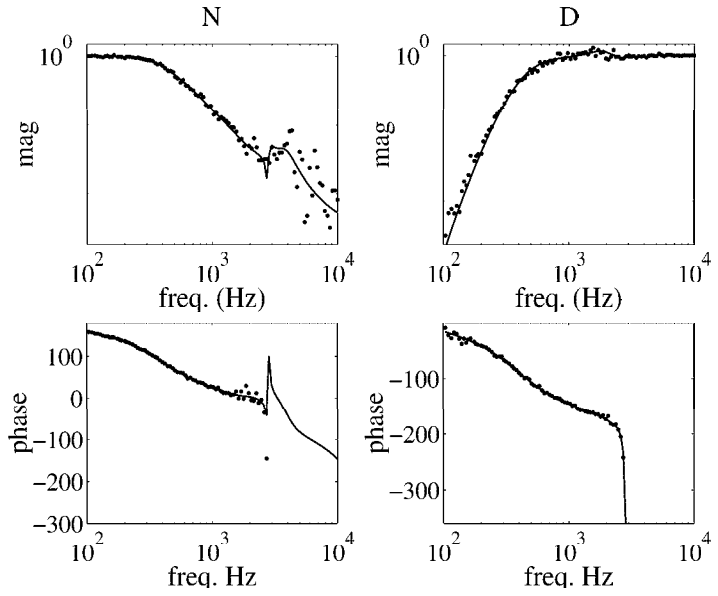

fig. 9.16: Bode diagram of 8th order coprime factor models.

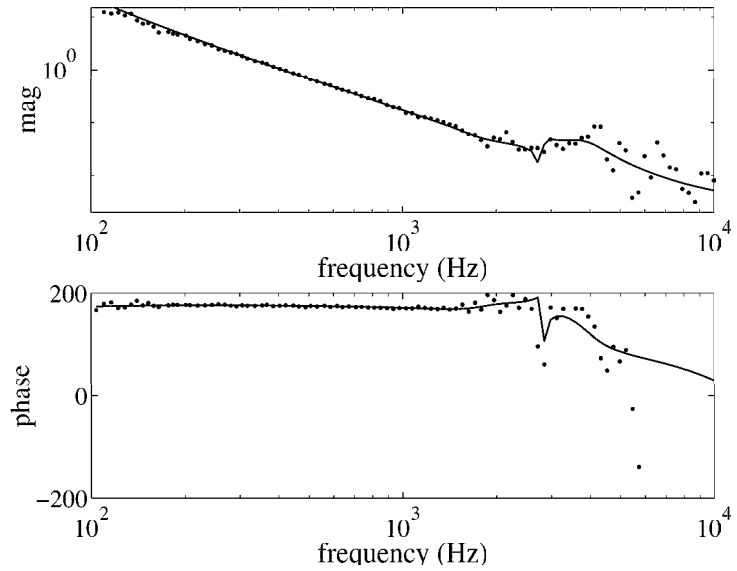

fig. 9.17: Bode diagram of the 8th order approximate model corresponding with the coprime factor models of figure 9.16.

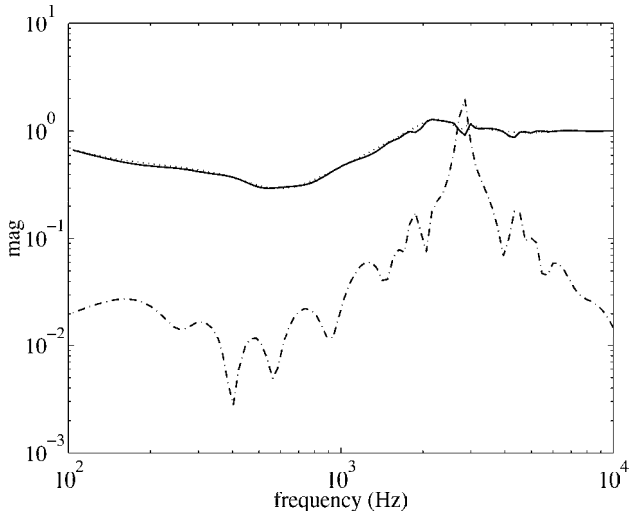

fig. 9.18: A posteriori evaluation of the parametric constraint $\frac{U}{R}(D_x + CN_x) + C\frac{Y}{R}(D_x + CN_x) = D(\hat{\theta}) + CN(\hat{\theta})$; Bode magnitude diagram of $D_x + CN_x$, $D(\hat{\theta}) + CN(\hat{\theta})$ and $(D_x + CN_x) - (D(\hat{\theta}) + CN(\hat{\theta}))$

9.4.4 Control design

Design of a robust controller is performed according to the design procedure proposed in section 4.5. The procedure consists of design of a suitable weighting function, calculation of a controller via a robustness optimization based on a nominal model and evaluation of robust performance utilizing a system uncertainty set. We address each of these step.

Weighting function design

The first stage in the control design is the design of a weighting function trajectory via loop shape compensator design based on an available nominal model. In chapter 4 we have introduced two lead-lag compensators, $W_4(\nu_b)$ of order 4 (expression (4.8)) and $W_3(\nu_b)$ of order 3 (expression (4.9)), both parametrized in a nominal design bandwidth ν_b:

$$W_3(\nu_b) := K\frac{\tau_0 s+1}{\tau_0 s}\frac{1}{\frac{s^2}{\omega_0^2}+2\beta\frac{s}{\omega_0}+1}$$

$$W_4(\nu_b) := K\frac{\tau_0 s+1}{\tau_0 s}\frac{\tau_1 s+1}{\tau_2 s+1}\frac{1}{\frac{s^2}{\omega_0^2}+2\beta\frac{s}{\omega_0}+1}$$

where

$$\tau_0=\frac{\nu_b}{5},\quad \tau_1=\frac{\nu_b}{3},\quad \tau_2=3\nu_b,\quad \omega_0=5\nu_b,\quad \beta=0.4$$

The difference between $W_4(\nu_b)$ and $W_3(\nu_b)$ is a phase lead in the cross-over frequency region which enables $W_4(\nu_b)$ to stabilize a nominal model having a double integrator, opposed to $W_3(\nu_b)$ that is structurally incapable of stabilizing a double integrator. Considerations regarding the choice of weighting function are that the robust design must not alter the nominal design too much and that the robust controller must be of lowest possible order. The weighting $W_3(\nu_b)$ provides robust controllers of degree 2 lower than the weighting $W_4(\nu_b)$, which gives preference to $W_3(\nu_b)$ in view of controller order.

Design of a robust controller has been narrowed down to selecting one parameter ν_b that has an interpretation of the nominal bandwidth of a double integrator. Selection of ν_b that establishes an acceptable increase of the bandwidth of the closed system typically is an exercise of repeated trial and evaluation of robust performance. As the design bandwidth of the initial compensator is 500 Hz, a first choice is to construct a number of lead-lag compensators that enhance the nominal design bandwidth by 50 Hz.

The weightings are designed in the s-domain; the robust design is based on models in the z-domain, therefore the designed weightings are transformed into the z-domain by mapping the poles in the complex s-plane into the complex z-plane by means of the expression $\mu = e^{\lambda \Delta T}$ where ΔT is the sample time for controller implementation (see Åström and Wittenmark [3]). Although a similar expression of mapping zeros in the s-domain into the z-domain is not available, for high sample rates the same mapping as applied to the poles can be performed. In order not to complicate notation, in the sequel the notations $W_3(\nu_b)$ and $W_4(\nu_b)$ refer to weigthings in the z-domain.

The Bode diagrams of figures 9.19 resp. 9.20 depict weighting functions $W_3(\nu_b)$ resp. $W_4(\nu_b)$ for design bandwidths $\nu_b = 550, 600, 650$ and 700 Hz.

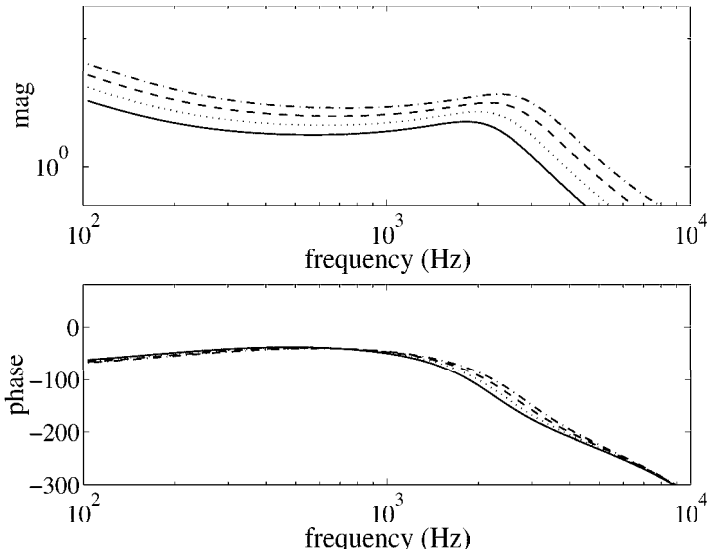

fig. 9.19: Bode diagram of weighting functions $W_3(\nu_b)$ for $\nu_b = 550$ Hz (solid), $\nu_b = 600$ Hz (dot), $\nu_b = 650$ Hz (dash) and $\nu_b = 700$ Hz (dash-dot).

Robustness optimization

With the weightings assigned as $W_3(\nu_b)$ (expression (4.9)) and $W_4(\nu_b)$ (expression (4.8)) for $\nu_b \in \{550, 600, 650, 700\}$ Hz, controllers are designed via the $\mathcal{H}_\infty$ loop shape design defined in definition 4.3.1 in chapter 4:

$$C_{\hat{P},\nu_b} = \arg_{\tilde{C}} \min \left\| \begin{bmatrix} W(\nu_b)\hat{P} \\ I \end{bmatrix} [I + \tilde{C}\hat{P}]^{-1} [\tilde{C}/W(\nu_b) \;\; I] \right\|_\infty . \qquad (9.5)$$

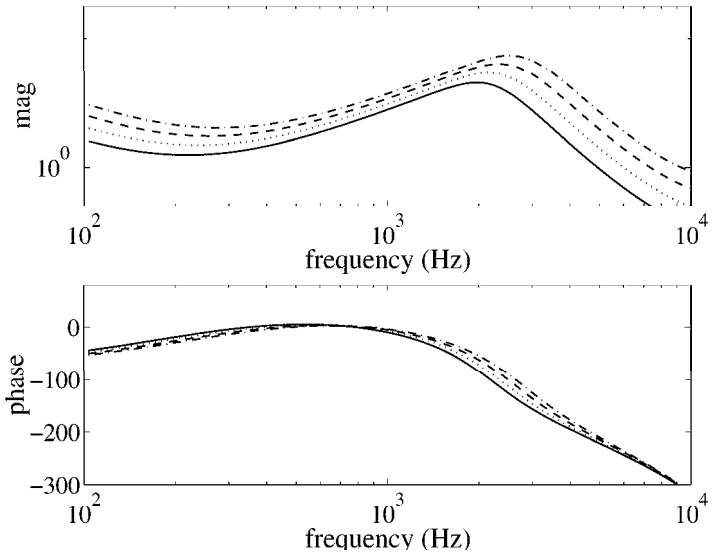

fig. 9.20: Bode diagram of weighting functions $W_4(\nu_b)$ for $\nu_b = 550$ Hz (solid), $\nu_b = 600$ Hz (dot), $\nu_b = 650$ Hz (dash) and $\nu_b = 700$ Hz (dash-dot); phase lead is present in the cross-over frequency region to ensure robustness.

The design is carried out in two steps:

1. $C'_{\hat{P},\nu_b}$ is computed as

$$C'_{\hat{P},\nu_b} = \arg_{\tilde{C}} \min \left\| \begin{bmatrix} W(\nu_b)\hat{P} \\ I \end{bmatrix} [I + \tilde{C}\ W(\nu_b)\hat{P}]^{-1} [\tilde{C} \quad I] \right\|_\infty ,$$

2. The final controller is constructed as

$$C_{\hat{P},\nu_b} = W(\nu_b) C'_{\hat{P},\nu_b}.$$

The optimization-based design is carried out utilizing the procedure described by Bongers ([5]). As we have discussed in section 4.4.2, the controller order is determined twice by the order of the weigthing function $W_3(\nu_b)$ or $W_4(\nu_b)$. As the maximum controller order is set to 15 due to hardware restrictions (see also section 9.2.2) this implies that nominal models underlying the design should have a maximum order of 9 resp. 7; consequently, for both weightings approximately half of the controller order is claimed by the weighting order! Our objective is to employ nominal models of largest possible order within the limitations of controller implementation and therefore we wish to keep the weigthing order contribution to the controller order as little as possible. Therefore, a controller reduction is performed as is described in [5] such that the weigthing order effects the controller only once. This implies that a model of order 11 underlies the robustness optimization for weightings of order 3 and 4.

The Bode diagram of figure 9.21 depicts the robust controllers designed using $W_3(\nu_b)$ for $\nu_b \in \{550, 600, 650, 700\}$ Hz.
The Bode diagram of figure 9.22 depicts the robust controllers designed using $W_4(\nu_b)$ for $\nu_b \in \{550, 600, 650, 700\}$ Hz.
We mention that the controllers shown in the Bode diagrams of figures 9.21 and 9.22 are not reduced, as an approximate model of order 8 leads to controllers of order 14 resp. 16. We have deliberately limited the model order to 8 in order to clearly illustrate the mechanisms that underly the model-based control design, which is elaborated next.

Performance evaluation

To ensure robust performance enhancement prior to implementation, controllers resulting from the robustness optimization design are evaluated in view

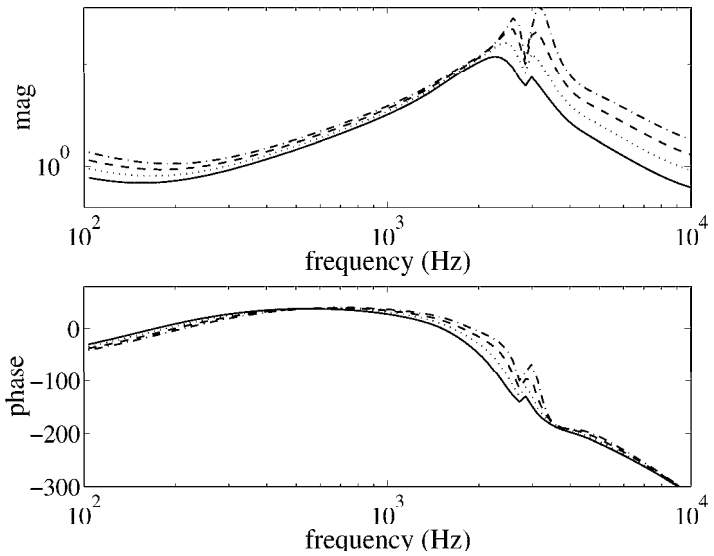

fig. 9.21: Bode diagram of robust controllers designed with $W_3(\nu_b)$ for $\nu_b = 550$ Hz (solid), $\nu_b = 600$ Hz (dot), $\nu_b = 650$ Hz (dash) and $\nu_b = 700$ Hz (dash-dot).

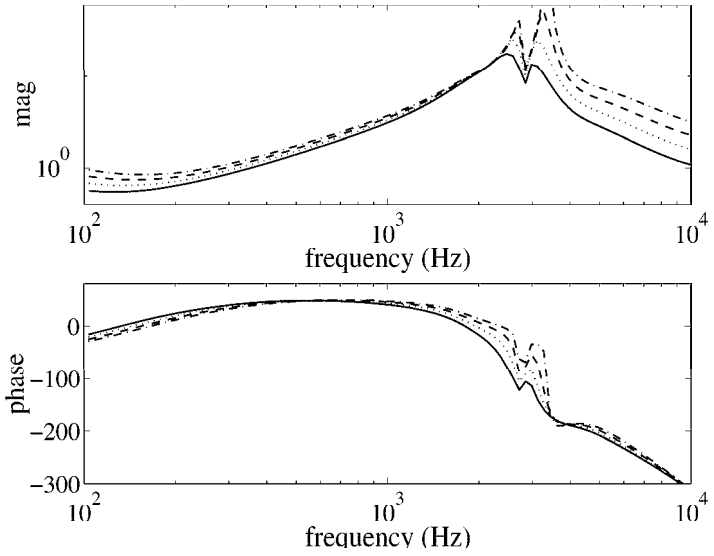

fig. 9.22: Bode diagram of robust controllers designed with $W_4(\nu_b)$ for $\nu_b = 550$ Hz (solid), $\nu_b = 600$ Hz (dot), $\nu_b = 650$ Hz (dash) and $\nu_b = 700$ Hz (dash-dot).

of the performance they achieve for the system. Based on the outcome of the evaluation, one controller is selected for implementation.

Robust performance evaluation is addressed in chapter 7 and amounts to evaluation of

$$\sup_{P\in\mathcal{P}_R}\ ,\ \inf_{P\in\mathcal{P}_R}\left|J(P,C_{\hat{P},\nu_b})\right|,\ \omega\in[0,\pi),$$

where $J(P,C_{\hat{P},\nu_b}) = W_{\text{out}}T(P,C_{\hat{P},\nu_b})W_{\text{in}}$ and $\mathcal{P}_R$ denotes the system uncertainty set identified in section 9.4.2.

The sensitivity function embodies the closed loop transfer function that reflects the most important performance specification for the radial servo system, as is clarified in chapter 3. Therefore we restrict the performance evaluation to the $(2,2)$-element of $J(P,C_{\hat{P},\nu_b})$; it is noted that similar performance evaluation is feasible for every element of $J(P,C_{\hat{P},\nu_b})$.

Using the expressions of proposition 7.3.1, magnitude bounds of the closed loop transfer function $J(P,C_{\hat{P},\nu_b})$ are constructed element-wise in a non-conservative way, employing a system uncertainty set $\mathcal{P}_R(N_x,D_x,N_c,D_c,R,\delta_R)$. The magnitude of $J_{22}(P,C_{\hat{P},\nu_b})$ thus is bounded by following expressions:

$$|J_{22,\text{nom}}| - \delta_{J_{22}} \le |J_{22}(P,C_{\hat{P},\nu_b})| \le |J_{22,\text{nom}}| + \delta_{J_{22}} \tag{9.6}$$

where $J_{22,\text{nom}}$ is the $(2,2)$-element of (7.4) and $\delta_{J_{22}}$ is the $(2,2)$-element of (7.5) in proposition 7.3.1, expressed as

$$J_{22,\text{nom}}(\mathcal{P}_R,C_{\hat{P},\nu_b}) := \tag{9.7}$$
$$\frac{(D_x-N_cR)(D_x+C_{\hat{P},\nu_b}N_x)^* + \left(D_xR^*-N_c(RR^*-\delta_R^2)\right)(C_{\hat{P},\nu_b}D_c-N_c)^*}{D(\mathcal{P}_R,C_{\hat{P},\nu_b})}$$

$$\delta_{J_{22}}\mathcal{P}_R,C_{\hat{P},\nu_b} := \frac{|C_{\hat{P},\nu_b}|.|D_x+CN_x)|.\delta_R}{D(\mathcal{P}_R,C_{\hat{P},\nu_b})} \tag{9.8}$$

with

$$D(\mathcal{P}_R,C_{\hat{P},\nu_b}) =$$
$$\left|D_x+C_{\hat{P},\nu_b}N_x+(C_{\hat{P},\nu_b}D_c-N_c)R\right|^2 - \left|C_{\hat{P},\nu_b}D_c-N_c\right|^2\delta_R^2.$$

The Bode magnitude diagrams of figure 9.23 show the nominal sensitivity function and magnitude error bounds for controllers $C_{\hat{P},\nu_b}$ designed using $W_3(\nu_b)$ for $\nu_b\in\{550,600,650,700\}$ Hz.

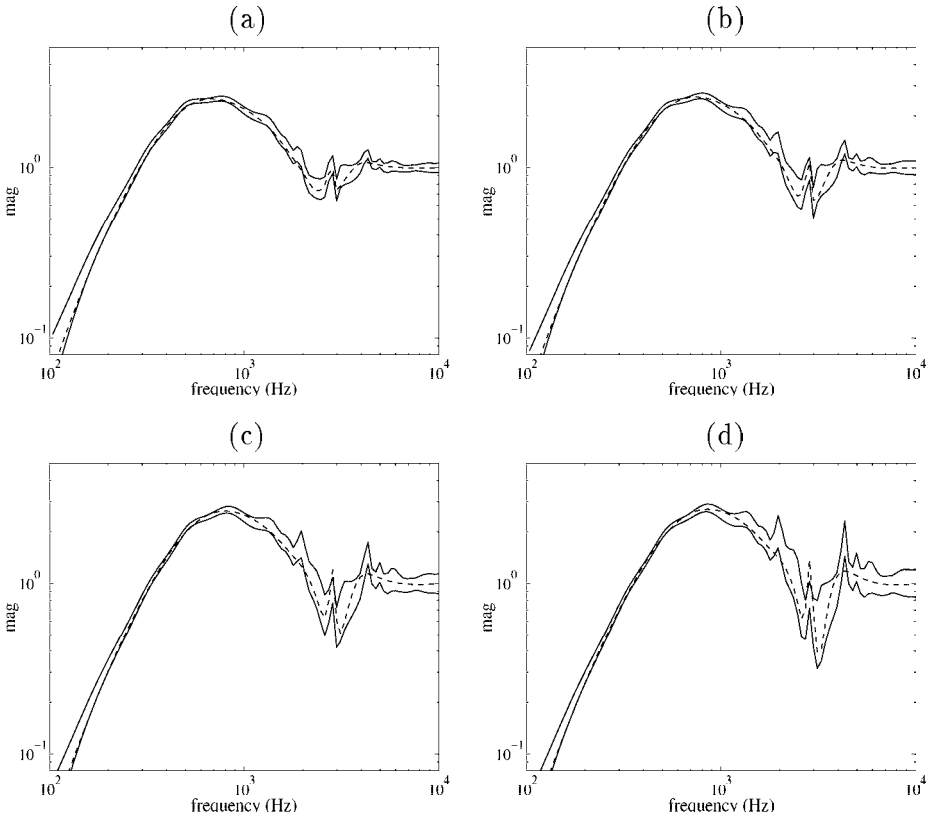

fig. 9.23: Bode magnitude diagram of the sensitivity function: robust controllers designed with $W_3(\nu_b)$ for $\nu_b = 550\,(a), 600\,(b), 650\,(c), 700\,(d)$ Hz in conjunction with the nominal model (dash) and the system uncertainty set bounds (solid).

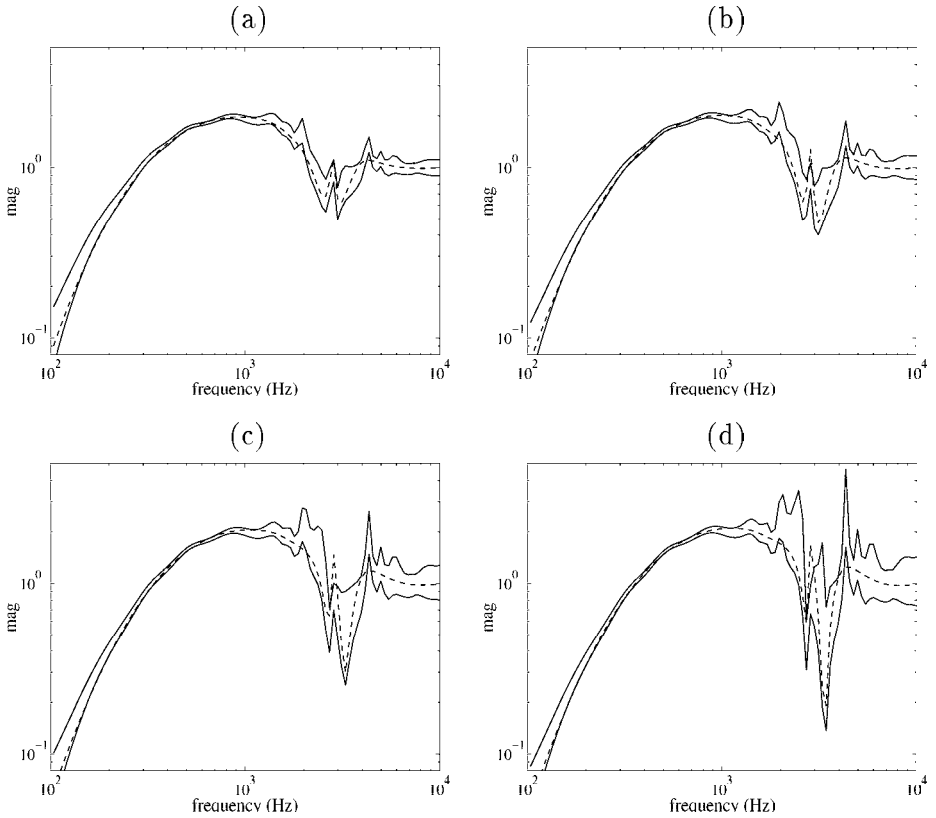

fig. 9.24: Bode magnitude diagram of the sensitivity function: robust controllers designed with $W_4(\nu_b)$ for $\nu_b = 550\,(a), 600\,(b), 650\,(c), 700\,(d)$ Hz in conjunction with the nominal model (dash) and the system uncertainty set bounds (solid).

The Bode magnitude diagrams of figure 9.24 depict the nominal sensitivity function and magnitude error bounds for controllers $C_{\hat{P},\nu_b}$ designed using $W_4(\nu_b), \nu_b \in \{550, 600, 650, 700\}$ Hz.

The Bode magnitude diagrams in figures 9.23 and 9.24 exhibit the mechanisms that are discussed in chapter 8, which underly our approach to restricted complexity controller design. Let us first consider both figures separately in view of the models utilized for design.

The sensitivity magnitude characterictics of figures 9.23.a, 9.23.b, 9.23.c and 9.23.d exhibit a gradual enhancement of nominal as well as robust performance, in view of the "ideal" Bode magnitude characteristic shown in figure 3.6 in chapter 3. Up to 1.5 kHz the nominal sensitivity is tightly captured by the error bounds, implying that the approximate model underlying the design provides an adequate system desription as embodied by the bounds. At frequencies from 1.5 kHz on we observe a gradually increasing discrepancy between the nominal sensitivity and the error bounds, which indicates that the nominal model is an insufficiently accurate system description at these frequencies. Note specifically the "emerging" peaks described by the error bounds at approximately 2 and 4 kHz, which might endanger our desired performance objective.

A similar evolution of sensitivity magnitudes is to be observed in figures 9.24.a, 9.24.b, 9.24.c and 9.24.d. Up to 1.5 kHz the sensitivity magnitudes of the nominal model and the error bounds exhibit an even more desirable characteristic as the magnitudes are of a significantly lower value than in figure 9.24. However, the discrepancies between nominal sensitivity and error bounds are more obvious from 1.5 kHz on! Especially at 4 kHz a resonance mode that is adequately described by the system uncertainty set proves to cause a disastrous effect with respect to noise attenuation and production of audible noise.

Regarding the utilization of weighting $W_3(\nu_b)$ or $W_4(\nu_b)$ for control design, it can be concluded that up to 1.5 kHz the weighting $W_4(\nu_b)$ provides better robust performance in terms of a lower magnitude. This can be attributed to a larger phase lead in the cross-over frequency region of the controllers designed with $W_4(\nu_b)$, as follows from the Bode diagram of figure 9.22 compared to the one of figure 9.21.

From 1.5 kHz on however, $W_3(\nu_b)$ is to be preferred as the error bounds, constructed from the identified system uncertainty set, indicate that the resonances present at higher frequencies are less endangering in view of disturbance attenuation. It clearly follows that the design of adequate weighting functions is crucial in view of achieving an enhanced *robust* performance. Regarding the observations above, a system uncertainty set that underlies the perfor-

mance evaluation can play an important part in an iterative design of adequate weightings.

Two situations may occur in evaluation of robust performance that lead to rejection of a controller for implementation:

1. the nominal performance exceeds the performance bounds while the bounds comply with prespecified performance bounds $\Gamma_{\text{lo}}, \Gamma_{\text{up}}$. This situation is likely to occur in case the non-tunable model error plays a minor role in view of the tunable model error, which typically is the case if tight error bounds can be identified from closed loop measurements.

2. the performance magnitude bounds exceed prespecified performance magnitude bounds $\Gamma_{\text{lo}}, \Gamma_{\text{up}}$ while the nominal performance is adequately captured by the bounds. This situation is likely to occur in case the non-tunable model error constitutes a significant part of the overall model error.

In either case the latest controller evaluated that complies with prespecified performance is implemented in order to acquire measurements for a renewed identification of a system uncertainty set and approximate model.

9.5 A second iteration

9.5.1 Results

A second iteration is performed with a controller, obtained from a design with $W_3(\nu_b), \nu_b = 750$. We have deliberately designed a controller in view of a high bandwidth in order to experimentally explore any limitations of our design approach. The Bode diagram of the controller is shown in figure 9.25.
With this controller in the loop, closed loop measurement data are acquired employing the same periodic excitation signal as in the previous section (see figure 9.5).

The first issue to address is validation of the system uncertainty set $\mathcal{P}_R$, where $\{N_c, D_c\}$ are nrcf's of controller $C_{\hat{P},500}$, identified in sections 9.4.1 and 9.4.2 in view of their capability of predicting the plant performance. To that end the error bounds on the transfer functions of $P(I+CP)^{-1}$ and $(I+CP)^{-1}$ in conjunction with controller $C_{\hat{P},750}$ are constructed based on the identified system uncertainty set and evaluated in view of the actually measured averaged frequency response estimates with $C_{\hat{P},750}$ in the loop; the error bounds and frequency response measurements are shown in the Bode magnitude diagrams of figure 9.26.

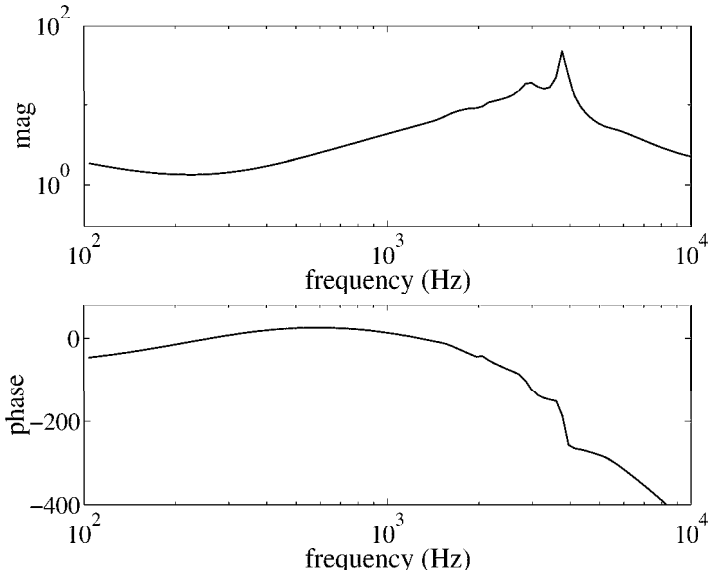

fig. 9.25: Bode diagram of a 15th order controller, resulting from a design with weighting $W_3(\nu_b)$ and $\nu_b = 750$ Hz.

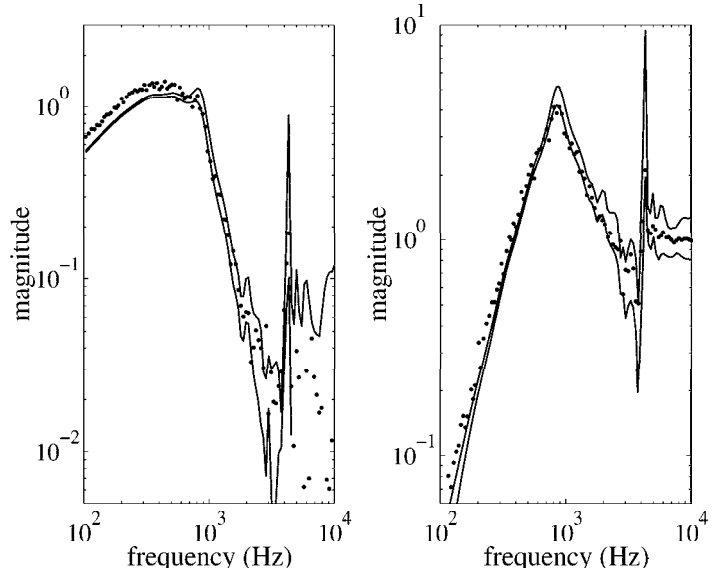

fig. 9.26: $P(I + CP)^{-1}$ (left) and $(I + CP)^{-1}$ (right) with controller $C_{\hat{P},750}$ in the loop: system uncertainty set (solid), identified with controller $C_{\hat{P},500}$, and frequency response estimate (dot).

A remarkable and undesired feature of the Bode magnitude diagram in figure 9.26 is that the transfer function error bounds do not adequately capture the measurements at low frequencies, while at higher frequencies they predict the measurements in a reliable and tight way. To examine this phenomenon, a system uncertainty set is identified based on measurement data with controller $C_{\hat{P},750}$ in the loop. We want to evaluate whether a system uncertainty set, identified from closed loop measurement data with the corresponding controller in the loop, provides a more reliable performance evaluation, which in fact amounts to performance monitoring. An auxiliary model of order 48 is estimated based on an ORTFIR model structure (8 basis functions of order 6); the Bode diagrams of the auxiliary model and the frequency response $Y_N^{\mathrm{av}}(e^{j\omega_k})/U_N^{\mathrm{av}}(e^{j\omega_k})$ are shown in figure 9.27.

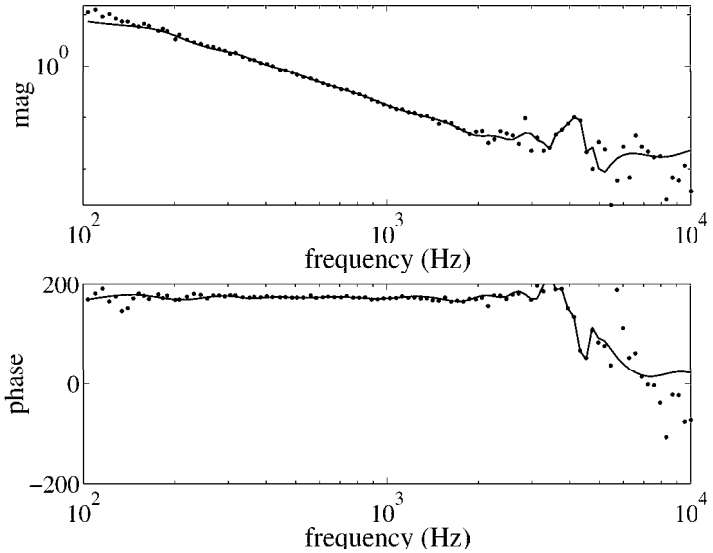

fig. 9.27: Auxiliary model P_x constructed on the basis of normalized coprime factors.

Figure 9.28 shows the normalizedness of the filtered data $\{\frac{Y}{X}(e^{j\omega_k}), \frac{U}{X}(e^{j\omega_k})\}$ and frequency response measurements $\{\frac{Y}{R}(e^{j\omega_k}), \frac{U}{R}(e^{j\omega_k})\}$, where $X(e^{j\omega_k}) := (D_x + CN_x)^{-1}R(e^{j\omega_k})$.

We see from figure 9.28 that the differences in normalization between filtered frequency response data $\{Y(e^{j\omega_k}), U(e^{j\omega_k})\}$ and employing a dual Youla parametrization are more evident than in figure 9.9 and, moreover, that fre-

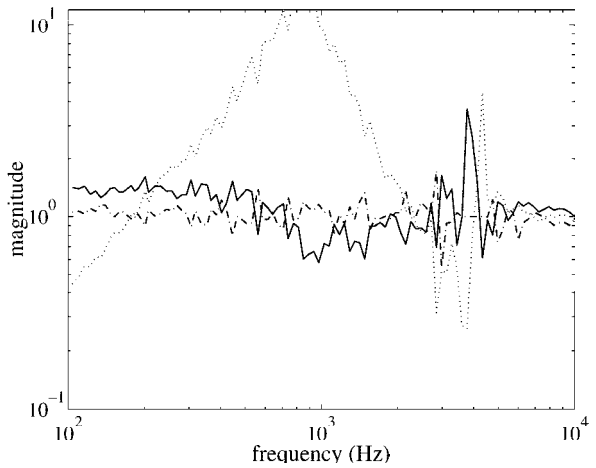

fig. 9.28: Normalization of frequency response data: measured frequency responses (dot), filtered via coprime factor representation (solid) and dual Youla representation (dash-dot).

quency response data constructed according to

$$N_x + D_c \frac{Z}{X}(e^{j\omega_k}), \quad D_x - N_c \frac{Z}{X}(e^{j\omega_k}).$$

exhibit better normalization than data filtered according to

$$\frac{Y}{R}(e^{j\omega_k})(D_x + CN_x), \quad \frac{U}{R}(e^{j\omega_k})(D_x + CN_x).$$

A possible explanation for the differences in normalization is that the controller used for filtering does not exactly match the controller that is actually implemented. As the controller enters in different manners in both filter operations, this may cause the observed differences.

A nonparametric and parametric model error bound is estimated based on data that correspond to the dual Youla parameter associated with N_x, D_x, N_c, D_c; the bounds are shown resp. in figure 9.29.a and 9.29.b.

To verify whether the error bounds account for the system frequency response, upper and lower magnitude bounds of the open loop system and the averaged ETFE $Y_N^{\mathrm{av}}(e^{j\omega_k})/U_N^{\mathrm{av}}(e^{j\omega_k})$ of the system are shown in the Bode magnitude diagram of figure 9.30.

Error bounds of the closed loop transfers $P(I + CP)^{-1}$ and $(I + CP)^{-1}$ are shown in the Bode diagrams of figures 9.31 and 9.32.

The Bode diagram of figure 9.31 indicates that the identified system uncertainty set is not capable of a reliable evaluation of performance in the frequency

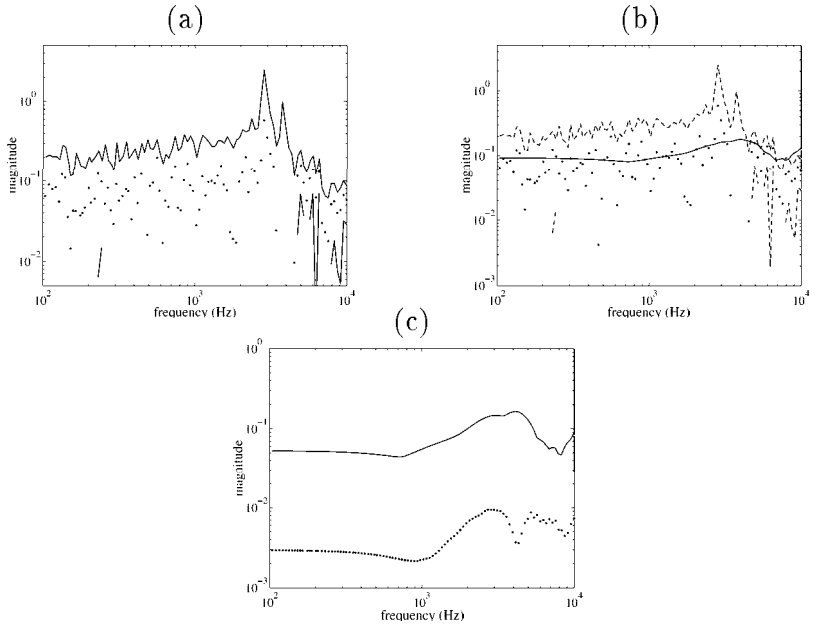

fig. 9.29: Error bounds of a dual Youla parameter: discrete (a) and continuous (b) transfer function error bound and ETFE; figure (c) shows the separate error bounds due to noise (probabilistic, solid) and undermodelling (deterministic,dot), unknown previous inputs have negligible effect on the bounds.

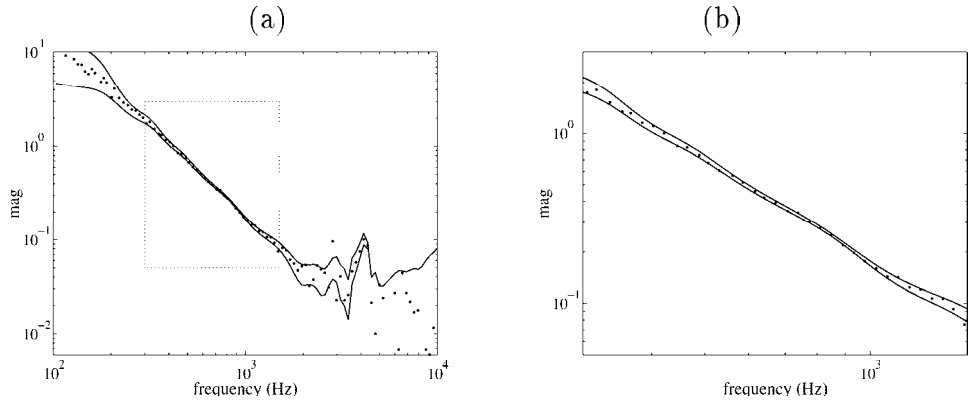

fig. 9.30: Upper and lower continuous magnitude bounds and averaged ETFE (dot) of the radial actuator: frequency range [100, 10.000] Hz (a) and [300, 1.500] Hz (b).

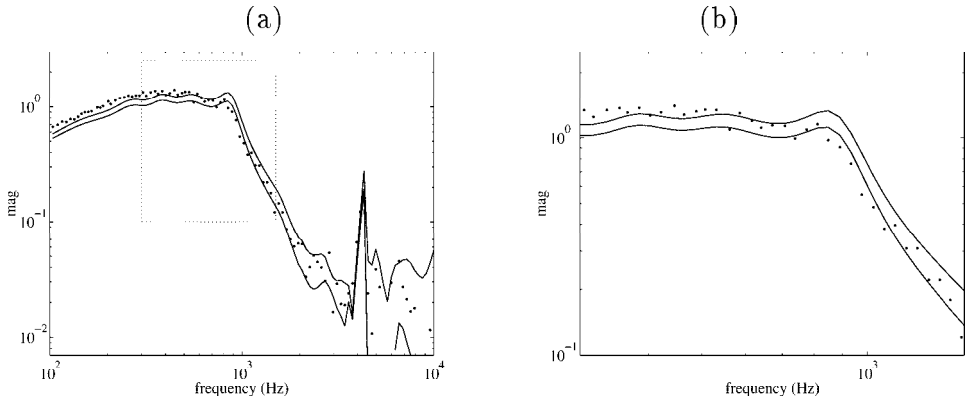

fig. 9.31: Upper and lower continuous magnitude bounds and averaged ETFE (dot) of $P(I+CP)^{-1}$: frequency range [100, 10.000] Hz (a) and [300, 1.500] Hz (b).

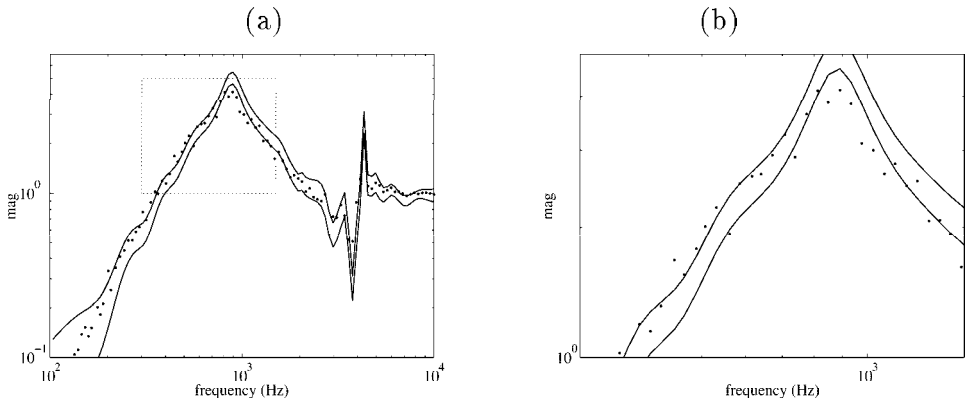

fig. 9.32: Upper and lower continuous magnitude bounds and averaged ETFE (dot) of $(I+CP)^{-1}$: frequency range [100, 10.000] Hz (a) and [300, 1.500] Hz (b).

region up to 500 Hz. As we previously observed, normalization of a fractional representation of frequency response data is insufficient in the frequency region up to 500 Hz, as indicated in figure 9.28. Due to the significant differences between normalization via a coprime factor filter structure and via a dual Youla parametrization, we have concluded that the knowledge of the controller present in the feedback loop is inadequate up to 500 Hz. Our conclusion is subscribed by the deficient performance evaluation on figure 9.31, as the identification of the system uncertainty set employs knowledge of the controller. Consequently, a severe limitation of our model-based design approach is confined in the fact that the identification is sensitive to inaccurate controller knowledge.

9.5.2 Evaluation of the results

What is done ?

In the preceeding two sections two iterations of the model-based control design procedure proposed in chapter 8, are carried out.

What can we conclude from the results ?

We summarize the following observations in view of identification of approximate models and model error bounds:

- Approximate identification of coprime factor models based on closed-loop measurement data delivers models that emphasize the system dynamics that are relevant in view of the feedback controller present in the loop.
- Identification of a system uncertainty set based on closed-loop measurement data, employing a model uncertainty structure $\mathcal{P}_R$, and subsequent transformation into additive magnitude error bounds of the open loop system provide error bounds that are reliable and tight specifically in the cross-over frequency region. Transformation of the error bounds into additive error bounds on the closed loop transfer functions of $T(P, C)$ provides bounds that are reliable and tight for all frequencies. This observation emphasizes the utility of an uncertainty structure employing a dual Youla parametrization of the system in view of feedback related identification of model error bounds.
- Error bounds on the dual Youla parameter due to variance, accounted for in the employed uncertainty bounding procedure, exhibit a larger contribution to the total model error bound for the controller that achieves a higher bandwidth, see figures 9.11 and 9.29.

Measurement data are acquired under closed loop conditions, as depicted in the block scheme of figure 9.3, which makes it evident that the controller present in the loop affects the signal-to-noise ratio of the plant input u_p and output y_p for a given excitation signal r_1 (r_2 is set to 0) in the presence of a disturbance d. From

$$\begin{aligned} y_p &= P_0(I + CP_0)^{-1}r_1 + (I + CP_0)^{-1}d \\ u_p &= (I + CP_0)^{-1}r_1 - C(I + CP_0)^{-1}d \end{aligned}$$

it follows that the noise contribution in y_p and u_p is determined by the sensitivity function. The above observation is consistent with theoretical results presented in [30] where an analysis of the merits and demerits of closed loop experiments is carried out in view of errors due to variance. We conclude that closed loop experimental conditions are not always favourable in view of control relevant tuning of the model uncertainty when viewed from the point of variance.

The following observations are made on the control design:

- the control design roughly consists of design of a weighting function and a subsequent optimization problem. The weighting functions used have a prefixed structure and are parametrized in one parameter ν_b that reflects the frequency for which $|\frac{K}{s^2}W(\nu_b)| = 1$ holds.
- Implementation of high bandwidth controllers may lead to a bad-conditioned subsequent identification, as the identification procedure based on fractional model representations is sensitive to inaccurate controller knowledge. This clearly imposes a restriction to the maximum achievable performance employing an iterative approach of identification and model-based control design. This observation stresses the importance of performing a control design (which amounts to design of weighting functions) in such a way that that controller knowledge remains accurate.

9.6 Uncertainty set identification of a batch of systems

9.6.1 Introduction

An essential problem in feedback control applications in consumer electronic products is that one feedback controller should exhibit a prespecified performance for a large number of systems. As consumer electronic products are produced in large numbers at limited production costs, different systems exhibit

slight deviations in dynamical behaviour. Design of a high robust performance controller for a batch of systems requires availability of a system uncertainty set that encompasses the dynamics of the batch of systems without becoming overly large. To that end an evaluation of the model error bounding technique discussed in chapter 7 is at place in view of providing a system uncertainty set for a number of different systems. The problem addressed in this section is formalized as follows:

Problem 9.6.1 *Presume that we have available measurement data obtained from a batch of systems $P^s(e^{j\omega}), s = 1, \ldots, L$, operating in a feedback configuration with a known controller C. Can we use the model error bounding technique of section 7.4 to identify a system uncertainty set $\mathcal{P}_R(N_x, D_x, N_c, D_c, R, \delta_R)$ such that $P^s \in \mathcal{P}_R$ holds for $s = 1, \ldots, L$?*

A straightforward approach is to apply model error bounding to each system separately following the approach in chapter 7, resulting in a set of error bounds, and to pick those bounds that enwrap the whole set. In case the number of systems L is large this winds up to be a very elaborate undertaking. A more amenable approach is to combine the measurement data in a way such that error bounding needs to be performed only once, yet resulting in tight and accurate bounds.

For each system, DFT's of the external excitation signal $r^i(t)$, input signals $u^{s,i}(t)$ and output signals $y^{s,i}(t), i = 1, \ldots, M$, are presumed available, denoted

$$\begin{aligned}
\mathcal{R}(e^{j\omega_k}) &:= [R^1(e^{j\omega_k}) \;\; R^2(e^{j\omega_k}) \;\; \ldots \;\; R^M(e^{j\omega_k})] \\
\mathcal{U}^s(e^{j\omega_k}) &:= [U^{s,1}(e^{j\omega_k}) \;\; U^{s,2}(e^{j\omega_k}) \;\; \ldots \;\; U^{s,M}(e^{j\omega_k})] \\
\mathcal{Y}^s(e^{j\omega_k}) &:= [Y^{s,1}(e^{j\omega_k}) \;\; Y^{s,2}(e^{j\omega_k}) \;\; \ldots \;\; Y^{s,M}(e^{j\omega_k})]
\end{aligned}$$

where M denotes the number of periods measured for each system and that satisfy the system equations:

$$\begin{aligned}
\frac{Y^{s,i}}{R^i}(e^{j\omega_k}) &= P^s(I + CP^s)^{-1} + (I + CP^s)^{-1}\frac{D^{s,i}}{R^i}(e^{j\omega_k}) + \frac{S^{s,i}}{R^i}(e^{j\omega_k}) \\
\frac{U^{s,i}}{R^i}(e^{j\omega_k}) &= (I + CP^s)^{-1} - (I + CP^s)^{-1}C\frac{D^{s,i}}{R^i}(e^{j\omega_k}) + \frac{S^{s,i}}{R^i}(e^{j\omega_k}),
\end{aligned}$$

where $s = 1, \ldots, L$. Basically, identification of a system uncertainty set $\mathcal{P}_R$ of a batch of different systems is constituted of the following 4 steps:

1. Acquisition of measurement data $\{\mathcal{R}, \mathcal{U}^s, \mathcal{Y}^s\}$ for $s = 1, \ldots, L$;

2. Identification of an auxiliary model P_x based on $\{\mathcal{R}, \mathcal{U}^s, \mathcal{Y}^s\}$;

3. Filtering of the measurement data $\{\mathcal{R}, \mathcal{U}^s, \mathcal{Y}^s\}$ into $\{\mathcal{X}, \mathcal{Z}\}$, corresponding to a dual Youla parameter, based on nrcf's $\{N_x, D_x\}$ of P_x and $\{N_c, D_c\}$ of the controller C;

4. Identification of a nominal model $\hat{R}$ and an upper bound δ_R based on the filtered data $\{\mathcal{X}, \mathcal{Z}\}$.

The main difference with uncertainty bounding of one system lies within steps 2 and 3. It is not evident how to combine measurement data $\{\mathcal{R}, \mathcal{U}^s, \mathcal{Y}^s\}$, $s = 1, \ldots, L$, such that a resulting P_x and $\hat{R}, \delta_R$ provide a reliable and tight uncertainty set. In subsequent subsections we will address two different ways of combining measurement data.

The approach adopted to tackle the problem stated above is a pragmatic one. A second experimental set up is at our disposal to experimentally verify the feasibility of the model error bounding procedure in view of providing a system uncertainty set for a batch of systems.

The controller C is depicted in the Bode diagram of figure 9.7 and the excitation signal displayed in figure 9.5. The Bode diagrams of the corresponding open loop frequency responses are shown in figure 9.33.

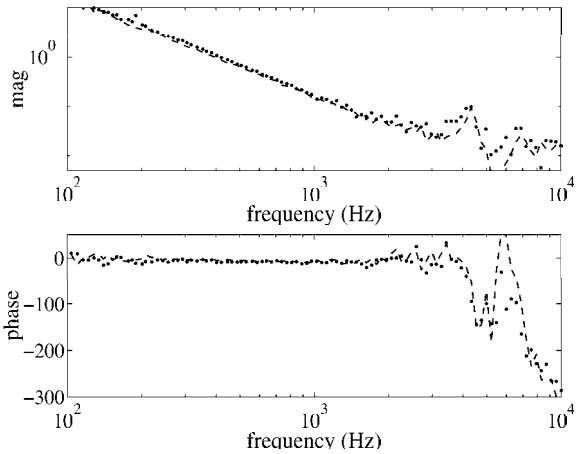

fig. 9.33: Bode diagram of frequency response measurements of two radial actuators: set up 1 (dash - dash) and set up 2 (dot).

It is seen from figure 9.33 that a difference in dynamical behaviour predominantly occurs at higher frequencies. At low frequencies set up 2 has a slightly larger magnitude.

In our elaboration the measurement data are presumed to satisfy the following presumptions:

- Disturbances present in measurement datum obtained from different systems are stochastic signals of a similar random process.
- The excitation signal $r^{s,i}(t)$ is periodic and equivalent for every system; measurements are performed such that the periodic excitations for each and every system are in exact phase. This implies that $R^{s,i}(e^{j\omega_k}) = R^{s+1,i+1}(e^{j\omega_k})$ for $s = 1, \ldots, L-1$ and $i = 1, \ldots, M-1$.

9.6.2 Data concatenation

A measurement data set can be constructed by simply concatenating the measurements as follows

$$\begin{aligned}
&[\mathcal{R}^1(e^{j\omega_k})\ \mathcal{R}^2(e^{j\omega_k})\ \ldots\ \mathcal{R}^L(e^{j\omega_k})] &&\in \mathbb{C}^{N_f \times (L \cdot M)} \\
&[\mathcal{U}^1(e^{j\omega_k})\ \mathcal{U}^2(e^{j\omega_k})\ \ldots\ \mathcal{U}^L(e^{j\omega_k})] &&\in \mathbb{C}^{N_f \times (L \cdot M)} \\
&[\mathcal{Y}^1(e^{j\omega_k})\ \mathcal{Y}^2(e^{j\omega_k})\ \ldots\ \mathcal{Y}^L(e^{j\omega_k})] &&\in \mathbb{C}^{N_f \times (L \cdot M)},
\end{aligned}$$

where N_f is the number of frequency points.

Closed loop measurement data $\mathcal{R}(e^{j\omega_k}), \mathcal{U}^s(e^{j\omega_k}), \mathcal{Y}^s(e^{j\omega_k}) \in \mathbb{C}^{N_f \times M}$ for $N_f = 99$ and $M = 40$, are available, obtained from two experimental set ups of a radial Compact Disk actuator ($L = 2$). Both experiments are performed using the same periodic excitation signal and the periods of both measurements are exactly in phase; in this way measurements from different experiments can be easily combined.

The nonparametric and parametric error bounds are depicted in the Bode magnitude diagrams of figure 9.34

The magnitude bounds of the set of open loop actuators are shown in figure 9.35; error bounds of $P(I + CP)^{-1}$ and $(I + CP)^{-1}$ are shown in 9.36 resp. 9.37.

The identified error bounds are evidently too tight to reliably capture both separate frequency response measurements, although this does not imply that the bounds are invalid at first instant. Note that continuous error bounds are not invalidated by discrete bounds as measurement noise is substantially better reduced in continuous uncertainty bounds than in discrete bounds. A closer look at the above figures however shows that the frequency responses are systematicly not captured in the frequency range of 300 to 1.500 Hz.

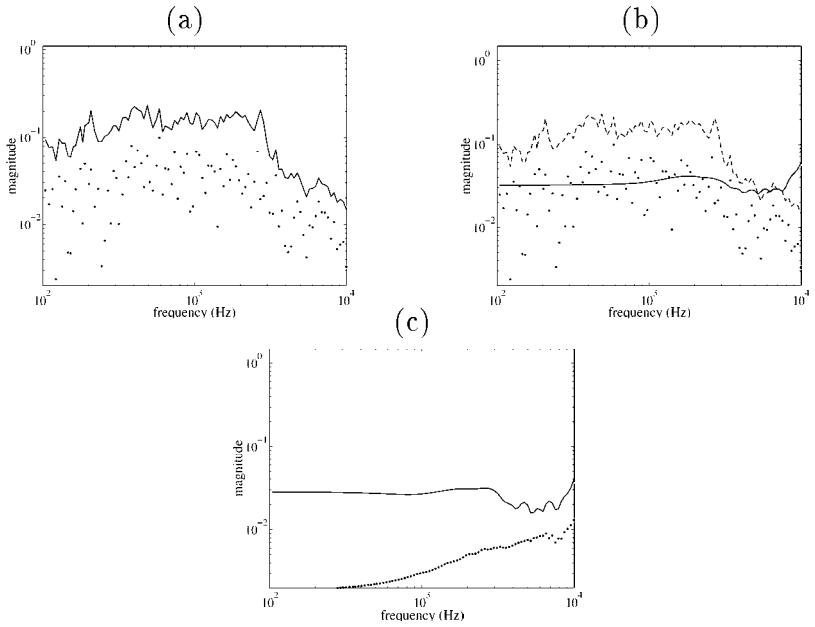

fig. 9.34: Error bounds of a dual Youla parameter: discrete (a) and continuous (b) transfer function error bound and ETFE; figure (c) depicts the separate error bounds due to noise (probabilistic, solid) and undermodelling (deterministic, dot), error due to unknown inputs is neglegible.

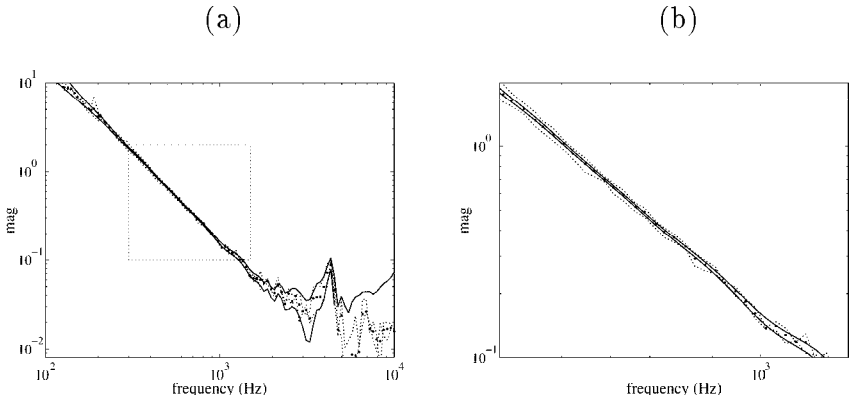

fig. 9.35: Upper and lower continuous magnitude bounds of the radial actuator, the average frequency response (big dot) and the two frequency responses of set up 1 and 2 (small dot); frequency range [100, 10.000] Hz (a) and [300, 1.500] Hz (b).

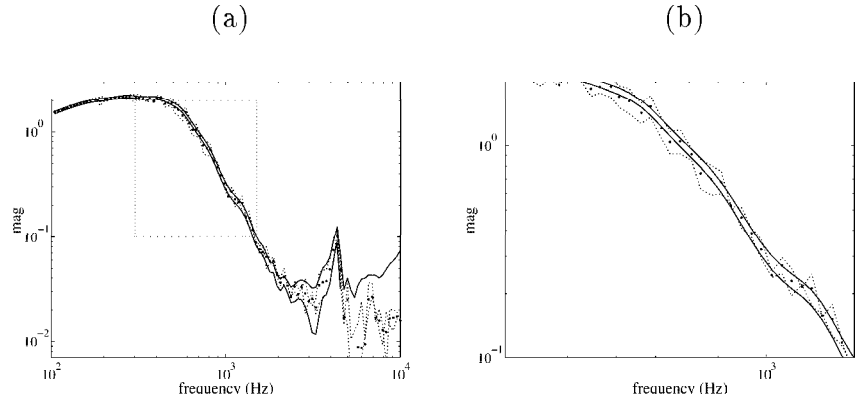

fig. 9.36: Upper and lower continuous magnitude bounds of $P(I+CP)^{-1}$, the average frequency response (big dot) and the two frequency responses of set up 1 and 2 (small dot); frequency range [100, 10.000] Hz (a) and [300, 1.500] Hz (b).

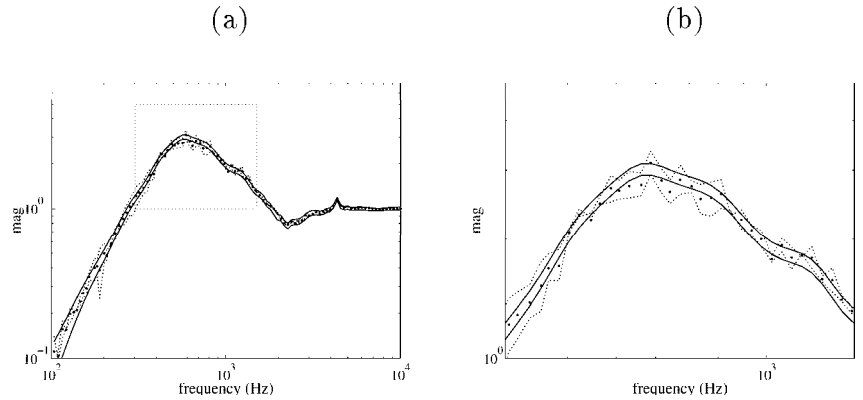

fig. 9.37: Upper and lower continuous magnitude bounds of $(I+CP)^{-1}$, the average frequency response (big dot) and the two frequency responses of set up 1 and 2 (small dot); frequency range [100, 10.000] Hz (a) and [300, 1.500] Hz (b).

Although the above experimental verification based on concatenated measurement data obtained from two systems constitutes an insufficient basis for invalidating the proposed approach in view of a *large* number of systems, we yet can explain the results. Important to note is that the error bounds are mainly the result of variance, since a utilization of a high order model results in a minor undermodelling part of the error and transient system responses are not present in measurement data, due to periodic excitation. In that case the bounding procedure of section 7.4 attributes the model error solely to measurement noise. The issue is whether computation of an error bound due to measurement noise also accounts for errors that are not only due to measurement noise, but also due to differences between several physical systems.

Error bounding due to noise contributions according to the procedure in section 7.4 amounts to construction of a confidence region based on an estimated variance, expressed as (see expression (7.12), chapter 7)

$$\hat{\sigma}^2(\hat{P}(e^{j\omega_k})) = \frac{1}{L \cdot M(L \cdot M - 1)} \sum_{i=1}^{M} \sum_{s=1}^{L} \left| \hat{P}(e^{j\omega_k}) - \hat{P}^{s,i}(e^{j\omega_k}) \right|^2 \tag{9.9}$$

where

$$\hat{P}(e^{j\omega_k}) := \frac{1}{M} \sum_{i=1}^{M} \frac{1}{L} \sum_{s=1}^{L} \hat{P}^{s,i}(e^{j\omega_k}),$$

denotes a noise corrupted estimate of a physically non-existent average system

$$\frac{1}{L} \sum_{s=1}^{L} \hat{P}^{s}(e^{j\omega_k}).$$

The number of periods available for estimation is $L \cdot M$; as the variance estimate (9.9) will tend to 0 as the number of periods tends to infinity (see [90]), the probabilistic part of the bounds vanishes asymptotically with the number of periods underlying the estimation. Expression (9.9) is asymptotic in the number of periods M measured for each system, or for the number of systems L, or both. In either case, $\hat{\sigma}^2(\hat{P}(e^{j\omega_k}))$ will tend to 0. This implies that attributing varying system dynamics to a model error by construction of a confidence region, the bounds tend to 0 in case the number of systems tends to infinity ($L \to \infty$). This is an undesirable feature as errors that describe the difference between a number of systems should not decrease; stronger, they are expected to increase for $L \to \infty$ such that all systems are captured by the bounds.

9.6.3 Alternative approach

In order to construct error bounds that capture a batch of systems for $L, M \rightarrow \infty$ we propose an alternative way of combining measurement data obtained from a number of systems. Consider available measurement data

$$\hat{\mathcal{P}}^s(e^{j\omega_k}) = [\hat{P}^{s,1}(e^{j\omega_k}) \;\; \hat{P}^{s,2}(e^{j\omega_k}) \;\; \ldots \;\; \hat{P}^{s,M}(e^{j\omega_k})]$$

for $s = 1, \ldots, L$. For every frequency ω_k we select data that correspond to two systems having the maximum resp. minimum magnitude, denoted as

$$\begin{aligned}
\hat{\mathcal{P}}_{\mathrm{up}}(e^{j\omega_k}) &:= \left\{ \hat{\mathcal{P}}(e^{j\omega_k}) | \hat{\mathcal{P}}(e^{j\omega_k}) = \hat{\mathcal{P}}^s(e^{j\omega_k})|_{|\hat{P}^s(e^{j\omega_k})|=\max_{s=1,\ldots,L}|\hat{P}^s(e^{j\omega_k})|} \right\} \\
\hat{\mathcal{P}}_{\mathrm{lo}}(e^{j\omega_k}) &:= \left\{ \hat{\mathcal{P}}(e^{j\omega_k}) | \hat{\mathcal{P}}(e^{j\omega_k}) = \hat{\mathcal{P}}^s(e^{j\omega_k})|_{|\hat{P}^s(e^{j\omega_k})|=\min_{s=1,\ldots,L}|\hat{P}^s(e^{j\omega_k})|} \right\}
\end{aligned}$$

where

$$\begin{aligned}
\hat{\mathcal{P}}^s(e^{j\omega_k}) &:= [\hat{P}^{s,1}(e^{j\omega_k}) \; \hat{P}^{S,2}(e^{j\omega_k}) \; \ldots \; \hat{P}^{s,M}(e^{j\omega_k})] \\
\hat{P}^s(e^{j\omega_k}) &:= \frac{1}{M} \sum_{i=1}^{M} \hat{P}^{s,i}(e^{j\omega_k})
\end{aligned}$$

In this way frequency response data are constructed of two (physically non-existent) systems that correspond to a worst case magnitude, to which the error bounding procedure of section 7.4 can be straightforwardly applied. In this way two error boundings have to be performed for constructing a system uncertainty set for L systems where averaging is performed over M periods. The identified error bounds of the dual Youla parameter are depicted in the Bode magnitude diagrams of figure 9.38.
The resulting error bounds of the open loop system are shown in the Bode magnitude diagrams of figure 9.39; the corresponding error bounds of $P(I + CP)^{-1}$ and $(I + CP)^{-1}$ in figures 9.40 resp. 9.41. As opposed to the results based on data concatenation, the error bounds identified from a worst case data combination prove to be reliable, as they capture both frequency response estimates, yet are less tight.

The transfer function error bounds on the open loop system in figure 9.39 tightly capture the two frequency response estimates in the frequency region [300, 700] Hz, while the error bounds of $P(I+CP)^{-1}$ and $(I+CP)^{-1}$ in figure 9.40 resp. 9.41 capture the corresponding frequency response estimates not specificly tight in the same frequency region. This, once again, stresses the utility of identifying error bounds within a dual Youla model parametrization in view of closed loop relevant uncertainty modelling.

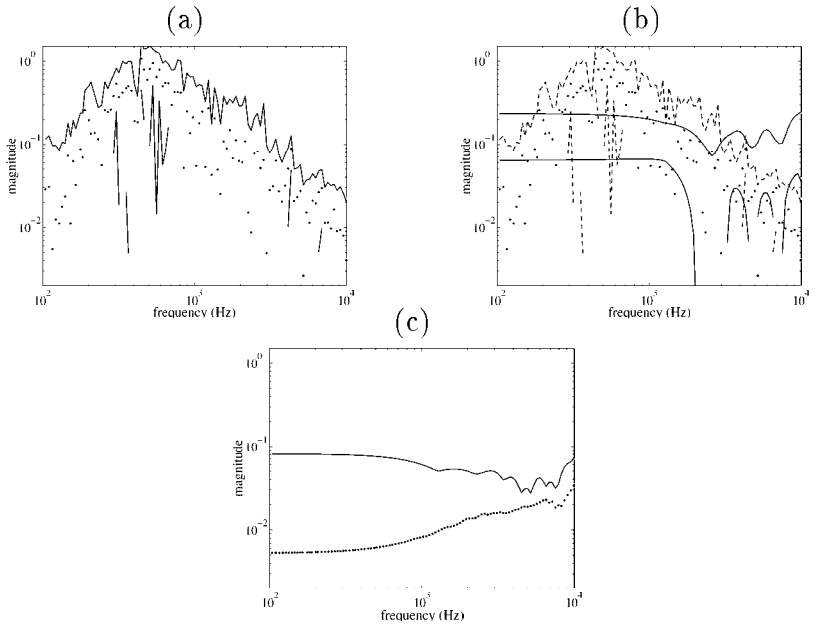

fig. 9.38: Error bounds of a dual Youla parameter: discrete (a) and continuous (b) transfer function error bound and ETFE; figure (c) depicts the separate error bounds due to noise (probabilistic, solid) and undermodelling (deterministic, dot), error due to unknown inputs is neglegible.

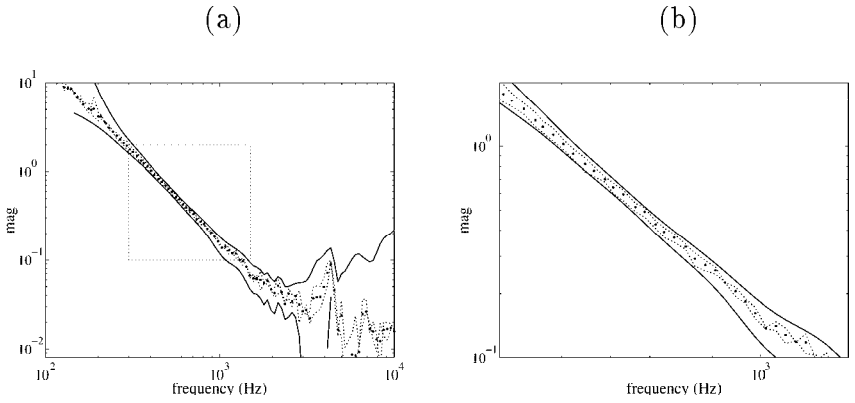

fig. 9.39: Upper and lower continuous magnitude bounds of the open loop system, the average frequency response (big dot) and the two frequency responses of set up 1 and 2 (small dotted line); frequency range [100, 10.000] Hz (a) and [300, 1.500] Hz (b).

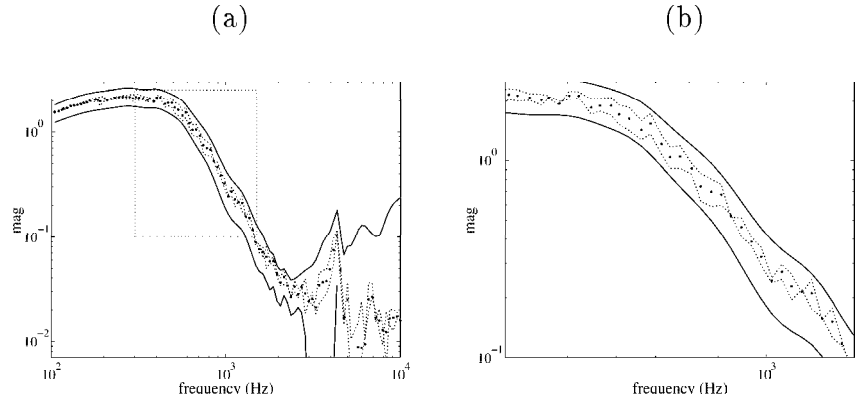

fig. 9.40: Upper and lower continuous magnitude bounds of $P(I+CP)^{-1}$, the average frequency response (big dot) and the two frequency responses of set up 1 and 2 (small dotted line); frequency range [100, 10.000] Hz (a) and [300, 1.500] Hz (b).

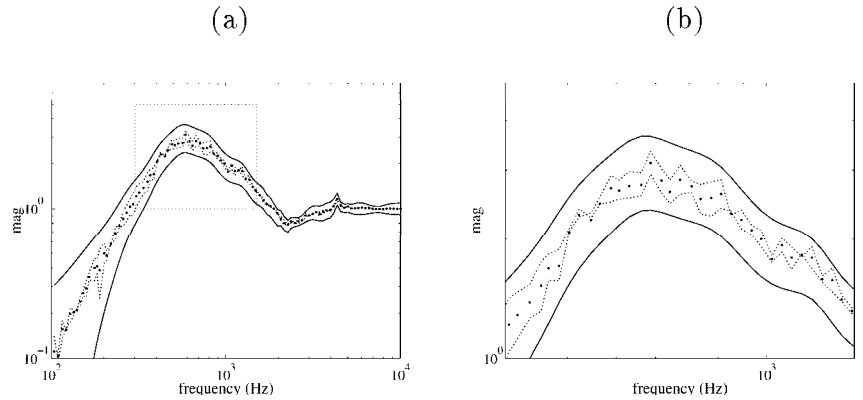

fig. 9.41: Upper and lower continuous magnitude bounds of $(I+CP)^{-1}$, the average frequency response (big dot) and the two frequency responses of set up 1 and 2 (small dot); frequency range [100, 10.000] Hz (a) and [300, 1.500] Hz (b).

9.7 Discussion

Based on the experimental results presented in this chapter, we summarize our main findings in view of our proposed model-based control design procedure.

- Utilizing approximate models for control design and a system uncertainty set for evaluation of robust performance in a model-based control design procedure for design of *restricted* complexity controllers constitutes a design approach that requires some skills in choosing the right identification parameters and assigning adequate weightings in the control design. The results achieved in this research are promising, given the limited loop shape skills of the researcher, yet a further experimental exploration is required in order to fully examine the procedures merits.

- From the experimental results in this chapter it follows that digital controller implementation exhibits discrepancies with the designed controller. A similar observation is made in chapter 5. Discrepancies between dynamics of a designed compensator and its actually implemented version may be a result of unknown gains, computational delay, quantization and saturation. Even in case of utilizing a floating point arithmetic processor board, these phenomena may drastically affect the compensators' dynamical behaviour, as is also stressed in [38].

  Inadequate controller knowledge effects the identification of approximate models based on closed-loop measurement data as well as the identification of a system uncertainty set based on a dual Youla parametrization. This stresses a disadvantage of using prior controller knowledge, which in our approach is indispensible in the approximate idenitfication of models in view of closed loop properties. In case a compensator is not exactly known, bad models are likely to come out and, subsequently, resulting controllers will also be bad, and thus a divergence from the desired enhanced performance may be the result. Concluding, in view of establishing an enhanced robust performance design procedure, controller inaccuracy should be systematically accounted for.

  Robustness with respect to inaccurate controller implementation can be incorporated by means of utilizing model error bounds as well as controller error bounds in the evaluation of robust performance. As controller knowledge is employed in filtering of DFT'd measurement data, an alternative to employing prior controller knowledge is to measure the frequency response of the controller; this is feasible via measurement of an additional signal, being the controller output.

Chapter 10

Conclusions and recommendations

10.1 Review

The background motivation for the research reported in this thesis is twofold. Firstly, stricter specifications on tracking performance in optical disk drive systems require an enhanced technology for design of high robust performance feedback controllers. The limitations of present model-based feedback control design technology are predominantly determined by the lack of a quantitative measure of the model accuracy. Secondly, in the research field of system identification for the purpose of model-based control design, techniques have been developed for constructing nominal models and uncertainty models. These methods have potential in improving present control design technology. Our problem statement hence is to inventorise in what way identification techniques that have recently come available, can be merged into a model-based control design technology that complies with specifications imposed by optical disk drive systems.

The approach adopted to tackle our problem is incented by following two observations:

1. Present feedback control of optical disk drives is hindered by the fact that models underlying the design prove not to be sufficiently accurate in order to comply with stricter performance specifications.

2. Available system identification techniques deliver accurate yet complex models (nominal models and uncertainty models) of disk drive actuators, resulting in controllers that are too complex for implementation.

In order to keep the controller order restricted, low order (hence approximate) nominal models are utilized for control design; robustness in view of inaccu-

rate models is accounted for by utilizing a data-based, accurate system uncertainty set (constituted of a high complexity nominal model in conjunction with a model error bound) for analysis of performance achieved for the system. Performance is evaluated in terms of the magnitude of the closed loop transfer functions that reflect disturbance attenuation (sensitivity) and power consumption and production of audible noise (controller times sensitivity).

10.2 Contributions of this research

In the elaboration of the outlined strategy for restricted complexity controller design based on nominal models and uncertainty models, the following issues have been elaborated:

- Frequency response measurements obtained from a radial Compact Disk servo actuator (swing-arm type, Philips CDM9) are found to be insufficiently accurate to provide a reliable analysis of robust performance (chapter 5). This observation necessitates the utilization of model error bounds in the evaluation of robust performance.
- An available mixed worst case-probabilistic error bounding technique is made operational to cope with a large amount of data points to enable estimation of model error bounds that are of surplus value in respect of measurements obtained with a dynamic signal analyzer.
- Identification of model error bounds from closed loop measurement data is performed employing a dual Youla parametrization of the model. Transformation of an error bound on a dual Youla parameter (which has no direct physical interpretation) into an additive model error bound on the open loop system (proposition 7.3.2) as well as (!) any closed loop system (sensitivity, complementary sensitivity, controller times sensitivity and plant times sensitivity) for *any* stabilizing controller (proposition 7.3.1) is feasible in a non-conservative way.
- Application of the restricted complexity controller design procedure, proposed in chapter 4, to an experimental Compact Disk player has shown the following:
  - Identified model error bounds of a dual Youla parameter enable a *reliable* and *useful* evaluation of robust performance in terms of magnitude bounds on the closed loop transfer function, provided the controller that is evaluated does not differ too much from the present controller.

  - Critical issue in design of an enhanced robust performance is the choice of the weighting function in the $\mathcal{H}_\infty$ loop shape control design. Two weightings have been considered: one that achieves nominal stability, resulting in robust controllers that establish a cautious performance enhancement yet are robust, and one that destabilizes the nominal model, resulting in robust controllers that achieve a vigorous performance enhancement yet are insufficiently robust.

- From experimental results we have observed two important aspects with respect to design and implementation of high bandwidth controllers in an iterative approach towards identification and model-based control design:

  1. A high bandwidth controller in a feedback loop impairs subsequent identification of approximate models and model error bounds, based on closed loop measurements. The noise contribution in the loop signals (plant input and output) increases for higher frequencies and the cross-over frequency region, especially in case the control results from a bad design; this has resulted in an increase of the variance contributions in the identified model error bounds, specifically in frequency regions that are crucial in a subsequent identification.
  2. The identification of approximate models and model error bounds employs knowledge of the controller present in the loop during data measurement. We have observed from experiments that the available controller knowledge may no longer be sufficiently accurate in case of high bandwidth designs, hence potentially leading to erroneous identification results in a subsequent iteration.

Issues that have emerged in the course of this research yet have not been given proper attention and aspects that are no specific contributions of this work yet are of significant importance in the elaboration, are listed next.

- Utilization of a frequency domain representation of measurement data has played an important role throughout the modelling part in this research. The main motivation for employing a frequency domain data format is the fact that data filtering is much more amenable in the frequency domain than in the time domain. As identification in a fractional model framework based on a large number of measurement data requires a great deal of filtering, a significant cut-down in computation time is achieved while refraining from additional transients in the filtered data.

An additional feature is concerned with estimation of error bounds for a batch of systems (section 9.6). Frequency domain data representations allow for simple manipulation of data attained from a large number of different systems.

- Validation of frequency response measurements in view of robust performance analysis (chapter 5) has indicated that the controller that is to be implemented (the controller resulting from the design) and the controller that is actually operative in the loop after downloading on a digital signal processor, exhibit different dynamical behaviour and that differences become more evident in case of high bandwidth controllers. The same observation is made in chapter 9.

  We have not looked extensively into improving digital controller implementation, which in itself is an important issue. In view of identification of coprime factor models, accurate knowledge of the controller that is actually operational in the loop is indispensable. A possible way of reducing the effect of bad controller implementation on a subsequent coprime factor identification, is to utilize an identified model of the controller instead of relying on the designed controller. Closed loop controller identification is dual to closed loop system identification and requires measurement of one additional signal (controller output). This has not been done.

10.3 Recommendations for further research

- The incentive of this research has been the perception that model-based control design for a physical system requires a sound understanding of model uncertainty and the need for a systematic way to deal with model uncertainty in a robust design. We have limited our scope to uncertainty due to inaccurate modelling of an electro mechanical actuator in disk drive systems. The actual tracking performance however is determined by yet another uncertain phenomenon, being the limited accuracy of knowledge of a feedback controller that operates in a feedback loop. Usage of data-based models and model error bounds in a control design technology should therefore be extended to modelling of system *and* controller.

- A phenomenon that has received no attention in this work but is nevertheless of major influence on tracking, is the presence of disturbances. As we have observed in the estimation of model error bounds based on closed loop measurement data, a controller that achieves a higher bandwidth may lead to larger error bounds, resulting from an increased effect of

disturbances on the signals in the closed loop. It is worthwhile to give attention to whether these error bounds are informative with respect to the nature and extent of the disturbances that effect the feedback system as the availability of accurate models that account for disturbances in a model-based control design approach may substantially contribute to an enhanced tracking performance.

- A problem encountered in mass-produced servo systems in consumer products is the variability of dynamical behaviour. In view of enhanced tracking performance control design, there is a clear need for models and model error bounds that accurately describe varying dynamical behaviour for a large number of systems. A first pragmatic approach towards model error bounding of a batch of systems has been proposed and experimentally verified on two experimental set ups of a radial Compact Disc actuator, resulting in uncertainty sets that are tight and reliable.

  However, the utility of this approach in view of a *large* number of systems remains unclear. A sound analysis of error bounding in view of a batch of systems is required together with a thorough investigation of alternative techniques of data-based error bounding.

- An iterative approach of identification and model-based control design requires a large number of user choices. Application of an iterative procedure to an electro mechnical servo system as is reported in this research still has left many open issues concerning suitable choices of weightings for control design and choices of the identification procedure. From an industrial perspective more insight in suitable user choices is required in order to make an iterative approach amenable for usage in industry.

Appendix A

Performance representation in the graph

In this appendix an interpretation of the approximation problem (2.20) is given in terms of a performance representation of a feedback system that shows a close relation to a graph representation of a feedback system.

In the next proposition the graph of a feedback system, depicted in figure A.1, is characterized in terms of fractional representations of P and C.

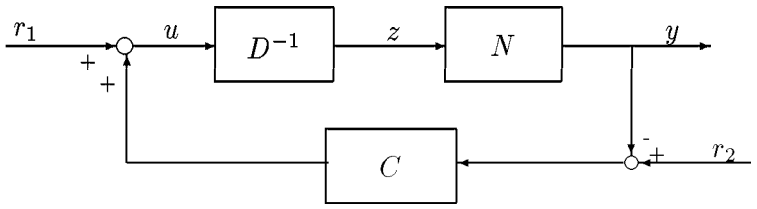

fig. A.1: Fractional system representation in feedback configuration with a compensator.

Proposition A.0.1 *Consider a feedback system system consisting of a plant P and a controller C, as depicted in figure A.1 where r_1, r_2, u, y are scalar signals. Consider a right coprime factor (r.c.f.) representation of the system $P := ND^{-1}$ and a left coprime factor (l.c.f.) representation of the controller $C := \tilde{D}_c^{-1}\tilde{N}_c$. The transfer function (2.4) that maps $[r_2\ r_1]^T \rightarrow [y\ u]^T$ is expressed as*

$$T(P,C) := \begin{bmatrix} P \\ I \end{bmatrix} [I + CP]^{-1}[C \quad I] = \begin{bmatrix} N \\ D \end{bmatrix} [\tilde{D}_c D + \tilde{N}_c N]^{-1}[\tilde{N}_c \quad \tilde{D}_c]$$

Recalling $\Lambda := \tilde{D}_c D + \tilde{N}_c N$, $([N^T\ D^T]^T, \Lambda, [\tilde{N}_c, \tilde{D}_c])$ *is a bicoprime factorization of* $T(P,C)$ *in case* (N,D) *are right coprime and* $(\tilde{N}_c, \tilde{D}_c)$ *are left coprime. The graph of the feedback system* $T(P,C)$ *can be represented in terms of coprime factor representations of* $\{P,C\}$ *as follows:*

$$\mathcal{G}_T = \left\{ \begin{bmatrix} y_p \\ u_p \\ r \end{bmatrix} \middle| \begin{bmatrix} y_p \\ u_p \\ r \end{bmatrix} = \begin{bmatrix} N \\ D \\ \Lambda \end{bmatrix} z,\ z \in l_{\mathcal{P}},\ r := [\tilde{N}_c\ \tilde{D}_c][r_2\ r_1]^T \right\}$$

Note that $[y_p\ u_p\ r]^T \in l_{\mathcal{P}} \times l_{\mathcal{P}} \times l_{\mathcal{P}}$ *for any* $z \in l_{\mathcal{P}}$, *even if* $T(P,C)$ *is unstable.*

Proof: *From lemma 2.5.2 the graph of a (possibly unstable) system is parametrized by any right coprime factorization. What is left to show is that* $([N^T\ D^T]^T, \Lambda)$ *is an r.c.f. and that the signal* r *is well-defined due to left coprimeness of* $([\tilde{N}_c\ \tilde{D}_c], \Lambda)$, *which can easily be verified in case* (N,D) *are right coprime and* $(\tilde{D}_c, \tilde{N}_c)$ *are left coprime. Additionally,* $r := [\tilde{N}_c\ \tilde{D}_c][r_2\ r_1]^T$ *is bounded as* r_2, r_1 *are both presumed bounded and* $\tilde{N}_c, \tilde{D}_c$ *are both stable. Consequently, the graph of a (possibly unstable) feedback system with input* $r := [\tilde{N}_c\ \tilde{D}_c][r_2\ r_1]^T$ *and output* $[y_p\ u_p]^T$ *can be represented as*

$$\begin{bmatrix} y_p \\ u_p \\ r \end{bmatrix} = \begin{bmatrix} N \\ D \\ \Lambda \end{bmatrix} z,$$

for any $z \in l_{\mathcal{P}}$. □

A performance representation based on a graph oriented parametrization of a feedback system hence is a transfer function that maps a bounded signal z onto the input r and output $[y_p\ u_p]^T$ of the feedback system. The role of the intermediate signal z is equivalent to the role of the signal x in the coprime factor representation of P in figure 2.2. In chapter 6 it is shown that this intermediate signal can be constructed from data measured from the closed loop system for identification purposes.

In line with the above proposition, performance of a feedback system, employing a fractional system representation, can alternatively be represented as follows

$$J_f(P,C) := W_{\text{out},f} \begin{bmatrix} N \\ D \\ \tilde{D}_c D + \tilde{N}_c N \end{bmatrix} W_{\text{in},f} \qquad \text{(A.1)}$$

where $W_{\text{out},f}, W_{\text{in},f} \in \mathbb{R}\mathcal{H}_\infty$ are weighting functions. As we assume that an available controller C_i stabilizes the system, we restrict to feedback systems (2.4) that are stable, which implies $\Lambda^{-1} \in \mathbb{R}\mathcal{H}_\infty$. The signal $z := \Lambda^{-1} r$ consequently is bounded and well-defined for any bounded signal r. Important to note is that a performance representation according to (A.1) is equivalent to (2.6),

$$W_{\text{out}} T(P, C) W_{\text{in}},$$

in terms of mutual relations of the signals r_1, r_2, u, y if we choose $W_{\text{out},f} = diag(W_{\text{out}}, I)$ and $W_{\text{in},f} = (\tilde{D}_c D + \tilde{N}_c N)^{-1} \begin{bmatrix} \tilde{N}_c & \tilde{D}_c \end{bmatrix} W_{\text{in}}$.

Appendix B

Properties of the averaged periodogram

Proof proposition 5.2.1

If we substitute the Discrete Fourier Transforms of $u^i(t)$ and $y^i(t)$ in the expression for $\widehat{\Phi}^i_{yu}(e^{j\omega})$, it is rewritten as

$$\begin{aligned}\widehat{\Phi}^i_{yu}(e^{j\omega}) &= \frac{1}{N}\left(\sum_{s=0}^{N-1} u^i(s)e^{-j\omega s}\right)^* \sum_{t=0}^{N-1} y^i(t)e^{-j\omega t} \\ &= \frac{1}{N}\sum_{s=0}^{N-1}\sum_{t=0}^{N-1} u^i(s)y^i(t)e^{-j\omega(t-s)}.\end{aligned}$$

Defining $\tau := t - s$ and rearranging the order of summation gives:

$$\begin{aligned}\widehat{\Phi}^i_{yu}(e^{j\omega}) &= \frac{1}{N}\sum_{t=0}^{N-1}\sum_{\tau+t=0}^{N-1} y^i(t)u^i(t-\tau)e^{-j\omega\tau} \\ &= \sum_{\tau=-(N_o-1)}^{N-1} \underbrace{\frac{1}{N}\sum_{t=\max\{0,\tau\}}^{\min\{N-1,N-1+\tau\}} y^i(t)u^i(t-\tau)}_{\widehat{R}^i_{yu}(\tau)}\, e^{-j\omega\tau}.\end{aligned}$$

For abbreviation of notation we denote $t_i := (i-1)N + n_i$ and define

$$\widehat{R}^i_{yu}(\tau) := \frac{1}{N}\sum_{t=\max\{0,\tau\}}^{\min\{N-1,N-1+\tau\}} w(t)w(t-\tau)y(t_i+t)u(t_i+t-\tau),$$

which is an estimate of the cross-correlation $R_{yu}(\tau)$, defined for $|\tau| < N-1$, based on a single data segment.

The asymptotic cross-periodogram $\hat{\Phi}_{yu,\infty}$ can be expressed as follows [60]

$$\widehat{\Phi}_{yu,\infty} = \sum_{\tau=-\infty}^{\infty} R_{yu}(\tau)R_w(\tau)e^{-j\omega\tau} = \frac{1}{2\pi}\int_{-\pi}^{\pi} \Phi_{yu}(e^{j\xi})W(e^{j(\omega-\xi)})\, d\xi \quad \text{(B.1)}$$

where $W(e^{j\omega})$ is the Fourier transform of $R_w(\tau)$. As $\Phi_{yu}(e^{j\omega}) = P(e^{j\omega})\Phi_u(\omega)$ holds, this is rewritten as

$$\frac{1}{2\pi}\int_{-\pi}^{\pi} P(e^{j\xi})\Phi_u(\xi)W(e^{j(\omega-\xi)})\, d\xi. \quad \text{(B.2)}$$

Proof proposition 5.2.2

A measured output signal $y^i(t)$ can be expressed employing a Finite Impulse Response representation of the system:

$$y^i(t) = \sum_{\chi=0}^{\infty} g(\chi)u(t_i + t - \chi) + d(t_i + t)$$

where $g(\chi), \chi = 0, \ldots, \infty$ represent the Markov parameters of the system. As data segments are of finite length, a cross-correlation of measurements of $\{u^i(t), y^i(t)\}$ does not completely capture the system dynamics. This is seen by splitting up the part of $y^i(t)$ due to known $u^i(t), t \in \{0, \ldots, N-1\}$ and the part due to (previous) unknown inputs as

$$y^i(t) = \underbrace{\sum_{\chi=0}^{t} g(\chi)u(t_i + t - \chi)}_{y_s^i(t)} + \underbrace{\sum_{\chi=t+1}^{\infty} g(\chi)u(t_i + t - \chi)}_{r^i(t)} + d(t_i + t)$$

where the second term, denoted as $r^i(t)$, reflects the transient effects in the measured output sequence due to previous inputs. The measured output is rewritten as $y^i(t) = y_s^i(t) + r^i(t)$, leading to an asymptotic estimate:

$$\bar{E}R_{yu}^i(\tau) := \lim_{M\to\infty} \frac{1}{M}\sum_{i=1}^{M} E\{(y_s^i(t) + r^i(t))u^i(t-\tau)\}, \qquad \begin{matrix} |\tau| & \leq N-1, \\ t & \leq N-|\tau| \end{matrix} \quad \text{(B.3)}$$

Defining

$$R_w(\tau) := \lim_{N\to\infty} \frac{1}{N}\sum_{t=0}^{N-1} \frac{1}{N} w(t)w(t-\tau)$$

it is evident that

$$R_w(\tau) = \sum_{t=\max\{0,\tau\}}^{\min\{N-1,N-1+\tau\}} \frac{1}{N} w(t)w(t-\tau)$$

holds as $w(t)w(t-\tau) = 0, |\tau| > N-1$ holds. This leads us to the following expression:

$$\begin{aligned}
&\lim_{M\to\infty} \frac{1}{M} \sum_{i=1}^{M} R_w(\tau) y(t_i+t) u(t_i+t-\tau) \\
&= R_w(\tau) \lim_{M\to\infty} \frac{1}{M} \sum_{i=1}^{M} \{E y_s(t_i+t) u(t_i+t-\tau) + r(t_i+t) u(t_i+t-\tau)\} \\
&= R_w(\tau)(R_{yu_s}(\tau) + R_{ru}(\tau)). \qquad \text{(B.4)}
\end{aligned}$$

Appendix C

Invalidation frequency response estimates

In this appendix the state space descriptions of the controllers are given that have been utilized for validation of frequency response measurements in chapter 5, employing swept sine excitation. Further, l_1 scaling of the controllers is clarified and the validation results for plant times sensitivity $P(I+CP)^{-1}$ are shown.

Implemented controllers

In view of validation of frequency response measurements of the radial Compact Disk servo mechanism, 3 controllers are implemented.

The state space description of controller C_{dr} (order 4) is:

$$A_{C_{dr}} = \begin{bmatrix} 0.0804 & -15.2114 & 0 & 0 \\ 0.0289 & 0.4842 & 0 & 0 \\ -1.2994 & -21.6445 & 0.6401 & -0.0016 \\ -0.1533 & -3.5038 & 0.1834 & 0.9998 \end{bmatrix}; \quad B_{C_{dr}} = \begin{bmatrix} 26.0352 \\ 0.8827 \\ 37.0714 \\ 6.0002 \end{bmatrix}$$

$$C_{C_{dr}} = [0 \;\; 0 \;\; 0 \;\; -0.1930], \qquad D_{C_{dr}} = 0$$

The state space description of controller C_{30} (order 8) is:

$A_{C_{30}} =$

$$\begin{bmatrix} 0.9884 & 0.0001 & -0.0003 & 0.0001 & 0.0001 & -0.0011 & 0.0005 & -0.0124 \\ -0.4268 & 0.5731 & -0.1205 & 0.1406 & -0.0183 & -0.1131 & 0.1676 & -0.4348 \\ 0 & 1.4326 & 0.1578 & -0.4761 & 0.0008 & -0.1612 & -0.5878 & 1.2969 \\ 0 & 0 & 0.9094 & 0.1286 & -0.0226 & -0.0885 & 0.1261 & -0.3354 \\ 0 & 0 & 0 & 0.8697 & -0.0052 & -0.1846 & -0.7219 & 1.3938 \\ 0 & 0 & 0 & 0 & 0.8986 & -0.0291 & -0.0681 & 0.0872 \\ 0 & 0 & 0 & 0 & 0 & 0.3743 & -0.2494 & -0.5189 \\ 0 & 0 & 0 & 0 & 0 & 0 & 0.3169 & 0.3181 \end{bmatrix};$$

$$B_{C_{30}} = \begin{bmatrix} 0.1864 \\ 0.8016 \\ 0.4329 \\ 0.7372 \\ 0.0781 \\ 0.3919 \\ 3.8387 \\ 1.0051 \end{bmatrix}; \quad C_{C_{30}} = [0 \;\; 0 \;\; 0 \;\; 0 \;\; 0 \;\; 0 \;\; 0 \;\; 1.2602]; \quad D_{C_{30}} = -4.0815$$

The state space description of the controller C_{62} (order 8) is:

$A_{C_{62}} =$

$$\begin{bmatrix} 0.9884 & 0.0002 & -0.0017 & 0.0002 & 0.0002 & -0.0058 & 0.0018 & -0.0259 \\ -0.2467 & 0.5731 & -0.3787 & 0.3934 & -0.0608 & -0.3306 & 0.3139 & -0.5245 \\ 0 & 0.4556 & 0.1579 & -0.4236 & 0.0008 & -0.1498 & -0.3501 & 0.4975 \\ 0 & 0 & 1.0222 & 0.1286 & -0.0268 & -0.0887 & 0.0845 & -0.1446 \\ 0 & 0 & 0 & 0.7326 & -0.0052 & -0.1624 & -0.4070 & 0.5061 \\ 0 & 0 & 0 & 0 & 1.0215 & -0.0291 & -0.0436 & 0.0360 \\ 0 & 0 & 0 & 0 & 0 & 0.5841 & -0.2494 & -0.3342 \\ 0 & 0 & 0 & 0 & 0 & 0 & 0.4920 & 0.3182 \end{bmatrix};$$

$$B_{C_{62}} = \begin{bmatrix} 0.4722 \\ 1.1733 \\ -0.2015 \\ 0.3859 \\ 0.0344 \\ 0.1963 \\ 3.0003 \\ 1.2197 \end{bmatrix}; \quad C_{C_{62}} = [0 \;\; 0 \;\; 0 \;\; 0 \;\; 0 \;\; 0 \;\; 0 \;\; 2.2016]; \quad D_{C_{62}} = -8.6528.$$

Closed loop scaling factors

Goal of l_1 signal scaling is to find scaling factors for the controller input, output and states such that during operation the signal magnitude covers most of the digital signal range most of the time.

The calculation of the scaling factors is adopted from [78] and amounts to calculation of

$$\sum_{k=0}^{\infty} |h(k)| \cdot |r|_{max}$$

where $\{h(k)\}$ denotes the Markov parameter sequence of the closed loop transfer from some external signal r (reference or disturbance) to the loop controller input, output and states.

The Markov parameters are constructed from state space descriptions of the controller and some model of the plant. With a state space model of the system (A_m, B_m, C_m, D_m) (an 8th order model that sufficiently describes the resonance modes of the radial actuator) and the controller (A_c, B_c, C_c, D_c) a state space model of the closed loop system is expressed as

$$A_{cl} = \begin{bmatrix} A_c - B_c D_m (1 + D_c D_m)^{-1} C_c & B_c C_m - B_c D_m (1 + D_c D_m)^{-1} D_c C_m \\ -B_m (1 + D_c D_m)^{-1} C_c & A_m - B_m (1 + D_c D_m)^{-1} D_c C_m \end{bmatrix}$$

$$B_{cl} = \begin{bmatrix} B_c D_m \\ B_m \end{bmatrix} (1 + D_c D_m)^{-1}, \quad D_{cl} = (1 + D_c D_m)^{-1}.$$

The C matrix determines the controller input, output and state signals that are scaled.

As the external signal r is characterized in terms of its maximum magnitude the scaling results may become too conservative for instance in case $|r(k)|$ reaches its maximum value only at a few time instants and remains low at

others. To obtain the least conservative scaling results we propose the following desirable property for r:

$$|r(k)|_\infty - \frac{1}{N_1 - N_0} \sum_{k=N_0}^{N_1-1} |r(k)| \ll |r(k)|_\infty \qquad \text{(C.1)}$$

where $N_1 - N_0$ $(N_1 > N_0)$ denotes the length of an arbitrary segment of the time domain data sequence.

In case of random noise excitation (C.1) is more or less satisfied for a white random process. In case the process is known to be coloured the filter characterizing the process should be included in calculation of $|h(k)|_1$ as is advocated by [78].

In case of sine sweep excitation (C.1) is satisfied in case a large number of cycles is present in a measured time sequence. Since the scaling applies to all frequencies the number of cycles should be the same for each frequency if the magnitude is constant. For this reason we use the auto integration facility of the analyzer. Scaling factors are calculated for 3 controllers.

Closed loop invalidation: *PS*

Here the measured and constructed frequency responses of the plant times sensitivity transfer function are shown.

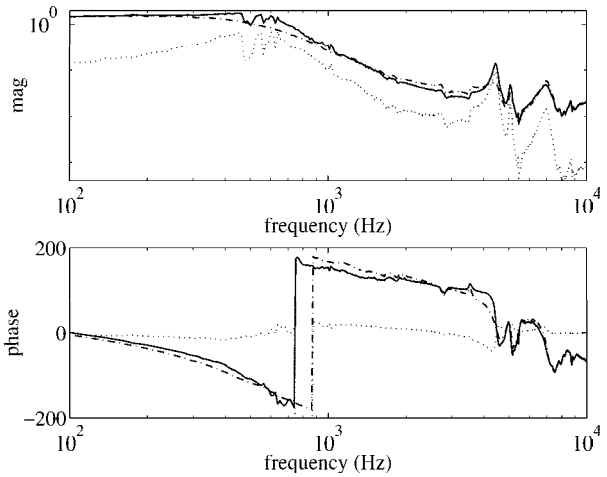

fig. C.1: $\widehat{PS}_{C_{dr}}$ (dash-dot), $\widehat{PS}_{C_{dr}}(\hat{S}_{C_{dr}} + C_{dr}\widehat{PS}_{C_{dr}})^{-1}$ (solid), $|\widehat{PS}_{C_{dr}} - \widehat{PS}_{C_{dr}}(\hat{S}_{C_{dr}} + C_{dr}\widehat{PS}_{C_{dr}})^{-1}|$ (dot, upper) and $\arg(\widehat{PS}_{C_{dr}}) - \arg(\widehat{PS}_{C_{dr}}(\hat{S}_{C_{dr}} + C_{dr}\widehat{PS}_{C_{dr}})^{-1})$ (dot, lower).

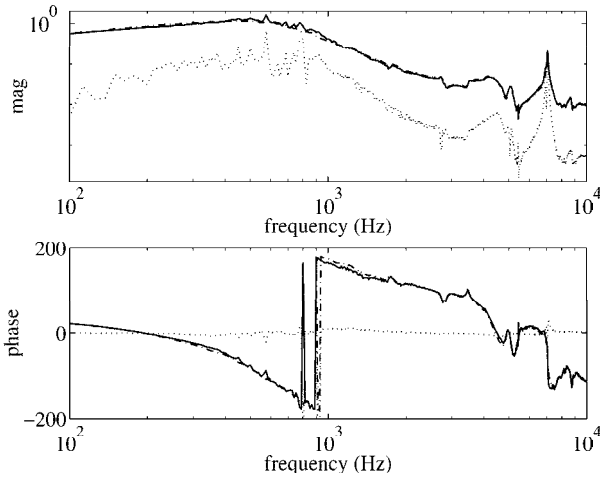

fig. C.2: $\widehat{PS}_{C_{30}}$ (dash-dot), $\widehat{PS}_{C_{30}}(\hat{S}_{C_{30}} + C_{30}\widehat{PS}_{C_{30}})^{-1}$ (solid), $|\widehat{PS}_{C_{30}} - \widehat{PS}_{C_{30}}(\hat{S}_{C_{30}} + C_{30}\widehat{PS}_{C_{30}})^{-1}|$ (dot, upper) and $\arg(\widehat{PS}_{C_{30}}) - \arg(\widehat{PS}_{C_{30}}(\hat{S}_{C_{30}} + C_{30}\widehat{PS}_{C_{30}})^{-1})$ (dot, lower).

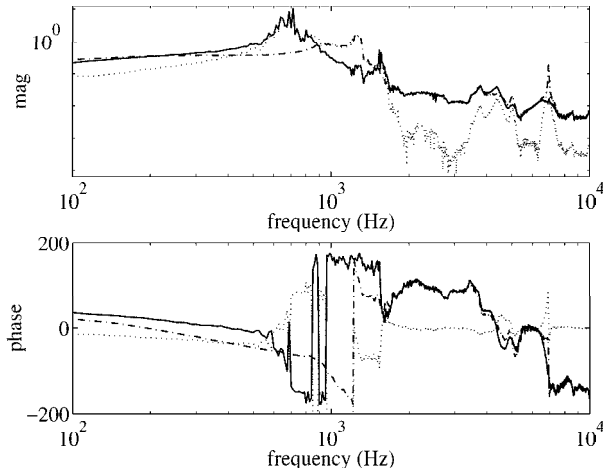

fig. C.3: $\widehat{PS}_{C_{62}}$ (dash-dot), $\widehat{PS}_{C_{62}}(\hat{S}_{C_{62}} + C_{62}\widehat{PS}_{C_{62}})^{-1}$ (solid), $|\widehat{PS}_{C_{62}} - \widehat{PS}_{C_{62}}(\hat{S}_{C_{62}} + C_{62}\widehat{PS}_{C_{62}})^{-1}|$ (dot, upper) and $\arg(\widehat{PS}_{C_{62}}) - \arg(\widehat{PS}_{C_{62}}(\hat{S}_{C_{62}} + C_{62}\widehat{PS}_{C_{62}})^{-1})$ (dot, lower).

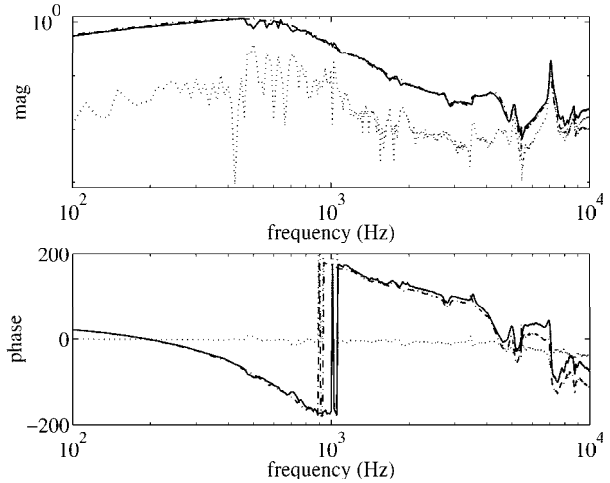

fig. C.4: $\widehat{PS}_{C_{dr}}$ (dash-dot), $\widehat{PS}_{C_{30}}(\hat{S}_{C_{30}} + C_{dr}\widehat{PS}_{C_{30}})^{-1}$ (solid), $|\widehat{PS}_{C_{dr}} - \widehat{PS}_{C_{30}}(\hat{S}_{C_{30}} + C_{dr}\widehat{PS}_{C_{30}})^{-1}|$ (dot, upper) and $\arg(\widehat{PS}_{C_{dr}}) - \arg(\widehat{PS}_{C_{30}}(\hat{S}_{C_{30}} + C_{dr}\widehat{PS}_{C_{30}})^{-1})$ (dot, lower).

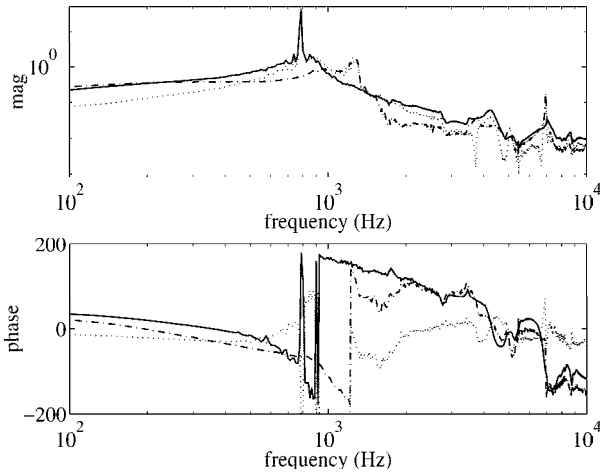

fig. C.5: $\widehat{PS}_{C_{30}}$ (dash-dot), $\widehat{PS}_{C_{62}}(\hat{S}_{C_{62}} + C_{30}\widehat{PS}_{C_{62}})^{-1}$ (solid), $|\widehat{PS}_{C_{30}} - \widehat{PS}_{C_{62}}(\hat{S}_{C_{62}} + C_{30}\widehat{PS}_{C_{62}})^{-1}|$ (dot, upper) and $\arg(\widehat{PS}_{C_{30}}) - \arg(\widehat{PS}_{C_{62}}(\hat{S}_{C_{62}} + C_{30}\widehat{PS}_{C_{62}})^{-1})$ (dot, lower).

Appendix D

Robust performance analysis employing model error bounds

We address robust performance analysis based on model error bounds. In section D.1 non-conservative expressions of upper and lower bounds of performance $|J(P,C)|$, as specified in chapter 2, are derived utilizing the system set $\mathcal{P}_R(N_x, D_x, N_c, D_c, R, \delta_R)$. Additionally, an upper and lower bound are derived for $\|J(P,C)\|_\infty$.

D.1 Proof proposition 7.3.1

Instrumental for construction of non-conservative bounds is the observation that $\mathcal{P}_R$ has the following structure

$$\frac{a+b\Delta}{c+d\Delta}$$

where $a, b, c, d, \Delta \in \mathbb{C}$. The mapping

$$\Delta \rightarrow \frac{a+b\Delta}{c+d\Delta}$$

is known as a Linear Fractional Transformation (LFT) [65]. A result known from complex analysis (see [65]) is that an LFT maps a disc in the complex plane onto another disc. This is phrased in the next proposition.

Proposition D.1.1 *Consider the disc $\mathcal{D}$ of complex variables in the complex plane $\mathcal{D} := \{\Delta | \Delta = \Delta_c + \Delta_r, |\Delta_r| < \delta_r\}$. Then the Linear Fractional Transformation*

$$\Delta \rightarrow \frac{a+b\Delta}{c+d\Delta}$$

maps $\mathcal{D}$ into a disc with centre

$$\xi_c = \frac{(a + b\Delta_c)(c + d\Delta_c)^* - bd^*\delta_r^2}{(c + d\Delta_c)(c + d\Delta_c)^* - dd^*\delta_r^2} \tag{D.1}$$

and radius

$$\delta_\xi = \frac{|ad - bc|\ \delta_r}{(c + d\Delta_c)(c + d\Delta_c)^* - dd^*\delta_r^2} \tag{D.2}$$

provided $(c + d\Delta_c)(c + d\Delta_c)^* > dd^*\delta_r^2$ holds.

Proof: *A disc in the complex plane can be expressed as a set of circles*

$$\left\{\Delta | \Delta\Delta^* - \Delta\Delta_c^* - \Delta^*\Delta_c + \Delta_c\Delta_c^* - r_\Delta^2 = 0, \quad 0 \le r_\Delta < \delta_r\right\} \tag{D.3}$$

where Δ_c is the centre of the disc and δ_r the radius. The LFT can be rewritten as

$$\alpha + \frac{\beta}{\gamma + \Delta}.$$

provided $d \neq 0$, where α, β, γ satisfy

$$\alpha = \frac{b}{d}, \quad \beta = \frac{ad - bc}{d^2}, \quad \gamma = \frac{c}{d}. \tag{D.4}$$

From

$$\xi = \alpha + \frac{\beta}{\gamma + \Delta}$$

follows

$$\Delta = -\gamma + \frac{\beta}{\xi - \alpha}.$$

Substitution in the equation of a circle in (D.3) *and subsequent rearrangement of the variables gives the following expression:*

$$\xi\xi^* - \xi\xi_c^* - \xi^*\xi_c + \xi_c\xi_c^* - r_\xi^2 = 0$$

reflecting a circle with

$$\xi_c = \alpha + \frac{\beta(\gamma + \Delta_c)^*}{(\gamma + \Delta_c)(\gamma + \Delta_c)^* - r_\Delta^2}$$

being the centre and

$$r_\xi = \frac{|\beta| r_\Delta}{(\gamma+\Delta_c)(\gamma+\Delta_c)^* - r_\Delta^2}$$

being the radius, which leads to following expressions in a, b, c, d*:*

$$\begin{aligned}
\xi_c &= \frac{b}{d} + \frac{(ad-bc)(c+d\Delta_c)^*}{d\left((c+d\Delta_c)(c+d\Delta_c)^* - dd^* r_\Delta^2\right)} \\
&= \frac{(a+b\Delta_c)(c+d\Delta_c)^* - bd^* r_\Delta^2}{(c+d\Delta_c)(c+d\Delta_c)^* - dd^* r_\Delta^2}, \\
r_\xi &= \frac{|ad-bc| r_\Delta}{(c+d\Delta_c)(c+d\Delta_c)^* - dd^* r_\Delta^2}.
\end{aligned}$$

What remains to be shown is that the mapping of a smaller circle is completely captured by the mapping of a larger one. This is trivial in case the centre of the mapping remains unaltered as the radius r_ξ *is an increasing function of* r_Δ*. However, the centre* ξ_c *moves along with* r_Δ*, so we have to verify whether*

$$|\xi_c(r_{\Delta,1}) - \xi_c(r_{\Delta,0})| < |r_\xi(r_{\Delta,1}) - r_\xi(r_{\Delta,0})|$$

holds for $0 \le r_{\Delta,0} < r_{\Delta,1} < \delta_r$*. Substitution of the above expressions for* ξ_c, r_ξ *gives the necessary condition* $(\gamma+\Delta_c)(\gamma+\Delta_c)^* > r_\Delta^2$*. So a disc defined according to* (D.3) *is mapped onto a disc*

$$\left\{\xi \mid \xi\xi^* - \xi\xi_c^* - \xi^*\xi_c + \xi_c\xi_c^* - \delta_\xi^2 = 0\right\} \tag{D.5}$$

where ξ_c *and* δ_ξ *are expressed as* (D.1) *resp.* (D.2). □

The construction of upper and lower bounds of $|J(P,C)|$ for *any* stabilizing controller, employing a system set $\mathcal{P}_R$,

$$\sup_{|\Delta_R|<\delta_R}, \inf_{|\Delta_R|<\delta_R} \left| \begin{bmatrix} N_x + D_c(R+\Delta_R) \\ D_x - N_c(R+\Delta_R) \end{bmatrix} \quad \times \right.$$
$$\left. \left(\tilde{D}_{cn} D_x + \tilde{N}_{cn} N_x + \tilde{D}_{cn}(C_n - C) D_c (R+\Delta_R)\right)^{-1} \begin{bmatrix} \tilde{N}_{cn} & \tilde{D}_{cn} \end{bmatrix} \right|, \quad \omega \in [0, \pi),$$

is attained by applying above result elementwise to

$$\begin{bmatrix} a_1 + b_1(\Delta_c + \Delta_r) \\ a_2 + b_2(\Delta_c + \Delta_r) \end{bmatrix} (c + d(\Delta_c + \Delta_r))^{-1} [f \quad g].$$

where

$$\begin{array}{lllll} \Delta_c = R & a_1 = N_x & a_2 = D_x & c = \tilde{D}_{cn}D_x + \tilde{N}_{cn}N_x & f = \tilde{N}_{cn} \\ \Delta_r = \Delta_R\,, & b_1 = D_c\,, & b_2 = -N_c\,, & d = \tilde{N}_{cn}D_c - \tilde{D}_{cn}N_c\,, & g = \tilde{D}_{cn} \end{array}$$

Expressions of lower and upper magnitude bounds follow in a straightforward manner from substitution of the above expressions:

$$\inf_{P\in\mathcal{P}_R} |J(P,C_n)| = |J(N_x,D_x,N_c,D_c,R,\delta_R,C_n)| - \delta_J(N_x,D_x,N_c,D_c,R,\delta_R,C_n)$$

$$\sup_{P\in\mathcal{P}_R} |J(P,C_n)| = |J(N_x,D_x,N_c,D_c,R,\delta_R,C_n)| + \delta_J(N_x,D_x,N_c,D_c,R,\delta_R,C_n)$$

where C_n denotes the newly designed controller for which robust performance is evaluated and

$$J_{\text{nom}}(N_x,D_x,N_c,D_c,R,\delta_R,C_n) = \begin{bmatrix} N_x + D_cR & -D_c \\ D_x - N_cR & N_c \end{bmatrix} \begin{bmatrix} (D_x + C_nN_x + (C_nD_c - N_c)R)^* \\ (C_nD_c - N_c)^*\delta_R^2 \end{bmatrix} \times D(N_x,D_x,N_c,D_c,R,\delta_R,C_n)^{-1} \begin{bmatrix} C_n & I \end{bmatrix} \quad \text{(D.6)}$$

$$\delta_J(N_x,D_x,N_c,D_c,R,\delta_R,C_n) = \begin{bmatrix} I \\ |C_n| \end{bmatrix} |(D_x + CN_x)D_c|\delta_R \times D(N_x,D_x,N_c,D_c,R,\delta_R,C_n)^{-1} \begin{bmatrix} |C_n| & I \end{bmatrix} \quad \text{(D.7)}$$

with

$$D(N_x,D_x,N_c,D_c,R,\delta_R,C_n) := |D_x + C_nN_x + (C_nD_c - N_c)R|^2 - |C_nD_c - N_c|^2\delta_R^2. \quad \text{(D.8)}$$

D.2 Proof proposition 7.3.2

The expressions of upper and lower magnitude bounds of a system P, employing a dual Youla parametrization

$$P = \frac{N_x + D_c(R + \Delta_R)}{D_x - N_c(R + \Delta_R)}, \quad |\Delta_R| < \delta_r$$

as shown in proposition 7.3.2 are found by subsitution of

$$\begin{array}{lll} \Delta_c = R & a = N_x & c = D_x \\ \delta_r = \delta_R \ , & b = D_c \ , & d = -N_c \end{array}$$

in expressions (D.1) and (D.2).

D.3 Bounds on $\|J(P,C)\|_\infty$

Analysis of robust performance in terms of an upper and lower bound of $\|J(P,C)\|_\infty$ can be derived from error bounds of $|J(P,C)|$ by virtue of the results of proposition 2.2.3 and proposition 7.3.1, which leads to the following inequality:

$$\begin{array}{c} \dfrac{\sqrt{J^F - \delta_J^F}}{|(D_x + C_n N_x + (C_n D_c - N_c)R)|^2 - |(C_n D_c - N_c)|^2 \delta_R^2} \\ \leq \quad \|J(P,C_n)\|_F \quad \leq \\ \dfrac{\sqrt{J^F + \delta_J^F}}{|(D_x + C_n N_x + (C_n D_c - N_c)R)|^2 - |(C_n D_c - N_c)|^2 \delta_R^2} \end{array} \tag{D.9}$$

where

$$\begin{aligned} J^F &:= |J_{11}|^2 + |J_{12}|^2 + |J_{21}|^2 + |J_{22}|^2 + |(D_x + CN_x)D_c|^2(|C_n|^2 + 1)^2\delta_R^2 \\ \delta_J^F &:= 2|D_x + CN_x|\delta_R \left(|C_n|^2|J_{21}| + |C_n|(|J_{11}| + |J_{22}|) + |J_{12}|\right) \end{aligned}$$

Appendix E

Data based model error bounds

E.1 Discrete transfer function bounds

In this section we present results used in this thesis for error bounding, adopted from the work by de Vries ([90]). The results hold for periodic input signals $u^i(t)$ with period length N; furthermore, $M \geq 1$ periods of measurement data $\{u^i(t), y^i(t)\}$ are available such that $u^i(t) = u^{i+1}(t)$ holds for $i = 1, \ldots, M-1$.

E.1.1 Error due to unknown inputs

Consider the error expression due to unknown input signals

$$Q(e^{j\omega_k}) := \hat{P}(e^{j\omega_k}) - \tilde{P}(e^{j\omega_k}) = \frac{1}{M}\sum_{i=1}^{M} Q_i(e^{j\omega_k})$$

then the following expressions hold:

$$|Q_i(e^{j\omega_k})| = \frac{1}{\sqrt{N}} \frac{2\bar{u}}{|U^i(e^{j\omega_k})|} \frac{K\rho(1-\rho^{-N})}{(\rho^2-1)^2} \rho^{-(i-1)N-N_s} \tag{E.1}$$

$$|Q(e^{j\omega_k})| = \frac{1}{M\sqrt{N}} \frac{2\bar{u}}{|U^i(e^{j\omega_k})|} \frac{K\rho(1-\rho^{-N_o})}{(\rho^2-1)^2} \rho^{-N_s} \tag{E.2}$$

where the system pulse response is presumed bounded by $L\rho^{-k}, \rho > 1$, $\bar{u}^p = \max|u^i(t)|$ and N_s is the number of data samples that the system is excited with $u^i(t)$ preceding measurement.

E.1.2 Bound on the variance estimation error

Consider the estimates $\hat{\sigma}^2(\tilde{P}(e^{j\omega_k}))$ and $\hat{\sigma}^2(\hat{P}(e^{j\omega_k}))$ as defined in expressions (7.11) resp. (7.12). A bound on the error of the variance estimate is expressed

as:

$$|\hat{\sigma}^2(\tilde{P}(e^{j\omega_k})) - \hat{\sigma}^2(\hat{P}(e^{j\omega_k}))| \leq \mathcal{S}(\omega_k)$$

where

$$\mathcal{S}(\omega_k) = \frac{1}{M(M-1)} \sum_{i=1}^{M} (2|A_i(e^{j\omega_k})||B_i(e^{j\omega_k})| + |B_i(e^{j\omega_k})|^2)$$

and

$$\begin{aligned} |A_i(e^{j\omega_k})| &= |\hat{P}(e^{j\omega_k}) - \hat{P}_i(e^{j\omega_k})| \\ |B_i(e^{j\omega_k})| &= \frac{M-2}{M}|Q_i(e^{j\omega_k})| + \frac{1}{M}\sum_{q=1}^{M}|Q_q(e^{j\omega_k})| \end{aligned}$$

hold and where $|Q_i(e^{j\omega_k})|$ is defined according to (E.1).

Chapter 6

Bibliography

Bibliography

[1] Anderson, B.D.O., F. De Bruyne and M. Gevers, Computing LQG plant and controller perturbations, *Proc. 33rd Conf. on Decision and Control*, Lake Buena Vista, FA, USA, 1994.

[2] Åström, K., Matching criteria for control and identification (1993). *Proc. European Conference on Control*, pp. 248-251, 1993.

[3] Åström, K. and B. Wittenmark, *Computer Controlled Systems*, Prentice Hall, Englewood Cliffs, New Jersey, 1990.

[4] Balas, G.J. and J.C. Doyle, Identification for robust control of flexible structures. *Proc. American Control Conference*, Pittsburgh, PA, USA, pp. 2566-2571, 1989.

[5] Bongers, P.M.M., *Modeling and Identification of Flexible Wind Turbine Systems and a Factorizational Approach to Robust Control.* PhD.-thesis, Delft University of Technology, The Netherlands, 1994.

[6] Bongers, P.M.M. and O.H. Bosgra, Low order robust $\mathcal{H}_\infty$ controller synthesis, *Proc. 29th Conf. on Decision and Control*, Honolulu, Hawaii, December 1990, pp.194-199.

[7] Bouwhuis, G., J. Braat, A. Huijser, J. Pasman, G. van Rosmalen, K. Schouhamer Immink , *Principles of Optical Disc Systems*, Adam Hilger Ltd, Bristol, UK, 1985.

[8] Brillinger, D.R., *Time Series: Data Analysis and Theory.* McGraw-Hill, Inc., 1981.

[9] de Callafon, R.A., *Control relevant Identification of a Compact Disc Pick-up Mechanism*, Report A-617, Mechanical Engineering Systems And Control Group, Delft University of Technology, The Netherlands, 1992.

[10] de Callafon, R.A., P.M.J. Van den Hof and D.K. de Vries, Identification and control of a Compact Disc mechanism using fractional representations *Proc. 10th IFAC Symposium SYSID '94, July 4-6 1994, Copenhagen.*

[11] de Callafon, R.A., P.M.J. Van den Hof, Filtering and parametrization issues in feedback relevant identification based on fractional model representations. *Proc. 3rd European Control Conference*, pp. 441-446, 1995.

[12] de Callafon, R.A., D. de Roover and P.M.J. Van den Hof, Multivariable least squares frequency domain identification using polynomial matrix fraction descriptions. *Internal Report N-495*, Mechanical Engineering Systems and Control Group, Delft University of Technology, The Netherlands, 1996.

[13] de Callafon, R.A. and P.M.J. Van den Hof, Suboptimal feedback control by a scheme of iterative identification and control design, *Mathematical Modelling of Systems*, Vol. 3, No. 1, pp. 77-101, 1997.

[14] Chait, Y., M.S. Park and M. Steinbuch, Design and implementation of a QFT controller for a Compact Disk Player. *Proc. American Control Conference*, Baltimore, Maryland, June 29- July 1, pp. 3204-3208, 1994.

[15] Daraei, M., *Control-relevant Iddenitfication of a Compact Disc Pick-up mechanism* (in Dutch), Report A-711, Mechanical Systems and Control Group, Delft University of Technology, The Netherlands, June 1995.

[16] dSPACE GmbH, *" DSP-CIT pro IMPEX (Implementation Expert) User's Guide Version 3.0 "*, Paderborn, Germany, 1992.

[17] dSPACE GmbH, *User's and Reference Guides Version 3.0*, Paderborn, Germany, 1995.

[18] Desoer, C.A., R.W. Liu, J. Murray and R. Saeks, feedback system design: the fractional representation approach to analysis and synthesis. *IEEE Trans. on Autom. Control*, AC-25, pp. 399-412, 1980.

[19] Donkelaar, E.T., *Identification of Model Uncertainty for a Compact Disc Pick-up Mechanism*, Report A-747, Mechanical Engineering Systems and Control Group, Delft University of Technology, August 1995.

[20] Donkelaar, E.T., H.G.M. Dötsch and P.M.J. Van den Hof, Identification of model uncertainty of a Compact Disc Pick-up mechanism. *Selected Topics in Identification, Modelling and Control*, Vol. 8, Delft University Press, 1995, pp. 47-56, 1995.

[21] Doyle, J.C., M. Newlin, F. Paganini and J. Tierno, Unifying robustness analysis and system ID. *Proceedings 33rd Conf. on Dec. and Control*, Lake Buena Vista, Fl., USA, pp. 3667-3672, 1994.

[22] Dötsch, H.G.M., P.M.J. Van den Hof, H.G. Smakman, M. Steinbuch, *Adaptive repetitive control of a compact disc mechanism.* Proc. 34th Conf. Decision and Control, 13-15 Dec. 1995, New Orleans, Louisiana, USA, pp. 1720-1725.

[23] Dötsch, H.G.M., P.M.J. Van den Hof, O.H. Bosgra and M. Steinbuch, *Identification in view of Control Design of a CD player*, Selected Topics in Identification, Modelling and Control, Vol. 9, December 1996, Delft University Press.

[24] Draijer, W., *Parametric System Identification of the Philips Compact Disc Servo System*, Report 284/89, Philips research Laboratories Eindhoven, The Netherlands, 1989.

[25] El-Sakkary, A.K.,The gap metric: robustness of stabilization of feedback systems, *IEEE Trans. on Autom. Control*, Vol AC-30, No. 3, pp.240-247, 1985.

[26] Francis, B.A., *A Course in $\mathcal{H}_\infty$ Control Theory.* Lecture Notes in Control and Information Sciences, Vol. 88, Springer Verlag, 1987.

[27] Freudenberg, J.S. and D.P. Looze, Right Half Plane Poles and Zeros and Design Tradeoffs in Feedback Systems. *IEEE Trans. on Autom. Control*, Vol. AC-30, No. 6, pp. 555-565, 1985.

[28] Freudenberg, J.S. and D.P. Looze, An analysis of $\mathcal{H}_\infty$-Optimization Design Methods. *IEEE Trans. on Autom. Control*, Vol. AC-31, No. 3, pp. 194-200, 1986.

[29] Gevers, M., *Towards a joint design of identification and control?* In: Trentelman H.L., Willems J.C. (Eds.), Essays on Control: Perspectives in the Theory and its applications. Birkhäuser, Boston, 1993, pp. 111-151, 1993.

[30] Gevers, M., L. Ljung and P.M.J. Van den Hof, Asymptotic variance expressions for closed-loop identification and their relevance in identification for control. *Accepted for presentation at 11th IFAC Symposium on System Identification*, 8-11 July 1997, Fukuoka, Japan.

[31] Gianone, L., *System Identification for Robust Control using Noncanonical Bases*, Ph.D.-thesis, Systems and Control Laboratory, Computer and Automation Research Institute, Hungarian Academy of Sciences, 1996.

[32] Godfrey, K. (editor). *Perturbation signals for system identification*, Prentice Hall Int. (UK), 1993.

[33] Goh, H.T., *Implementation of Digital Controllers: l_1 scaling*, Technical Report 107/93, Philips Research Laboratories Eindhoven, The Netherlands, 1993.

[34] Goodwin, G.C., M. Gevers and B.M. Ninness, Quantifying the error in estimated transfer functions with application to model order selection. *IEEE Trans. on Autom. Control, Vol. 37, No.7*, July 1992, pp. 913-928.

[35] van Groos, P.J.M., M. Steinbuch and O.H.Bosgra, Multivariable Control of a Compact Disc Player using μ-Synthesis. *Proc. European Control Conf. 1993*, Groningen, The Netherlands, pp. 981-985.

[36] van Groos, P.J.M., *Robust control of a compact disc player.* M.Sc.-thesis, technical note 143/93, Philips Research Laboratories, 1993.

[37] Hakvoort, R.G., *System Identification for Robust Process Control: Nominal Models and Error Bounds*, PhD-thesis, Delft University of Technology, The Netherlands, 1994.

[38] Hanselmann, H., Implementation of digital controllers - a Survey. *Automatica*, Vol. 23, No. 1, pp. 7-32, 1987.

[39] Hansen, F.R., and G. Franklin, On a fractional representation approach to closed-loop experiment design. *Proc. American Control Conf.*, Atlanta, GA, USA, pp. 1319-1320, 1988.

[40] Hansen, F.R., G. Franklin and R. Kosut, Closed-loop identification via the Fractional Representation: Experiment Design. *Proc. American Control Conf.*, Pittsburgh, PA, USA, pp. 1422-1427, 1989.

[41] Heuberger, P.S.C., *On Approximate System Identification with System Based Orthonormal Functions*, PhD.-thesis, Delft University of Technology, The Netherlands, 1990.

[42] Heuberger, P.S.C., P.M.J. Van den Hof and O.H. Bosgra, A generalized orthonormal basis for linear dynamical systems, *IEEE Trans. on Autom. Control*, AC-40, 1995, pp. 451-465.

[43] Hjalmarsson, H., S. Gunnarson and M. Gevers, A convergent iterative restricted complexity control design scheme. *Proc. 33rd Conf. on Decision and Control*, Lake Buena Vista, Florida, December 1994, pp. 1735-1740.

[44] Hewlett Packard 3562A Dynamic Signal Analyzer - Operating Manual, Hewlett-Packard Co., Everett, WA, USA, 1985.

[45] Jenkins, G.M. and D.G. Watts, *Spectral Analysis and its Applications*. Holden-Day, San Francisco, CA, USA, 1968.

[46] Kosut, R.L., Uncertainty model unfalsification: a system identification paradigm compatible with robust control design. *Presentation at 13-th Benelux Meeting, 1994, Houthalen, Belgium.*

[47] Kosut, R.L., M.K. Lau and S.P. Boyd, Set-membership identification of systems with parametric and nonparametric uncertainty. *IEEE Trans. on Autom. Control, Vol. 37, No. 7*, July 1992, pp.929-941.

[48] Kwakernaak, H. and R. Sivan, *Modern Signals and Systems*, Prentice-Hall International Inc., Englewood Cliffs, New Jersey, 1991.

[49] McFarlane, D. and K. Glover, An H_∞ design procedure using robust stabilization of normalized coprime factors. *Proc. 27th Conf. Decision and Control*, Austin, Texas, December 1988, pp. 1343-1348.

[50] McFarlane, D.C. and K. Glover, *Robust Controller Design Using Normalized Coprime Factor Plant Descriptions*. Lecture Notes in Control and Information Sciences, no. 138, Springer Verlag, 1990.

[51] Milanese, M. and A. Vicino, Optimal estimation theory for dynamic systems with Set Membership Uncertainty: an overview. *Automatica, Vol. 27, No. 6*, pp. 997-1009, 1991.

[52] Lambrechts, P.F., *The Application of Robust Control Theory Concepts to Mechanical Servo Systems*, Ph.D.-thesis, Mechanical Engineering Systems and Control Group, Delft University of Technology, 1994.

[53] Lee, W.S., B.D.O. Anderson, R.L. Kosut, I.M.Y. Mareels, A new approach to adaptive robust control. Int. Journal of adaptive control and signal processing, vol. 7, pp. 183-211, 1993.

[54] Lee, W.S., B.D.O. Anderson, I.M.Y. Mareels and R.L. Kosut, On some key issues in the Windsurfer Approach to adaptive robust control. *Automatica*, Vol. 31, no. 11, pp. 1619-1636, 1995.

[55] Ljung, L. *System identification: Theory for the user.* Prentice Hall, Englewood Cliffs, New Jersey, 1987.

[56] Ljung, L. and T. Glad, *Modeling of Dynamic Systems*, Prentice-Hall, Englewood Cliffs, New Jersey.

[57] Maciejowski, J.M., *Multivariable Feedback Design*, Addison-Wesley Publishing Company, Inc., 1989.

[58] Naylor, A.W. and G.R. Sell, *Linear Operator Theory in Engineering and Science*, Springer Verlag NewYork, Inc., 1982.

[59] Ninness, B.M., *Stochastic and Deterministic Modelling*, PhD-thesis, University of Newcastle, New South Wales, Australia, 1993.

[60] Oppenheim, A.V., Schafer, R.W. *Discrete Time Signal Processing.* Prentice Hall, Englewood Cliffs, New Jersey, 1989.

[61] Park, M.S., Y. Chait and M. Steinbuch, A new approach to multivariable Quatitative Feedback Theory: thereticalk and experimental results. *Proc. American Control Conference*, Baltimore, Maryland, June 29- July 1, pp. 340-344, 1994.

[62] Partanen, A.G. and R.R. Bitmead, Two stage iterative identification/controller design and direct experimental controller refinement. *Proc. 32nd Conf. on Decision and Control*, San Antonio, Texas, December 1993, pp. 2833-2838.

[63] Partanen, A.G., Z. Zang, R.R Bitmead and M. Gevers, Experimental restricted complexity controller design. *Proc. 10th IFAC SYSID Symposium on System Identification*, July 4-6 1994, Copenhagen.

[64] Pintelon, R., P. Guillaume, Y. Rolain, J. Schoukens and H. van Hamme. Parametric Identification of Transfer Functions in the Frequency Domain - a Survey. *IEEE Trans. on Automatic Control.* Vol. 39, No. 11, pp. 2245-2260, 1994.

[65] Rudin, W., *Real and Complex Analysis*, McGraw-Hill Inc., 1970.

[66] Sanathanan, C.K. and J. Koerner. Transfer function synthesis as a ratio of two complex polynomials, *IEEE Trans. on Autom. Control*, Vol. AC-8, pp. 56-58, 1963.
[67] Schootstra, G., CDM9 compact disc servo manual, Philips Research Laboratories, Eindhoven, The Netherlands, 1993.
[68] Schoukens, J. and R. Pintelon, *Identification of Linear Systems - A Practical Guideline to Accurate Modeling*, Pergamon Press, 1991.
[69] Schrama, R.J.P., *Approximate identification and control design*. Ph.D.-thesis, Delft University of Technology, The Netherlands, 1992.
[70] Schrama, R., Accurate identification for control: the necessity of an iterative scheme, *IEEE Trans. on Autom. Control*, Vol AC-37, pp. 991-994, 1992.
[71] Schroeder, M.R., Synthesis of low peak factor signals and binary sequences of low auto-correlation. *IEEE Trans. Information Theory*, 16 : 85-89, 1970.
[72] Skelton, R.E., Model error concepts in control design. *Int. Journal of Control*, Vol. 49, No. 5, pp. 1725-1753, 1989.
[73] Smakman, H.T., *Adaptive Repetitive Control of the Radial Servo System of a CD Pick-up Mechanism*, Report A-695, Mechanical Engineering Systems and Control Group, Delft University of Technology, March 1995.
[74] Smith, R.S. and J.C. Doyle, Model validation: a connection between robust control and identification. *IEEE Trans. on Automatic Control*, Vol. 37, No. 7, pp. 942-952, 1992.
[75] Smith, R. S., Model validation for robust control: an experimental process control application. *Automatica*, Vol. 31, No. 11, pp. 1637-1647, 1995.
[76] Söderström, T. and P. Stoica, *System Identification*, Prentice-Hall Int., (UK), Ltd., 1989.
[77] Steinbuch, M., *Linear Dynamic Analysis of CD Portable*, Report 073/91, Philips Research Laboratories Eindhoven, The Netherlands, 1991.
[78] Steinbuch, M., G. Schootstra, H.-T. Goh and O.H. Bosgra, Closed Loop l_1 scaling for Fixed-point Digital Control Implementation. *Proc. American Control Conference*, Baltimore, Maryland, June 29- July 1, pp. 1157-1161, 1994.
[79] Steinbuch, M., G. Schootstra and O.H. Bosgra, Robust Control of a Compact Disc Player. *Proc. Conf. on Dec. Control*, December 1992, Tucson, Arizona, pp. 2596-2600.
[80] Steinbuch, M., P. Wortelboer, P.J.M. van Groos and O.H. Bosgra, Limits of implementation: a CD player control case study. *Proc. American Control Conference*, Baltimore, Maryland, June 29 - July 1 1994, pp. 3209-3213.

[81] Steinbuch, M., *Personal communication*, 1996.

[82] Steinbuch, M. and M.L. Norg, Industrial feedback. *Proc. 4th European Control Conference*, Brussels, July 1-4 1997.

[83] Tomizuka, M. and K.K.Chew, Steady-state and stochastic performance of a modified discrete-time prototype repetitive controller, *Journal of Dynamic Syetems, Measurement and Control*, Vol. 112, 1990, pp. 35-41.

[84] Tsao, T.-C. and M. Nemani, Asymptotic rejection of periodic disturbances with uncertain period. *Proc. American Control Conference*, Chicago, Ill., pp. 2696-2699.

[85] Van den Hof, P.M.J. and R.J.P. Schrama, Identification and control - closed loop issues. *Automatica*, Vol. 31, No. 12, pp. 1751-1770, 1995.

[86] Van den Hof, P.M.J., R.J.P. Schrama, R.A. de Callafon, O.H. Bosgra, Identification of Normalised Coprime Plant Factors from Closed Loop Experimental Data. European Journal of Control, 1:62, pp. 62-74, 1995.

[87] Van den Hof, P.M.J., E.T. van Donkelaar, H.G.M. Dötsch and R.A. de Callafon, Control-relevant uncertainty modelling directed towards performance robustness. Proceedings 13th IFAC World Congress in San Fransisco, USA, Vol. I, pp. 103-108, 1996.

[88] Vidyasagar, M., *Control System Synthesis: A Factorization Approach*, MIT Press, Cambridge, Massachussets, 1985.

[89] Vinnicombe, G., Frequency domain uncertainty and the Graph topology, *IEEE Trans. on Autom. Control*, Vol. 38, No. 9, pp.1371-1383, 1993.

[90] De Vries, D.K., *Identification of model uncertainty for control design.* Ph.D.-thesis, Delft University of Technology, The Netherlands, 1994.

[91] De Vries, D.K. and P.M.J. Van den Hof, Quantification of model uncertainty from data, *Int. Journal of Robust and Nonlinear Control*, Vol. 4, pp. 301-319.

[92] De Vries, D.K. and P.M.J. Van den Hof, Frequency domain identification with generalized orthonormal basis functions, in *Selected Topics in Identification, Modelling and Control*, Vol. 8 December 1995, Delft University Press, pp.65-74.

[93] De Vries, D.K. and P.M.J. Van den Hof, Quantification of uncertainty in transfer function estimation: a mixed probabilistic-worst-case approach, *Automatica*, Vol. 31, No. 4, pp. 543-557, 1995.

[94] De Vries, D.K. and P.M.J. Van den Hof, Quantification of uncertainty in transfer function estimation: a mixed probabilistic-worst case approach. *Automatica, Vol. 31, No. 4*, pp. 543-557, 1995.

[95] Wortelboer, P.M.R., Frequency-weighted Balanced Reduction of Closed-Loop Mechanical Servo-systems: Theory and Tools. *PhD. dissertation*, Delft University of Technology, The Netherlands, 1994.

[96] Younce, R.C and C.E. Rohrs, Identification with Nonparametric Uncertainty, *IEEE Trans. on Autom. Control*, Vol. 37, No.6, pp. 715-728.

[97] Zhou, K., J.C. Doyle and K. Glover, *Robust and Optimal Control*, Prentice Hall, Upper Saddle River, New Jersey, 1996.

[98] Zhou, T., H.G.M. Dötsch and P.M.J. Van den Hof, Model set determination and its application to the control of Compact Disc players. *Submitted to European Journal of Control*, 1997.

Chapter 7

Glossary of symbols

Glossary of symbols

Roman

a_k	real coefficient
b_k	real coefficient
d	disturbance
$g(k)$	k-th pulse response parameter
j	$\sqrt{(}-1)$
n_b	order basis generating system
n_i	number of intermediate data samples up to the i-th segment
n_p	order ORTFIR model
$\bar{n}_p$	number of basis functions
p	index number
q	shift operator
$r_{1,2}$	reference signals
$r^i(t)$	i-th segment of reference signal r
t	time index
u	input signal
u_c	controller input
u_p	plant input
$\bar{u}^p$	maximum amplitude past input signal
$u^i(t)$	i-th segment of input signal u
$w^i(t)$	i-th segment of window w
x	auxiliary signal
y	output signal
y_c	controller output
y_p	plant output
$y^i(t)$	i-th segment of output signal y

A	complex matrix
$A(e^{j\omega_k})$	numerator polynomial of coprime factor D
$B(e^{j\omega_k})$	numerator polynomial of coprime factor N
C	controller
D_c	right coprime factor of C
$\tilde{D}_c$	left coprime factor of C
$\tilde{D}_{cn}$	normalized left coprime factor of C
D_n	normalized right coprime factor of system P
D_x	right coprime factor of P_x
$E, \bar{E}$	expectation operator
$F(e^{j\omega_k})$	denominator polynomial of coprime factors N, D
$F_\alpha(n, m)$	F-distribution with n degrees in numerator and m degrees in denominator
G	general system
H	noise model
I	identity matrix
$J(P, C)$	weighted feedback system
L_k	parameter ORTFIR model
N	right coprime factor of P; signal segment length
N_o	total length of measured data sequence
N_c	right coprime factor of controller C
$\tilde{N}_c$	left coprime factor of controller C
$\tilde{N}_{cn}$	normalized left coprime factor of controller C
N_l	left bicoprime factor
N_n	normalized factor of system P
N_r	right bicoprime factor
N_x	right coprime factor of P_x
P	plant
PS_i	plant times sensitivity with controller C_i
$\widehat{PS}_i$	frequency response estimate of PS_i
$\hat{P}$	identified model
$Q(e^{j\omega_k})$	error bound due to unknown past inputs
R	dual Youla parameter
$\hat{R}$	identified model of dual Youla parameter
$R_x(\tau)$	auto-correlation of $x(t)$
$R_{yx}(\tau)$	cross-correlation of $y(t)$ and $x(t)$
$R_N^{s,i}(e^{j\omega_k})$	DFT of i-th segment of r, measured from plant number s

S_i	sensitivity function with controller C_i
$\hat{S}_i$	frequency response estimate of S_i
S^i	error due to unknown past input signals of the i-th data segment
$T(P, C)$	general feedback system
$U_N^{r,i}(e^{j\omega_k})$	DFT of i-th segment of u, measured from plant number s
V_{in}	input weighting
V_{out}	output weighting
W_3	3rd order weighting for $\mathcal{H}_\infty$ loop shape design
W_4	4th order weighting for $\mathcal{H}_\infty$ loop shape design
W_{in}	input weighting
W_{out}	output weighting
$X_N^{r,i}(e^{j\omega_k})$	DFT of i-th segment of x, corresponding to plant number s
$Y_N^{r,i}(e^{j\omega_k})$	DFT of i-th segment of y, measured from plant number s
$Z_N^{r,i}(e^{j\omega_k})$	DFT of i-th segment of z, corresponding to plant number s

Greek

α	probability
β	relative damping
γ	performance measure
γ_{desired}	desired performance measure
δ_N	error bound of coprime factor N
δ_D	error bound of coprime factor D
δ_R	error bound of dual Youla parameter R
ϵ_{max}	maximum robustness margin
η	bound for generalized pulse response parameters
θ	parameter
$\hat{\theta}$	parameter estimate
$\vartheta(e^{j\omega_k})$	vector of orthonormal basis functions
ν_b	design bandwidth (Hz)
$\bar{\sigma}$	maximum singular value
$\hat{\sigma}^2$	variance estimate
τ	time index
$\tau_{0,1,2}$	time constants
ϕ_l	phase of sinusoid with frequency ω_l
ω, ω_k	frequency (radians)
$\Gamma_{\text{lo,up}}$	performance bounds on $\lvert J(P,C)\rvert$
Δ	uncertainty model
$\Delta_{N,D,R}$	additive uncertainty of N, D resp. R
Λ	$D_x\tilde{D}_c + N_x\tilde{N}_c$
$\Phi_x(\omega)$	auto-spectrum of x
$\widehat{\Phi}_x(\omega)$	estimate of $\Phi_x(\omega)$
$\Phi_{yx}(e^{j\omega})$	cross-spectrum of y and x
$\widehat{\Phi}^i_{yx}(e^{j\omega})$	cross-periodogram of y^i and x^i
$\widehat{\Phi}_{yx,M}(e^{j\omega})$	estimate of $\Phi_{yx}(\omega)$ based on M averages of $\widehat{\Phi}^i_{yu}(e^{j\omega})$
Ψ	matrix of $\vartheta(e^{j\omega_k})$ for N frequencies

Calligraphic

$\mathcal{F}^i$	error due to measurement noise in parameter estimate θ^i
$\mathcal{P}$	system uncertainty set
$\hat{\mathcal{P}}$	vector of frequency response estimates
$\mathcal{P}_R$	system uncertainty set based on dual Youla model structure
$\mathcal{P}_{ND}$	system uncertainty set based on coprime factor model structure
$\mathcal{R}^s(e^{j\omega_k})$	vector of DFT of r corresponding to a batch of systems
$\mathcal{S}$	error due to (unknown) input signals prior to measurement in parameter estimate θ
$\mathcal{S}^i$	error due to (unknown) input signals prior to measurement in parameter estimate θ^i
$\mathcal{U}^s(e^{j\omega_k})$	vector of DFT of u corresponding to a batch of systems
$\mathcal{V}_k(e^{j\omega_k})$	orthonormal basis function
$\mathcal{W}$	diagonal matrix of single input single output weighting $W(e^{j\omega_k})$
$\mathcal{Y}^s(e^{j\omega_k})$	vector of DFT of y corresponding to a batch of systems
$\mathcal{Z}$	undermodelling error in parameter estimate θ^i

Chapter 8

Samenvatting

Samenvatting

Identificatie ten behoeve van Regelaarontwerp met toepassing op een Compact Disk Mechanisme

Hans Dötsch

Toepassingen van optische disk drive systemen in consumentenelectronische producten vereisen een verbetering van het spoorvolggedrag om te kunnen voldoen aan hogere prestatie-eisen, welke worden ingegeven door een hogere informatiedichtheid op een optische schijf en een snellere toegankelijkheid tot die informatie. Tevens vereist een toepassing in een consumentenproduct een ongevoeligheid voor verstoringen zoals trillingen en schokken. Spoorvolging en storingsonderdrukking kunnen worden gerealiseerd door ontwerp van een terugkoppelregeling.

Huidige specificaties ten aanzien van spoorvolggedrag en storingsonderdrukking van Compact Disk systemen worden behaald door regelingen die ontworpen zijn op grond van "loop shape" ontwerptechnieken. Hierbij wordt een regelaar "getuned" op grond van heuristische ontwerpregels. Hogere prestatie-eisen ten aanzien van het systeem vragen echter veelal om een systematisch gebruik van beschikbare modelkennis in een ontwerpprocedure. Een verbetering van spoorvolggedrag en storingsongevoeligheid wordt derhalve beoogt door toepassing van modelgebaseerd regelaarontwerp, waarbij een mathematisch parametrisch model van het systeem dient als basis voor ontwerp van een regeling. Het ontwerpprobleem is geformuleerd als een optimalisatieprobleem. De kwaliteit van de verkregen regeling hangt onder andere af van de kwaliteit van het parametrische model en daarenboven worden in het algemeen regelingen verkregen van een hoge complexiteit. Een belangrijke eis ten aanzien van regelaarim-

plementatie echter is dat regelingen een beperkte complexiteit dienen te hebben.

In dit onderzoek ligt de nadruk op de constructie van parametrische modellen en modelfoutgrenzen op basis van metingen (systeem identificatie) die specifiek geschikt dienen te zijn met het oog op regelaarontwerp. Identificatie van parametrische modellen ten behoeve van regelaarontwerp heeft veel aandacht gekregen in de literatuur wat heeft geresulteerd in de beschikbaarheid van gereedschappen voor identificatie van benaderende parametrische modellen en modelfoutgrenzen. Wat tot op heden nog niet voorhanden is, is een systematische procedure voor ontwerp van een modelgebaseerde regeling met een *beperkte* complexiteit ten behoeve van een verbeterd spoorvolggedrag van een niet exact bekend systeem.

In dit proefschrift wordt een modelgebaseerde regelaarontwerpstrategie voorgesteld ten behoeve van ontwerp van regelingen met een beperkte complexiteit en wordt experimenteel getoetst aan een Compact Disk mechanisme. De voorgestelde procedure behelst identificatie van een benaderend model, identificatie van modelfoutgrenzen, ontwerp van een regeling op basis van het benaderende model en evaluatie van de voor het systeem gerealiseerde prestatie op basis van een zogenaamde systeemonzekerheidsbeschrijving, waarbij gebruik wordt gemaakt van modelfoutgrenzen. De complexiteit van ontworpen regelingen wordt beperkt door de complexiteit van het parametrische model laag te houden. Dientengevolge dienen de beperkingen van de ontworpen regeling met betrekking tot de prestatie voor het systeem geëvalueerd te worden alvorens tot implementatie over te gaan. Een systeemonzekerheidsbeschrijving volgens een zogenaamde duale Youla modelstructuur blijkt geschikt ten behoeve van een niet-conservatieve evaluatie van de gerealiseerde storingsonderdruking, uitgedrukt in de sensitivity overdrachtsfunctie.

De procedure is experimenteel getoetst aan twee Compact Disk mechanismen. Op grond van experimentele resultaten kan worden geconstateerd dat het gebruik van modelfoutgrenzen in een duale Youla modelstructuur een betrouwbare en bruikbare evaluatie van de gerealiseerde prestatie voor het systeem mogelijk maakt. Een belangrijk aspect van de voorgestelde procedure is dat kennis van de regeling aanwezig in de terugkoppellus vereist is voor identificatie en dat inaccurate regelaarkennis kritischer wordt naarmate een hogere prestatiemaat wordt nagestreefd.

Chapter 9

Curriculum Vitae

Curriculum Vitae

6 april 1966	Geboren te Tegelen.
1978 - 1984	Gymnasium B, Rooms-Katholieke scholengemeenschap St. Thomascollege te Venlo.
1984 - 1991	Studie Werktuigbouwkunde aan de Technische Universiteit Delft te Delft. Het afstudeerwerk is verricht binnen de vakgroep Meet- en Regeltechniek, sectie Technische Systemen, getiteld: "Identificatie van fysisch gestruktureerde modellen van een Nauta-menger".
1991 - 1992	Vervulling militaire dienstplicht als Officier Civiele Vakopleiding.
1992 - 1998	Assistent in Opleiding aan de Technische Universiteit Delft, faculteit Werktuigbouwkunde en Maritieme Techniek, vakgroep Meet- en Regeltechniek.